P-y Curves for Laterally Loaded Drilled Shafts

Embedded in Weathered Rock

by

Mohammed A. Gabr, Ph.D., P.E.

Roy H. Borden, Ph.D., P.E.

Kook Hwan Cho

Shane Clark

Joseph B. Nixon

Department of Civil Engineering

North Carolina State University

Technical Report Documentation Page

1. Report No. FHWA/NC/2002-008	2. Government Accession No.	3. Recipient's Catalog No.
4. Title and Subtitle P-y Curves for Laterally Loaded Drilled Shafts Embedded in Weathered Rock		5. Report Date December, 2002
		6. Performing Organization Code
7. Author(s) M.A. Gabr, R.H. Borden, K.H. Cho, S.C. Clark, J.B. Nixon		8. Performing Organization Report No.
9. Performing Organization Name and Address Department of Civil Engineering CB 7908 Mann Hall North Carolina State University Raleigh, NC 27695-7908		10. Work Unit No. (TRAIS)
		11. Contract or Grant No. 2002-01
12. Sponsoring Agency Name and Address North Carolina Department of Transportation Research and Analysis Group 1 South Wilmington Street Raleigh, North Carolina 27601		13. Type of Report and Period Covered July 1999 - June 2002
		14. Sponsoring Agency Code 2000-01 and 2002-13
15. Supplementary Notes		

16. Abstract

In areas of weathered and decomposed rock profiles, the definition of soil parameters needed for the analysis and design of laterally loaded drilled shafts poses a great challenge. The lack of an acceptable analysis procedure is compounded by the unavailability of a means for evaluating the weathered profile properties, including the lateral subgrade modulus, which often leads to the conservative design. Results from this research revealed that currently proposed P-y approaches to design drilled shafts embedded in weathered Piedmont profiles do not provide reasonable estimates of load-deflection response. Results in this report are used to develop and validate a procedure for the analysis of laterally loaded drilled shafts embedded in a weathered rock mass. The developed procedure is based on the P-y method of analysis in which the shape and magnitude of the P-y function are defined. The research proceeded along four complementary tracks: i) Finite Element modeling , ii) Laboratory work, iii) Field testing using full scale shafts; field work also included estimation of in situ modulus of subgrade reaction using "rock" dilatometer, and finally iv) Performance predictions. The proposed P-y curves are developed as hyperbolic functions. A method to evaluate in situ stiffness properties of the weathered rock by utilization of the rock dilatometer, as well as by using geologic information of joint conditions, RQD, and the strength properties of cored samples, is proposed. A computational scheme for lateral behavior is advanced by which different lateral subgrade responses are assigned in the model based on the location of the point of rotation. Above the point of rotation, a coefficient of lateral subgrade reaction is assigned on the basis of evaluated modulus as computed from rock dilatometer data or from index geologic properties. A stiffer lateral subgrade reaction is assigned below the point of rotation in order to model the relatively small shear strains in this region. Predictions based on the proposed P-y model for weathered rock show good agreement with field test results, which were performed in various rock profiles. The proposed method is also verified by comparisons with published results of an additional field test. Concepts of the proposed weathered rock model have been encoded into the computer program LTBASE.

17. Key Words Laterally Loaded Drilled Shafts, Weathered Rock, P-y Curves, Rock Dilatometer, Subgrade Reaction		18. Distribution Statement	
19. Security Classif. (of this report) Unclassified	20. Security Classif. (of this page) Unclassified	21. No. of Pages 289	22. Price

Form DOT F 1700.7 (8-72)   **Reproduction of completed page authorized**

DISCLAIMER

The contents of this report reflect the views of the author(s) and not necessarily the views of the University. The author(s) are responsible for the facts and the accuracy of the data presented herein. The contents do not necessarily reflect the official views or policies of either the North Carolina Department of Transportation or the Federal Highway Administration at the time of publication. This report does not constitute a standard, specification, or regulation.

ABSTRACT

In areas of weathered and decomposed rock profiles, the definition of soil parameters needed for the analysis and design of laterally loaded drilled shafts poses a great challenge for engineers and contractors. The lack of an acceptable analysis procedure is compounded by the unavailability of a means for evaluating the weathered profile properties, including the lateral subgrade modulus, which often leads to the conservative design.

One of the acceptable approaches to analyze laterally loaded shaft is to model the in situ media as springs, usually characterized in literature as P-y curves. However, results from this research revealed that currently proposed P-y approaches to design drilled shafts embedded in weathered Piedmont profiles do not provide reasonable estimates of load-deflection response.

Results of the research study presented in this report are used to develop and validate a procedure for the analysis of laterally loaded drilled shafts embedded in a weathered rock mass. The developed procedure is based on the P-y method of analysis in which the shape and magnitude of the P-y function are defined. The research proceeded along four complementary tracks: i) Finite Element modeling using computer program ABAQUS for 3-dimensional analysis of resistance forms, ii) Laboratory work to study the characteristics of P-y curves in simulated material. iii) Field testing using full scale shafts to develop and verify P-y curves in the weathered rock. Field work also included estimation of in situ modulus of subgrade reaction using "rock" dilatometer, and finally iv) Performance predictions using the developed, and proposed, P-y model to predict measured shaft performances, and validate the proposed P-y model.

The proposed P-y curves are developed as hyperbolic functions as this shape is found to best fit the laboratory and field data. The P-y curves are established as a function of relative stiffness of the shaft and in situ material. A method to evaluate in situ stiffness properties of the weathered rock by utilization of the rock dilatometer, as well as by using geologic information of joint conditions, RQD, and the strength properties of cored samples, is proposed.

A computational scheme of lateral behavior is advanced by which different lateral subgrade responses are assigned in the model based on the location of the point of rotation. Above the point of rotation, a coefficient of lateral subgrade reaction is assigned on the basis of evaluated modulus as computed from rock dilatometer data or from index geologic properties. A stiffer lateral subgrade reaction is assigned below the point of rotation in order to model the relatively small shear strains in this region and. Predictions based on the proposed P-y model for weathered rock show good agreement with field test results, which are performed in various rock profiles. The proposed method is also verified by comparisons with published results of an additional field test. Concepts of the proposed weathered rock model have been encoded into the computer program LTBASE. Details for creating input files using the proposed weathered rock (WR) P-y model are presented in this report.

TABLE OF CONTENTS

LIST OF TABLES

LIST OF FIGURES

CHAPTER 1. INTRODUCTION

1.1 Background

In locations where geologic discontinuities have resulted in relatively soft soils overlying massive hard rock, the geometry of the soil-rock boundary can be reasonably defined with existing subsurface exploratory techniques. In areas of weathered and decomposed rock profiles, such as that of the Piedmont physiographic province of the southeastern United States, definition of the soil-rock boundary is a recurring challenge for engineers and contractors. In this situation, the subsurface conditions typically consist of surface soils derived from extensive weathering of the parent rock. With depth, the soils grade into less-weathered material and more evidence of the parent rock features are retained. At some depth, virtually no sign of weathering within the rock mass can be detected. Quantitative definitions of the soil-rock interface have been addressed in the literature. Coates (1970) recommended that the Rock Quality Designation (RQD) value could be used to estimate depth to sound rock. RQD values less than 25% designate very poor rock quality that could be classified as soil for engineering purposes. Peck (1976) stated that the distinction between rock-like and soil-like material in transition zones is usually unpredictable. Figure 1, presented by Kulhawy et al (1991), showed the depiction of different residual profiles based on definitions proposed by different researchers.

In these types of transitional subsurface profiles, definition of the soil parameters needed for the analysis and design of laterally loaded drilled shafts is challenging. The lack of an acceptable analysis procedure is compounded by the unavailability of a means for evaluating the weathered profile properties, including the lateral subgrade modulus, which often leads to overly conservative design of the shaft foundation.

Generally the two most common deformation-based analytical models used in the analysis of laterally loaded shafts placed in deforming soils and rock are:

1. Subgrade reaction approach (based on the assumption of Winkler foundation).
2. Linear approach based on the theory of elasticity.
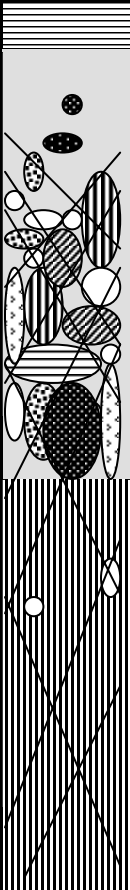
Idealized Profile	Sowers (1963) Igneous & Metamorphic	Deer & Patton (1971) All Rocks		Demean (1976) All Rocks	Engineering Properties & Behavior	General Profile
	Soil	Residual Soil	A-Horizons	Soil or True Residual Soil	Soil Structure Controlled	Top Soil
			B-Horizons			Soil
	Saprolite		C-Horizons (Saprolite)	Completely Weathered		
	Partially Weathered Rock	Weathered Rock	Saprolite to Weathered Rock Transition	Highly Weathered	Relict Discontinuity Controlled	
			Partly Weathered Rock	Moderately Weathered		Weathered to Unweathered Rock Mass (Bedrock)
	Solid Rock	Unweathered Rock		Slightly Weathered	Discontinuity Controlled	
				Fresh Rock		

Figure 1. Some Comparisons of Residual Weathering Profiles (Kulhawy et al., 1991)

Numerical models using finite element, finite difference, and boundary element techniques, with the soil idealized by the subgrade or elastic theory approaches, are often used as the solution scheme due to the limitations associated with closed-form solutions. These limitations are mainly related to the difficulty of modeling complicated boundaries, nonlinearity, inhomogenouity often encountered in geotechnical engineering problems.

1.2 Problem Statement

Past work on the deformation-based analysis of drilled shafts in weathered rock is scarce. Notable studies recently reported in literature include work by Zhang et al.

(2000), Reese (1997), and Digioia and Rojas-Gonzalez (1994). Zhang et al. (2000) considered nonlinear behavior of soil and rock by assuming that the soil and rock mass are elastic-perfectly plastic materials. Reese (1997) extended the P-y method and utilized it for the analysis of a single pile in rock. The method was termed "interim" principally because of the dearth of load test data to validate the design equations. Digioia and Rojas-Gonzalez (1994) performed seven tests on drilled shafts supporting transmission towers and reported the applicability of their design model (MFAD) in predicting the measured field behavior. They concluded that "classical methods for prediction the load-deflection relationship for drilled shafts in soil consistently over-predict drilled shaft deflection." They also stated that additional research is necessary to assist the designer with various rock profiles.

According to the literature reviewed, none of the previous work has been performed by fully investigating the load-deflection behavior of shafts embedded in weathered rock. Therefore, it appears that the stiff clay model has been most frequently used in industry to design shafts embedded in weathered rock, which may be yielding non-cost effective geometry due to the underestimation of lateral shaft resistance. Generally, the cost to construct a 1.0 meter diameter drilled shaft is approximately $1,200 per foot. If advanced knowledge can lead to shortening the length of shaft by developing a P-y curve model for weathered rock, a significant cost saving can be expected.

1.3 Objectives

The general objective of the research program presented in the report is to develop, validate, and verify a procedure for the design and analysis of laterally loaded drilled shafts embedded in North Carolina weathered rock profiles. The procedure developed is based on the P-y method of analysis, in which the shape and magnitude of the P-y curves will be defined. As previously mentioned, the soil-rock boundary is largely undefined for the case of a residual soil profile. The current state-of-practice used by NCDOT for drilled shafts embedded in a weathered Piedmont rock profile is considered to be over conservative, as it relies on modeling the weathered rock as stiff clay. Accordingly, cost savings could be realized, while maintaining an acceptable and safe performance, if a rational method is developed.

From an engineering perspective, the distinction between transitional material and rock is important in understanding the long-term behavior of a drilled shaft foundation. Evaluating the lateral stiffness characteristics of the weathered profiles is an essential analysis component. Such evaluation can be accomplished, in rock profiles, by using in-situ measuring devices such as the rock dilatometer. However, no in-situ stiffness values are presently available for discerning the lateral modulus in the Piedmont transitional profiles.

Specifically, the research program described herein has the following objectives:

1. Enhancement of current understanding of the behavior of drilled shafts embedded in weathered rock profiles through establishment of performance data from instrumented field load tests.

2. Development of a P-y model for weathered rock on the basis of laboratory and field testing, complimented by F.E.M. analysis.

3. Development of a method to estimate the coefficient of subgrade reaction on the basis of material properties and degree of fixity, as well as in-situ modulus properties measured using rock dilatometer.

4. Establishment of a database of weathered rock moduli from the North Carolina Piedmont area using rock dilatometer.

5. Definition of the shape and magnitude of P-y curves and development of a method to construct these curves for weathered rock using the measured in-situ properties from the rock dilatometer.

6. Validation of the developed P-y curve model by comparing predicted with measured load-deformation responses.

7. Verification of the developed P-y curve model utilizing performance predictions of field tests independent of those used for model development.

1.4 Scope of Work

The scope of work for development of P-y curves in weathered rock proceeded along four complementary tasks. The first task involved Finite Element modeling using the ABAQUS computer program for 3-dimensional analysis of resistance media forms. The second task included laboratory work to study the characteristics of P-y curves in

simulated material. The third task included field testing using full scale shafts to develop and validate P-y curves in natural weathered rock materials. And, the final task involved the application of the developed P-y curve model to field load tests, for which performance predictions were made prior to testing and then compared with measured shaft responses. Each of four phases of work is described in the following sections.

1.4.1 Finite Element Method Modeling

Finite Element modeling was performed using the computer program ABAQUS to design the laboratory testing program and investigate the effects of various field conditions on the lateral response. Boundary analyses were conducted to discern boundary effects during laboratory testing based on the diameter and length of the model pile, the size of testing chamber, and the depth of the soil.

F.E.M. analyses were also used to systematically investigate the effect of relative stiffness of weathered rock and shaft, and the degree of fixity on the load-deformation characteristics. In addition, the F.E.M. analyses were utilized for the investigation of various, possible, field conditions. The comparison and combination of results from F.E.M. analysis, laboratory testing, and field testing were used to explore situations beyond those encountered during the laboratory and field experimental programs. Fifty (50) different scenarios were simulated using F.E.M. by varying analyses parameters including the magnitude of loading, depth of embedment, and relative stiffness of the shaft.

1.4.2 Laboratory Testing

Two (2) large scale laboratory tests were performed to evaluate the characteristics of the P-y curve in simulated material under controlled conditions. The test model shafts were installed approximately 1 meter into compacted Aggregate Base Course material (ABC) obtained from Godwin Sand and Gravel in Raleigh, NC. The material was selected as a weathered rock simulant based on the percentage of recovery from rock cores obtained in the field from weathered rock profiles. The shape of the P-y curves were investigated under two different conditions. The first test was performed under self-weight of simulated material, and the second test under a surcharge of 24 kPa.

The test results were used to study the phenomena of changing lateral stiffness with depth and with deformation level. The subgrade modulus and ultimate resistance measured from laboratory test were compared with those from field test results. The laboratory test results were used to develop the shape of a mathematical P-y curve function and to increase the range of relative stiffness within the overall database.

1.4.3 Field Testing

The field load tests were used to develop and verify the P-y curve model for weathered rock. As a part of the P-y model development, six (6) lateral load tests were performed in Nash-Halifax County, Caldwell County, and Wilson County in North Carolina. In addition, four (4) load tests were performed in Durham County as a part of verification study. All tests were performed on 0.762 meter diameter drilled shafts instrumented with vibrating wire strain gages. The deflection profile of each shaft was measured with continuous inclinometer probes. These data were collected to enable the back-calculation of measured P-y curves with depth. The results of the field test were used to generate field P-y curves and demonstrate their validity in predicting the measured load-deformation response of the tested shafts. Results are discussed in view of measured and predicted responses.

1.4.3.1 Rock Dilatometer Test

Lateral material modulus is needed in order to construct P-y curve for weathered rock. When the geological conditions were such that the weathered rock is highly fractured and weathered, it is very difficult to take samples for laboratory test. Furthermore, when tested in laboratory, the strength and the stiffness properties of the intact rock fragments were not representative of the in-situ weathered rock mass. Therefore, if geological conditions vary with depth, in-situ measured properties are expected to provide the best data for design. An in-situ test method available to measure rock-mass properties is borehole pressuremeter (referred to as a rock dilatometer model Probex 1 by ROCTEST, Plattsburgh, NY). The rock dilatometer, manufactured by ROCTEST is a specialized probe that uses an expandable bladder to apply pressure to the walls of a N-size borehole. Volume change of the probe is measured at the probe level under stress increments.

Nine (9) rock dilatometer tests were performed to provide modulus data for weathered rock material. A method to construct P-y curve for weathered rock using rock dilatometer test data, performed at the locations of test shafts, is proposed in this research.

1.4.4 Verification Testing

Four field load tests are used to verify the applicability of the developed P-y curve model. Prior to shaft testing, performance predictions were made based on the developed P-y curve model utilizing strength, stiffness, and geologic parameters measured from laboratory and field investigations. Performance predictions were also developed using both of Reese's Methods for P-y curves in weak rock, and Stiff Clay. Results from the comparison of predicted and measured behavior are discussed. Recommended design procedures are given based on the results of the verification testing.

CHAPTER 2. LITERATURE REVIEW

Estimation of load-deflection profiles for laterally loaded shaft has been reported in literature using several approaches. Poulos (1971) proposed a linear approach based on the theory of elasticity. Nonlinear load-deflection techniques using the principle of subgrade reaction is considered most useful for the analysis of laterally loaded piles and piers.

Reese (1997) proposed a P-y curve method for weathered rock. Zhang et al. (2000) published a method to estimate the load-resistance profiles for a shaft embedded in a weathered rock zone. This method assumes that soil and rock have elastic perfectly plastic characteristics. In either approach, the engineering properties of weathered rock should be properly determined. The properties of weathered rock can be determined from either in-situ tests, such as rock dilatometer testing, or using index geological properties such as unconfined compressive strength, mass joint conditions, and Rock Quality Designation (RQD). Methods reported in literature for estimating lateral response of shafts in weathered rock material and lateral modulus properties are discussed in this chapter.

2.1 Elastic Approach for Analysis of Laterally Loaded Shafts

The theory of elasticity is often used to estimate lateral movement of piles and shafts in a variety of geomaterial types. One approach, based on the theory of elasticity, was suggested by Poulos (1971). As presented by Poulos (1971), the lateral behavior of a given pile was generally influenced by the length-to-diameter ratio, L/d, stiffness of the pile, and soil strength and stiffness properties The soil in this case was assumed as an ideal, elastic, homogeneous, isotropic medium, having elastic parameters of E_s and ν_s with depth. The pile was assumed to be a thin rectangular vertical strip of width (d), Length (L), and constant flexibility ($E_p I_p$). In order to apply the analysis to a circular pile, the width (d) can be taken as the diameter of the pile. To simplify the analysis, horizontal shear stresses, that develop between the soil and the sides of the pile, were not taken into account.

A dimensionless factor K_R describing the relative stiffness of the pile/soil material was defined as follows (Poulos, 1971):

$$K_R = \frac{E_p I_p}{E_s L^4} \quad (1)$$

Where, E_p = modulus of elasticity of pile;

I_p = moment of inertia of pile;

E_s = modulus of elasticity of soil; and,

L = length of pile.

K_R has limiting values of ∞ for an infinitely rigid pile and zero for a pile of infinite length but with no stiffness. The displacement of the pile at the ground surface was presented using equation 2 and Figures 2 and 3 as follows (Poulos, 1971):

$$\rho = I_{\rho H} \frac{H}{E_s L} + I_{\rho M} \frac{M}{E_s L^2} \quad (2)$$

Where, H = applied horizontal load;

M = applied moment;

$I_{\rho H}$ = the displacement influence factor for horizontal load only, acting on ground surface (Figure 2); and,

$I_{\rho M}$ = the displacement influence factor for moment only, acting on ground surface (Figure 3).

The theory of elasticity approach provides a means to estimate the behavior of drilled shaft based on mathematical derivation. However, in reality, soils and weathered rock are highly inelastic materials especially under relatively large deformations. Accordingly, predicted shaft deflections commonly match field deflections at low loads (20~30% of total capacity). At higher load levels, the predicted deflections are too small (DiGioia and Rojas-Gonzalez, 1993).
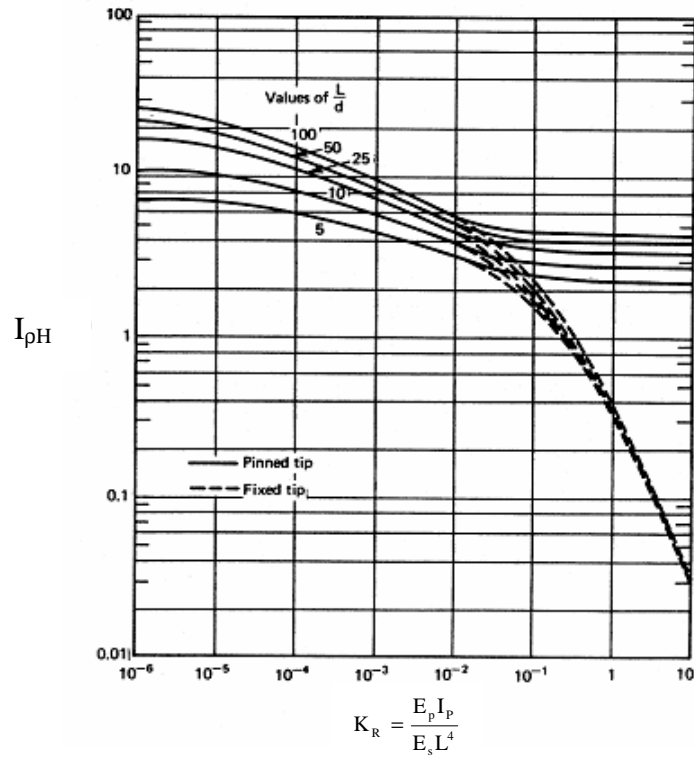
Figure 2. Displacement Influence Factor for Horizontal Load (from Poulos, 1971)
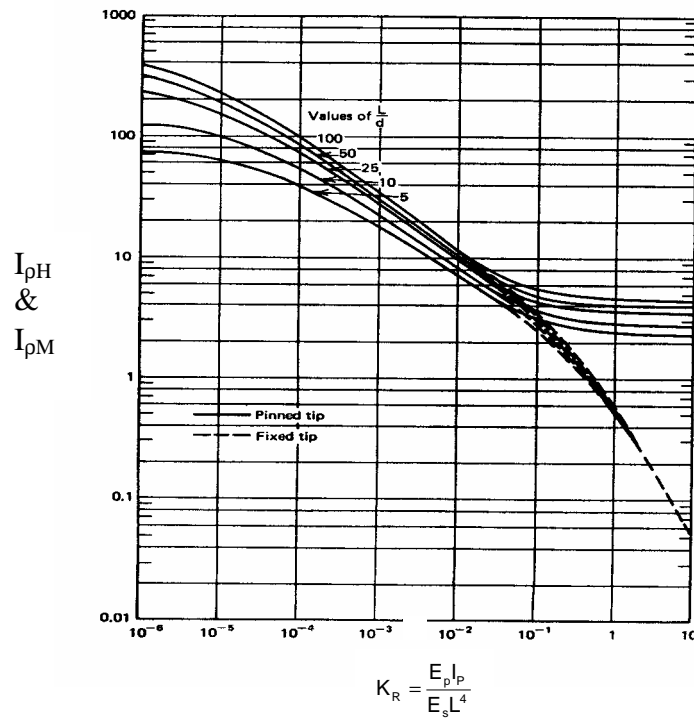
Figure 3. Displacement Influence Factor for Moment (from Poulos, 1971)

10

2.2 P-y Analysis Method

Based on the subgrade reaction approach, the soil pressure, p (kN/m^2) is correlated to the lateral deformation as follows (Matlock, 1970):

$$p = k_{ho}y \tag{3}$$

Where, k_{ho} = the coefficient of subgrade reaction that is normally defined on the basis of Winkler foundation (kN/m^3); and,

y = the lateral displacement of the pile (m).

Mltiplying the soil pressure, p (kN/m^2), by the pile width, b (m) (or diameter, if circular), the force per unit length, P (kN/m), is obtained. Accordingly, the soil reaction P is expressed as the follows:

$$P = k_h y \tag{4}$$

Where

P (kN/m) = soil reaction force per unit length;

k_h (kN/m^2) = subgrade modulus = k_{ho} b;

k_{ho} (kN/m^3) = coefficient of subgrade reaction; and,

y (m) = pile displacement.

In the subgrade reaction approach for analysis of laterally loaded piles and shafts, the soil is replaced by a series of springs attached to an element of foundation, as shown in Figure 4. P-y curves are defined at various depth, as a function of soil type and geometry.

According to Mattlock (1970), the proper form of a P-y relation is influenced by many factors, including: (i) natural variation of soil properties with depth, (ii) the general form of the pile deflection, (iii) the corresponding state of stress and strain throughout the affected soil zone, and (iv) the rate sequence and history of load cycles. In order to perform an analysis for a given design, the complex pile-soil interaction is reduced at each depth to a simple P-y curve.
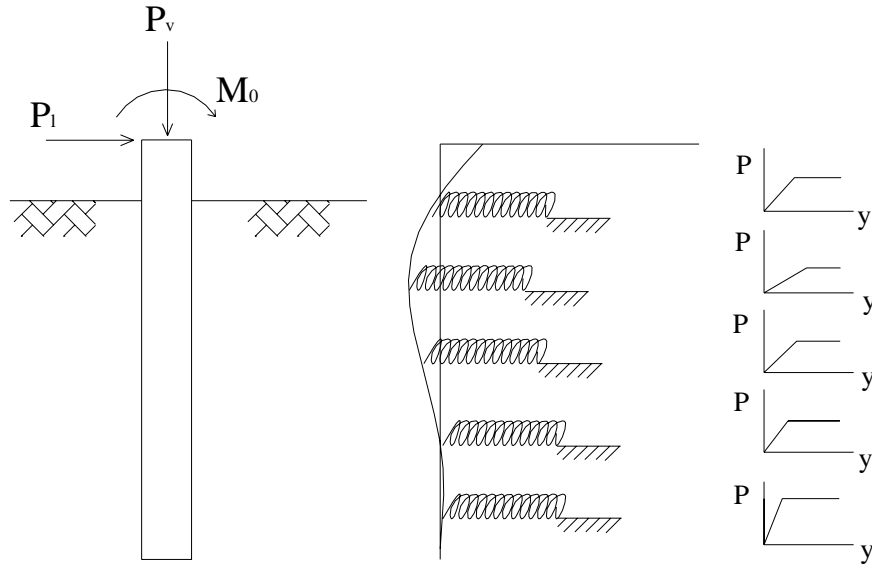
Figure 4. Model of a Laterally Loaded Pile (Reese, 1997)

2.2.1 P-y Curve from Measured Strain Data

P-y curves from measured data can be evaluated using principles of statics. Two sets of equations are used to establish the governing differential equation based on geometry and structural element: the constitutive equation for the pile and the equilibrium equations for the pile element, as shown in Figure 5. The constitutive equation for the pile is defined as:

$$M = EI\phi = EI\frac{d^2y}{dz^2} \tag{5}$$

Where, M = bending moment at depth, z;

      E = modulus of elasticity of the pile;

      I = moment of inertia of the pile around the centroidal axis of the pile

         section;

      ϕ = pile curvature;

      y = pile lateral displacement; and,

      z = depth.
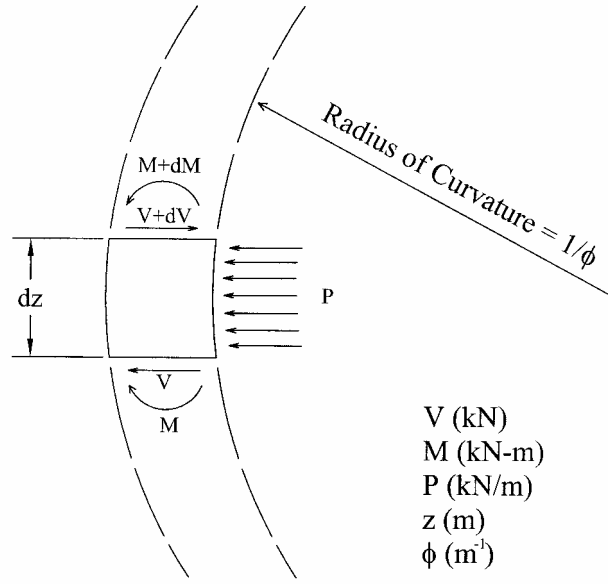
Figure 5. Equilibrium of an Element of Pile

Note that the moment of inertia is taken around the centroidal axis of the pile cross section. In the case of concrete piles which may crack, the pile cross section is reduced to account for cracking. In this case it is necessary to first find the neutral axis of the section, under moments and axial loads, in order to evaluate the part of section that remains uncracked. Then the centroidal axis of the uncracked section is found and the a new moment of inertia is calculated around that axis. The horizontal force equilibrium equation for an element of pile is given as (Figure 5):

$$dV = P \, dz \tag{6}$$

The moment equilibrium equation for the pile element is given as:

$$dM = V \, dz \tag{7}$$

Equations 5, 6, and 7 are combined and lead to the commonly used governing differential equation (Reese and Welch, 1975):

$$\mathbf{EI} \frac{\mathbf{d^4 y}}{\mathbf{dz^4}} + \mathbf{V} \frac{\mathbf{d^2 y}}{\mathbf{dz^2}} - \mathbf{P} = \mathbf{0} \tag{8}$$

For pile load tests commonly performed in the field, the major data measured are strains. Stresses acting normal to the cross section of the pile are determined from the normal strain, ε_x, which is defined as follows:

$$\varepsilon_x = -\frac{y}{\rho} = -\kappa y \tag{9}$$

Where, y = distance to the neutral axis;

ρ = radius of curvature; and,

ϕ = curvature of the beam.

Assuming the pile material to be linearly elastic within a given loading range, Hooke's Law for uniaxial stress ($\sigma = E\varepsilon$) can be substituted in to equation 9 to obtain equation 10.

$$\sigma_x = E\varepsilon_x = -\frac{Ey}{\rho} = -E\kappa y \tag{10}$$

Where, σ_x = stress along the x axis; and,

E = Young's Modulus of the material.

This equation indicates the normal stresses acting along the cross section vary linearly with the distance (y) from the neutral axis. For a circular cross section, the neutral axis is located along the centerline of the pile. Given that the moment resultant of the normal stresses is acting over the entire cross section, this resultant can be estimated as follows:

$$\mathbf{M_o} = -\int \boldsymbol{\sigma_x} \, \mathbf{y} \, \mathbf{dA} \tag{11}$$

Noting that $-M_o$ is equal to the bending moment, M, and substituting for σ_x from equation 11, the bending moment can be expressed by equation 12 as:

$$M = -\kappa EI \tag{12}$$

Where, $I = \int y^2 dA$.

This equation can be rearranged as follows:

$$\kappa = \frac{1}{\rho} = \frac{M}{EI} \tag{13}$$

This equation is known as the moment-curvature equation and demonstrates that the curvature is directly proportional to the bending moment and inversely proportional to EI, where EI is the flexural stiffness of the pile.

During a load test, collected strain-evaluated moment data are used to curve fit the function plotted with depth from the point of load application. Through integration and differentiation, these data can provide soil reaction values with depth. For example, a fourth order regression line is selected to curve fit the data shown in Figure 6 and corresponding variable are obtained as follows:

$$y = a + bx + cx^2 + dx^3 + ex^4 \tag{14}$$

Where: a, b, c, d, e = the coefficients of the regression line; and,

x = pile segment length (m).
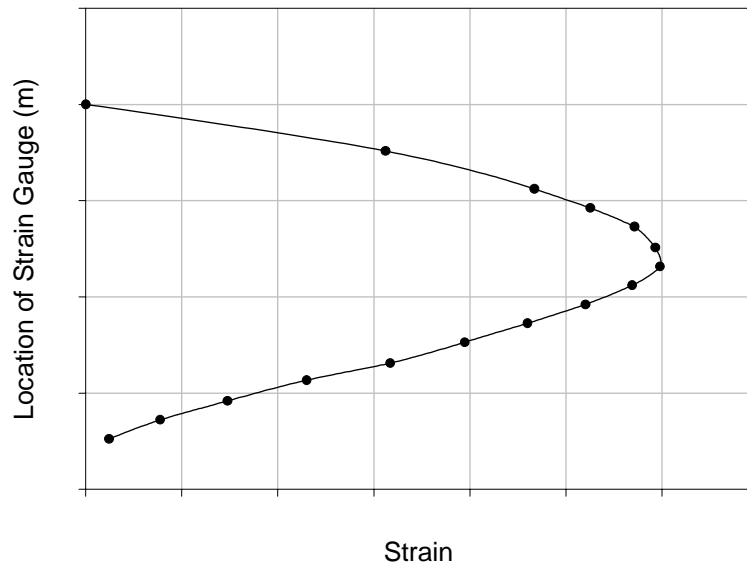
Figure 6. Typical Measured Strain from Testing

Once this equation is obtained, it is differentiated, with respect to depth, three times to estimate the resistance of soil P (kN/m). This equation can be integrated twice to obtain y (m). Alternatively, the lateral deflection can be directly monitored during testing using inclinometer system. These values are then used to create P-y curves with depth .

2.3 P-y Curves in Weathered Rock

Residual profiles, such as those found in the piedmont area of the eastern United States exhibit a transition zone between sound rock and unconsolidated sediments. Over geologic times, parent rocks are weathered into residual soils, which retain much of the fabric and many of the structural features of the original rock. The degree of weathering decreases with depth, usually with no well-defined boundary between soil and rock. Although the weathering materials have the texture of soils, they retain enough of the fractures of rock that their behavior under load is often better modeled using methods of rock mechanics, rather than soil mechanics (Sowers, 1983). The zone between soil and rock is the focus of this research since many drilled shafts built in Piedmont weathered rock are placed in, or transgress, this transition zone.

Quantitative definitions of the soil-rock interface have been addressed in the literature. Deere and Patton (1971) have illustrated idealized residual profile for metamorphic rock as shown in Figure 7 (a), and intrusive igneous rocks as shown in Figure 7 (b).
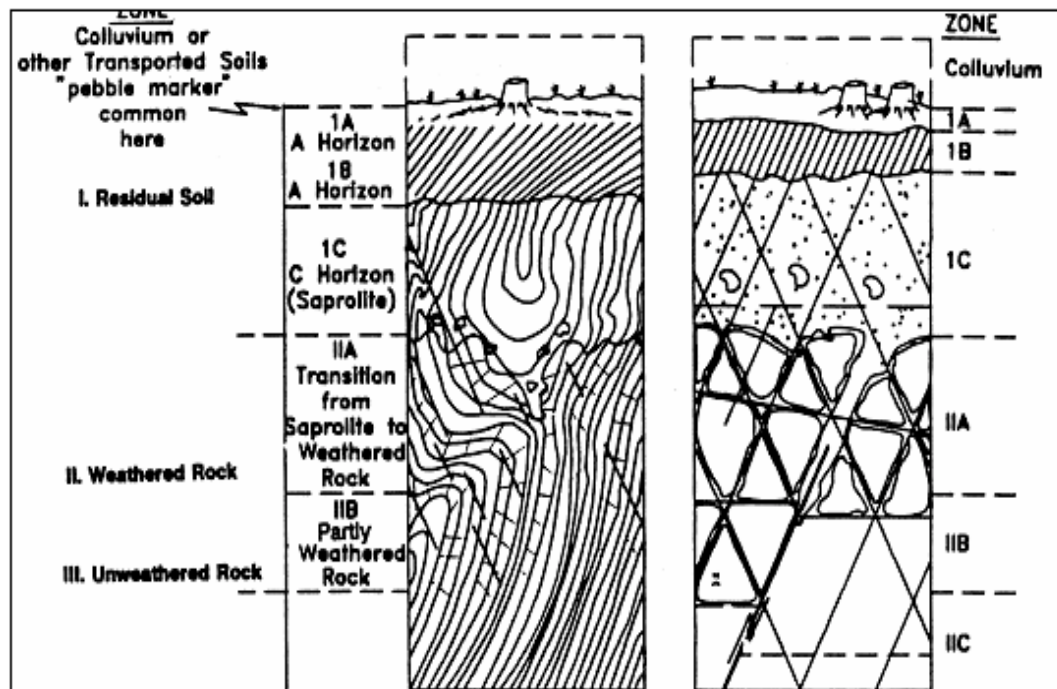
(a) Metamorphic Rock   (b) Igneous Rock

Figure 7. Transition between Residual Soil and Unweathered Rock
(from Deer and Patton, 1971)

16

Coates (1970) recommended that the Rock Quality Designation (RQD) values be used to estimate depth to sound rock. RQD values smaller than 25% designated very poor rock quality that could be classified as soil for engineering purposes. Peck (1976) stated that the distinction between rock-like and soil-like material in transition zones is usually unpredictable.

2.3.1 P-y Curves for Weak Rock

Reese (1997), based on two load tests, proposed the only method currently reported in the literature to construct P-y curves for "weak" rock. The ultimate resistance P_{ur} for weak rock was calculated as follows based on limit equilibrium as a function of depth below ground surface:

$$P_{ur} = \alpha_r q_{ur} b(1+1.4x_r/b), \ for \ 0 \leq x_r \leq 3b \tag{15}$$

$$P_{ur} = 5.2\alpha_r q_{ur} b, \ for \ x_r > 3b \tag{16}$$

Where, q_{ur} = compressive strength of rock, (usually lower-bound as function of depth);

α_r = strength reduction factor;

b = width, or diameter of pile; and,

x_r = depth below rock surface.

If a pile were considered to be a beam resting on an elastic, homogeneous, and isotropic media, the initial modulus K_{ir} (p_i divided by y_i) may be shown to have the following value (Reese, 1997):

$$K_{ir} = k_{ir} E_{ir} \tag{17}$$

Where, E_{ir} = initial modulus of rock; and,

k_{ir} = dimensionless constant.

Reese (1997) suggested equation 18 and 19 for k_{ir}, which were empirically derived from experiments and reflected the assumption that the presence of the rock surface will have a similar effect in k_{ir}, as was shown for p_{ur}.

$$k_{ir} = (100 + 400x_r/3b), \ for \ 0 \leq x_r \leq 3b \tag{18}$$

$$k_{ir} = 500, \ for \ x_r \geq 3b \tag{19}$$

Equations 18 and 19 yield the initial portions of the P-y curves and normally provide very stiff response in order to model the relatively low deflections observed during initial loading.

With guidelines for computing p_{ur} and K_{ir}, equations for the three-parts of P-y curve are illustrated in Figure 8.
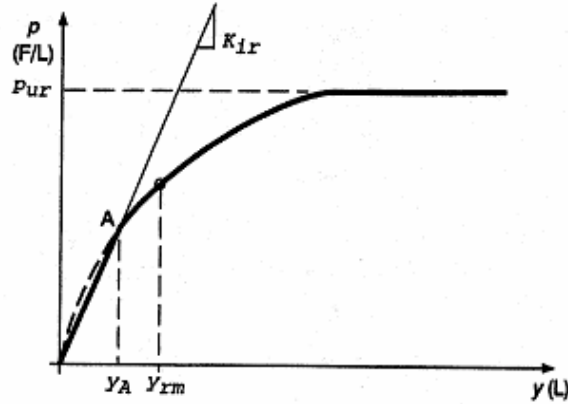
Figure 8. Sketch of P-y Curve for Rock (from Reese, 1997)

Equation 20 defines the straight-line, initial portion of the curves, while the second and third segments are defined by equations 21 and 22. respectively, Reese (1997):

$$P = K_{ir}y, \text{ for } y \leq y_A \tag{20}$$

$$P = \frac{P_{ur}}{2} (\frac{y}{y_{rm}})^{0.25}, \text{ for } y \geq y_A \text{ and } p \leq p_{ur} \tag{21}$$

$$y_{rm} = k_{rm} b \tag{22}$$

Where, k_{rm} = constant, ranging from 0.0005 to 0.00005 and serves to establish
overall stiffness of curves.

The value of y_A is found by solving for the intersection of equations 20 and 21, and is shown by equation 23:

$$y_A = [\frac{P_{ur}}{2(y_{rm})^{0.25} K_{ir}}]^{1.333} \tag{23}$$

Reese (1997) comments on these equations were as follows: "First, the equations have no influence on solutions beyond the value y_A (Figure 8) and probably will have no influence on the designs based on the ultimate bending moment of a pile. Second, available theory, while incomplete, shows much lower values of K_{ir} in relation to the modulus of rock or soil. Third, the increase in K_{ir} with depth in equation 17 is consistent with results obtained from the lateral loading of piles in overconsolidated clays."

Using equations 20-23, typical P-y curves for Sandstone, Mudstone, and Granite are constructed and presented in Figure 9. The representative material properties needed for calculations are based on data summarized in Table 1 (Coon and Merrit, 1970). The moduli of elasticity for these rock types are decreased by factor of 10 to consider weathering effects. The diameter of shaft is assumed to 0.762 meter and the depth of interest is assumed to be greater than 3b (2.3 meters).

Table 1. Material Properties of Rocks

Item	Mudstone	Sandstone	Granite
Elastic Modulus (kN/m^2)	7.0×10^7	2.0×10^7	4.0×10^7
E_r (Factor of 10)	7.0×10^6	2.0×10^6	4.0×10^6
Compressive Strength (q_{ur}) (kN/m^2)	10,000	70,000	150,000
P_{ur} (kN/m)	3962.4	27736.8	59436.0
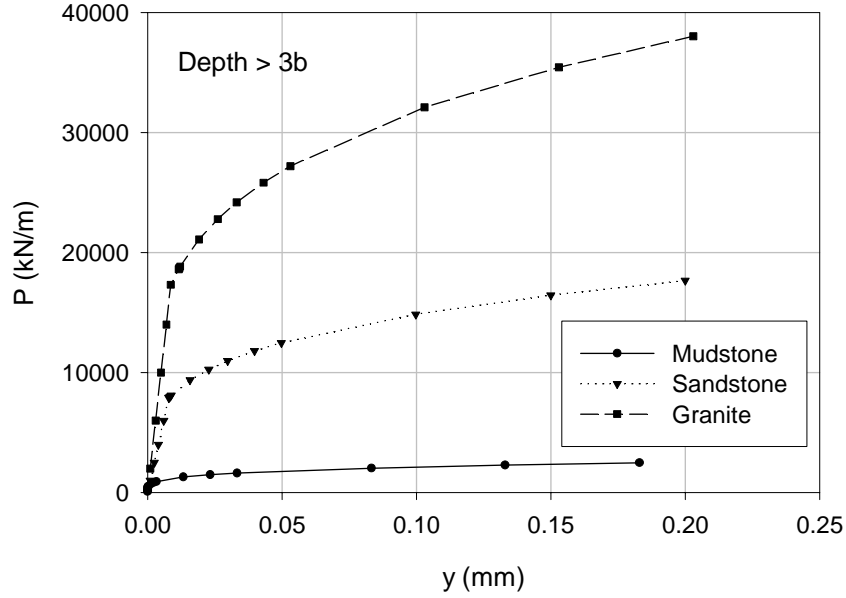
Figure 9. Typical P-y Curves Estimated from Reese's Method

The P-y curves illustrated in Figure 9 show that the value of K_{ir} is inconsequential, given its influence at small y. The ultimate resistances for the three curves are reached a relatively small deflection, in the range of 0.2 mm. It seems for the data illustrated in Figure 9 that the magnitude of P-y curve is largely dependent on the strength of the rock. However, in weathered profiles, one can expect that the strength may depend on the frequency and condition of joints.

2.3.2 P-y Curve Prediction using Stiff Clay Model

Anther possible approach for construction of P-y curves in weathered rock could be synthesized from that presented by Reese, Cox, and Koop (1975) to model P-y curves in stiff clay above the groundwater. The shape of the P-y curve for stiff clay was generated by Reese et al. (1975) using following equation,

$$\frac{P}{P_{ur}} = (\frac{y}{16y_{50}})^{\frac{1}{4}} \tag{24}$$

Comparisons of measured and predicted behavior of piers embedded in rock were performed using equation 24 by Gabr (1993). A stiffer response of P-y curve was simulated by assuming $y_{50} = \varepsilon_{50} B$ to parametrically study the effect of P-y magnitude on

the predicted behavior. Predictions were performed using the computer program LTBASE by Gabr and Borden (1988).

Using $y_{50} = \varepsilon_{50}$ B, compared to $y_{50} = 2.5\varepsilon_{50}$ B, produced a stiffer P-y response with shorter initial slope. Consequently, by using $y_{50} = \varepsilon_{50}$ B, the non-linearity effect is more represented at the early stage of loading as shown in Figure 10. Results showed the ability to predict the test piers lateral response using P-y model in comparison to the use of elastic theory.

2.4 Laterally-Loaded, Rock-Socketed, Shafts

Zhang (1999) proposed a method to predict the resistance of laterally loaded rock-socketed shafts. Figure 11 shows a typical drilled shaft of length L, radius R, and flexural stiffness E_pI_p, embedded within a soil and rock profile. The deformation modulus of the soil was assumed to increase linearly from E_{s1} at the ground surface to E_{s2} at the soil and rock mass interface. The elastic modulus of the rock mass varies linearly from E_{m1} at the soil and rock mass interface to E_{m2} at the shaft tip.
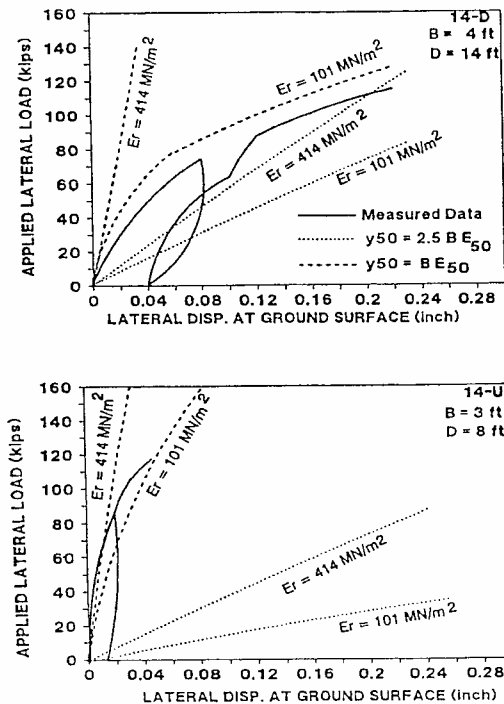
Figure 10. Predicted versus Measured Response (Stiff Clay Model, from Gabr, 1993)

21

Zhang et al. proposed a simple method that considered local yielding of the soil and rock mass and assumed the soil and rock mass to be elastic-perfectly plastic. A summary of this approach was described as follows (Zhang and Einstein, 2000):

1. Assuming the soil and rock mass are elastic, lateral reaction force (P) is determined after applying lateral load H and moment M.

2. Compare the computed lateral load reaction force (P) with the ultimate resistance P_{ult}, and, if $P > P_{ult}$, determine the yield depth z_y in the soil and/or rock mass.

3. Consider the portion of the shaft in the unyielded ground (soil and/or rock mass) ($z_y \leq z \leq L$) as a new shaft, and analyze it by ignoring the effect of the soil and/or rock mass above the level $z = z_y$.

4. Repeat Steps (2) and (3). The iteration is continued until no further yielding of the soil or rock mass occurs.

Figure 11. (a) Shaft and Soil/Rock Mass System; (b) Coordinate System and Displacement Components; (c) Shear Force V(z) and Moment M(z) Acting on Shaft at depth, z (from Zhang and Einstein, 2000)
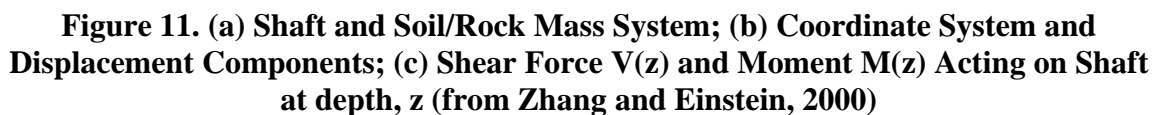
2.4.1 Determination of Ultimate Resistance (P_{ult}) of Rock Mass

As shown in Figure 12, the total reaction of the rock mass consists of two parts: the side shear resistance and the front normal resistance. Thus the ultimate resistance P_{ult} can be estimated as follows (Briaud and Smith, 1983; Carter and Kulhawy, 1992):

$$p_{ult} = (p_L + \tau_{max})B \qquad (25)$$

Where, B = diameter of the shaft;

τ_{max} = maximum shearing resistance along the sides of the shaft; and,

p_L = normal limit resistance.
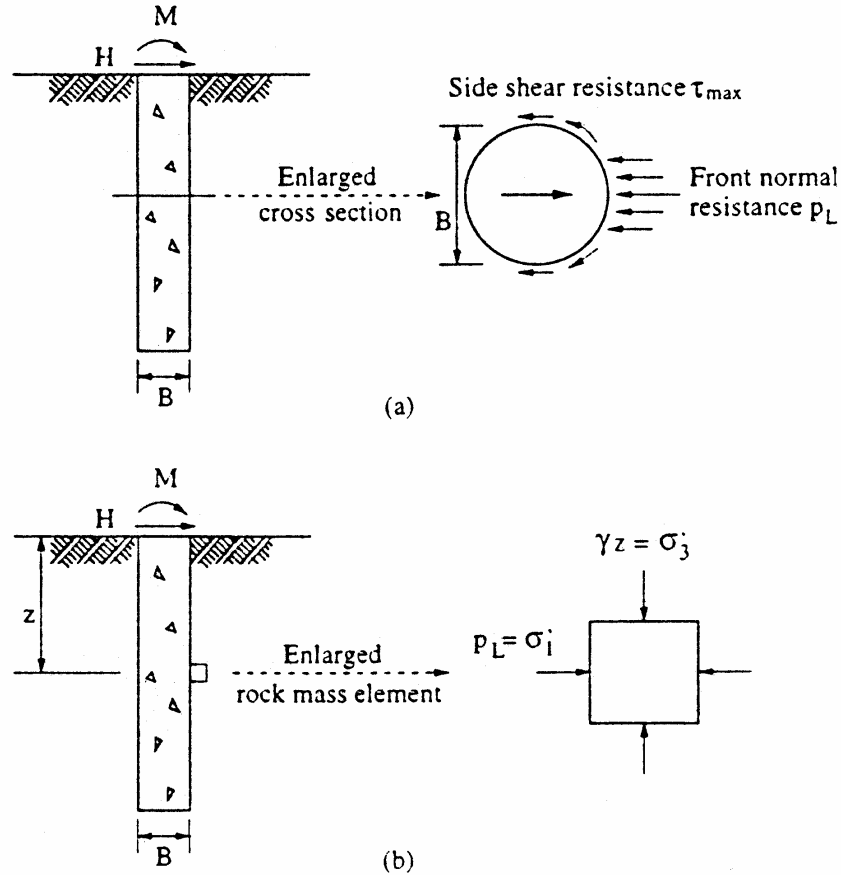
Figure 12. (a) Components of Rock Mass Resistance, (b) Calculation of Normal Limit Stress P_L (from Zhang and Einstein, 2000)

For simplicity, τ_{max} was assumed to be the same as the maximum side resistance under axial loading and was given as follows (Zhang, 1999)

23

Smooth socket:

$$\tau_{max} = 0.20 \, (\sigma_c)^{0.5} \quad \text{(MPa)} \tag{26}$$

Rough socket:

$$\tau_{max} = 0.80 \, (\sigma_c)^{0.5} \quad \text{(MPa)} \tag{27}$$

Where, σ_c = unconfined compressive strength of the intact rock (MPa).

To determine the normal limit stress P_L, the strength criterion for rock masses developed by Hoek and Brown (1980, 1988) was used. For intact rock, the Hoek-Brown criterion was expressed in the following form:

$$\sigma_1' = \sigma_3' + \sigma_c \left(m_i \frac{\sigma_3'}{\sigma_c} + 1 \right)^{0.5} \tag{28}$$

Where, σ_c = uniaxial compressive strength of the intact rock material;

σ_1' and σ_3' = major and minor effective principal stresses, respectively;

m_i = material constant for the intact rock.

For jointed rock masses, the Hoek-Brown criterion was given by:

$$\sigma_1' = \sigma_3' + \sigma_c \left(m_b \frac{\sigma_3'}{\sigma_c} + s \right)^{a} \tag{29}$$

Where, m_b = value of the constant m for the rock mass; and,

s and a = constants that depend on the characteristics of the rock mass.

Assuming that the minor principal effective stress, σ_3', was the effective overburden pressure, $\gamma'z$, and the limit normal stress, P_L, was the major principal effective stress, σ_1', [Figure 12 (b)], the following expression for p_L is developed from equation 29 (Hoek and Brown, 1988):

$$p_L = \sigma_1' = \gamma'z + \sigma_c \left(m_b \frac{\sigma_3'}{\sigma_c} + s \right)^{a} \tag{30}$$

Where, γ' = effective unit weight of the rock mass; and,

24

z = depth from the rock mass surface.

2.5 Strength of Jointed Rock Mass

The strength of a jointed rock mass depends on the properties of the intact rock pieces and also on the movements of these pieces under different stress conditions, such as sliding and rotation. This characteristic is controlled by the geometric shape of the intact rock pieces and the interface condition of the surface between pieces. The Geotechnical Strength Index (GSI) introduced by Hoek (1994) provides a method to estimate criteria which are used to calculate rock strength characteristics, as described in Figure 13.
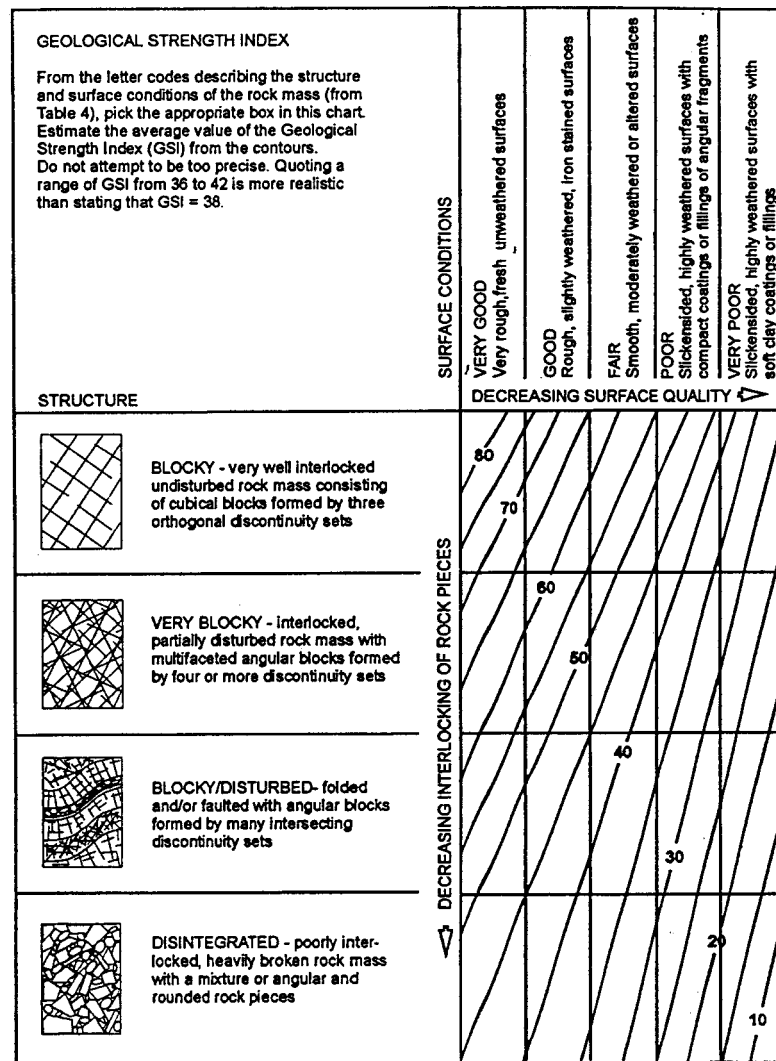
Figure 13. Geotechnical Strength Index (Hoek and Brown, 1997)

According to Figure 13, angular rock pieces with clean and rough surface discontinuities will have greater shearing resistance than a weathered rock mass which contains rounded pieces surrounded by soil. After the GSI has been determined, the parameters which described the rock mass strength characteristics can be calculated based on Hoek et al. (1995) and Hoek and Brown (1997), who proposed the set of relationships shown in Table 2.

Table 2. Relationships between m_b, S, a, and GSI (from Hoek et al., (1995))

Parameter	Quality of Rock Mass (GSI)	
	Good to reasonable (> 25)	Good to poor (< 25)
m_b	$\exp(\dfrac{GSI-100}{28})m_i$	$\exp(\dfrac{GSI-100}{28})m_i$
S	$\exp(\dfrac{GSI-100}{9})$	0
A	0.5	$0.65 - \dfrac{GSI}{200}$

Table 3 shows values for the parameter m_i, which is essentially a function of rock type (texture and mineralogy) and can be selected according to Hoek and Brown (1988).

The GSI method to define rock mass quality is somewhat imprecise for better quality rock with GSI > 25. In order to estimate a more precise GSI value for better quality rock masses, with GSI > 25, it is recommended to use Rock Mass Rating (RMR, Bieniawski, 1976) method with the ground water rating set to 10 (dry) and the adjustment for Joint Orientation set to 0, as shown in Table 4 (Hoek and Brown, 1997). However, for very poor quality rock masses (GSI < 25), the value of RMR is very difficult to estimate and the balance between the different rating systems no longer gives a reliable basis for estimating rock mass strength (Hoek and Brown, 1997). Therefore, it would be better to estimate the GSI value from Figure 13.

Table 3. Value of mi Parameter (Hoek and Brown, 1988)

Rock type	Class	Group	Texture			
			Coarse	Medium	Fine	Very fine
SEDIMENTARY	Clastic		Conglomerate (22)	Sandstone 19	Siltstone 9	Claystone 4
				—Greywacke— (18)		
	Non-Clastic	Organic		—Chalk— 7		
				—Coal— (8–21)		
		Carbonate	Breccia (20)	Sparitic Limestone (10)	Micritic Limestone 8	
		Chemical		Gypstone 16	Anhydrite 13	
METAMORPHIC	Non-foliated		Marble 9	Hornfels (19)	Quartzite 24	
	Slightly foliated		Migmatite (30)	Amphibolite 25–31	Mylonites (6)	
	Foliated*		Gneiss 33	Schists 4–8	Phyllites (10)	Slate 9
IGNEOUS	Light		Granite 33		Rhyolite (16)	Obsidian (19)
			Granodiorite (30)		Dacite (17)	
			Diorite (28)		Andesite 19	
	Dark		Gabbro 27	Dolerite (19)	Basalt (17)	
			Norite 22			
	Extrusive pyroclastic type		Agglomerate (20)	Breccia (18)	Tuff (15)	

*These values are for intact rock specimens tested normal to bedding or foliation. The value of m_i will be significantly different if failure occurs along a weakness plane.

2.6 Database for North Carolina Rock Properties

A database for engineering characteristics of weathered rock in the Durham Triassic Basin (DTB) in North Carolina State was presented by Parish (2001).

2.6.1 Site Locations

Twelve locations within the DTB were used to test the engineering properties of the rock found in the region. Figure 14 shows an area highway map with the locations of each site identified. Rock cores were retrieved from in-situ materials at all but one location.

2.6.2 Sample Collection

The collection of samples from DTB area was performed using HX, NX, and BX size coring. The majority of material recovered was drilled using a 54 mm diameter core or NX barrel. Larger diameter cores were also used to enable in-situ rock dilatometer

Table 4. Rock Mass Rating (RMR) Method (Bieniawski, 1976)

	Parameter		Range of Values						
1	Strength of Intact Rock Material	Point Load Strength Index	< 8 MPa	> 8 MPa	4-8 MPa	1-2 MPa	For this low range uniaxial compressive test is preferred		
		Uniaxial Compression Strength	< 200 MPa	> 200 MPa	50-100 MPa	25-50 MPa	10-25 MPa	3-10 MPa	1-3 MPa
	Rating		15	12	7	4	2	1	0
2	R.Q.D.		90-100 %	75-90 %	50-75 %	25-50 %	<25 %		
	Rating		20	17	13	8	3		
3	Spacing of Joints		>3 m	1-3 m	0.3-1 m	50-300 mm	<50 mm		
	Rating		30	25	20	10	5		
4	Condition of Joints		Very rough surfaces, Not continuous, No Separation, Hard joint wall rock	Slightly rough surfaces Separation < 1 mm Hard joint wall rock	Slightly rough surfaces Separation < 1 mm Soft joint wall rock	Slickensided surfaces Gouge < 5 mm thick or Joint open 1-5 mm Continuous joints	Soft gouge > 5 mm thick or Joint open > 5 mm Continuous joints		
	Rating		25	20	12	6	0		
5	Ground Water	Inflow per 10 m tunnel length	None or	< 25 liter/min or	25-125 liters/min or	25 liters/min or			
		Ratio ($\frac{\text{Joint water pressure}}{\text{Major principal stress}}$)	0 or	0.0-0.2 or	0.2-0.5 or	> 0.5 or			
		General Conditions	Completely dry	Moist only (Interstitial water)	Water under mod. pressure	s			
	Rating		10	7	4	0			

testing. Cores were taken at varying depths from 1.0 m to 15.5 m. Material from each run was geologically classified by type, rock quality designation (RQD), and percent recovery (REC). Samples were retrieved from the twelve different locations within the DTB identified by NCDOT personnel. Locations where weak materials had previously been discovered during construction projects were selected for the study. Different rock types were obtained at varying depths from each site. Thus, within one location, layered

rock structures occasionally provided alternate types of rock. When the material properties differed, specimens from each sample depth were catalogued separately and tested as an independent set of specimens.
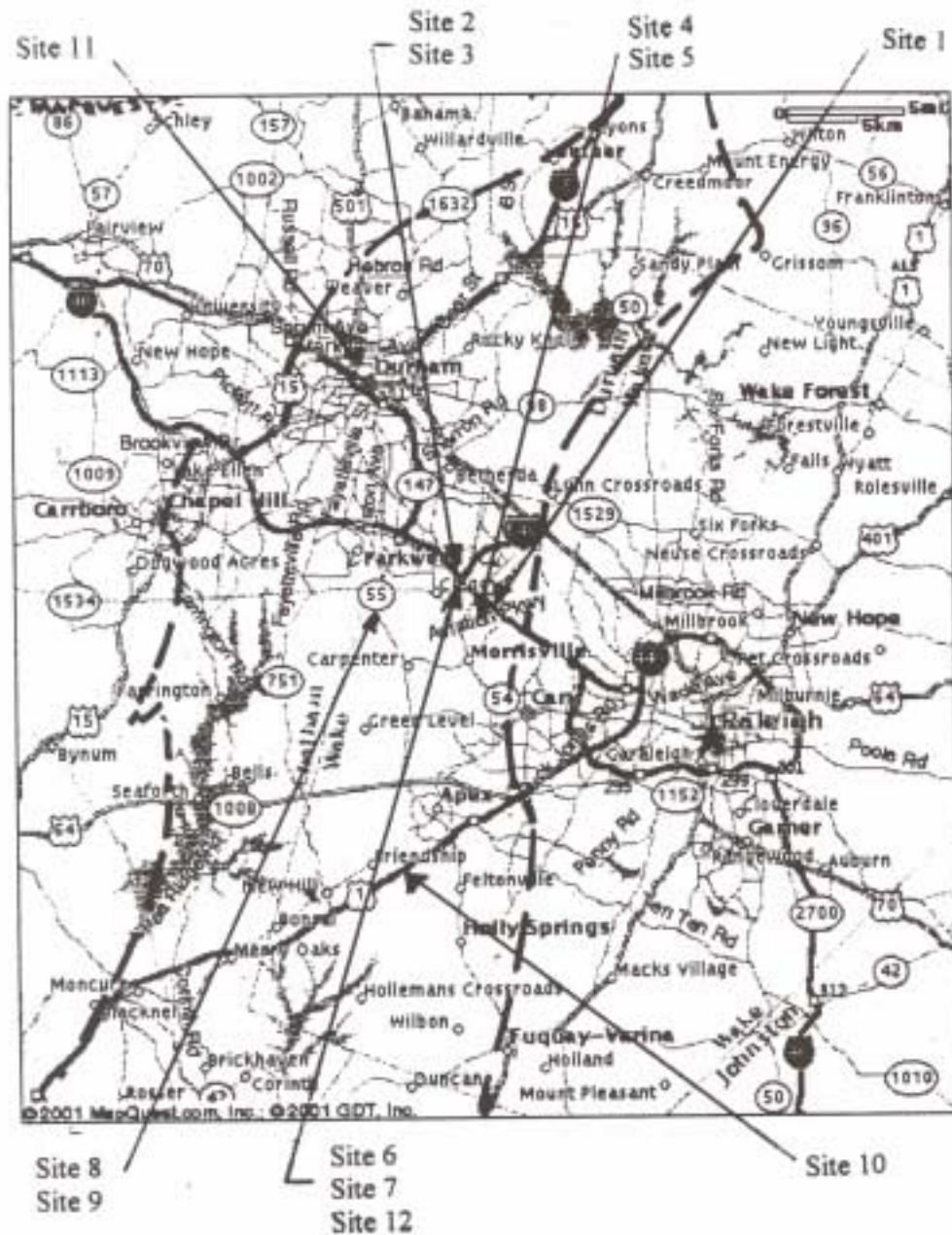
Figure 14. Test Site Locations within the Durham Triassic Basin (Parish, 2001)

2.6.3 Sample Identification

For identification purposes, samples taken from core runs at different locations within the basin were labeled with a site designation (i.e. Site 1 represented the samples taken from borings at I-85 and Gregson Street). In addition, depth and type of rock were also identified. The depth identifier represented the beginning depth at which the specimen was taken. For rock type, the s*and*stones were labeled as "a" and s*i*ltstones as "i". Thus a sample identified as "1-3.5i" represents a siltstone sample from Site 1 taken at a depth of 3.5 meter. The site details and sample identifications for materials collected for this study are listed in Table 5. In general, three specimens for unconfined compressive strength (q_u) testing were obtained for each sample.

2.6.4 Unconfined Compressive Strength

Testing was performed according to ASTM D2938-86, Test Method for Unconfined Compressive Strength of Intact Rock Core Specimens. Table 6 is a list of the means and standard deviations of q_u for all of the groups of specimens tested in this study. In general, these means and standard deviations were calculated from the results of tests on three specimens, as shown in Table 6. In case where less than three specimens were tested, a subscript is used for identification. In certain instances, for example specimen 7-4.4i, no standard deviation is listed since only one specimen was tested in that sample lot. The list also provides depth and sample identifier.

2.7 Rock Dilatometer

One of the most challenging aspects related to the determination of the required embedment length of drilled shafts in weathered rock is estimating the modulus of lateral subgrade reaction. A literature review yielded no documented research that was performed specifically for characterizing the lateral subgrade modulus of weathered rocks. In-situ investigation techniques are specially needed in this case since the profile materials are transitional between soils that can be excavated easily, and massive hard rock without weakened discontinuities. Since rock in this transition zone is decomposed, it is challenging to retrieve representative samples. Even when samples are retrieved, conventional tests, performed on cores, do not provide representative stiffness and strength characteristics. A relationship between in-situ rock mass modulus and

laboratory intact modulus values has been presented in the literature by Coon and Merrit (1970) for higher RQD rocks (typically RQD > 70%). No such relationship exists for the highly weathered and lower RQD rocks. Unfortunately, the weathering conditions and the inability to retrieve representative samples from the field necessitate the performance of in-situ testing if high-quality modulus values are needed.

Table 5. Site and Sample Identification (Parish, 2001)

Site No.	NCDOT Project No.	Location	Station	Depth (m)	Sample Identification	Rock Type
1	8.1640501 B-2634	Aviation Parkway Bridge over Nelson Wake Co.	Sta 14+26.3 10 RT	2.5-3.0 3.0-3.5 3.5-4.0 4.0-4.4 4.4-4.9	1-2.5a 1-3.0a 1-3.5i 1-4.0a 1-4.4i	Sandstone Sandstone Siltstone Sandstone Siltstone
2	6.408002 R2000BB	Bridge Site on I540 Wake Co.	Sta 113+63 180 RT	8.3-9.7 9.7-10.7	2-8.3i 2-9.7i	Siltstone Siltstone
3	6.408002 R2000BB	Bridge Site on I540 Wake Co.	Sta 395+00 25 RT	4.7-6.2	3-4.7i	Siltstone
4	6.408004T R2000BA	New Page Rd B-2 Bridge Wake Co.	Sta 205+05 Center	1.0-2.0 2.1-3.7	4-1.0a 4-2.1a	Sandstone Sandstone
5	6.408004T R2000BA	New Page Rd B-8 Bridge Wake Co.	Sta 203+34 77 RT	8.1-10.2 10.0-12.1 12.2-14.0	5-8.1i 5-10.0i 5-12.2i	Siltstone Siltstone Siltstone
6	8.U401706 R2000BA Site 2	I40 & I540 Interchange Wake Co.	Sta 297+50 76 LT	1.9-3.1 3.7-5.2 5.2-6.7 6.7-8.1 8.4-9.9 10.0-10.9	6-1.9i 6-3.7i 6-5.2i 6-6.7i 6-8.4i 6-10.0i	Siltstone Siltstone Siltstone Siltstone Siltstone Siltstone
7	8.U401706 R2000BA Site 3	I40 & I540 Interchange Wake Co.	Sta 232+80	4.4-5.3 5.3-6.9 6.1-6.7 6.7-7.7 6.9-8.2 8.2-9.8 8.8-9.8 9.9-11.4	7-4.4i 7-5.3i 7-6.1i 7-6.7a 7-6.9a 7-8.2i 7-8.8i 7-9.9a	Siltstone Siltstone Siltstone Sandstone Sandstone Siltstone Siltstone Sandstone

Table 5. Site and Sample Identification ((Parish, 2001, Continued)

Site No.	NCDOT Project No.	Location	Station	Depth (m)	Sample Identification	Rock Type
8	8.U401711 R2000AA	Proposed Outer Loop by Davis Drive Wake Co.	Sta 40 +22 31 RT	3.6-4.5	8-3.6i	Siltstone
				4.5-6.1	8-4.5i	Siltstone
				5.7-7.6	8-5.7a	Sandstone
				9.7-10.4	8-9.7a	Sandstone
				10.6-11.7	8-10.6a	Sandstone
9	8.U401711 R2000AB	Proposed Outer Loop by Davis Drive Wake Co.	Sta 47+60 40 RT	1.8-2.8	9-1.8i	Siltstone
				2.8-4.3	9-2.8i	Siltstone
				2.9-4.3	9-2.9i	Siltstone
				4.3-5.8	9-4.3i	Siltstone
				5.8-7.3	9-5.8i	Siltstone
				8.8-10.4	9-8.8a	Sandstone
				8.9-10.4	9-8.9i	Siltstone
				10.4-11.4	9-10.4i	Siltstone
10	6.409006T R2500B	Us Highway 1 Wake Co.	M.P. 91 Near Apex	6.2-8.0	10-6.2a	Sandstone
				6.5-7.7	10-6.5i	Siltstone
				7.9-8.5	10-7.9i	Siltstone
				8.0-9.3	10-8.0i	Siltstone
11	8.1414801	I85 & Greggson Durham Co.	Sta 4+563.47 47.83 RT	1.5-2.0	11-1.5a	Sandstone
				3.0-3.9	11-3.0a	Sandstone
				3.6-4.7	11-3.6a	Sandstone
				4.3-5.4	11-4.3a	Sandstone
				4.7-5.5	11-4.7i	Siltstone
				5.4-6.2	11-5.4a	Sandstone
				5.5-6.1	11-5.5a	Sandstone
12*	8.U401706 R2000BA Drilled Shaft	I40 & I540 Interchange Wake Co.	Sta 232+80 55 RT	2.9-3.6	12-2.9i	Siltstone
				9.9-10.4	12-9.9i	Siltstone
				13.4-14.0	12-13.4a	Sandstone
				14.0-15.5	12-14.0a	Sandstone

*Note: Sample depths for Site 12 are below grade in compacted embankment.

Table 6. Unconfined Compressive Strength Database in DTB (Parish, 2001)

Site No.	Depth (m)	Sample Identification	Mean (MPa)	Std Dev (MPa)
1	2.5-3.0	1-2.5a	50.6	7.3
1	3.0-3.5	1-3.0a	46.5	6.0
1	3.5-4.0	1-3.5i	-	-
1	4.0-4.4	1-4.0a	52.4	9.7
1	4.4-4.9	1-4.4i	-	-
2	8.3-9.7	2-8.3i	50.9	3.9
2	9.7-10.7	2-9.7i	63.8	6.3
3	4.7-6.2	3-4.7i	18.7	1.2
4	1.0-2.0	4-1.0a	59.9	2.5
4	2.1-3.7	4-2.1a	41.5	4.0
5	8.1-10.2	5-10.0i	-	-
5	10.0-12.1	5-10.0i	65.4	10.8
5	12.2-14.0	5-12.2i	32.8	2.0
6	1.9-3.1	6-3.7i	-	-
6	3.7-5.2	6-3.7i	13.1	2.0
6	5.2-6.7	6-5.2i	10.2	3.2
6	6.7-8.1	6-6.7i	10.7	1.6
6	8.4-9.9	6-8.4i	10.2^2	0.6
6	10.0-10.9	6-10.0i	20.5	3.0

Site No.	Depth (m)	Sample Identification	Mean (MPa)	Std Dev (MPa)
7	4.4-5.3	7-4.4i	9.8^1	-
7	5.3-6.9	7-5.3i	10.1^2	3.1
7	6.1-6.7	7-6.1i	25.1^1	25.1
7	6.7-7.7	7-6.7a	20.6	2.8
7	6.9-8.2	7-6.9a	17.8^1	-
7	8.2-9.8	7-8.2i	10.1	3.1
7	8.8-9.8	7-8.8i	10.4^1	-
7	9.9-11.4	7-9.9a	23.5^2	2.1
8	3.6-4.5	8-3.6i	11.9	6.4
8	4.5-6.1	8-4.5i	15.1	5.1
8	5.7-7.6	8-5.7a	21.2	6.4
8	9.7-10.4	8-9.7a	22.0	8.3
8	10.6-11.7	8-10.6a	33.9	4.9
9	1.8-2.8	9-2.8i	-	-
9	2.8-4.3	9-2.8i	32.1	12.4
9	2.9-4.3	9-2.9i	47.8	5.3
9	4.3-5.8	9-4.3i	46.1	5.0
9	5.8-7.3	9-5.8i	19.2	11.4
9	8.8-10.4	9-8.8a	26.6^1	-
9	8.9-10.4	9-8.9i	30.3	6.6
9	10.4-11.4	9-10.4i	18.1	2.4

Site No.	Depth (m)	Sample Identification	Mean (MPa)	Std Dev (MPa)
10	6.2-8.0	10-6.2a	1.7	0.4
10	6.5-7.7	10-6.5i	17.1	3.2
10	7.9-8.5	10-7.9i	-	-
10	8.0-9.3	10-8.0i	8.6^2	2.7
11	1.5-2.0	11-1.5a	-	-
11	3.0-3.9	11-3.0a	28.7^2	8.0
11	3.6-4.7	11-3.6a	45.5	6.9

Site No.	Depth (m)	Sample Identification	Mean (MPa)	Std Dev (MPa)
11	4.3-5.4	11-4.3a	33.0	13.4
11	4.7-5.5	11-4.7i	28.5^2	18.3
11	5.4-6.2	11-5.4a	35.8	7.5
11	5.5-6.1	11-5.5a	30.8	5.7
12	2.9-3.6	12-2.9i	53.6	14.1
12	9.9-10.4	12-9.9i	63.2	27.4
12	13.4-14.0	12-13.4a	42.3	7.2
12	14.0-15.5	12-14.0a	55.1^2	3.1

Note: supercript 1 = Only one (1) specimen tested
supercript 2 = Only two (2) specimen tested

Two methods of in-situ testing can be used to measure lateral modulus values in rock. The first method is commonly referred to as a plate jacking test. The plate jacking

test requires excavating a trench from grade to the desired test depth. A hydraulic ram and deformation measuring instrument are placed in the trench. The ram is used to provide a measurable force from which deformation is induced and measured. Obviously, performing such a test at a depth greater than perhaps 3 feet is challenging and cost prohibitive due to the magnitude of required shoring and excavation.

The second emerging method is based on using a borehole pressuremeter (referred to as a rock dilatometer model Probex 1). The rock dilatometer (manufactured by ROCTEST, Plattsburgh, NY) is a specialized probe that uses an expandable bladder to apply pressure to the walls of an N-size borehole. Volume change of the probe is measured at the probe level under stress increments. Lateral rock modulus can be derived based on the pressure-volume measurements in a manner similar to that employed for the pressuremeter test. The rock dilatometer can be incorporated into the subsurface investigation performed at a given site to estimate the in-situ lateral modulus as a function of depth. Maximum working pressures that can be applied, according to the manufacturer's literature, is approximately 30,000 kPa.

2.7.1 Calculation of Lateral Modulus

The rock dilatometer exerts a uniform radial pressure on the walls of the drilled hole by means of a flexible rubber sleeve. The expansion of the borehole is measured by the flow of oil, or antifreeze liquid, into the sleeve as the pressure is raised (Goodman et al., 1968). Figure 15 shows the components of the rock dilatometer. The expansion volume of the borehole is measured with a digital read-out box. Figure 16 shows typical pressure/dilation graphs for a calibration of probe carried out in a material of known modulus, and a test carried out in rock.
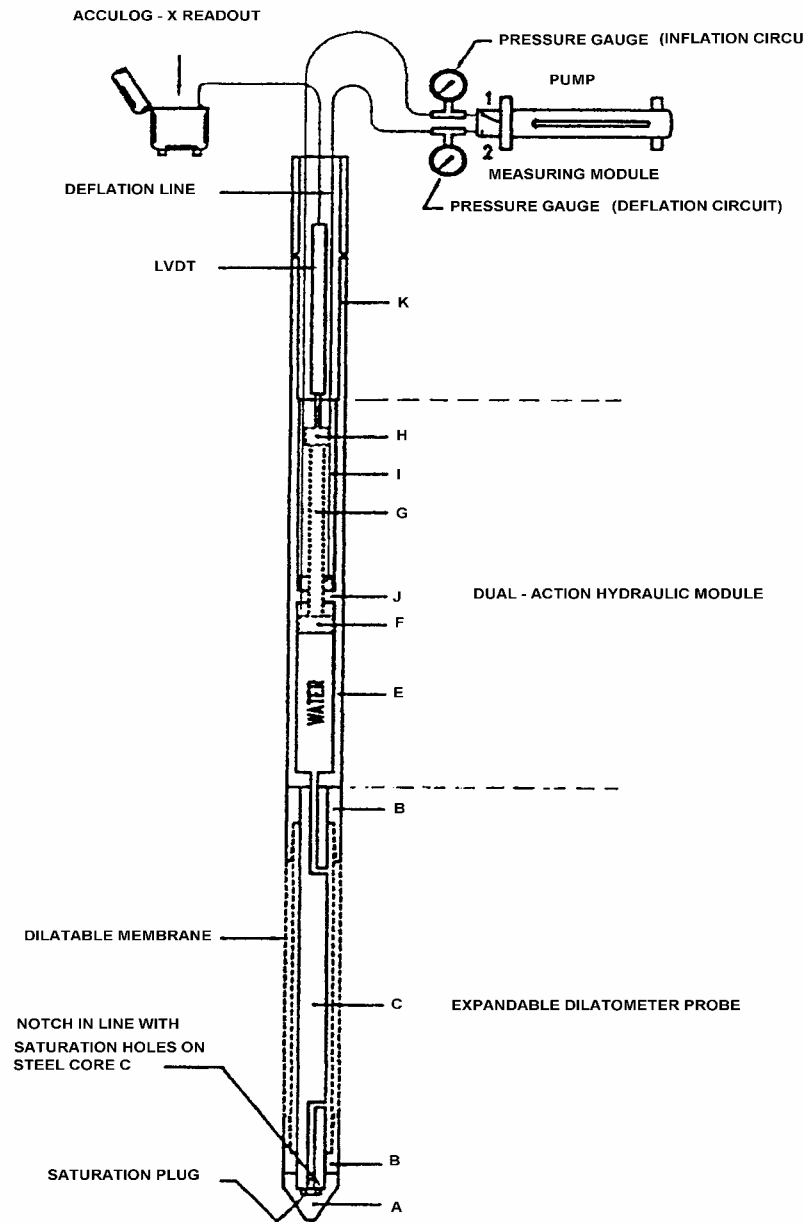
Figure 15. Component of Rock Dilatometer (Rock Dilatometer Manual, 1999)

35
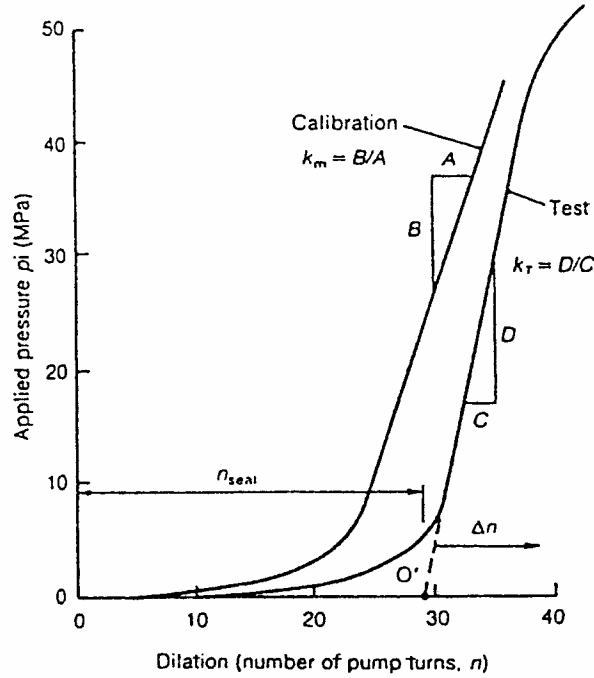
Figure 16. Typical Pressure/Dilation Graphs for a Pressuremeter Test (Briaud, 1988)

The data obtained during rock dilatometer testing are used to construct the pressure versus injected volume curves, similar to those shown in Figure 16, from which the rock modulus can be determined.

Lama (1852) expressed the radial expansion of an internally pressurized cylindrical cavity made in an infinitely elastic medium by the following equation:

$$G = V \times (\frac{\Delta p}{\Delta v}) \tag{31}$$

Where, G = the elastic shear modulus;

V = the volume of the cavity; and,

p = the pressure in the cavity.

The ratio $\Delta p/\Delta v$ corresponds to the slope of the pressure-volume curve obtained during a rock dilatometer test. Modulus determination from the pressure volume curve is performed over the pseudo-elastic part of the test (over a pressure range where curve is linear). The shear modulus (G) is estimated as follows:

36

$$G_m = V_m \times \left(\frac{\Delta p}{\Delta v}\right) \qquad (32)$$

To convert the shear modulus G_m to an elastic modulus, the following elastic relation is used:

$$G_m = \frac{E_r}{2(1 + \upsilon_r)} \qquad (33)$$

Where, E_r = modulus of deformation of the rock; and,

υ_r = Poisson's ratio of the rock.

Combining these equations and solving for E_r, one obtains:

$$E_r = 2(1 + \upsilon_r) \times V_m \times \left(\frac{\Delta p}{\Delta v}\right) \qquad (34)$$

The term V_m is the total cavity volume at the midpoint of the pressure range over which the rock modulus is determined. It is the sum of two volume components as defined followings:

$$V_m = v_0 + v_m \qquad (35)$$

Where, v_0 = normal initial or at rest volume of the deflated probe; this volume is approximately equal to 1,950 cc for this device which is used for the project; and,

v_m = mean additional volume (up to the selected pressure range midpoint) injected into the probe from the at rest condition.

Replacing v_m in previous equations, we obtain:

$$E_r = 2(1 + \upsilon_r) \times (v_0 + v_m) \times \left(\frac{\Delta p}{\Delta v}\right) \qquad (36)$$

As a calibration procedure, the two values of Δp and Δv must be corrected due to the stiffness of the membrane itself as well as due to any volume loss related to the intrinsic system dilation (i.e. due to increases in tube diameter with increasing fluid

pressure). When these corrections are applied to the previous equation, the resulting expression becomes:

$$E_r = 2(1 + \upsilon_r) \times (v_0 + v_m) \times \cfrac{1}{(\cfrac{\Delta v}{\Delta p - \Delta p_i}) - c}$$ (37)

The value of Δp_i is the change in pressure within the dilatable membrane corresponding to the applied pressure increment Δp. Parameter c is the volume correction factor of the rock dilatometer which is determined from calibration procedure. The value of c is 7.878×10^{-4} cc/kPa for the rock dilatometer used in this study.

For most tests, the relative importance of the inertia of the membrane in relation to the applied pressures attained during the tests leads to negligible Δp_i value. Accordingly, the previous equation can be simplified to the following (Rock Dilatometer Manual, 1999):

$$E_r = 2(1 + \upsilon_r) \times (v_0 + v_m) \times \cfrac{1}{(\cfrac{\Delta v}{\Delta p}) - c}$$ (38)

This equation is the basic equation used for rock modulus calculus when the rock dilatometer is used. If relatively soft material is tested, the user might have to use equation 37.

2.7.2 Calculation of the Pressure in Membrane

The water pressure which acts inside the rock dilatometer probe can be obtained from the following equation.

$$P_b = 0.955 P_g + 8.82 \Delta h(m)$$ (39)

Where, P_b = water pressure in the probe (kPa);

P_g = oil pressure read on the pressure gauge (kPa); and,

Δh = difference in elevation between the manual pump and the center of the dilatometer probe (m).

The factor 0.955 by which the reading on the pressure gauge is multiplied, takes into account the fact that the area on the downstream side of extremity F of the dual

38

piston is slightly larger than the area on its upstream side, this due to the diameter of rod G (Figure 15).

2.8 Summary of Literature Review

Review of literature revealed while the P-y curve approach has been extensively documented in literature for various soils, little work existed weathered rock profiles. Reese's method (1997) is the only developed P-y curve model for "weak" rock. However, it was established based on data from two load tests, and was considered to be "interim research" (Reeese, 1997). Zhang (1999) presented a method to estimate the lateral ultimate resistance for shafts in weathered rock profiles. This method seems to be reasonable and is evaluated for inclusion in this research. While k_h and P_{ult} can be evaluated on the basis of rock mass quality and strength, better quality data for k_h can be obtained using the rock dilatometer. The rock dilatometer can either be used to provide rock properties or to actually provide "measured P-y curves". However, based on actual field experience with the rock dilatometer, it was difficult to apply pressure high enough to reach the ultimate strength of the rock mass. The rock dilatometer only allows 7 mm of membrane expansion at maximum volume injection. According to test results performed so far in North Carolina transitional material, this maximum displacement was not enough to mobilize the ultimate strength of the rock. Therefore, in this study, the rock dilatometer will be used only to measure the lateral modulus properties.

CHAPTER 3. LABORATORY TESTING

A major objective of laboratory testing was to investigate the load-deflection characteristics of shafts embedded in weathered rock under controlled conditions. The main benefits of laboratory testing versus field tests are the ability to more closely control test conditions. This chapter presents a description of the laboratory testing component of the overall research program. The scope of presentation includes sample preparation, test pile configuration and attached instrumentation, and back-figured laboratory P-y curves. In addition, a study using F.E.M. to investigate the potential influence of boundary effects on the results is included. Measured laboratory results are reduced and presented in the form of P-y curves as a function of depth. Further analyses of the laboratory data and their correlation with field behavior are presented in Chapter 5.

To develop a P-y curve model for weathered rock under lateral loading, the interaction of the foundation materials and the shafts must be investigated. The laboratory testing is undertaken to evaluate P-y curves from model piles tested in an Aggregate Base Course (ABC) mixture. This mixture is used to simulate in-situ weathered rock material. The compacted ABC has higher stiffness than compacted soil with a stiffness closer to that of weathered rock. The ABC contains a large portion of gravel particles, somewhat similar to that of highly fractured in-situ rock mass. After establishing the correlation between measured properties from laboratory and field tests, the test results will be used to suggest an appropriate P-y curve function for weathered rock.

3.1 Experimental Program

The laboratory testing program can provide more information than test data from field testing since the laboratory testing allows the installation of more instrumentation, minimizes variations in ground conditions, such as non-uniform properties along the shaft length and the location of the ground water table, and it is relatively easier to control load applied than while field testing. The testing program included performing two tests on instrumented model piles with the first test performed without a surcharge. In the no-surcharge test, the test pile was embedded 0.86 meter into the simulated weathered rock material. After a surcharging system was installed, a second test was conducted with a

surcharge of 24 kPa, and the pile was embedded 1.07 meter into the simulated testing medium. Load application in both tests continued until the maximum allowable strains in the pile were attained.

3.1.1 Test Setup

The test pit used for these experiments is located in the Geotechnical Testing Lab, in the Constructed Facilities Lab, on Centennial Campus at NC State University. These tests were performed in a 1.82 m wide × 3.66 m long × 2.55 m high concrete-walled chamber as shown in Figure 17. Based on a F.E.M. analysis for boundary effects, this chamber was considered to be large enough to allow two tests to be set up while avoiding fixed-boundary effects. To simulate overburden pressures found in field situations, a combined lateral loading and surcharging system was developed. Figure 18 shows the surcharge loading system, which is comprised of the following: 1) 0.61 m × 0.84 m × 0.025 m thick A36 steel plates, two W 0.15 × 0.51 × 1.83 meter loading members, and a W 0.15 × 0.51 × 0.76 meter cross member. A leveled surface was carefully maintained to ensure uniform contact across the ground surface.

The loading frame was used to attach two 267 kN hydraulic jacks that can apply load in the vertical direction. This loading system was capable of applying stress simulating up to 15 meter of overburden. To monitor the actual applied load, two 222 kN StrainSert load cells were placed between the loading points on the jacks and the reaction beam. The load signals were measured using a Vishay P-3500 digital readout box.

3.1.2 Testing Medium

One important question asked before testing was how to simulate weathered rock in the laboratory. It is difficult and challenging to bring a large volume of undisturbed weathered rock to the laboratory for testing. Even if it were possible, it was still questionable that the disturbed weathered rock mass could be a representative of in-situ conditions. Alternatively, measured rock recovery (REC) obtained during field testing was employed to simulate a material representative of weathered rock. To develop the testing media, the proportions of ABC and soil in the simulated mixture were based on

Figure 17. Testing Chamber
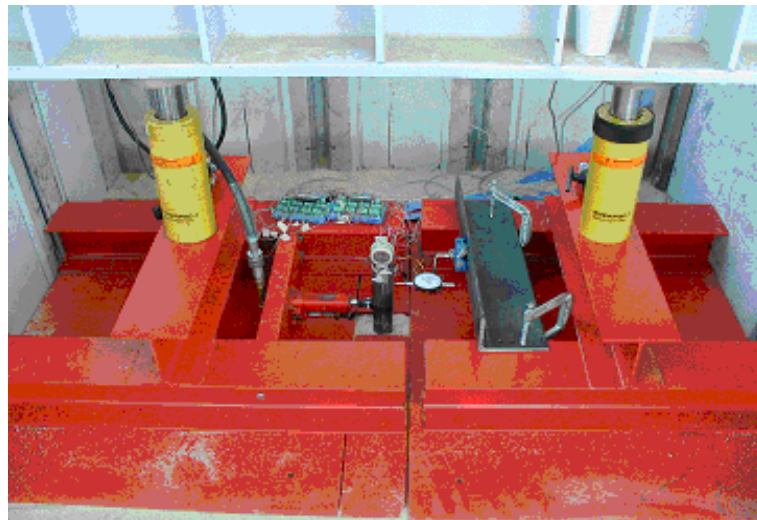
Figure 18. Surcharging and Lateral Loading System

analyses of boring logs and core samples obtained from load test field sites. Table 7 displays the location of these sites as well as the measured recovery (REC) and rock type. The data revealed that the recovered cores averaged approximately a 30% loss of material. This interpretation was based on an average REC of 70 %. Accordingly, it was assumed that the remaining 30% was finer materials that washed and/or slaked during the coring process. For testing purposes, these finer particles are assumed to be those smaller

than approximately 4.75 mm. This value is the dividing line between sands and gravels, according to the Unified Soil Classification System (USCS).

Table 7. Rock Test Data

COUNTY	REC (%)	ROCK TYPE
AVERY	69	GNEISS
	70	
	60	
	37	
	70	
	40	
	26	
CALDWELL	93	GNEISS
	86	
WILSON	76	METAVOLCANIC
	80	
	100	
	100	
	90	
GUILFORD	61	METADIORITE
	92	
AVERAGE	~ 72.0 %	

To create the testing media in the laboratory, Aggregate Base Course (ABC) was mixed with Number 467 stone and coarse concrete sand to create a well graded testing medium with an appropriate level of fines. To maintain a reasonable level of workability (due to the manual labor involved), the maximum particle size was limited to less than 51 mm. The ABC and sand were obtained from Godwin Sand and Gravel and the Number 467 stone came from Hamilton Landscaping, both of Raleigh, NC. The materials were mixed with a Bobcat Loader until the desired consistency was created. Approximately, 16 cubic meters of ABC and sand mixture was used to create the test medium. Two grain

size distrubution (GSD) curves from samples of the simulated testing medium are displayed in Figure 19.
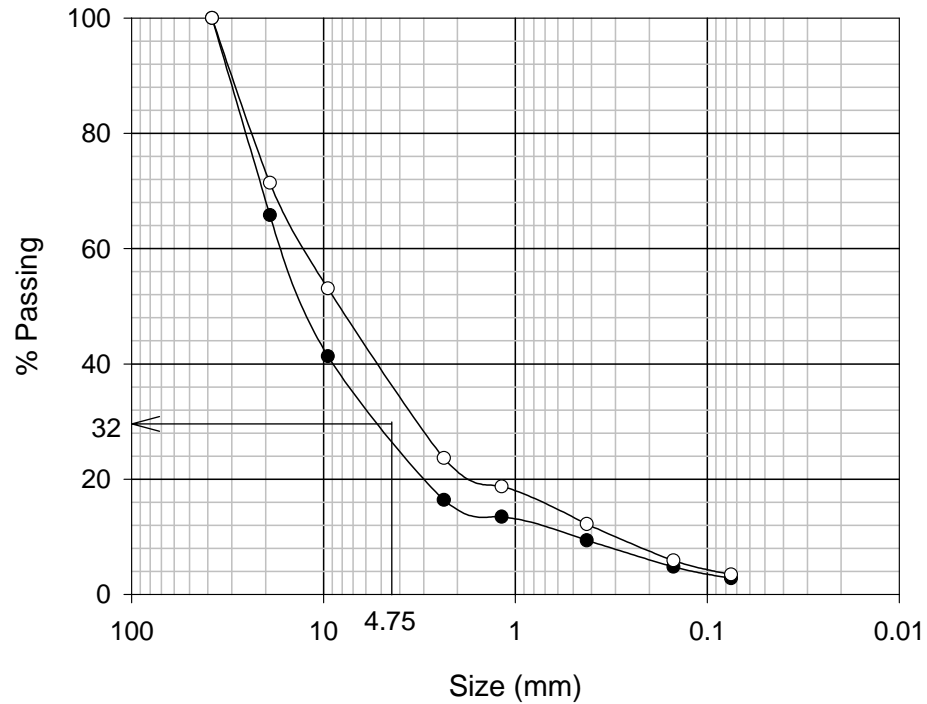
Figure 19. Grain Size Analysis of ABC Mixture

According to the GSD depicted in Figure 19, the average amount of soil passing the No. 4 sieve is approximately 32%, which is close to the targetted range. From this graph, the coeffiecient of uniformity and coefficient of curvature were calculated as follows:

$$c_u = \frac{D_{60}}{D_{10}} = \frac{12}{0.45} = 26$$

$$c_c = \frac{(D_{30})^2}{(D_{60} * D_{10})} = \frac{4^2}{(12 * 0.45)} = 2.96$$

These values indicated the testing medium to be well graded clean gravel with less than 4% fines passing No. 200 sieve.

3.1.3 Mechnical Properties of Simulated Weathered Rock

To investigate simulated weathered rock properties, Consolidated Drained (CD) triaxial testing was performed. This testing was performed on specimens prepared at two

different densities. The material tested was the ABC mix less any aggregate larger than 0.019 meter. The larger particles were removed due to the size of available testing equipment. The triaxial samples were prepared using a split mold sampler that was held together tightly with clamps. Then, the ABC mixture was spooned into the mold in three lifts and each lift was compacted using a modified Proctor Hammer. The compaction method consisted of full height drops (0.46 meter) and either 6 or 25 drops depending on the desired density. Compaction in this manner yielded unit weights ranging from 18.0 kN/m^3 to 22.3 kN/m^3. The samples were sheared at a rate of 0.25 mm/min. This value is approximately 0.18 percent strain per minute based on a desired 15 percent strain at failure for a 0.14 meter tall sample. Confining pressures of 34, 69, and 103 kPa were applied to samples, respectively, and each specimen was loaded to failure with drainage allowed. The results in terms of measured principal stress difference versus axial strain curves are shown in Figures 20 and 21 for the lower and higher density specimens, respectively. From these plots, the secant modulus of elasticity for the mixture was calculated at a strain level of 2 %. This value was chosen due to the ABC mixture nearing failure at this strain level, as seen in Figure 20.
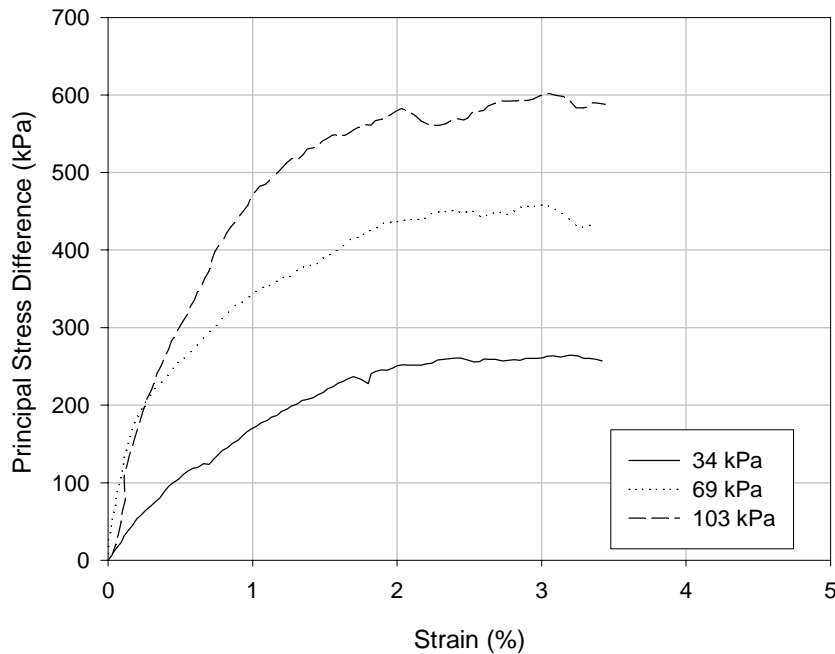
Figure 20. ABC Triaxial Tests (6 blows for density control)

Table 8 shows the secant moduli at 2 % strain under various conditions. The 2% strain value was used for consistency to evaluate the K_f line for each set of data, as shown in Figure 22.
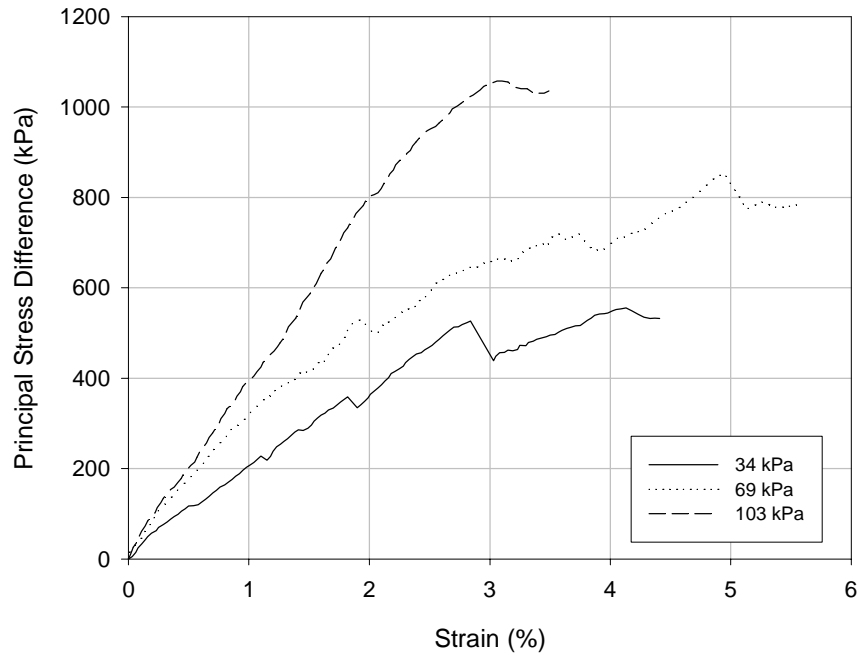
Figure 21. ABC Triaxial Tests (25 blows for density control)

Table 8. Modulus of Elasticity of ABC

Confining Pressure (kPa)	Modulus of Elasticity (kPa)	
	Number of Blows: 6 ($\gamma = 18.56$ kN/m^3)	Number of Blows: 25 ($\gamma = 20.17$ kN/m^3)
34	12,410	18,961
69	25,614	27,579
103	28,958	40,334

Figure 22 depicts the p-q diagrams based on a failure criterion of 2% strain. From these diagrams, the friction angles for the different density ABC mixtures can be calculated using the following equation:

$$\sin \phi = \tan \psi \tag{40}$$

Where, ϕ = the angle of internal friction; and,

ψ = the angle of the K_f line in the p-q diagram.

Accordingly, the friction angle of lower density ABC is 46.3° and the higher density ABC is 57.1°.
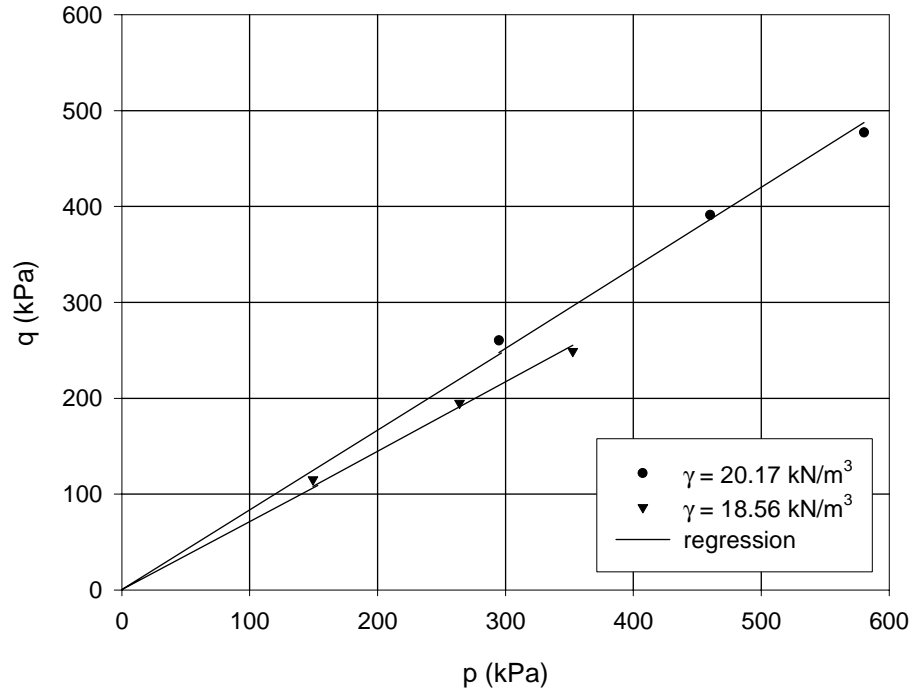
Figure 22. p-q diagram for ABC Mixture

3.2 F.E.M. Modeling of Laboratory Test

The laboratory test was modeled by approximately 3600 elements and 4300 nodes using the ABAQUS F.E.M. code. The dimensions of the volume modeled are same as the laboratory test chamber size described previously. Figure 23 shows the dimensions of the model and boundary conditions. For modeling the laboratory test setup, the lateral boundary condition was fixed against horizontal movement because of the rigid concrete

walls of the chamber. Table 9 shows the properties of ABC that were used as input data for F.E.M. modeling.
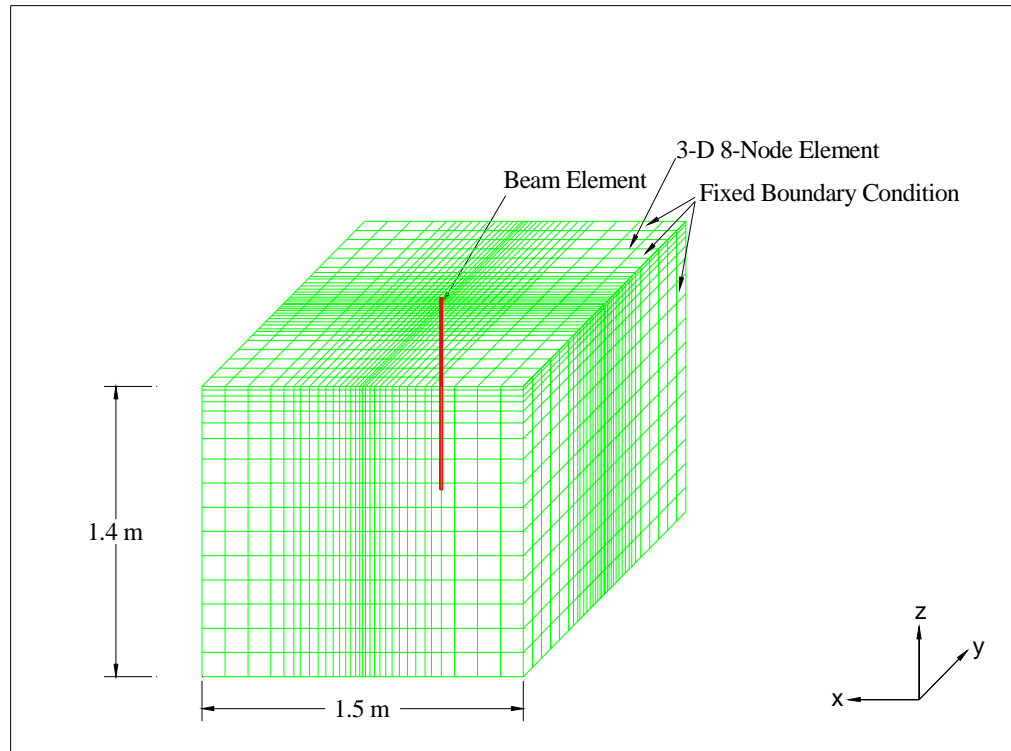
Figure 23. Dimensions and Boundary Conditions for Modeling of Laboratory Test

Table 9. Properties of ABC

Items	Values Uesd in Analysis
Modulus of Elasticity	2.5×10^4 kPa
Poisson's Ratio	0.15
Strain at Failure	2 %

The steel pipe used for the laboratory test pile was modeled with beam elements. The properties and dimensions of the test piles are summarized in Table 10.

Table 10. Properties of Test Piles

Items	Laboratory
Modulus of Elasticity (kN/m^2)	2.07×10^8
Poisson's Ratio (v)	0.15
Length of Pile (m)	1.22
Diameter of Pile (m)	0.051

Three-dimensional F.E.M. modeling using ABAQUS was used to evaluate the proposed design length and diameter of the test pile under load in order to investigate boundary effects. Figure 24 shows the stress contours estimated under lateral loading of the pile for the given diameter and embedded length, size of chamber, and depth of soil. These results suggested that no significant stress is transferred to the boundary. From these results, it can be inferred that the rigid boundaries will produce minimal effect on the measured pile strains and deformations during testing.

In addition, F.E.M. analyses were performed to evaluate the P-y characteristics of the model piles under different conditions (surcharged and non-surcharged loading tests). While the tests were performed with sophisticated measuring devices, it was difficult to measure every change along pile and soil during loading sequences. Therefore, the F.E.M. analysis provided enhanced understanding of the laboratory test data.

In order to include the plasticity of simulated weathered rock, the Drucker-Prager model was used in the modeling. The modified Drucker-Prager/Cap plasticity model in ABAQUS is intended for geological materials that exhibit pressure-dependent yielding and cohesionless properties. The yield criterion was defined based on the triaxial tests, which showed yield at 2 % vertical strain. The friction angle for the case of denser material, 57.1 degree, was used.
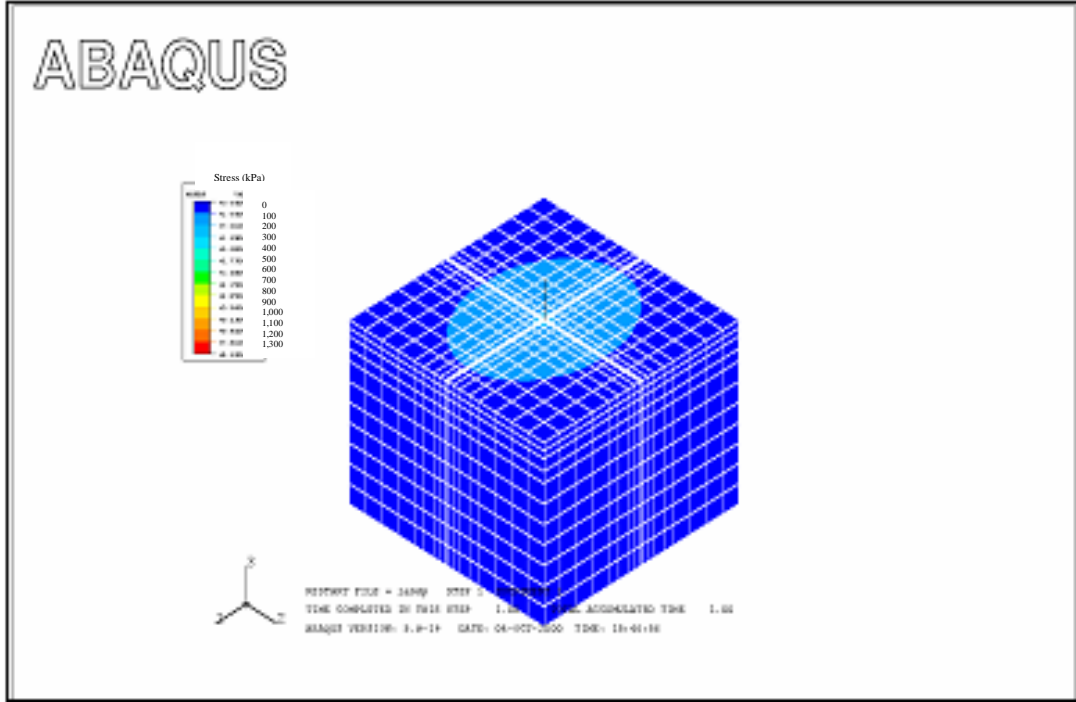
Figure 24. Stress Contour of the Laboratory Modeling under Design Load

Initial sets of model piles were constructed from 0.05-meter diameter A36 tubular steel. After initial testing with coarse concrete sand, the test soil did not fail but the ultimate yielding strain of steel was reached in the model pile, with the location of yield strain only a few centimeters deep. A re-design of the test pile was advanced under the following assumptions: 1) The P-y curves are linear; 2) the soil is uniform (all P-y curves are the same); and 3) the pile is infinitely long.

The governing differential was described as follows (Briaud, 1992):

$$EI\frac{d^4y}{dz^4} + Ky = 0 \tag{41}$$

or

$$y = \frac{l_0^4 d^4 y}{4dz^4} \tag{42}$$

with

50

$$l_0 = \sqrt[4]{\frac{4EI}{K}} \tag{43}$$

The parameter l_0 is called the transfer length. A pile will be considered as infinitely long if:

$$L \geq 3\, l_0$$

The pile is considered rigid if the embedded length L is smaller or equal to the transfer length:

$$L \leq l_0$$

Assuming K is equal to the elastic modulus of the simulated rock measured from laboratory triaxial tests, a second model pile was designed to cover the range of depth of embedment as described in Table 11.

Table 11. Properties of Piles

Items	Property Value
Length of Pile (m)	1.22
Outside Diameter of Pile (m)	0.09
Modulus of Elasticity (kPa)	2.07×10^8
Poisson's Ratio (ν)	0.15
Moment of Inertia (m^4)	1.01×10^{-6}
EI ($kN\text{-}m^2$)	2.09×10^5
l_0 (m)	0.45

3.3.1 Test Pile Construction

Two identical model piles were constructed of 0.09 meter O.D., A36, steel pipe with a wall thickness of 0.005 meter. The instrumentation strain gages were attached

along the outside of the pipe every 0.05 meters along its depth, beginning 0.1 meter from the tip. Prior to attachment of gages, surface preparation was performed as follows:

1. Solvent degreasing –surface oils, greases, organics, and soluble residues that occur during manufacture, transportation and installation were removed.

2. Surface Abrading – the surface is abraded to remove loosely bonded materials. In the case of the test pile surfaces, this was accomplished by using varying grades of sandpaper. The grades began with 100 or 200 grit and increased to a final grit of 400 to create the desired final surface finish.

3. Gage Layout and Location Lines – Great care was taken to ensure the gages were located along the centerline of the model with locations carefully marked.

4. Gage Attachment – once locations were identified, the cleaned surface was lightly coated with M-Bond 200 Catalyst to accelerate the bonding process. M-Bond 200 Adhesive was then applied and the gage followed. Care was taken to ensure that the bond did not contain air bubbles. The gage was then covered with Scotch © tape to hold the unit in place until curing was finished.

5. Final Cover – after curing was completed, the gages were covered with M-Coat to seal the edges. Once this coating dried, the gages were covered with an abrasion resistant rubber cover.

As the strain gages were attached, the gage wires were threaded through pre-drilled 3 mm holes, thus allowing the instrumentation wire to be protected within the pile member.

3.3.2 Test Chamber Filling Procedure and Density Control

The test chamber was filled with the ABC mixture using 4-6 inch lifts. These lifts were compacted with a Multiquip MVC-90H. This compactor is a gas operated vibrating plate tamper which can develop a tamping force of 14.9 kN based on a plate size of 0.5 meter $\times$ 0.56 meter (Sunbelt). On alternating layers, the edges were compacted further with a Bosch 11304 Electric Jackhammer equipped with a 0.3 meter $\times$ 0.3 meter steel foot. The effectiveness of the compaction effort was monitored with a Troxler Nuclear Density Gage. Both density and moisture content were measured in the Backscatter mode. Once the desired compaction was attained, additional layers were placed after scarifying the surface each time. The process continued until the desired tip location was

reached. At that point, the test piles were installed and held plumb using a 0.61 meter level. The testing medium was compacted around the piles. The process continued until the chamber was filled. Once the chamber was filled, the top was leveled and the loading system was installed.

3.4 Instrumentation and Data Acquisition

In order to collect data conveying laterally loaded model pile behavior, a variety of instrumentation was needed. To measure strains, electric resistance strain gages, Model CEA-06-250UW-120, obtained from Micro-Measurements, were used. Each gauge was designed with a 0.05 meter gauge length and overall dimensions of 11 mm by 5 mm. In addition to the strain measurement, the displacement behavior was also monitored. Lateral movements were measured with a Humboldt electronic dial gage with a resolution of 2.54×10^{-6} meter. Rotations at the point of load application were measured with a Schaevitz electronic inclinometer. As another aspect of these tests involved the application of a surface surcharge, the pressure distribution was monitored with depth using a series of Geokon pressure cells embedded in the test medium.

All instrumentation sensors were monitored using OPTIM Data Acquisition System. The unit was programmed to take readings every 2 seconds and store the data. These data sets were then downloaded in ASCII format and reduced using commercial software programs.

3.4.1 Analysis of Laboratory Strain Data

Tests were performed until the maximum allowable load was reached. The maximum load was estimated based on the yield strength of steel as follows:

$$\varepsilon_{yield} = \frac{\sigma_{yield}}{E} \tag{44}$$

Where, σ_y = yield stress of the steel pile (2.48×10^5 kPa);

E = Young's Modulus (2.07×10^{11} kPa); and,

ε_{yield} = yield strain.

The allowable strain was taken as 80% of the yield strain (approximately 1000 microstrain). Based on the measured strain values with depth, the calculated moment

diagrams along the pile length under a pile top lateral load of 2.66 kN is shown in Figure 25. A fourth order regression line was used to obtain functional representation of the moment diagram as follows:

$$y = b + b(1)x + b(2)x^2 + b(3)x^3 + b(4)x^4 \qquad (45)$$

Where, $b(i)$ = coefficients of the regression line; and,

x = pile segment depth.
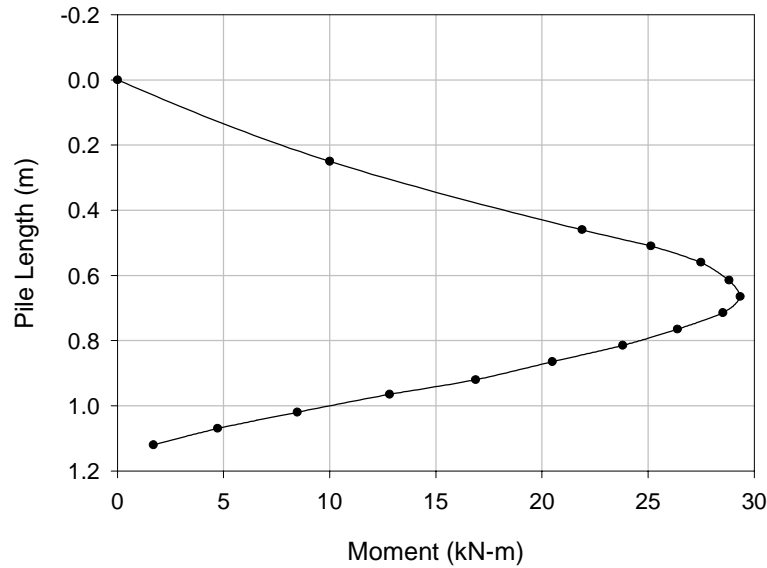
Figure 25. Typical Moment Curvature regression

From the function of the moment diagram, P, the load per unit length, and y, the deflection of the pile, were obtained through the differentiation and integration procedures as described in the literature review chapter. Performing the process for each load increment resulted in several points depicting P-y relationship at each depth.

3.5 Laboratory Pile Load Tests

The lateral loading of each test pile was applied using a 178 kN Enerpac hydraulic jack. The load was applied in 138 kPa pressure increments, which equal 0.44 kN, based on piston area of 0.003 m². The load was held until the lateral movement was stabilized and then the load was increased to the next level. This process was repeated until either maximum pile strain or soil failure was attained.

3.5.1 Load Test without Surcharge

The test pile was embedded 0.86 meter into the compacted simulated rock material. The pile was loaded laterally in approximately 0.44 kN increments. Once the test was completed, the chamber was excavated and set up for the next test. Utilizing the procedure as noted earlier, the deflected shape and corresponding P-y curves were derived from the measured test data.

3.5.2 Load Test with Surcharge

A test pile was embedded 1.07 meter into the compacted testing medium. The surcharging system was installed and a surcharge of 24 kPa was applied and allowed to stabilize for approximately one hour before starting the lateral load test. Again, the test continued until the maximum allowable strains were attained. To determine the stress distribution along the pile length, as induced by the surcharge system, a series of Geokon Earth Pressure Cells (EPC) were installed as shown in Figure 26.

Figure 26. Geokon EPC layout

Once the load was applied, the stress distribution was monitored adjacent to the pile. Figure 27 shows the stress with depth as measured from the pressure cells. These data are

compared to the stress distribution estimated using the Boussinesq solution and estimated stress distribution for the case without surcharge. (please recall that the surface surcharge was applied to the plates, and the pile was located between the two plates' gap of 0.61 meter). Assuming a linear stress distribution between the pressure cells point of measurement, the vertical stress adjacent to the pile increased from approximately 4.79 kPa at the surface to 21.5 kPa at a depth of 0.6 meter. The measured stresses then reduced to 19.2 kPa at a depth of 0.84 meter. This reduction may be due to inadequately compacted ABC at this depth (only around the EPC). The main goal in this case was not to obtain a specific distribution of stresses but to rather know the magnitude of stresses being applied.
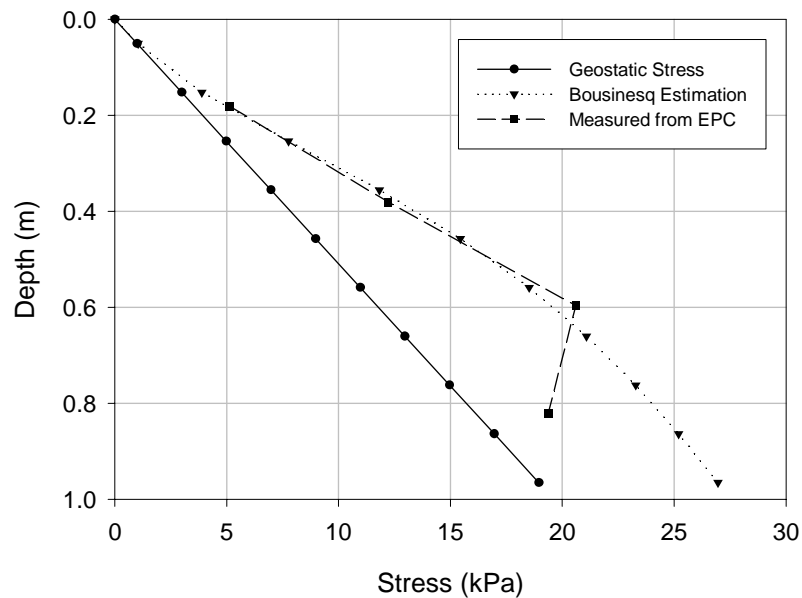
Figure 27. Stress Distribution

3.6 Measured P-y Curves

The measured P-y curves in the testing program are presented in Figure 28 for test with no surcharge case, and Figure 29 for test with surcharge case, and indicate a general trend where the initial slope of P-y curves becomes steeper as the depth increases.

Figure 28 shows results from the first successful test. The ABC material in this test was prepared with an average density of 18.1 kN/m^3 and moisture content of 4.5 percent. Figure 29 present results from the surcharged test with an average density of 19.6 kN/m^3 and a moisture content of 5.3 percent.
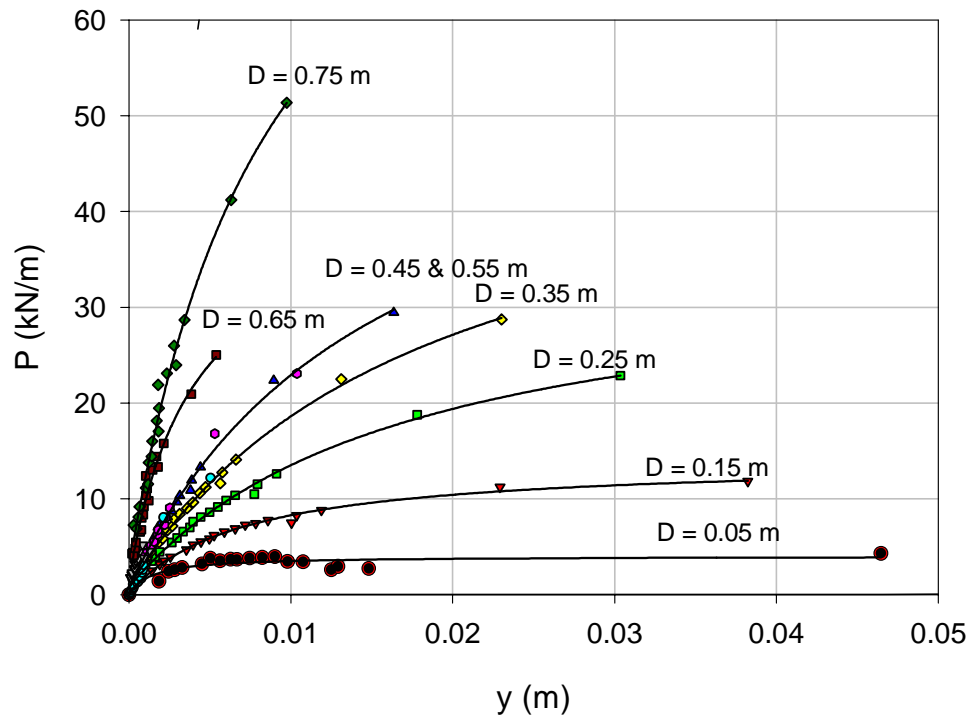
Figure 28. P-y Curves without Surcharge
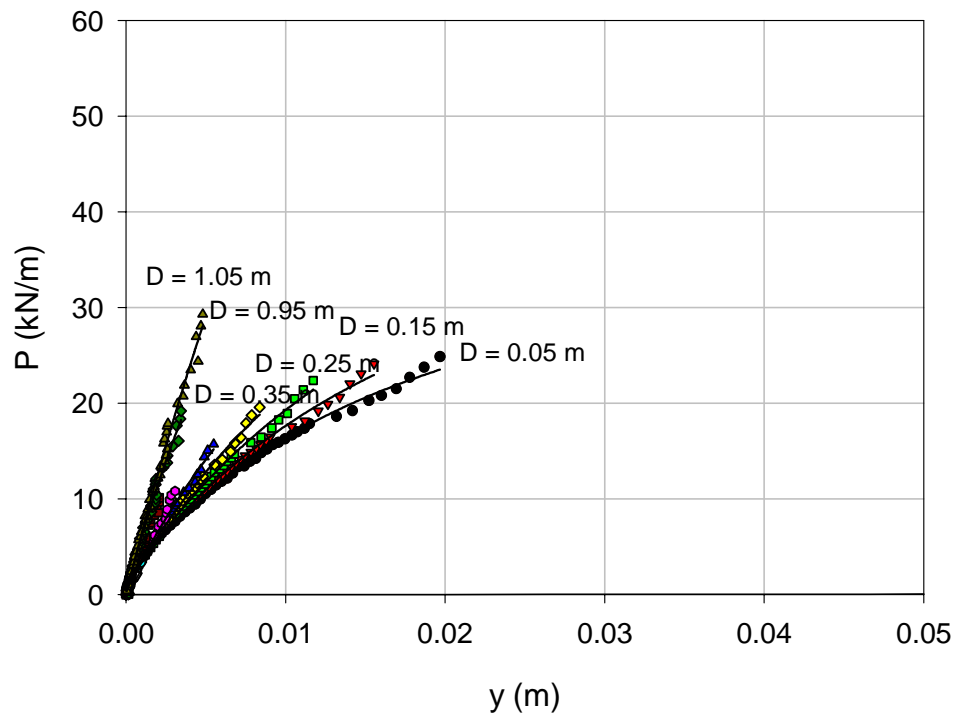
Figure 29. P-y Curves with Surcharge

3.7 Summary of Laboratory Tests

1.   Experimental work was conducted to investigate the possibility of using laboratory model tests to simulate lateral response of drilled shafts embedded in weathered rock and discern the shape of their P-y curve function. Two lateral load tests on instrumented model piles embedded in an Aggregate Base Course (ABC) medium were performed. The ABC material was selected to simulate the response of weathered rock encountered in the field. Based on the results of in this chapter, it seems that the model piles can be used to develop correlations that can yield P-y curves in the simulated material. The laboratory data is analyzed and compared with field results in chapter 5.

CHAPTER 4. FIELD TESTS

Six field tests were conducted at three different sites as a part of this research program to develop P-y curves in weathered rock. The purpose of field testing was to measure load and deflection response with depth for drilled shafts embedded in weathered rock (WR) profiles. A second component of the field work encompassed performing rock dilatometer testing. The rock dilatometer is a testing device that can be used to measure in-situ stiffness properties of rock. This aspect of work was necessary since the material of interest is highly fractured and weathered and therefore difficult to sample and test in the laboratory. Five test sites were selected to measure in-situ properties of WR. These data are presented in this chapter and Appendix B.

4.1 Field Load Testing

Field tests were performed in three different counties in North Carolina, as shown in Figure 30. Two load tests were performed at each of the three test sites in Nash-Halifax, Caldwell, and Wilson Counties. Local maps for test sites are shown in Appendix C. Table 12 presents the underlying rock types for each of the test sites.

At each site, two 0.762 meter diameter drilled shafts were constructed 7.62 meters apart. Figure 31 shows the general layout of these shafts. The shafts were drilled using conventional earth augers, preceded by the insertion (screwed in) of permanent casing to the tip. The 12.7 mm thick permanent casings were used to make these shafts stiffer in order to be able to induce lateral movement around the lower part of the shaft length (embedded in the weathered rock material).

Figure 31 shows a schematic diagram of the North Carolina Department of Transportation's test frame that was used to apply the lateral loads to both shafts simultaneously. The load frame was attached to the installed drilled shafts at a vertical distance of 0.3 meter above the excavated ground line. The maximum capacity of the load frame, including the factor of safety of 1.25, was 979 kN for the Nash-Halifax county tests and then increased to 1334 kN, through structural modifications, for the Caldwell and Wilson county tests.
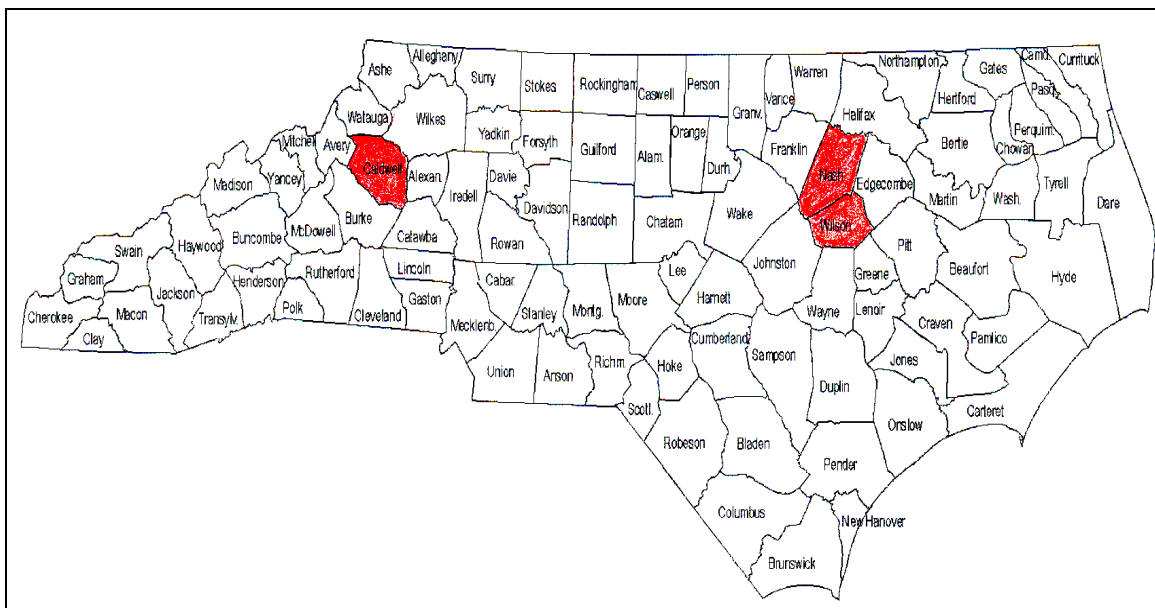
Figure 30. Locations of Test Sites

Table 12. List of test sites and Rock Types

Test Site	Rock Type
Nash-Halifax County	Sandstone
Caldwell County	Mica Schist
Wilson County	Crystalline Rock
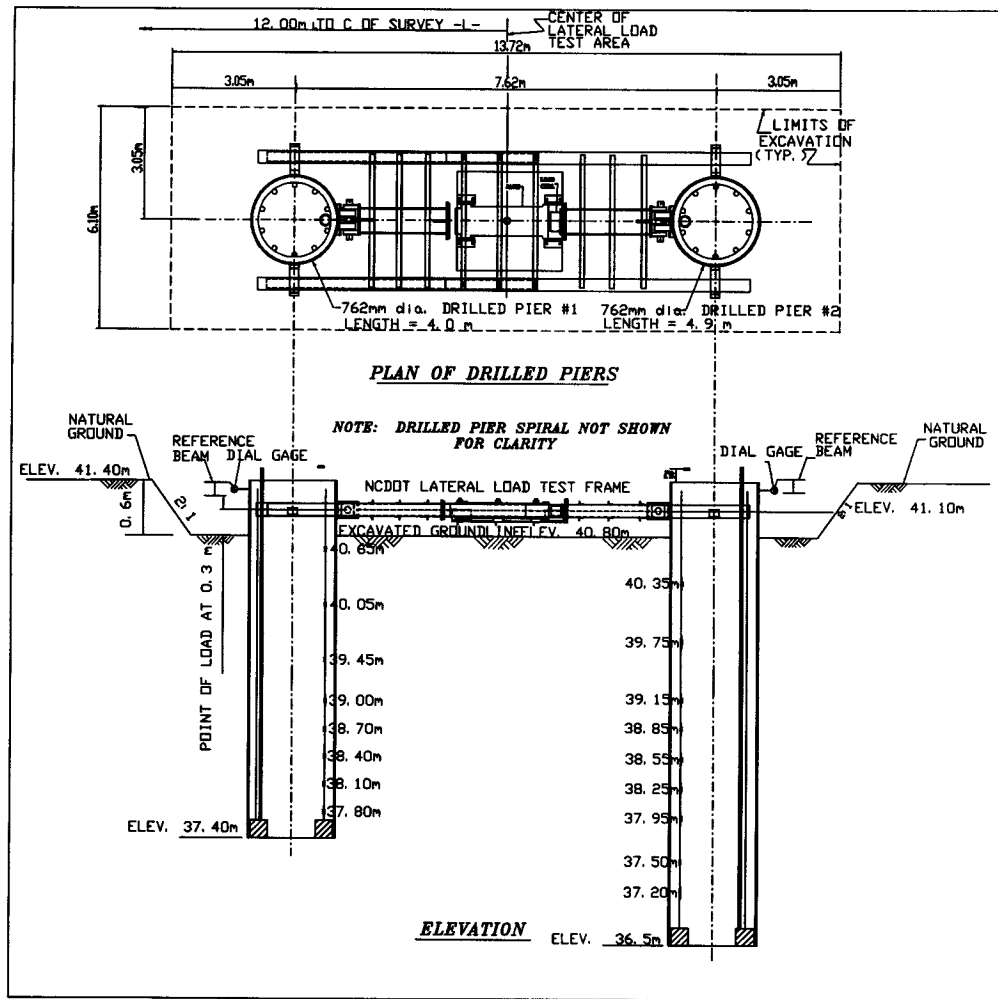
Figure 31. Layout of Test Shafts with Loading Frame

The loading sequence consisted of applying the lateral load in increments of 45 - 90 kN, followed by an unloading. Each load was held until there was no further appreciable deflection at the tops of the shafts (less than 0.127 mm per hour).

Monitored test data from the two load tests included the following: (1) load-deflection measurements at the top of the shafts; (2) deflection versus depth profiles measured by continuous inclinometer probes; and (3) measurements of strain with depth using Vibrating Wire (VW) strain gages. From the measured strains, moments were calculated along the depth each shaft by piece-wise numerical integration.

4.1.1 Instrumentation Plan

Shaft strains and deformations were monitored during field testing with a dial gage system, strain gages, and slope inclinometers. Some of these measuring systems are illustrated in Figure 31. Each shaft was instrumented above ground with four dial gages to measure surface deformation. A separate fixed reference beam was used for mounting the dial gages in accordance with section 5.1.1 of ASTM D3966-90. Two dial gages were used to measure shaft top rotation to calculate its deflection angle. One dial gage was used to measure lateral movement parallel to the direction of loading, and one dial gage was used to measure movement perpendicular to the loading direction.

Vibrating Wire (VW) strain gages were attached to the rebar cage along the shaft by sister bars tied to the vertical and spiral reinforcement. These gages were placed approximately at elevations shown in Figure 31 for the Nash-Halifax county tests, and similarly at the other test sites, to measure the strain induced by the lateral loading. The measured strain is then used to determine the moment and soil reaction as a function of depth. A CR-10 data logger was used to electronically acquire readings of strain and temperature.

Slope inclinometers were used to measure shaft lateral inclination as a function of depth. Electrolytic (EL) vertical in-place inclinometers were inserted into a plastic inclinometer casing installed during shaft construction. This plastic inclinometer casing was tied to the rebar cage prior to construction of the shafts. A continuous chain of inclinometer probes consisted of sensors with wheels that are attached to each other at pivot points approximately 0.50 meter apart. These probes were used to collect data along the entire length of each shaft. A signal cable extended up through the casing for each sensor and was connected to a data acquisition system. The data acquisition system consisted of an electronic measurement and control system monitored by a computer program.

Figure 32 shows installed strain gage and inclinometer casing attached to reinforcing rebar. After installation, the instrumented cages were inserted into theshaft drilled hole as shown in Figure 33.
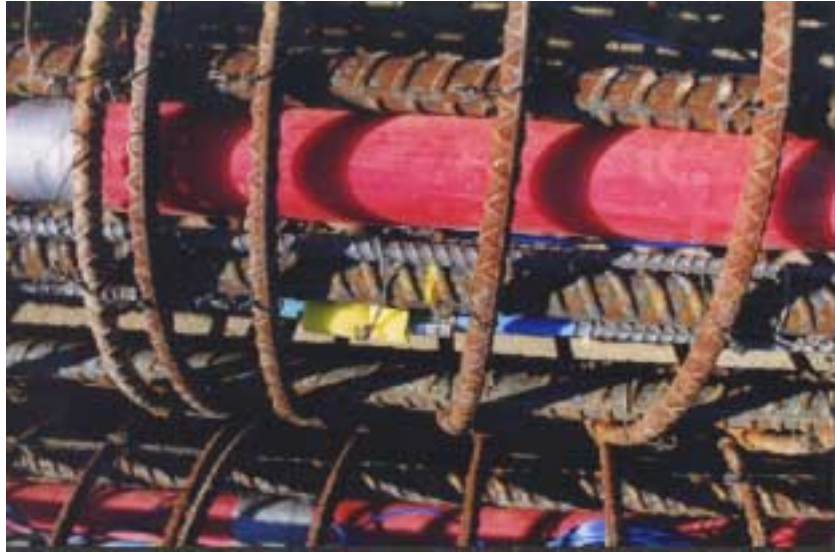
Figure 32. Strain Gage and Inclinometer Casing

Figure 33. Installation of Steel Cage

4.2 Nash-Halifax County Load Tests

This site is located at a bridge replacement project where bridge #153 crosses Fishing Creek at the Nash-Halifax County line, on NC 43. This area is situated in the

Northeasterly part of North Carolina near the town of Rocky Mount, which lies 18 miles to the southeast of the site.

Figure 34 (a) shows the installed test frame. A 1780 kN capacity jack with a 0.33 meter stroke, along with a 140 mm diameter load cell, were used to apply and monitor the test load, as shown in Figure 34 (b).

(a)   (b)

Figure 34. (a) Loading Frame, (b) Installed Loading Jack and Load Cell

4.2.1 Geology

The test site location is in gently rolling terrain along the easterly edge of the Piedmont Physiographic Province. Metamorphosed mudstone, siltstone, and sandstone of the Eastern Slate Belt underlie the area. The residual soils in this area were derived from the in-place weathering of the parent rock. The residual soils are mostly sandy silt (A-4) and silty clay (A-7). These soils are stiff to hard. The water table is located approximately 2 meters below the ground surface. Residual soils grade with depth into weathered rock. Weathered rock is derived from the underlying Meta-Argillite. A cross section of the subsurface profiles is shown in Figure 35.

The parent rock, which underlies the site, is metamorphosed sedimentary rock of the Eastern Slate Belt; Meta-argillite predominates. Foliation is poorly developed. The rock is mostly sound, but some natural fractures are present. These fractures predominately dip from 45 to 55 degrees and show no appreciable separation. Collected core samples had a tendency to break horizontally. Hard rock core recoveries exceeded 95% and Rock Quality Designation (RQD) for the lower 4.57 meter exceeded 75%. The

location of the tip of long shaft is approximately at the Elevation of 36 meters, near the middle of weathered rock zone.
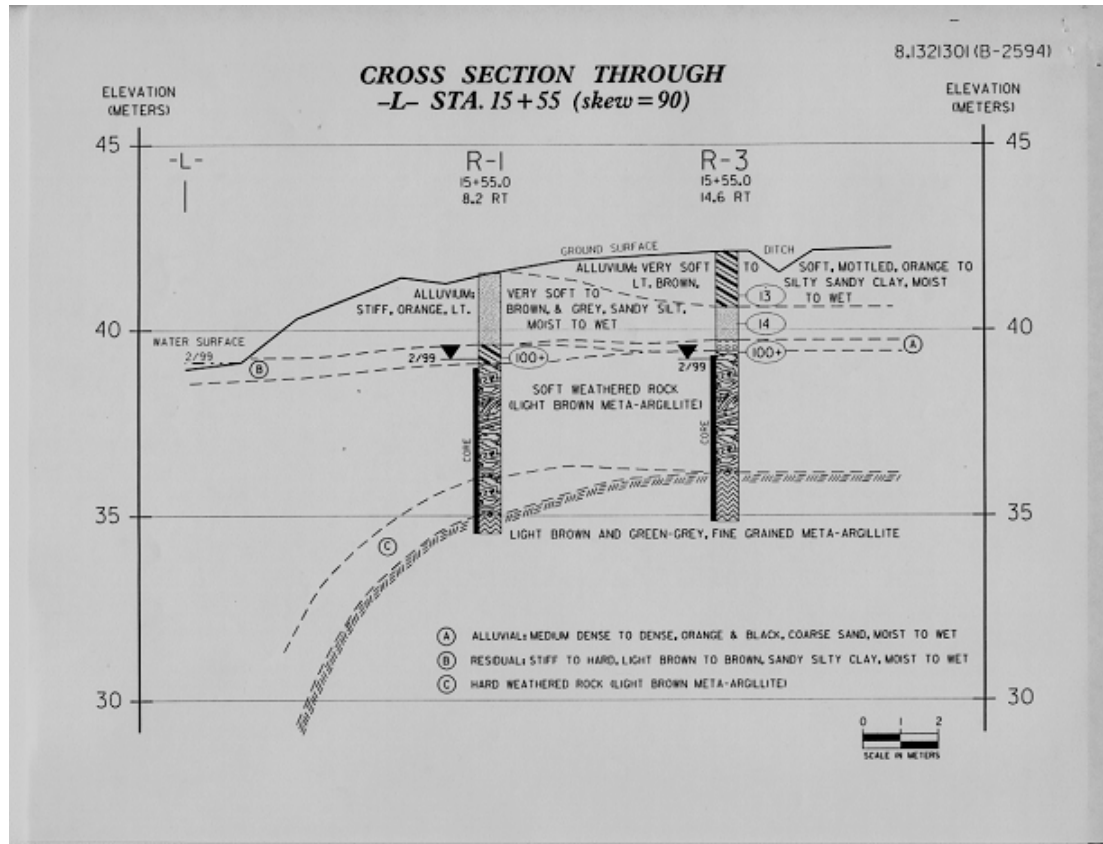
Figure 35. Test Area Subsurface Cross-section

4.2.2 Geotechnical Properties of Test Site

Two standard penetration test (SPT) profiles were performed near the test area. The site's alluvial soils consisted of stiff silt, sand, and clay and soft to very stiff sandy silt. Just below the alluvial layers is a thin residual, stiff to hard, silty clay. The groundwater is present at the interface of the alluvial soil and residual layers. Beneath the residual clay, a weathered meta-argillite rock grades into a hard weathered and finally into a competent rock around a depth of 6.10 meters.

The residual soils were cored from a depth of 2.44 meter to approximately 7.0 meter below the surface. The core size was an "H" core, to increase chances of sample recovery. Approximately 94% recovery from 12.80 meter of core was obtained. Most of the core is poor RQD rock, which can be classified as weathered rock.

All weathered rock core samples were inspected and specific samples were chosen for lab testing. Eight (8) samples were used for unconfined compression testing at the NCDOT, Materials and Test Unit laboratory. Table 13 summarizes the results of these tests.

Table 13. Nash-Halifax County Laboratory Test Results

Depth (m)	Unit Weight (kN/m^3)	Qu (kPa)	RQD (%)
4.58 – 4.76	24.6	33,095	< 25
5.27 – 5.57	26.1	19,305	< 25
5.62 – 5.92	22.4	31,026	< 25
6.15 – 6.35	26.1	126,864	50
6.64 – 6.80	25.5	48,263	50
6.80 – 7.00	25.4	55,158	50
10.42 – 10.61	27.0	154,443	85
12.71 – 12.94	26.4	135,827	98
14.35 – 14.58	26.4	50,332	100

4.2.3 Description of Test Shafts

Two drilled shafts 0.762 meter in diameter were constructed 7.62 meter apart. A shorter shaft was embedded approximately 3.35 m, and a longer shaft was embedded 4.57 m. Both shafts were constructed with approximately 0.61 m above ground length to facilitate the attachment of the loading frame. Figure 31 shows the layout of these shafts.

Prior to construction of these shafts, the test area measuring roughly, 10.67 m × 3.05 m was excavated by removing a 0.6 – 0.9 meter layer of soil. This excavation eliminated some of the overburden pressure and enabled the applied loads from the frame to be closer to the weathered rock elevation, therefore inducing movement in the subsurface layer of interest.

Seventeen strain gages were used for the two shafts, eight for the short shaft and nine for the long shaft. Each shaft was outfitted with the continuous inclinometer probes.

4.2.4 Load Test Results

During testing, the short shaft experienced over 0.135 meter of deformation at applied lateral load of 534 kN. After the failure of the short shaft, a concrete block was

installed behind it to add extra resistance, and loading of the long shaft was continued until the maximum load of 979 kN was reached. This load was the limit capacity of the testing frame.

4.2.4.1 Top Deflection and Inclinometer Data

The load-deformation response was obtained at the top of each shaft during incremental lateral loading. The top displacements of the short and long shaft are shown in Figure 36. Based on the measured response, the short shaft reached plastic deformation under the load of 534 kN, however the long shaft did not reach its ultimate resistance under applied test load of 979 kN. Lateral displacement under 534 kN was measured to be 0.135 m for the short shaft. In comparison, this displacement was 0.017 m for the long shaft.

Based on the inclinometer-measured deflection profile, the short shaft behaved as a rigid body with a linear displacement profile along the shaft's full length (Figure 37(a)). The long shaft behaved as a "restrained tip" shaft, as indicated by the non-linear displacement profiles along its length.
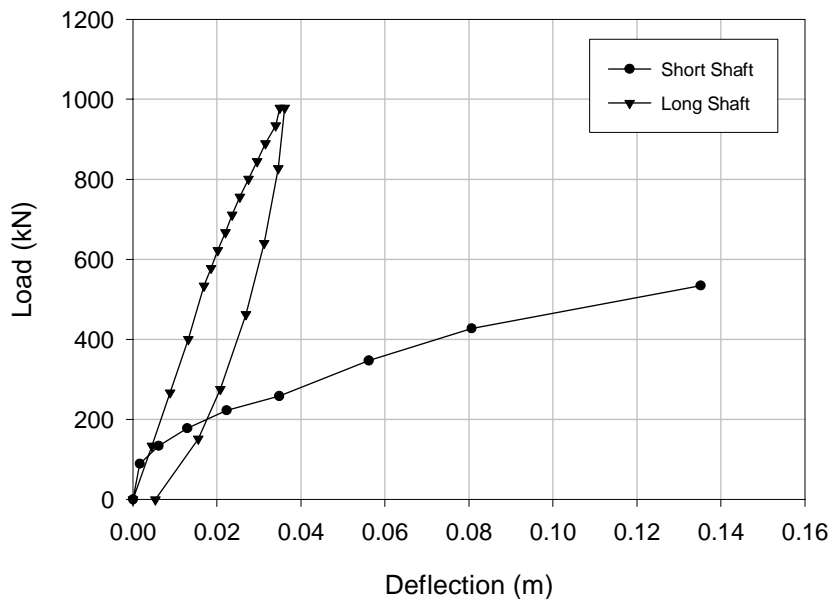
Figure 36. Top Displacements of the Short and Long Shaft Measured from Dial Gages
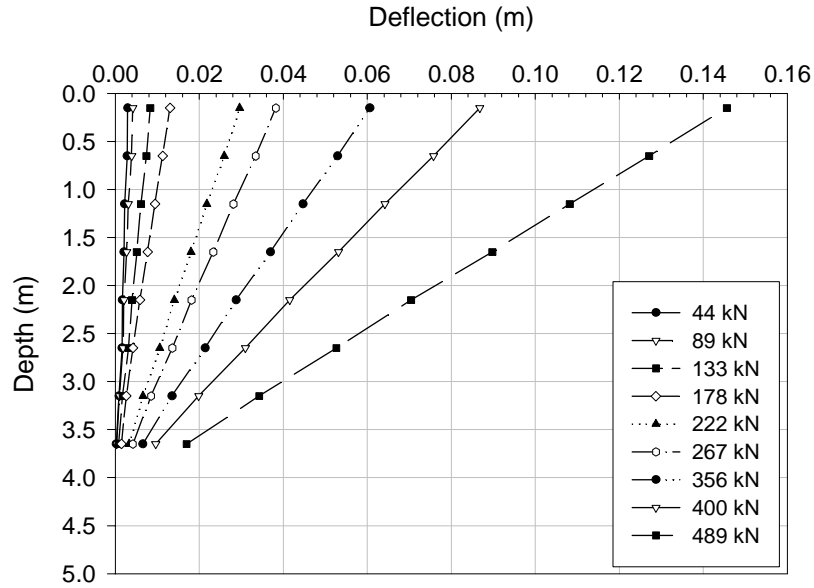
Figure 37. (a) Deflection Profile from Slope Inclinometer Readings -Short Shaft
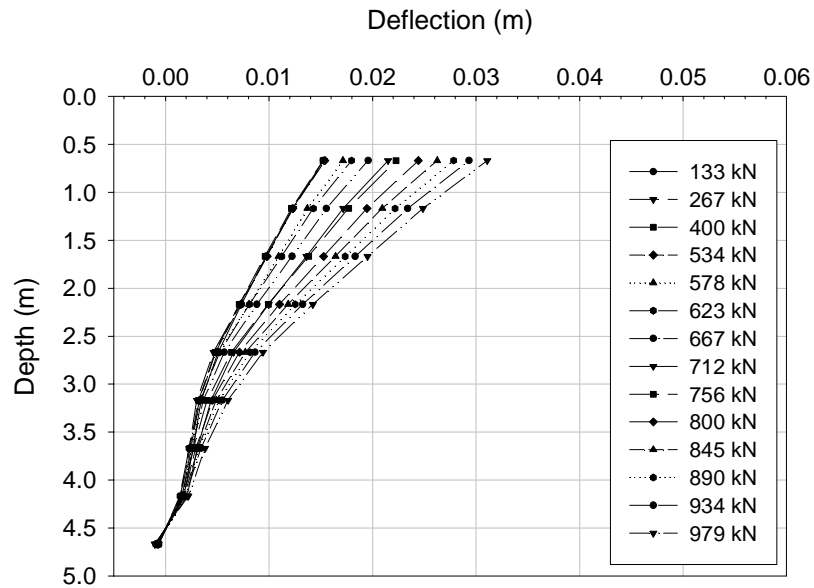
Figure 37. (b) Deflection Profile from Slope Inclinometer Readings - Long Shaft

4.2.4.2 Back-calculated P-y Curves

Strain measurements from vibrating wire strain gages were recorded by a readout box. From the measured strains, moments were calculated along the depth of the two shafts by piece-wise numerical integration. The soil reaction, P, calculated in kN/m, was determined using the calculated moment and EI (elastic modulus × moment of inertia) of

868630 kN-m^2. The y, measured in meters, was obtained from the inclinometer data. Figure 38 and Figure 39 show the estimated P-y curves in the WR region as calculated from the strain gages for the long and short shafts, respectively.
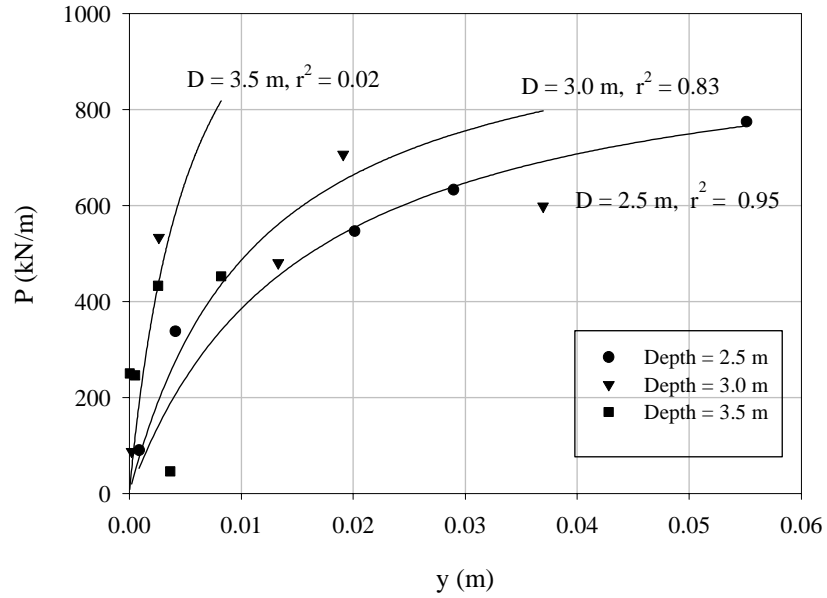
Figure 38. Back-calculated P-y Curves for the Weathered Rock – Short Shaft
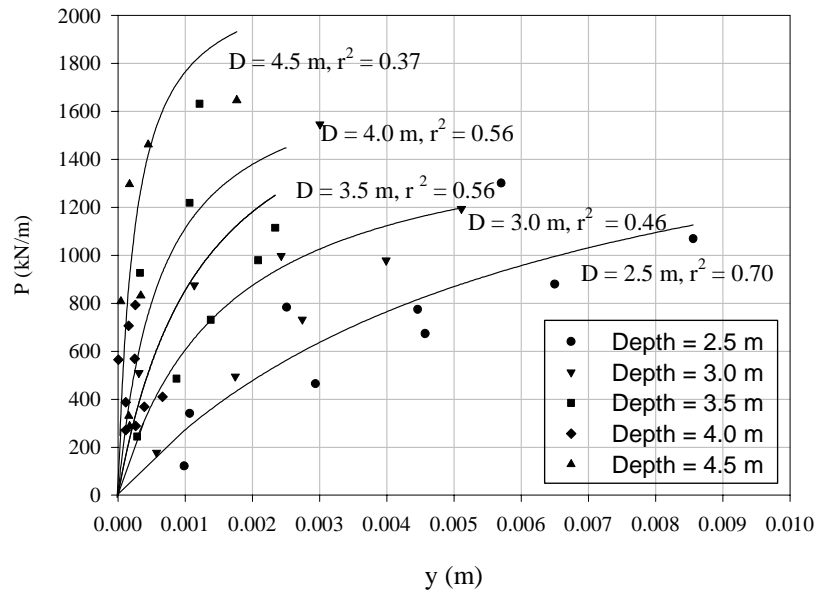
Figure 39. Back-calculated P-y Curves for the Weathered Rock – Short Shaft

4.2.4.3 Verifying Back-calculated P-y Curves

Using the P-y curves back-calculated from the strain gages, analyses were performed using the computer program BMCOL 76 to predict the shaft top deflection and compare with field measurements using dial gages. As shown in Figure 40, the calculated shaft-top deflection, determined from BMCOL 76, shows good agreement with measured data, with computed results yielding slightly less deflection.
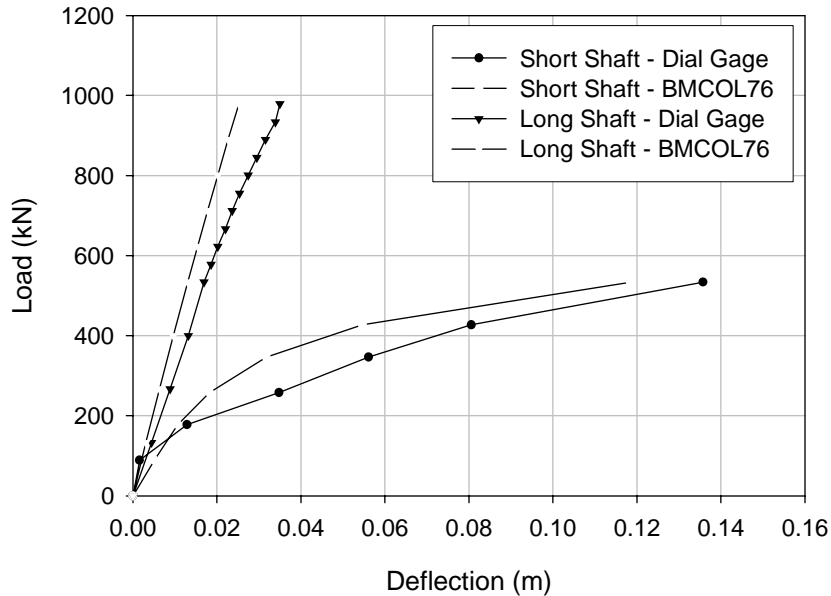
Figure 40. Verifying Back-calculated P-y Curves

4.3 Caldwell County Load Tests

This site is located in southern Caldwell County approximately one mile north of the town of Granite Falls. The lateral load tests were performed at a roadway widening project site that included a bridge replacement project.

Prior to performing load tests on these shafts, the test area roughly, 10.67 meter × 3.05 meter was excavated approximately 1.0 – 1.5 meter deep, as shown in Figure 41. This excavation removed soil layers above the weathered rock, so the entire lengths of the short and long shafts were embedded in weathered rock. Figure 42 shows the exposed rock profile at the test surface level. Figure 43 shows a photograph of the loading frame and constructed shaft with surface instrumentation.

Figure 41. Constructed Test Shaft and Excavated Test Site

Figure 42. Exposed Rock Profile at the Test Site Surface

Figure 43. Load Test Frame and Instrumentation Set-up Profile

4.3.1 Geology

Alluvium, sandy saprolite, weathered rock, and hard rock comprise the foundation materials that were encountered in the borings. The test area is underlain by a Cenozoic age biotite gneiss and schist rock unit of the Inner Piedmont Belt. Core borings revealed that locally much of the rock is granetiferous. This was also the case for the weathered rock horizon, though its extent was greater than the saprolite. Tan to brown medium dense silty to fine coarse sand, and micaceous residual material existed over a weathered rock layer. Figure 44 shows a subsurface profile near test site with RQD and % recovery values noted on the figure. The boring log at the exact test shaft location is shown in Appendix D.

4.3.2 Geotechnical Properties of Test Site

Two boring logs were performed in the vicinity of the test shafts. Rock dilatometer tests were also performed within the cored holes. Data indicated that the boring logs at the locations of long and short shafts were almost identical. No groundwater was encountered during the subsurface investigation. Beneath the residual soil, a weathered gneiss rock graded into a hard weathered rock and finally into a competent high RQD quality rock around a depth of 10.7 meters below the ground surface.
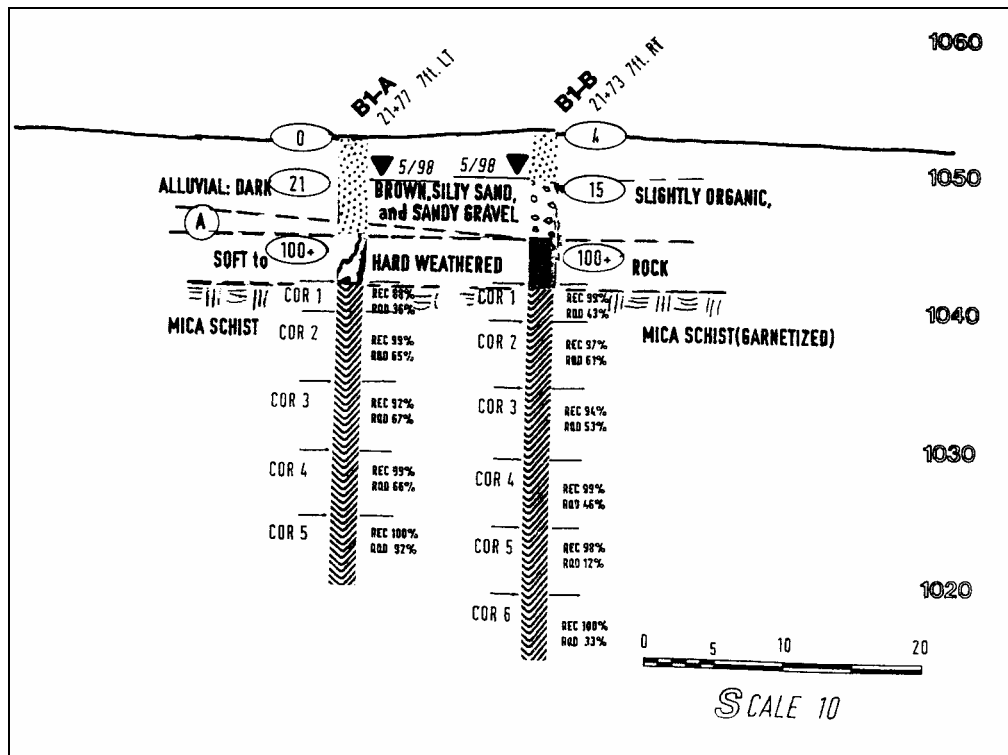
Figure 44. Test Area Subsurface Cross-section

The core size was "H" in order to increase chances of a better recovery. Most of the core samples had poor RQD values (RQD < 30 %) which can be classified as weathered rock.

All weathered rock core samples were inspected and specific samples were chosen for lab testing. Only two (2) samples were chosen for testing at the NCDOT, Materials and Test Unit laboratory due to poor coring. Table 14 summarizes the lab testing results. Rock core boring report is included in Appendix D.

Table 14. Caldwell County Laboratory Test Results

Depth (m)	Unit Weight (kN/m³)	Qu (kPa)	RQD (%)
9.7 – 9.2	26.67	59,128	30
9.92 – 10.05	27.01	61,578	27

4.3.3 Description of Test Shafts

Similar to the Nash County test, two drilled shafts 0.762 meter in diameter were constructed 7.62 meter apart. However, in this case, the short shaft was embedded approximately 4.0 meters, and the long shaft was embedded 4.8 meter. Both shafts were constructed with approximately 1.5-2.0 meter above the ground surface to facilitate attachment of the lateral load frame and subsurface instrimentation. The layout of these shafts is almost the same as the Nash-Halifax County test configuration shown in Figure 31.

Sixteen strain gages were used for the two shafts, seven for the short shaft and nine for the long shaft. The strain gages were installed with near uniform spacing of 0.5 meter.

4.3.4 Load Test Results

During testing, the short shaft experienced 0.089 meter of lateral displacement while the long shaft deflected 0.023 meter under the maximum load of 1334 kN. This load was approximately equal to the allowable load capacity of the test frame.

4.3.4.1 Top Deflections and Inclinometer Readings

The load-deformation response was obtained at the top of each shaft during incremental lateral loading. The top displacements of the short and long shaft are shown in Fig. 45. Although both shafts experienced some nonlinear response, neither reached their ultimate resistance under the maximum load of 1334 kN.

Initial large displacements were observed from dial gage measurements for both the long and short shafts, respectively, as shown in Figure 45. The presence of poor contact between the drilled holes and the shafts is evident by the concave shape of the load-deflection curves, as marked in Figure 45.
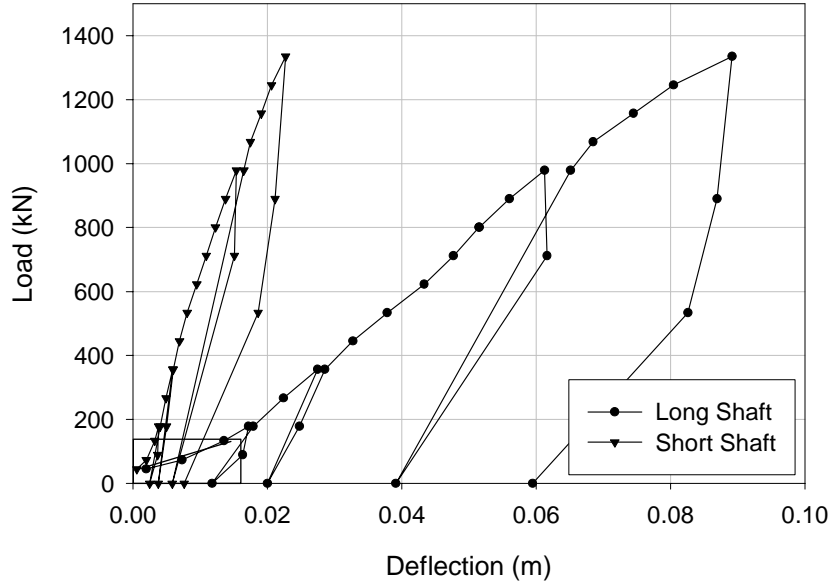
Figure 45. Top Displacements of Short and Long Shafts, Measured from Dial Gages

The interpreted data obtained from the continuous inclinometer measurement system in each shaft during loading is shown in Figures 46 (a) and (b). The short shaft behaved as a rigid body, with a linear displacement profile along the shaft's full length as shown in Figure 46(a). The long shaft behaved as an element with restrained tip, as indicated by the non-linear displacements along its length shown in Figure 46 (b).

4.3.4.2 Back-calculated P-y Curves

Strain measurements were collected using a CR-10 data logger attached to the vibrating wire strain gages. Figures 47 and 48 show the P-y curves back-calculated from the strain gage data for the long and short shafts, respectively. As observed before from the dial gage top-deflection measurements, initial non resisted deflection increments were observed from back-calculated P-y curves due to non-solid contacts.

The back-calculated P-y curves from the short shaft show non-linear response as shown in Figure 47. However, the P-y curves in Figure 48 for the long shaft are plotted as linear, since the load test yielded small deflections. Figures 47 and 48 have different scales for load and deflection axes due to the very different load-resistance characteristics. As shown in Figures 47 and 48, the k_h values increase with depth.
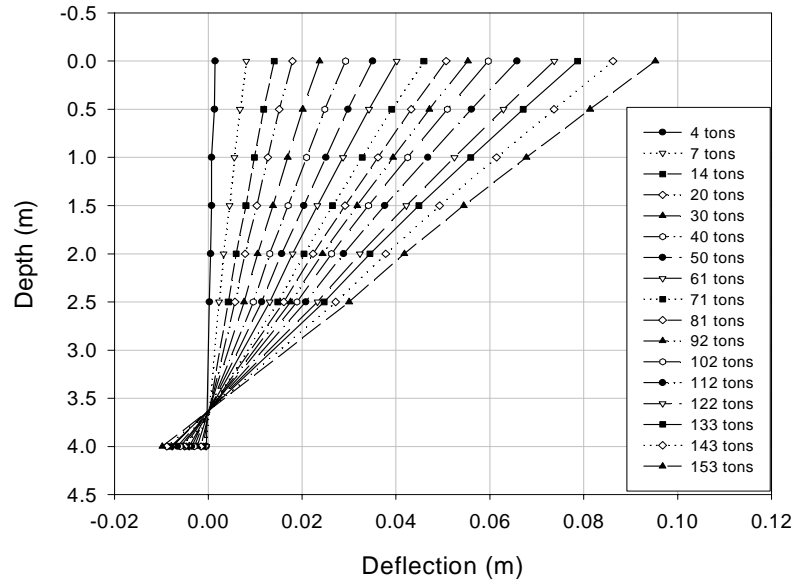
Figure 46. (a) Deflection Profile from Slope Inclinometer Readings - Short Shaft
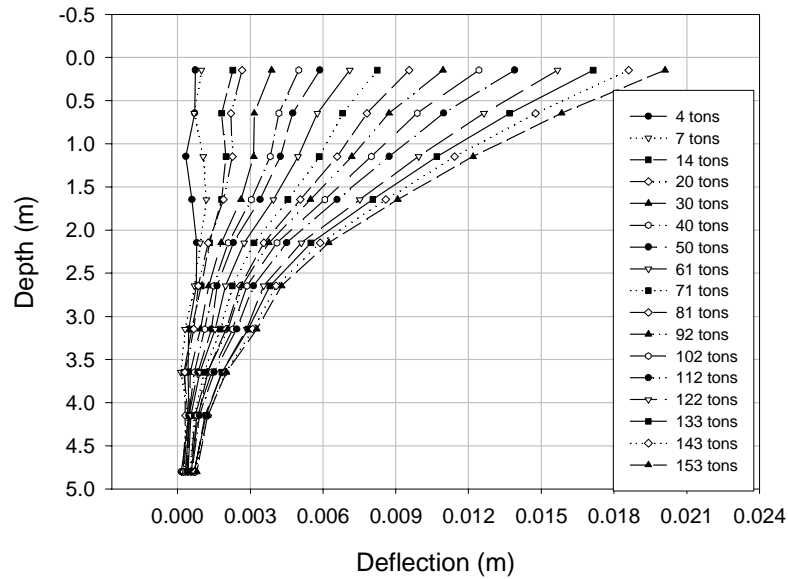
Figure 46. (b) Deflection Profile from Slope Inclinometer Readings - Long Shaft

However, the initial slope of curve related to k_h in P-y curves near the rotation point do not show clear incremental increases in k_h values with depth due to the very small deflections of shafts, especially in the short shaft.
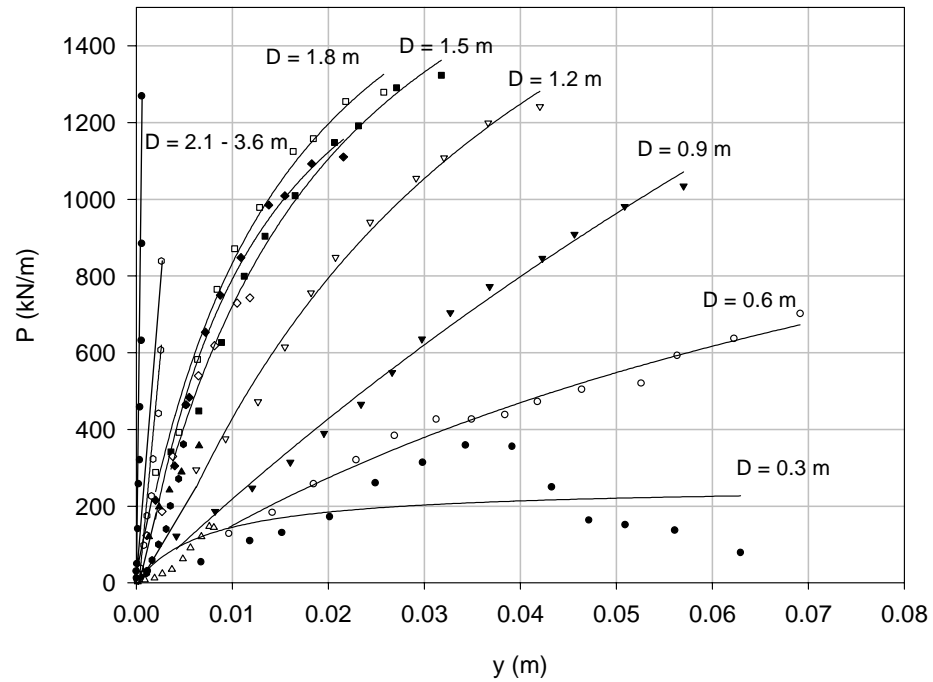
Figure 47. Back-calculated P-y Curves for the Weathered Rock – Short Shaft
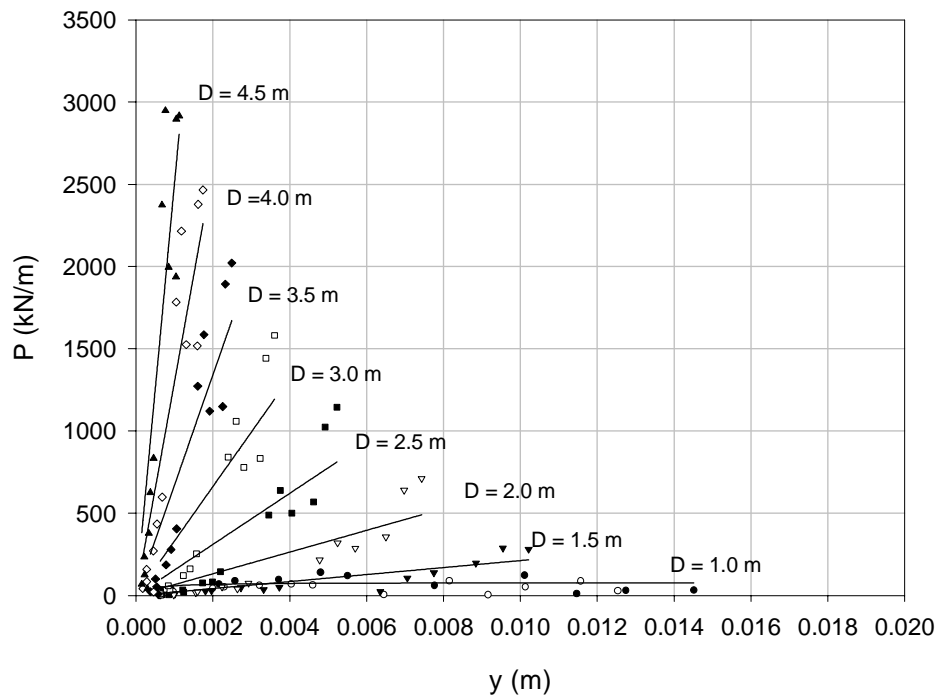
Figure 48. Back-calculated P-y Curves for the Weathered Rock – Long Shaft

4.3.4.3 Verifying Back-calculated P-Y Curves from Strain Gages

Using back-calculated P-y curves from the strain gages, top deflection of the test shafts were computed using the computer program BMCOL 76 and compared with deformation data from the dial gages. As shown in Figure 49, the deflection at the top of the shafts calculated from BMCOL 76 shows good agreement with measured data, with calculated results yielding slightly smaller deflections. The back-calculated P-y curves from the short shaft used as input data for BMCOL76 analysis were adjusted by removing the "free deformation" data points due to non-solid contacts. The non-solid contact deflection data from the dial gage measurements at the top of the short shaft were also adjusted.
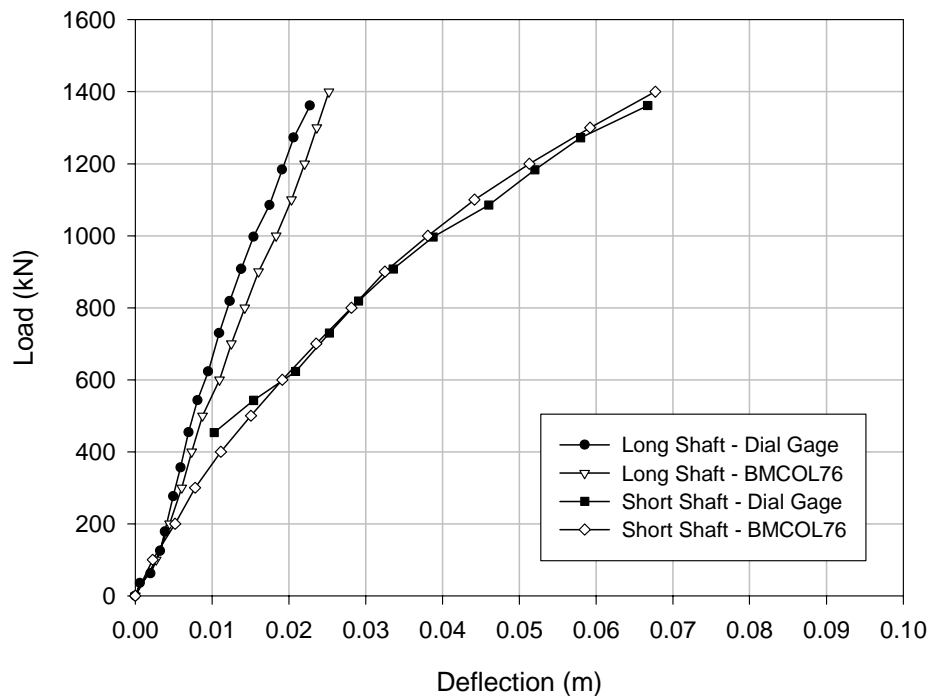
Figure 49. Verifying Back-Calculated P-y Curves

4.4 Wilson County Load Tests

This test site is located on NC 42, in southern Wilson County, approximately one mile west of the city of Wilson. The load tests were performed at a roadway straightening site around a bridge replacement project.

Prior to load testing, the test area roughly, 10.67 meter × 3.05 meter was excavated approximately 2.0 – 2.5 meter to remove most of soil above the weathered rock. Accordingly, the entire length of the short and long shafts were embedded in weathered rock. Figure 50 shows exposed weathered rock at the test surface level. A water pump was installed to pump-out inflow water to the test area, as the surface elevation was lower than the ground water table. Figure 51 shows a photograph of the loading frame and instrumentation set-up.

Figure 50. Exposed Weathered Rock at the Test Site Surface

4.4.1 Geology

In general, tan brown fine to coarse sand, weathered crystalline rock, and hard rock comprised the foundation materials that were encountered in test borings at the site. Alluvial material occurred to a variable extent. Rock was cored at two borings. It was found that this test site provided different subsurface profiles at the locations of the short and long shafts. This observation was also confirmed by the results of the rock dilatometer tests.

Figure 51. Loading Frame and Instrumentation Set-up

Those differences are shown in the rock core report attached in Appendix D. Figure 52 shows the subsurface profile (B2-B) near the test location. Boring logs at the locations of each shaft are provided in Appendix D.
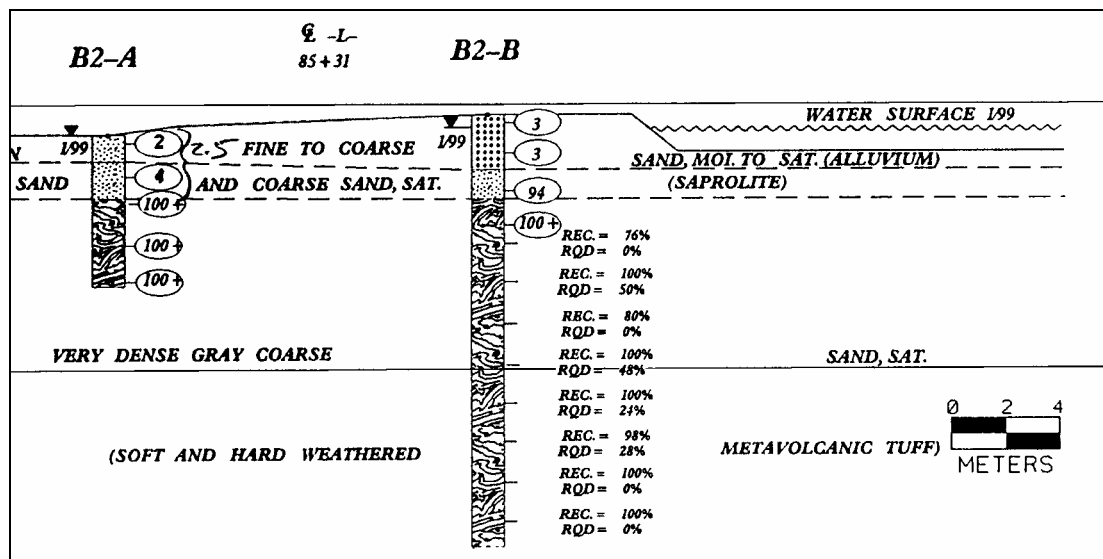
Figure 52. Test Area Subsurface Cross-section

4.4.2 Geotechnical Properties of Test Site

Two borings were performed at the location of test shafts groundwater was encountered almost near the ground surface. Beneath the alluvium, weathered crystalline rock was found, which graded into a weathered rock and finally into a competent high RQD quality rock around a depth of 9.1 meters below the ground surface (Appendix D).

The residual soil layer existed from the surface to a depth of approximately 2.4 meters. All weathered rock core samples were inspected and specific samples were chosen for lab testing. Only two (2) samples were tested; one each from the short and long shaft locations, respectively. Table 15 summarizes the lab test results. The short shaft location had higher RQD value (59 %) in comparison to the value of 13 % estimated at the long shaft location.

Table 15. Wilson County Laboratory Test Results

	Depth (m)	Unit Weight (kN/m^3)	Qu (kPa)	RQD (%)
Long Shaft	3.2-4.7	26.67	57,578	13
Short Shaft	3.0-4.5	27.01	62,567	59

4.4.3 Description of Drilled Shaft

The short shaft was embedded approximately 4.85 meters, and the long shaft was embedded 5.71 meter. The layout of these shafts is also similar to the Nash-Halifax County tests (shown in Figure 31). During the dilatometer tests, a collapse of the boring walls was experienced due to having weathered rock below the ground water table. In order to prevent hole collapse during shaft construction, steel casings were inserted, followed by augering. The drilled holes were constructed by first drilling approximately 1 meter, and then screwing the steel casing to the bottom of the hole. This procedure was repeated numerous times until the bottom of the proposed shaft was reached. Therefore, the contact between the weathered rock and the casing was solid.

Sixteen strain (16) gages were used for the two shafts, seven (7) for the short shaft and nine (9) for the long shaft. The strain gages were installed with approximately uniform spacing along the expected tension side of the shafts.

4.4.4 Load Test Results

During testing, the short shaft experienced 0.034 meters of shaft-top lateral displacement while the long shaft deflected 0.055 meter under the maximum load of 1681 kN.

4.4.4.1 Top Deflections and Inclinometer Readings

The load-deformation response at the top of each shaft was obtained during incremental lateral loading from the dial gage measurement system. The top displacements of the short and long shaft are shown in Figure 53.

The long shaft exhibited non-linear top deflection under the applied load of 1548 kN. However, the top deflection of the short shaft showed only slight non-linearity with loading. The reason for the different responses may be explained by the different geological conditions, as was shown in rock core reports.

Using the continuous inclinometer system previously described, deflection profiles along each of the shafts were measured. According to the inclinometer-measured deflection profile, both shafts behaved as partially fixed, as indicated by the non-linear displacements along their length. Refer to Figure 54 (a) and (b).

4.4.4.2 Back-calculated P-y Curves

Strain measurements from the vibrating wire strain gages, attached to vertical reinforcement with sister bars, were recorded by a CR-10 data logger. From the measured strains, moments were calculated along the depth of the two shafts by piece-wise numerical integration using the same procedure used for the Nash-Halifax County data analysis. Figures 55 and 56 show the back-calculated P-y curves for the long and short shafts, respectively.
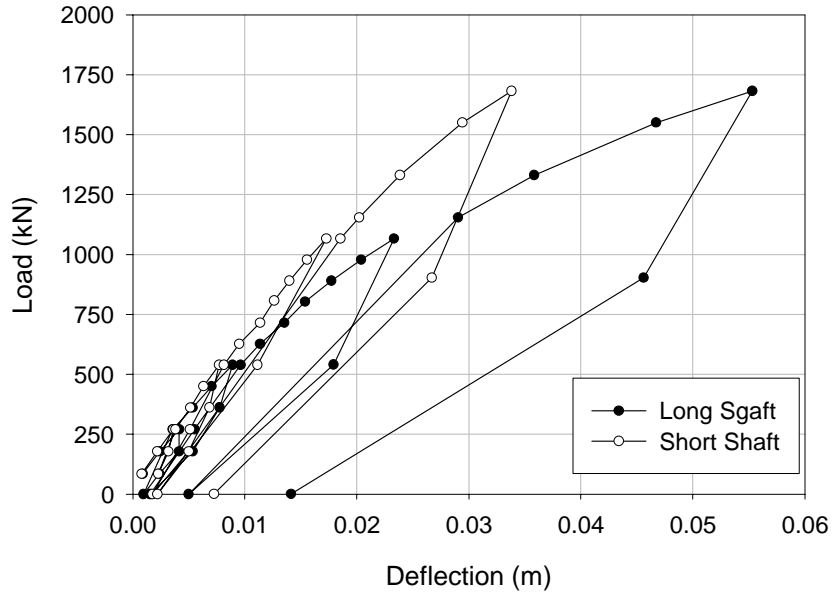
Figure 53. Top Displacements of the Short and Long Shaft Measured from Dial Gages
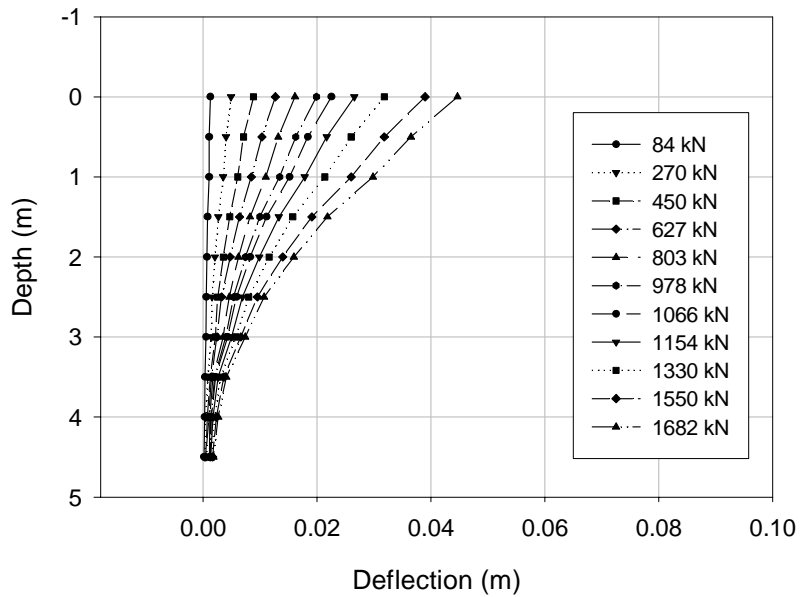
Figure 54. (a) Deflection Profile from Slope Inclinometer Readings -Short Shaft
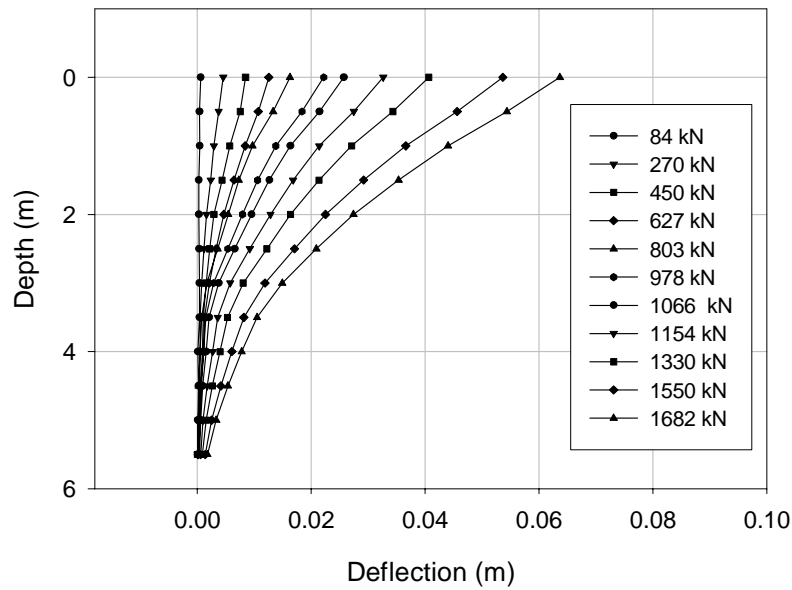
Figure 54. (b) Deflection Profile from Slope Inclinometer Readings - Long Shaft

As shown in these figures, the lateral load resistances calculated for the short shaft are higher than those for the long shaft. This behavior is in concert with the geological profiles and results from dial gage measurements.
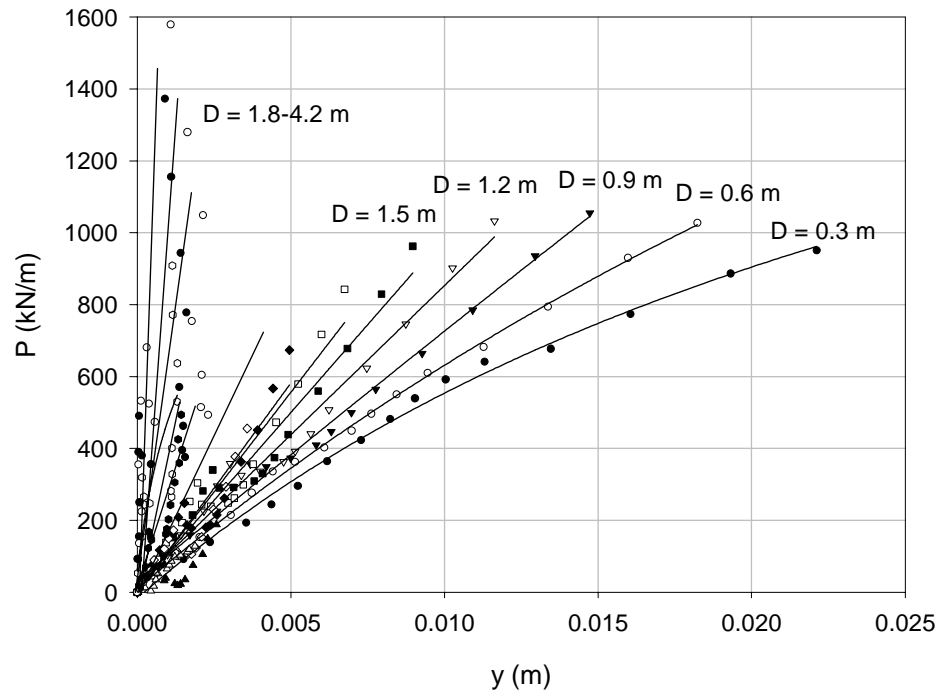
Figure 55. Back-calculated P-y Curves for the Weathered Rock – Short Shaft
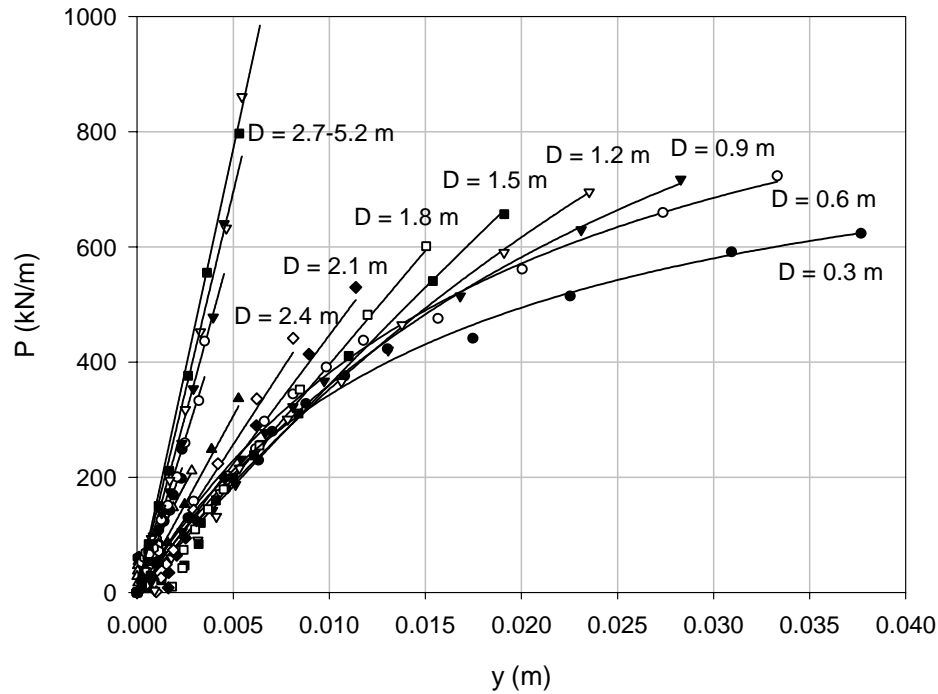
Figure 56. Back-calculated P-y Curves for the Weathered Rock – Long Shaft

Most of back-calculated P-y curves from the short shaft show a nearly linear response. For the longer shaft, only the P-y curves within the top 1.2 m of the profile show a non-linear response. Below this depth, the P-y curves also plot an essentially linear, because the test load did not produce enough deflection to reach the non-linear range of the P-y curves. Figures 55 and 56 have different scales for load and deflection axes due to different load-resistance characteristics. As shown in Figures 55 and 56, the k_h values increase with depth. However, the initial slope of curve related to k_h in P-y curves near the rotation point do not show clear incremental increases of k_h value with depth due to very small shaft deflections.

4.4.4.3 Verifying Back-calculated Results from Strain Gages

Using the back-calculated P-y curves from the strain gages, analyses were performed using the computer program BMCOL 76 and compared with the dial gage measurement data. As shown in Figure 57, the deflections calculated using the BMCOL

85

76 at the top of the long and short shafts, respectively, show good agreement with measured data.
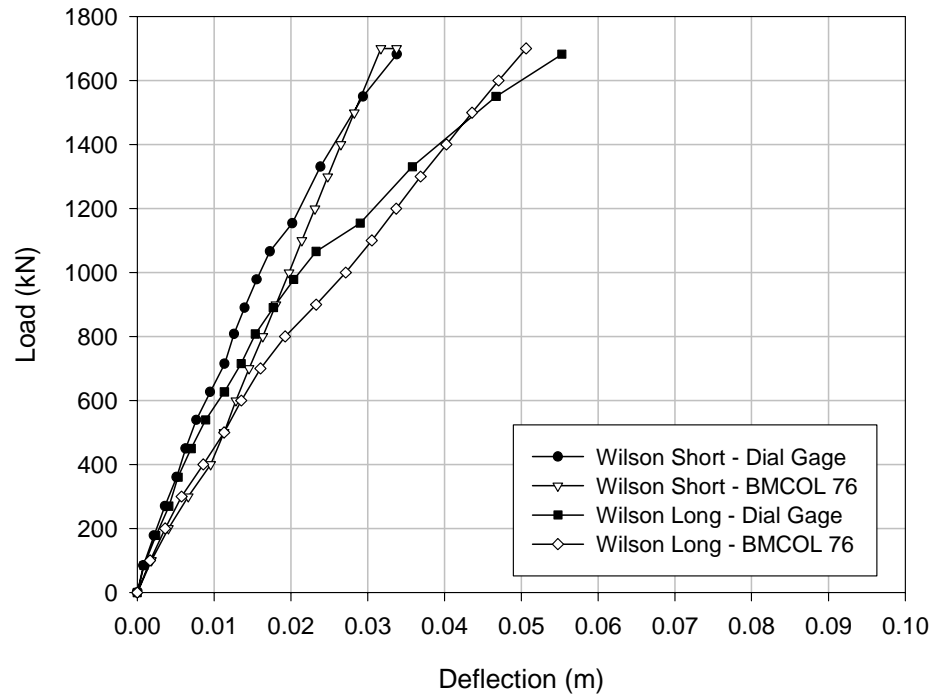
Figure 57. Verifying Back-calculated P-y Curves

4.5 Rock Dilatometer Testing

Field rock dilatometer tests were conducted as summarized in Table 16. The rock dilatometer was inserted into the borehole and test performed as a function of depth to obtain pressure-volume relationships within the soil, transition zone, and rock profile. The expanded volume of the membrane was measured by a digital read-out box, and the applied pressure was monitored through pressure gages attached to a hand pump.

Figures 58 and 59 show the results from tests at the Caldwell County test site. Other rock dilatometer test results are attached in Appendix B

Table 16. Rock Dilatometer Test Sites and Rock Type

Test Site	Rock Type
Nash County	Meta-Argillite Rock
Caldwell County	Gneiss
Durham County	Sandstone
Wilson County	Crystalline Rock
Wake County	Silty-Sandstone
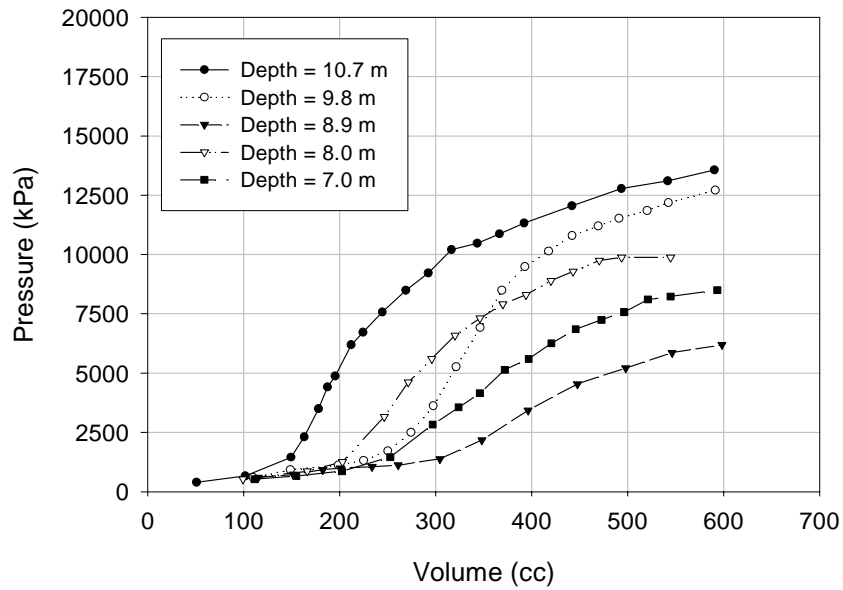
Figure 58. Rock Dilatometer Test Results (Pressure vs. Volume) – Caldwell Site A
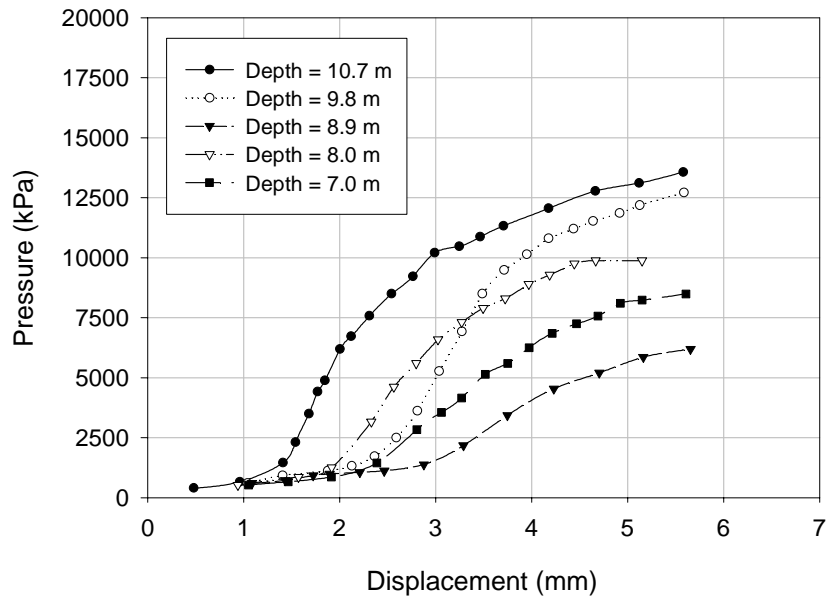
Figure 59. Rock Dilatometer Test Results -Caldwell Site A

4.6 Summary

Full-scale lateral load tests were completed on six (6) drilled shafts embedded in weathered rock. The test shafts were 0.762 m in diameter and varied in length from approximately 3.4m to 5.7 m.   Site characterization was performed at each test site and the instrumented drilled shafts were tested under lateral load in order to obtain data for the development of field P-y curves. Table 17 presents a summary of test results and characteristics of test sites. These results will be used to develop and validate a procedure for the design and analysis of laterally loaded drilled shafts embedded in the weathered rock profiles.

Eight rock dilatometer tests were performed in Nash, Wake, Caldwell, Durham, and Wilson counties. The resulting pressure versus volume curves will be used to back-calculate lateral modulus; a parameter need for the construction of P-y curves

Table 17. Summary of Field Load Tests

	Nash County		Caldwell County		Wilson County	
	Short Shaft	Long Shaft	Short Shaft	Long Shaft	Short Shaft	Long Shaft
Length (m)	3.35	4.57	4.0	4.8	4.85	5.71
Max. Load (kN)	534	979	1334	1334	1681	1681
Max Shaft-Top Deflection (m)	0.135	0.036	0.089	0.023	0.034	0.055
RQD (%)	<25	<25	<30	<30	≈ 60	≈ 15
Rock Type	Meta- Argillite		Gneiss		Crystalline	

CHAPTER 5. P-y Model FOR WEATHERED ROCK

5.1 P-y Curve Function

Analysis of test data and the development of a P-y curve model for weathered rock are presented in this chapter. The P-y curve development is based on F.E.M. analysis, and a combination of results obtained from laboratory testing and field lateral load tests. While there are many potential mathematical functions to represent non-linear curves (such as power, exponential, and hyperbolic functions) past research has suggested, in general, power or hyperbolic functions as appropriate for representation of P-y curves in soil. In this chapter, an appropriate form of P-y curves in weathered rock will be investigated and proposed. As the hyperbolic function can be expressed in terms of lateral modulus and ultimate lateral resistance, the analyses herein focused on the hypothesis that "P-y curves in SWR can be represented by a hyperbolic function".

For the proposed hyperbolic function, two parameters, the subgrade modulus (k_h) and the ultimate resistance (P_{ult}) are needed. The parameter, k_h, represents the initial tangent modulus of the P-y curve and can be back-figured from measured field values. However, the ultimate resistance (P_{ult}) will be estimated from curve fitting extrapolation, due to inability to achieve deformations large enough to develop ultimate resistance in the field.

Figure 60 shows the typical shape of a hyperbolic curve. The form of the function is as follows:

$$P = \frac{y}{a + by} \tag{46}$$

Where, $a = \dfrac{1}{k_h}$;

k_h = initial tangent modulus of P-y curve (subgrade modulus);

$b = \dfrac{1}{P_{ult}}$; and,

P_{ult} = ultimate lateral resistance.
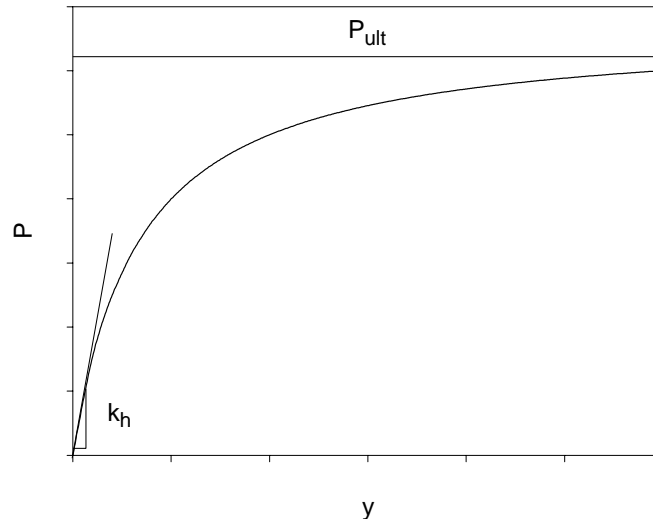
Figure 60. Shape of Assumed P-y Curve (Hyperbolic Curve)

Equation 47 can be rearranged into the form,

$$\frac{y}{P} = a + by \qquad (47)$$

This function indicates that the back-calculated P-y curve data plotted in y/P versus y space should be a linear function which has intercept, a, and slope, b, as shown in Figure 61. As described on Figure 61, the parameter "a" is equal to $1/k_h$ and "b" is equal to $1/P_{ult}$ (Kondner et al., 1963).
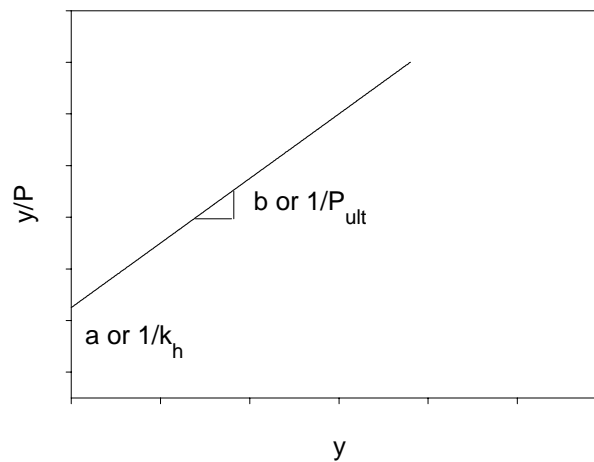
Figure 61. Transformed Hyperbolic Curve

5.1.1 Curve Fitting of Laboratory Tests Data

The hyperbolic curve fitting procedure was applied to the measured laboratory data down to the point of rotation of the model pile. The data at depth close to the rotation have very small deflections, which generate large errors in curve fitting, as deflections are divided by resistance, P. Accordingly, curve fitting was performed at each depth, excluding those around the point of rotation. For these small deflection points, the hyperbolic parameters were interpolated based on values determined from other depths above and below the point of rotation. Figures 62, 63, and 64 show transformed hyperbolic plots for depths of 0.15 m, 0.36 m, and 0.86 m, respectively. As shown in Figures 62, the regression lines have relatively high r^2 values around the top of the model shaft. Accordingly, the hypothesis of hyperbolic function seems to be valid for the simulated WR material at such depth. However, for areas around the point of rotation, wider scatter is observed, as shown in Figures 63 and 64, and deformation levels do not provide the full shape of P-y curves. Given the simplicity of hyperbolic function, such a function is used to represent P-y curves along the entire length of the model shaft.
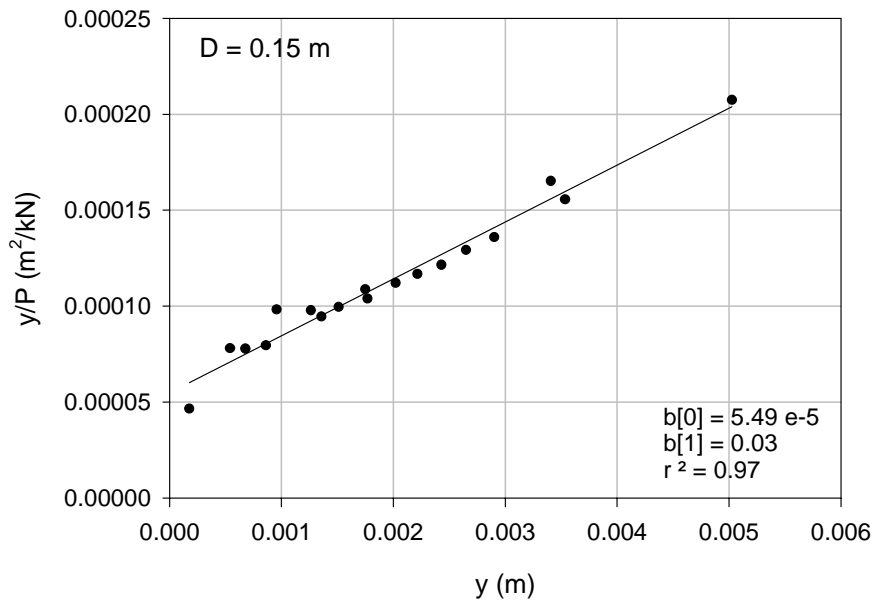
Figure 62. Curve Fitting Laboratory Tests (No Surcharge, Depth = 0.15m)

The evaluated P-y curves shown in Figure 28 (Chapter 3 - Laboratory Tests) indicated an increase in lateral stiffness with depth as well as increase in lateral resistance. At shallow depths, a P_{ult} was defined at a deformation level of approximately 0.076 meters. This is

equivalent to approximately 10% of the test pile diameter. After approximately 0.305 meter of pile embedment, it was hard to obtain such a level of deformation, and so only the initial slope of the P-y curves could be reasonably evaluated.
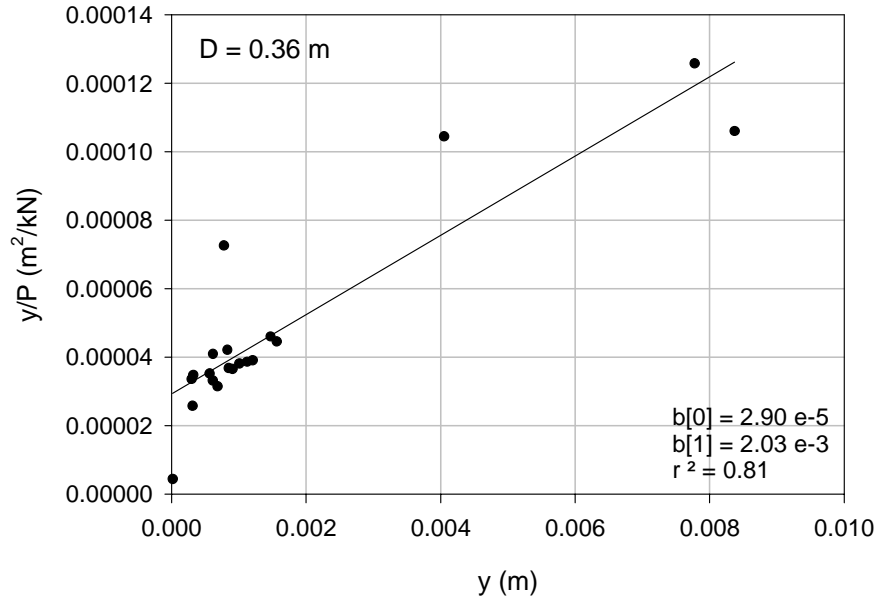
Figure 63. Curve Fitting Laboratory Tests (No Surcharge, Depth = 0.36m)
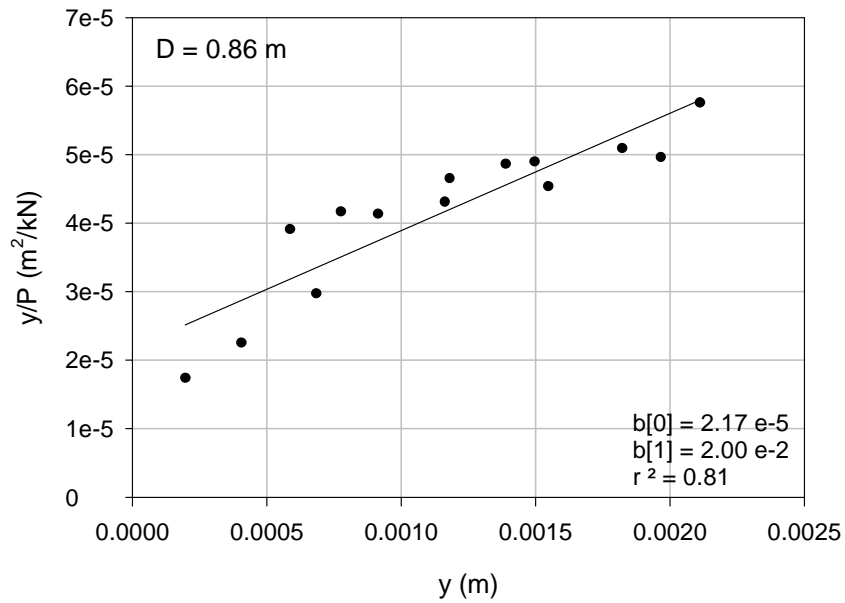
Figure 64. Curve Fitting Laboratory Tests (No Surcharge, Depth = 0.86m)

P-y results from the laboratory test with surcharge showed a trend similar to data shown in Figure 29 (Chapter 3 - Laboratory Tests). In the case of the surcharged test, the load-induced deformation was not large enough to achieve a P_{ult} value at any depth. However, the initial stiffness of the P-y curve corresponded well with the confining stress, whereby higher lateral stiffness values were obtained with increasing confining stress. A detailed analysis of these data is presented later. The overall conclusion from the laboratory test results is that the shape of P-y curves obtained from simulated weathered material can be reasonably represented by a hyperbolic function.

5.1.2 Curve Function Based on Field Tests

The back-calculated P-y curves from field tests were used to validate the hyperbolic function proposed for the P-y model in weathered rock. Figures 65 through 70 show hyperbolic curve fitting for two depths at each of the three field test sites. As explained before, the curve fitting procedure near the point of rotation was not robust due to small deflection magnitudes. Figures 65 and 66, Nash County data, are for depths of 2.5 m and 3.5 m, since the WR layer existed below a depth of 2.5 m. Figures 67 and 68, are for Caldwell County tests, and show curve fittings at depths of 0.6 m and 3.3 m, respectively. As shown in the Figures 65 through 70, the regression procedure produced correlations with relatively high r^2 values, on the order of 0.95, for both shallow and deeper depths of P-y curves. Figures 69 and 70, for Wilson County tests, shows r^2 value of 0.96 at a depth of 0.6 m, but at 3.9 m, the regression curve fitting has an r^2 value of 0.71. The rest of hyperbolic curve fitting figures are shown in Appendix E. According to the results of the curve fitting procedures, the proposed hyperbolic function seems to reasonably model the field-estimated P-y curves r^2 range from 0.5-0.99).
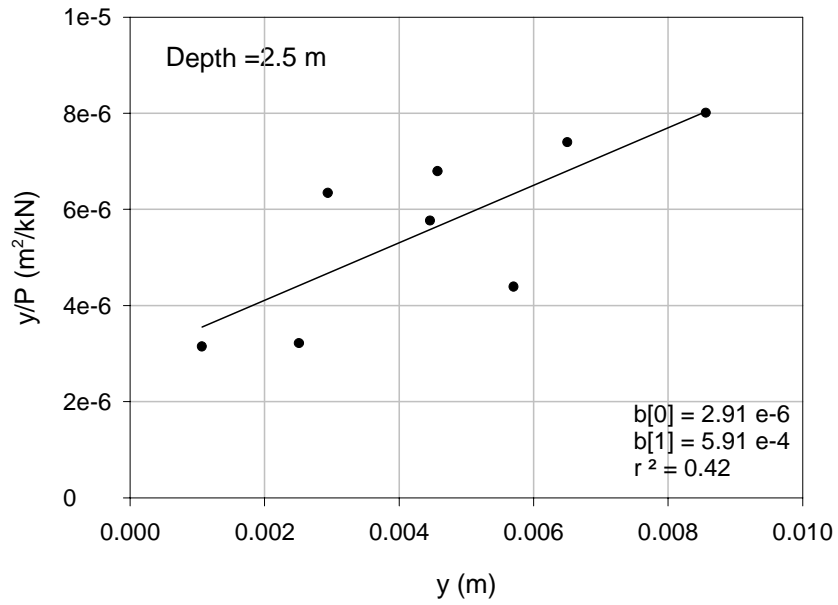
Figure 65. Curve Fitting Field Tests – Nash Long Shaft (Depth = 2.5m)
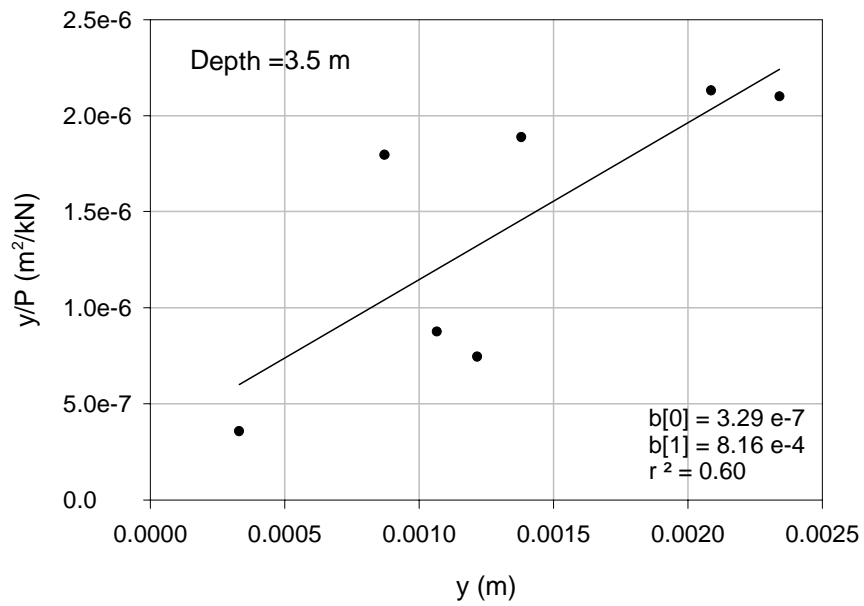
Figure 66. Curve Fitting Field Tests – Nash Long Shaft (Depth = 3.5m)
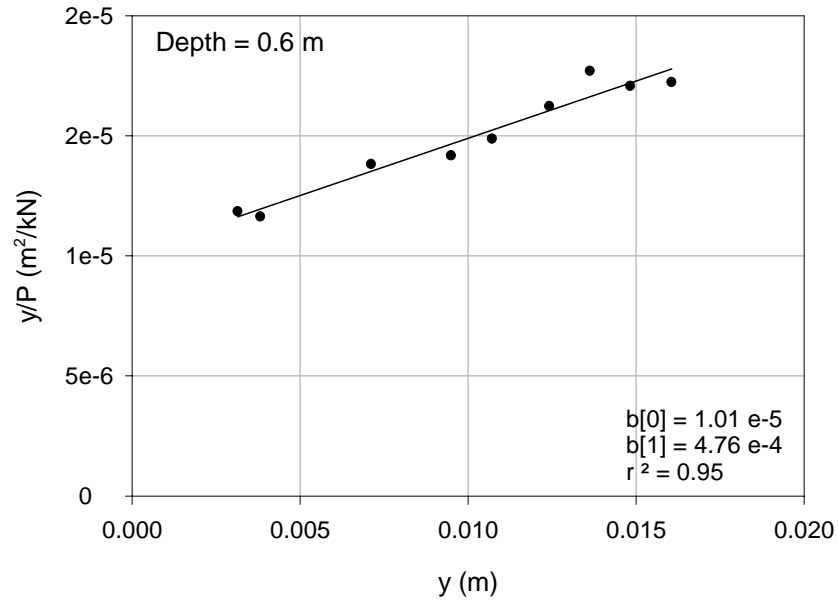
Figure 67. Curve Fitting Field Tests – Caldwell Long Shaft (Depth = 0.6m)
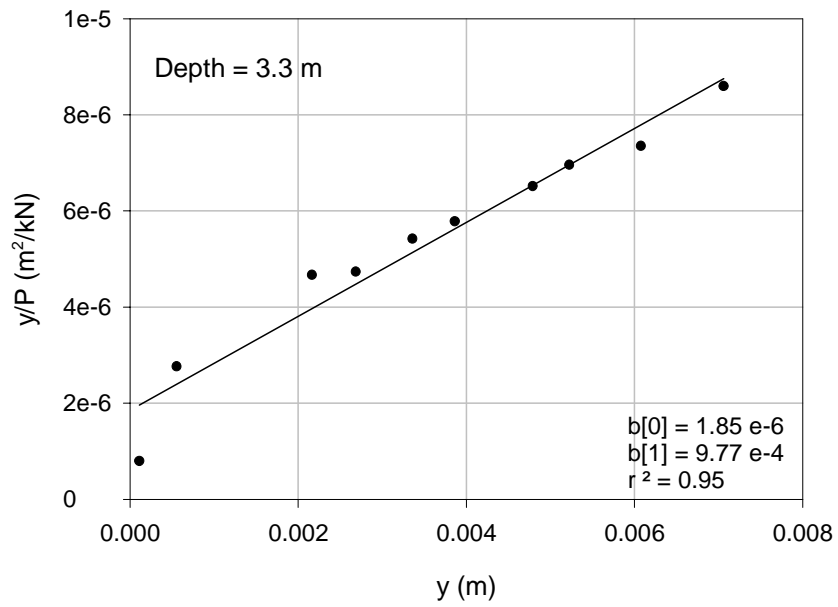
Figure 68. Curve Fitting Field Tests – Caldwell Short Shaft (Depth = 3.3m)
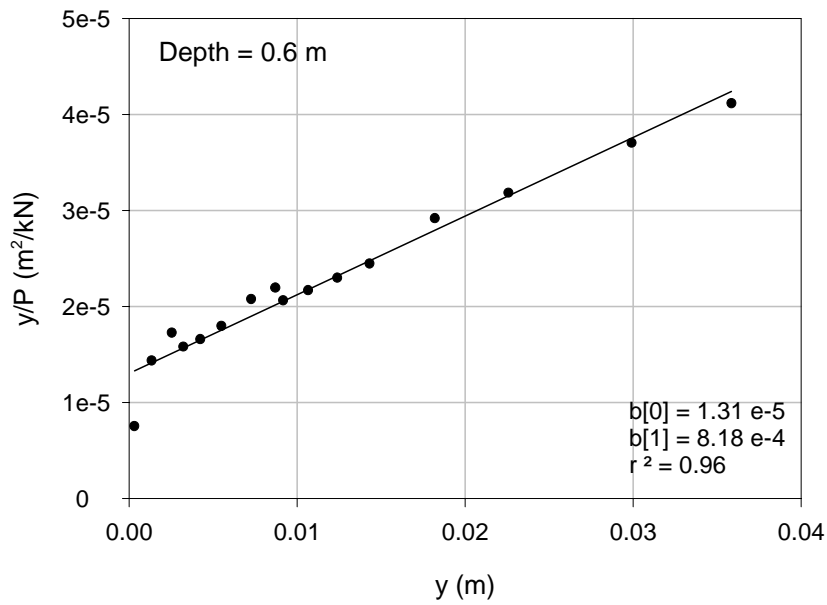
Figure 69. Curve Fitting Field Tests – Wilson Long Shaft (Depth = 0.6m)
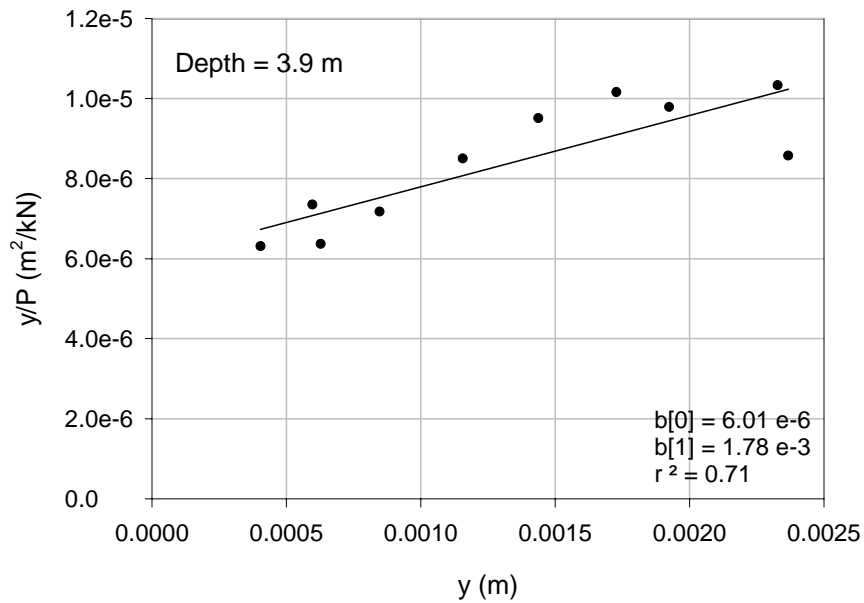
Figure 70. Curve Fitting Field Tests – Wilson Long Shaft (Depth = 3.9m)

The process of curve fitting back-calculated P-y curves from laboratory and field tests provided a basis for selecting an appropriate function to express the P-y curve for

weathered rock. Based on the results of the analysis, a hyperbolic function seems to be appropriate in this case.

5.2 Subgrade Modulus (k_h) for Weathered Rock

There is a dearth of data on the modulus of subgrade reaction in weathered rock. Based on data obtained in this study, the "a" parameter specified in equation 47 and back-figured from hyperbolic curve fitting (noted in Figures 62 through 70 as b[0]) was used to compute k_h value. The k_h value from data presented herein can be obtained either by taking the inverse of the 'a' parameter, or taking tangent slope of back-calculated P-y curves at a prescribed deformation or load level. The k_h value and its distribution will be investigated in this chapter.

5.2.1 Subgrade Modulus (kh)

Terzaghi (1955) considered k_h (F/L^2) to be directly proportional to the depth and independent of the diameter. On the other hand, he indicated that a coefficient of subgrade reaction k_{ho} (F/L^3) was proportional to diameter, where a larger pile diameter yielded a lower coefficient of subgrade reaction. Validity was granted to this hypothesis by Prakash (1962) when he demonstrated this assumption on a model scale. However, Prakash also indicated the actual variation of k_h with depth is not fully linear but grew with depth in a nonlinear fashion, as indicated in Figure 71 (a and b).

(a) Preloaded Cohesive Soil   (b) Granular Soils, Normally
                                                    Loaded Silts and Clays
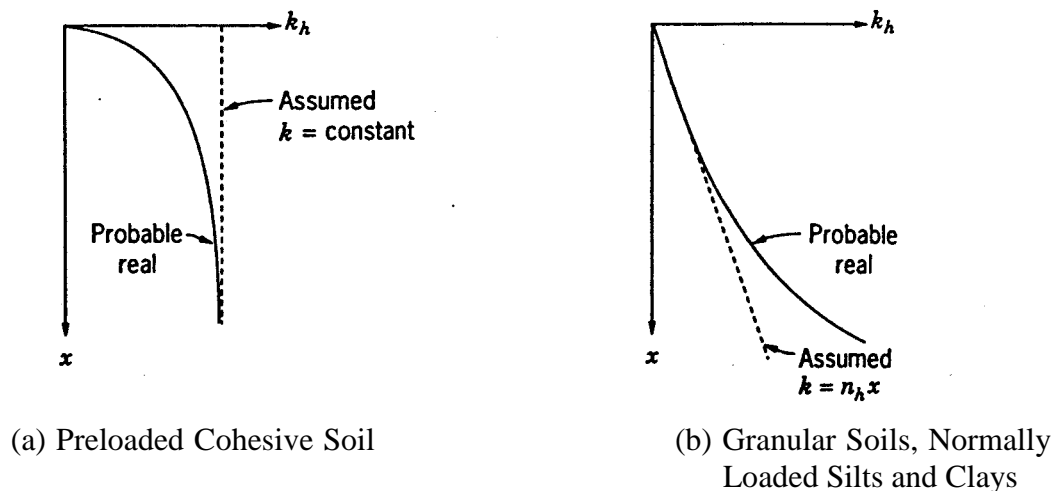
Figure 71. Variation of Subgrade Modulus (from Prakash, 1990)

Ashford and Juirnarongrit (2003) measured natural frequencies and damping of four cast-in-drilled-hole piles, with different diameters. The measured natural frequencies compared well with those estimated from a numerical model established with Terzaghi's concept of k_h. Ashford and Juirnarongrit (2003) indicated that these results confirmed the independence of k_h on pile diameter. In the work presented by Resse (1997), the modulus of subgrade reaction was assumed to be directly related to the weak rock modulus. Reese assumed **k_h** equal to 100 times the rock modulus at the rock surface and to linearly increase as a function of depth/diameter ratio. The maximum multiplier applied to rock modulus, to estimate **k_h**, was 500 at depth/diameter ratio of 3.

5.2.2 Modulus from Laboratory Tests

The subgrade modulus, k_h, was evaluated from the laboratory test results by taking the initial tangent modulus of backfigured P-y curves. The coefficient of subgrade reaction (k_{h0}) was calculated as k_h divided by B (pile width or diameter), as was explained in Chapter 3, Literature Review. The coefficient of subgrade reaction versus depth, normalized with respect to the diameter of the model shaft, is shown in Figure 72 for the two laboratory tests data.
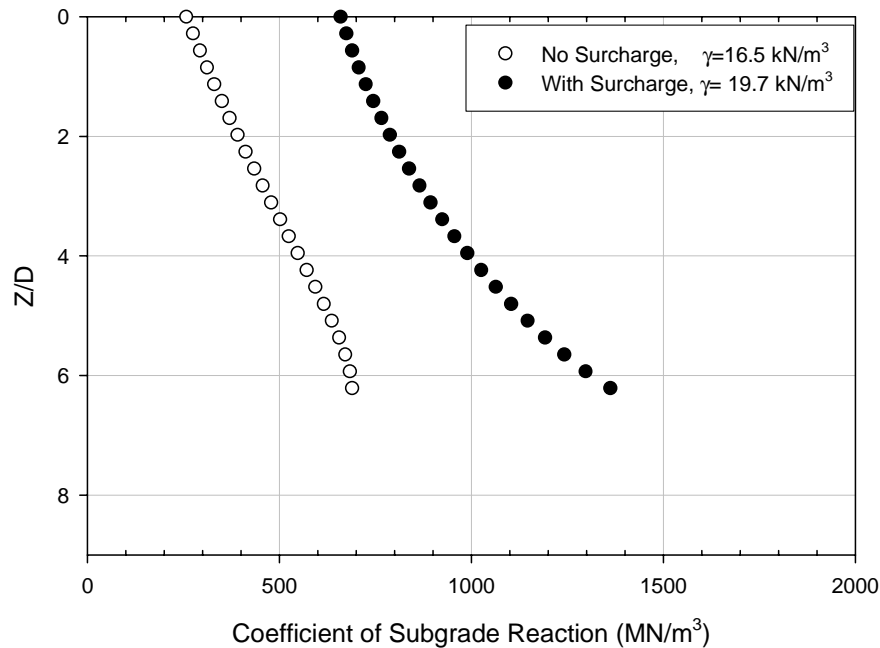
Figure 72. Depth vs. k_{h0} – No Surcharge and Surcharge

Plotting both curves on one graph shows the effect of the increased confining stress. The application of a surcharge appears to stiffen the k_{h0} response due to increase in effective stress with depth as well as increase in unit weight. As shown in Figure 72, the k_{h0} values linearly increased with depth ratio (Z/D) down to Z/D equal to approximately 4. The k_{h0} at Z/D of 6 was approximately 700 MN/m^3 for the no surcharge case versus 1400 MN/m^3 for the case with surcharge. The increase in k_{h0} can be explained by the increase in effective stress (18 kPa with surcharge versus 10 kPa with no surcharge) as well as the increase in soil unit weight, as data by Seed and Idriss (1970) reflected 40% increase in modulus as the relative density increased from 60% to 90%

5.2.3 Subgrade Modulus from Field Tests

Field subgrade moduli were calculated from backfigured P-y curves using the initial tangent modulus. After dividing by shaft diameter, the coefficients of subgrade reaction (k_{h0}) are shown in Figure 73 as a function of Z/D ratio. These values were obtained from the "a" parameter, mentioned in equation 47, and obtained by curve fitting a hyperbolic function to field-estimated P-y curves. There is a pronounced scatter in the data with Z/D ratio. On the average, the trend shows an increase of k_{h0} with depth. The average value of k_{h0} increased from approximately 80 MN/m^3 at the weathered rock surface to 250 MN/m^3 at Z/D ratio of 5. The rate of increase of the coefficient of subgrade reaction, will be defined here as n_h, with depth/diameter ratio was estimated to be 35. These values are approximately two orders of magnitude lower than values reported by Reese (1997) for two bored pile near San Fransisco, CA. For these two piles, k_{h0} according to Reese (1997) increased from approximately 8400 MPa at the surface to 143,000 at Z/D =3. Based on the data backfigured from field load tests, the variation of the coefficient of subgrade reaction with depth/diameter ratio can be represented as follows:

$$k_{h0} = 80 + 35 \frac{Z}{D} \qquad \text{in MN/m}^3 \tag{48}$$
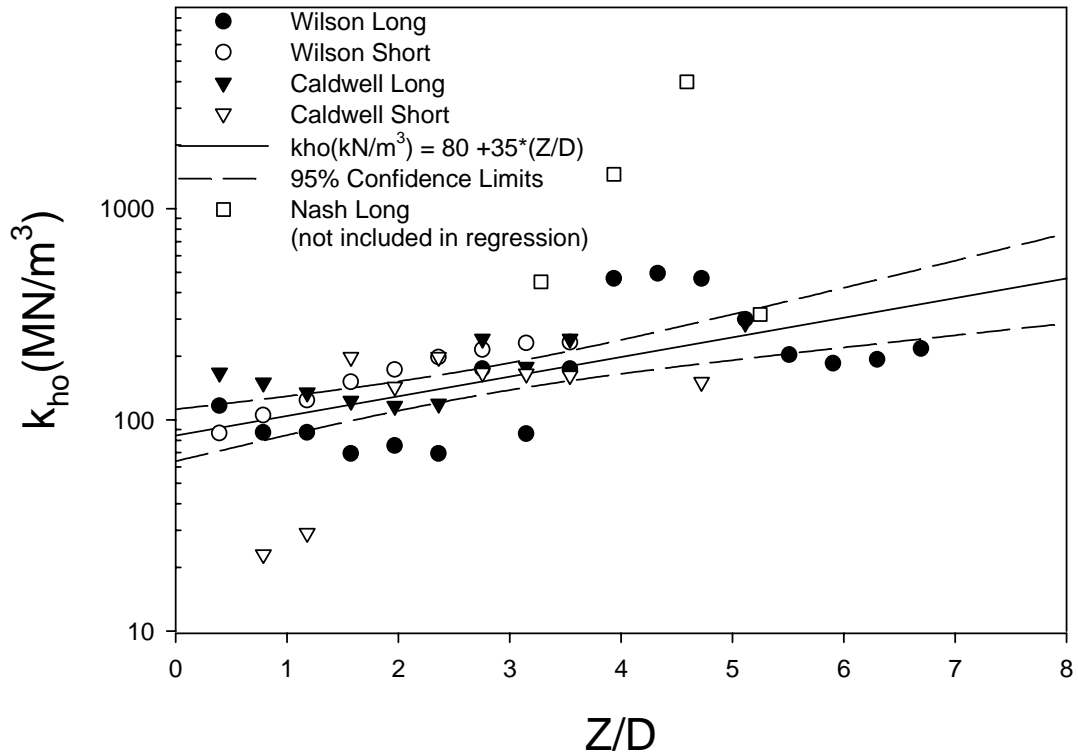
Figure 73. Measured k_{h0} Values from Field Tests

5.2.4 Comparison of k_{h0} from Laboratory and Field Tests

The k_{h0} relationships from the "no surcharge test" are compared with the field test results from testing in Caldwell and Wilson Counties. The laboratory and field values were divided by the diameter of the corresponding test shaft to convert k_h to k_{h0}. Also, normalized depth was obtained by dividing the depth by the diameter of the shaft for the laboratory and field results. A plot of Z/D versus k_{h0} is shown in Figure 74. As can be seen, the laboratory k_{h0} has a functional response and magnitude similar to that obtained from the field tests. Therefore, it appears that the use of the simulated weathered rock to investigate the characteristics shape of P-y curves in weathered rock was valid.
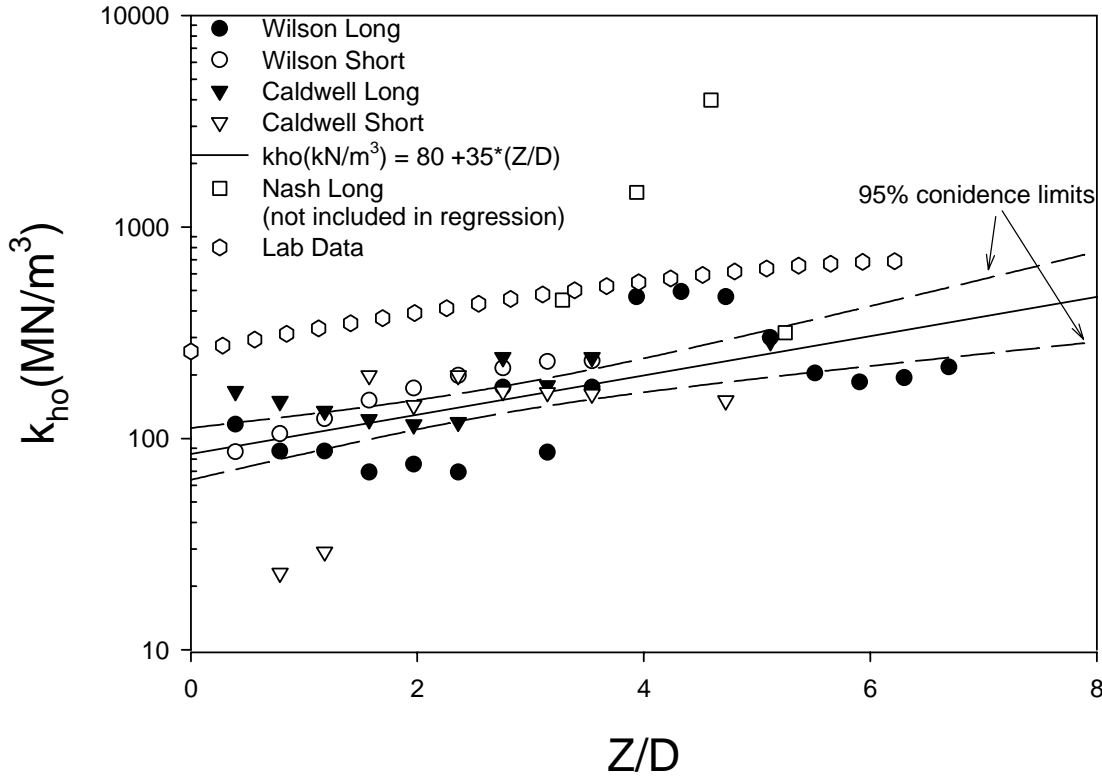
Figure 74. k_{h0} Comparison of Laboratory and Field Tests

5.2.5 Subgrade Modulus from Rock Dilatometer

Most weathered rock profiles in the Piedmont area are highly fractured and it is challenging to retrieve a sample by conventional methods for laboratory testing. As explained before, it is difficult to measure the ultimate resistance of weathered rock using a rock dilatometer due to the limited deformation. Therefore, the rock dilatometer data were only used for estimating the coefficient of subgrade reaction (k_{h0}) of weathered rock. For the sake of simplicity, the modulus of subgrade reaction was assumed equal to the lateral modulus as obtained from the rock dilatometer. As presented by Rocktest(1999), the equation to calculate the modulus from a rock dilatometer data is as follows:

$$E = 2(1 + v_r) \times (v_0 + v_m) \times \frac{1}{(\dfrac{\Delta v}{\Delta p - \Delta p_i}) - c} \quad (kN/m^2) \qquad (49)$$

102

Where, v_0 = normal initial or at rest volume of the deflated probe (1,950 cc);

   v_m = mean additional volume (370 cc);

   υ_r = Poisson's ratio of membrane (0.3);

   Δv= volume change under pressure increase;

   Δp_i = change of the pressure of the dilatable membrane (kPa);

   Δp = applied pressure increment (kPa); and

   c = volume correction factor (7.878×10^{-4} cc/kPa).

Vesic (1961) presented the following equation to estimate k_h based on the lateral modulus:

$$k_h = \frac{0.65E}{1-v_r^2}[\frac{E_s D^4}{EI}]^{1/12}$$ (50)

   D = diameter of shaft; and,

   EI = Shaft stiffness

It has been well recognized in literature that the 12th root of the relative stiffness of the shaft (or pile) to rock is approximately equal one. The coefficient of subgrade reaction, k_{h0}, can therefore be computed by dividing k_h from equation 50 by the shaft diameter (D). Accordingly, $k_{ho} = \frac{0.65E}{D(1-v_r^2)}$ (51)

For the test shafts with diameter equal to 0.762 m, k_{h0} is numerically taken to be approximately equal to E. The k_{h0} values evaluated from the rock dilatometer are generally lower than values backfigured from the field and laboratory data. Rock dilatometer-evaluated k_{h0} values ranged from 30 to 500 MN/m^3 at Caldwell county, and from 30 to 400 MN/m^3 at Wilson County. At Nash County, the test was performed deeper than the tip of the test shafts. Nonetheless, a test at depth of 4.8 m yielded E approximately equal to 270 MN/m^3, as compared to k_{h0} = 4000 MN/m^3 that was backfigured from the field P-y data. The E values evaluated from the rock dilatometer in this study are comparable to the range of E values reported by Hassan et al (2002) for soft

argillaceous rock for test sites in Dallas, Texas A&M, Toronto, and Honlulu, for which E varied from 154MPa to 730 MPa.

It is obvious that the E values computed from the rock dilatemeter data need to be modified in order to obtain reasonable prediction of lateral shaft response. This fact was recognized by Reese (1997). In his model, Reese addressed this need by introducing a modulus multiplier that increased from 100 at the surface and to 500 at a depth/diameter ratio of 3. The mechanics of k_h variation with deformation level and possible modification in order to reasonably predict shaft lateral response are discussed in the next section.

5.2.6 Evaluation of k_h with Deformation: Finite Element Study

Due to the restriction of performing a limited number of physical tests, Finite Element Method (F.E.M) analyses were used to study the deformation behavior of drilled shafts and corresponding subgrade modulus with the following conditions i) degree of fixity, ii) loading conditions, and iii) properties of shaft and subsurface material. In order to provide rigorous and systematic analyses, field conditions were modeled using three-dimensional finite element analysis with nonlinear material properties. The modeling and analysis were performed using the computer program, ABAQUS.

5.2.6.1 Boundary Analysis for Field Modeling

In modeling geotechnical problems involving soil-structure interaction, the soil medium is usually represented as a region of either infinite or semi-infinite extent. When considering numerical modeling of such problems, the conventional approach is to minimize the effect of boundaries by incorporating a large number of elements extending significant distances beyond the range of the loaded zone. However, the use of a large number of finite elements leads to an inordinate amount of computational effort. Nevertheless, the location of the truncated boundary is often selected on a trial and error basis before an acceptable degree of accuracy is achieved.

Infinite element methods representing the unbounded nature of a domain have been proposed by Bettess (1977), Lynn and Hadid (1981), and Curnier (1983). These methods utilized the reciprocal method or exponential decay terms to ensure the decay of the variables at large distances.

The purpose of the numerical investigation of the boundary problem presented herein was to address how large the mesh needs to be in order to model an unbounded domain. When using infinite elements, it is necessary to ascertain the location of such elements in relation to the loaded regions in order to achieve best solution accuracy. Modeling of soil domain in this study consisted of using both finite and infinite elements. In order to verify the effect of the location of the infinite elements, the distance to the coupling location was characterized by using remoteness factors. The remoteness factors, α and β, depicting the location of the infinite element in horizontal and vertical directions, respectively, were defined as follows:

$$\alpha = \frac{\text{Distance from the Center of Pile}}{\text{Length of Pile}} \tag{52}$$

$$\beta = \frac{\text{Distance from the Tip of Pile}}{\text{Length of Pile}} \tag{53}$$

In this analysis, the number of elements, and consequently the number of nodal points, have been increased for higher values of α and β. Instead of using infinite elements at the bottom of the model, fixed boundary conditions in x, y, and z direction were used.

Figure 75 shows the lateral displacement at top of shaft from the F.E.M. analyses. The magnitude of load used in the analysis was 1000 kN. The length and diameter of the shaft in the model were 17.5 meter and 0.3 meter, respectively. The properties of soil were assumed to be 50,000 kPa for the elastic modulus and 0.3 for the Poisson's ratio. The results showed that the displacement at the top of the shaft converged at an α factor of 1.5 and a β factor of 1.0. Therefore, these values were used to model field conditions with minimal boundary interference. The errors in these two parameters were calculated and tabulated in Table 18, and were and plotted in Figure 76. The error was defined as follows:

$$E(\%) = \frac{\delta - \delta^* (\textit{reference solution})}{\delta^*} \times 100 \tag{54}$$

As shown in Figure 76, if the α and β factor for a given mesh are larger than 1.0 and 1.5 respectively, the F.E.M. model can be used with minimal boundary effect. The transferred stress contour to the boundaries is shown later in this chapter to confirm the minimal interference of model boundaries on the results.
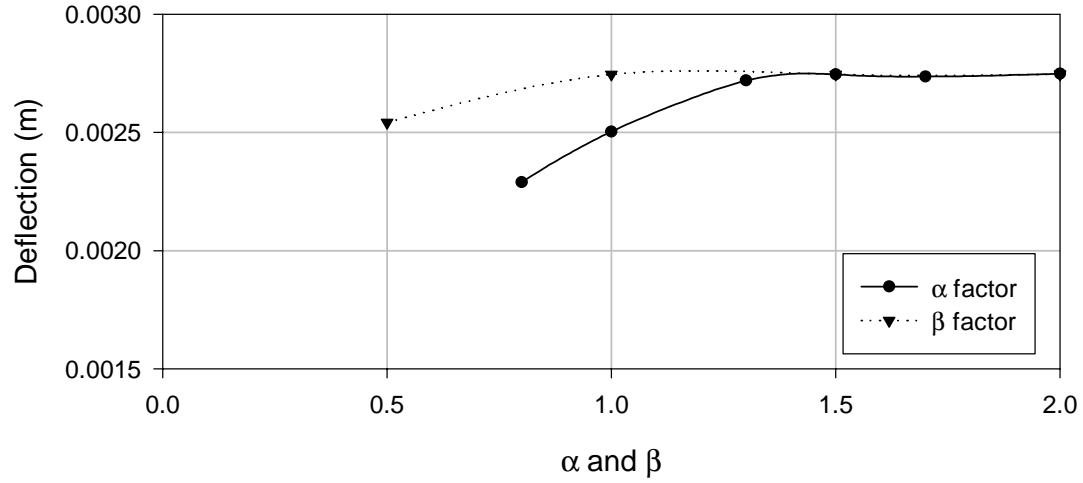
Figure 75. ABAQUS Results from Location of Infinite Element and Depth of Soil

Table 18. Results of the Lateral Boundary Analysis

Location of Infinite Element (α)	δ (m)	Error (%)	Location of Infinite Element (β)	δ (m)	Error (%)
0.8	2.289×10^{-3}	16.593	0.5	2.542×10^{-3}	7.390
1.0	2.503×10^{-3}	8.796	1.0	2.745×10^{-3}	0
1.3	2.719×10^{-3}	0.927	1.5	2.745×10^{-3}	-0.006
1.5	2.745×10^{-3}	0	2.0	2.746×10^{-3}	-0.033
1.7	2.736×10^{-3}	0.326	-	-	-
2.0	2.748×10^{-3}	-0.121	-	-	-
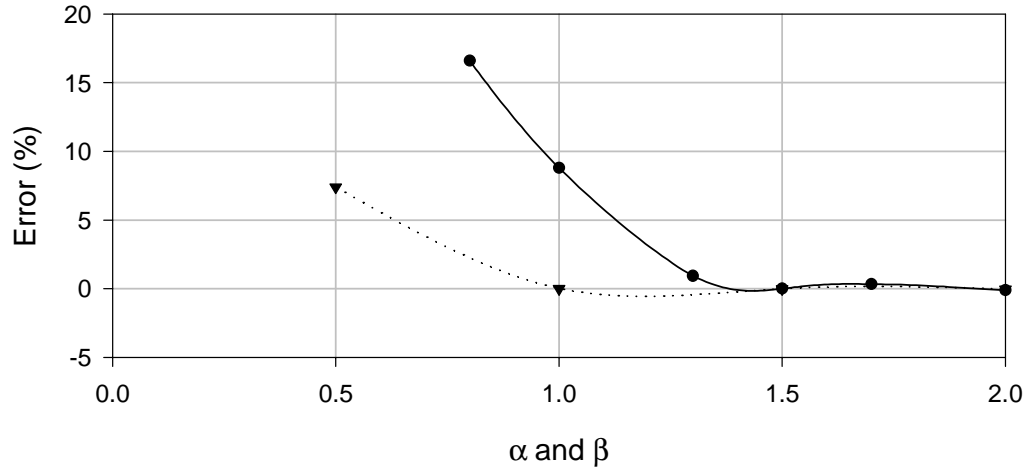
Figure 76. Error in ABAQUS Results from Various Location of Infinite Element and Depth of the Soil

5.2.6.2 Calibration of F.E.M. Modeling

The results from the F.E.M. analyses were compared with other closed-form solutions, or analytical solutions, to confirm that the modeled domain provides accurate results. The analysis data for a single shaft F.E.M. model were compared with results from Poulos (1976) method, which was based on elasticity theory. As previously explained in Chapter 2, Literature Review, the lateral displacement at the top of single pile can be calculated using equation 2. The results of the F.E.M. analysis and Poulos' method, under a lateral loading of 1000 kN, are plotted in Figure 77. As shown in Figure 77, results from the two analyses were well matched. Accordingly, it was concluded that the F.E.M. modeling of the subsurface domain with non-linear properties can yield reasonable representation of the shaft-soil system to be studied.

5.2.6.3 Modeling Field Parameters

The "field" three-dimensional finite element models are composed of 2245, 3527, 3528, 5157, and 5158 elements and 2857, 4285, 4285, 6119, and 6119 nodes for the cases of L/D = 2.5, 5.2, 7.5, 10.8, and 15.0, respectively. One example of the overall dimensions of a mesh used for field modeling is shown in Figure 78 for the case of L/D = 7.5. Figure 79 shows equivalent stress contours, as defined by equation 55, under the ultimate loading of 16,500 kN. These results indicated that no significant stresses were transferred to the boundaries of the model.
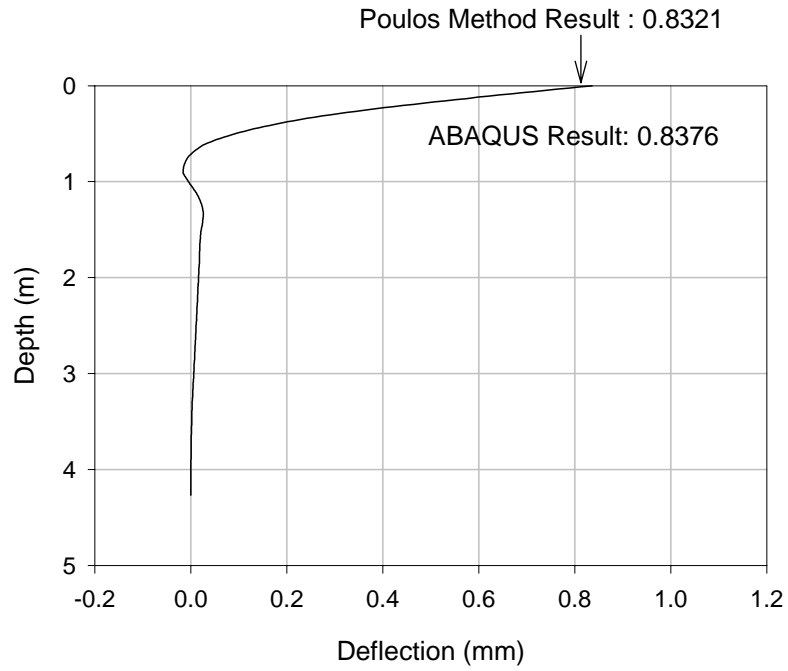
Figure 77. Comparisons between Poulos Method and ABAQUS Analysis
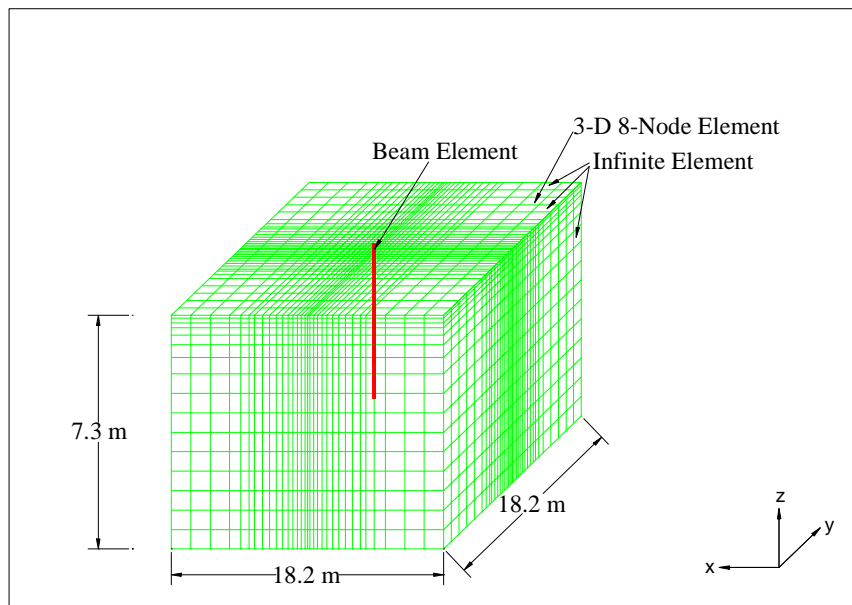
Figure 78. F.E.M. Modeling for Field Testing

$$q = \sqrt{\frac{2}{3} S_{ij} S_{ij}}$$ (55)

Where, $S_{ij} = \sigma_{ij} + p\delta_{ij}$;

$p = -\frac{1}{3}\sigma_{ii}$; and,

$\delta_{ij} = $ Kronecker delta.
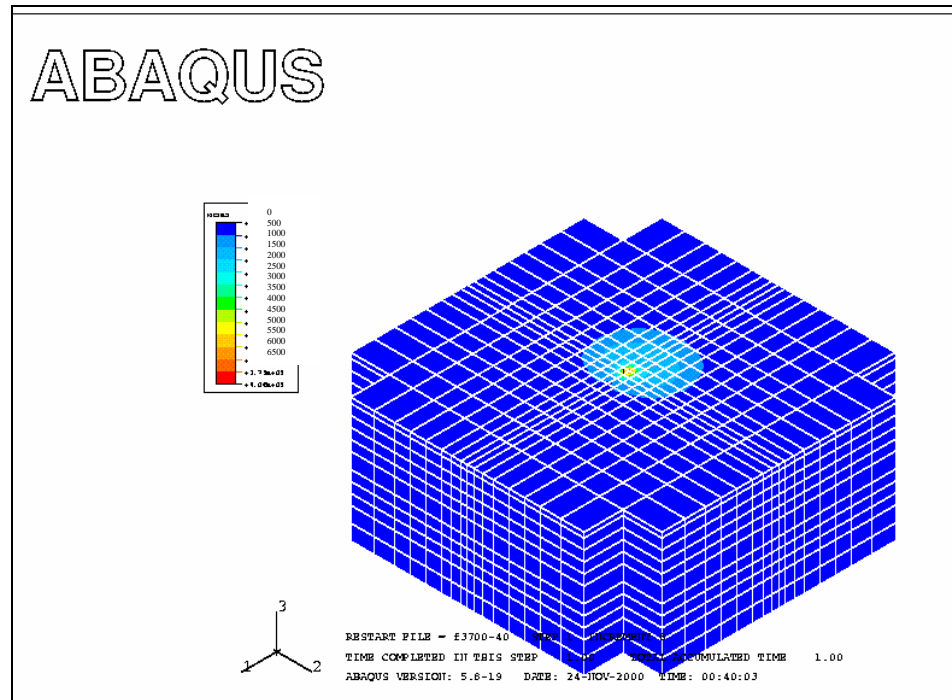
Figure 79. Stress Contour of the Field Modeling under Ultimate Loading Condition

The static analysis of a single shaft was performed using ABAQUS (version 6.1.1). Table 19 shows type of elements used to simulate the geologic material and drilled shaft. In modeling, the boundary conditions in the field were different from laboratory testing since in the field the ground was unbounded. The infinite elements were used to simulate the unbounded conditions.

The modified Drucker-Prager model was used to include the plasticity of weathered rock. Table 20 shows a summary of material properties for F.E.M. modeling. The elastic modulus of the weathered rock, used in analyses, was from data measured by the rock dilatometer at the Nash county test site.

Table 19. Elements used in F.E.M. Modeling

Type	Element Type	Element Name in ABAQUS
Geologic Material	8-node brick element	C3D8
Boundary (field model)	8-node linear, one-way infinite	CIN3D8
Pile	2-node beam element	B31

The Poisson's ratio and the strain at failure were those measured from laboratory triaxial tests using the simulated rock material.

Table 20. Properties of Element for Weathered Rock Simulation

Items	Values Uesd in Analysis
Modulus of Elasticity (kN/m^2)	2.220×10^5
Poisson's Ratio (ν)	0.15
Strain at Failure	2 %

The shaft properties were based on the dimensions of shafts used in field tests. These shafts were cased to full length and internally reinforced with steel rebar and concrete. The properties and dimensions of the shafts are summarized in Table 21.

Table 21. Properties of Piles

Items	Field
Modulus of Elasticity (kN/m^2)	2.00×10^7
Poisson's Ratio (ν)	0.15
Diameter of Pile (m)	0.762

As mentioned earlier, major variables influencing lateral shaft behavior included the length to diameter ratio (L/D), and a relative flexibility factor (K_R, as presented in equation 1). The F.E.M. analyses were performed by changing L/D ratio and flexibility factor (K_R) to study the influence of these parameters on the degree of fixity. Figure 80 shows the deformed shapes of analyzed shaft under the ultimate loads of 9800 kN, 13,000 kN, 16,500 kN, and 18,000 kN for cases of L/D = 2.5, 5.2, 7.5, and 15.0, respectively. These loads with the corresponding L/D ratios yielded comparable, if not equal, deformation levels. Figure 80 shows that at L/D = 2.5, the shaft behaves nearly as a rigid body versus a shaft with L/D = 15.0 where a fixed length was obtained below a point of fixity. The other L/D ratios show partially fixed tip conditions. These cases therefore cover a range of shaft behavior with different degrees of fixity, given the analysis parameters.

Figure 81 shows the shaft top-deflection as a function of model load, for each of the L/D ratios investigated. The top deflection in Figure 81 indicated that the applied load was large enough to induce non-linear load-deflection state for the analyses L/D ratios, and therefore allows for the study of the subgrade reaction characteristics of the shaft as a function of the degree of fixity in the non-linear deformation range.
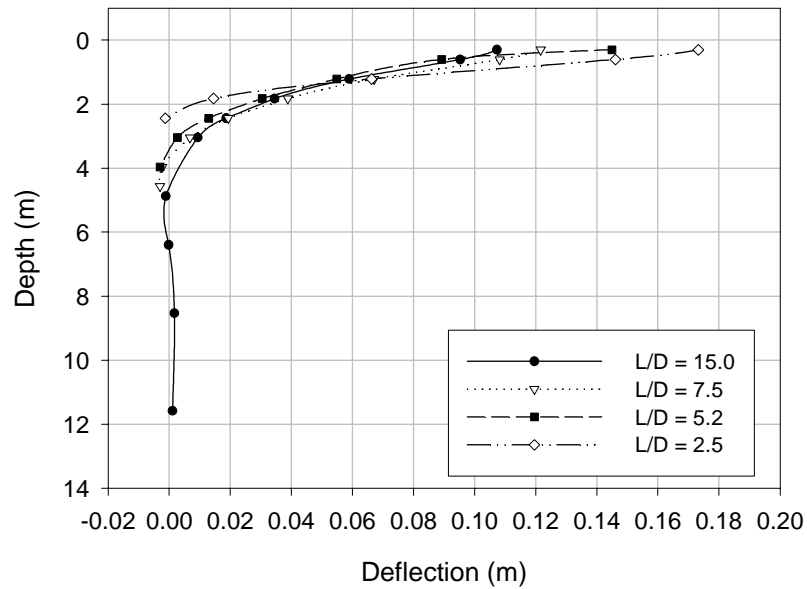
Figure 80. Deformed Shape of Shafts under Ultimate Loading

111
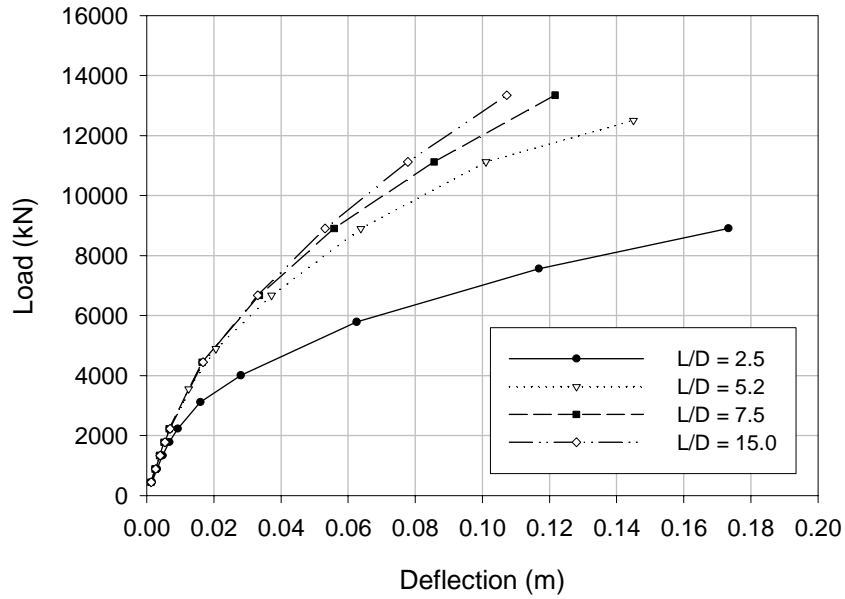
Figure 81. Top Deflections from F.E.M. Analysis

P-y curves were constructed from the results of the finite element analyses for the modeled L/D cases. The ABAQUS output file provided moment value at the center of each element of the shaft, and the deflections were given at specific depths along the length of the modeled shaft. Using the moments and deflections at given locations, the functional relationships, between the moment and deflection, were obtained from regression analysis. The reaction of the soil, P, was calculated by taking the second derivative of the moment function, and the deformation of the shaft, y, was directly obtained from the calculated deflection values at a given depth. Twenty regression analyses were performed for each of the five (5) L/D ratios, representing a different degree of fixity, to construct P-y curves along the shaft. Details of results are summarized and attached as Appendix F. P-y curves for the case of L/D = 7.5 are shown in Figure 82, and P-y curves for the cases of L/D = 2.5, 5.2, 10.8 and 15.0 are attached in Appendix G.
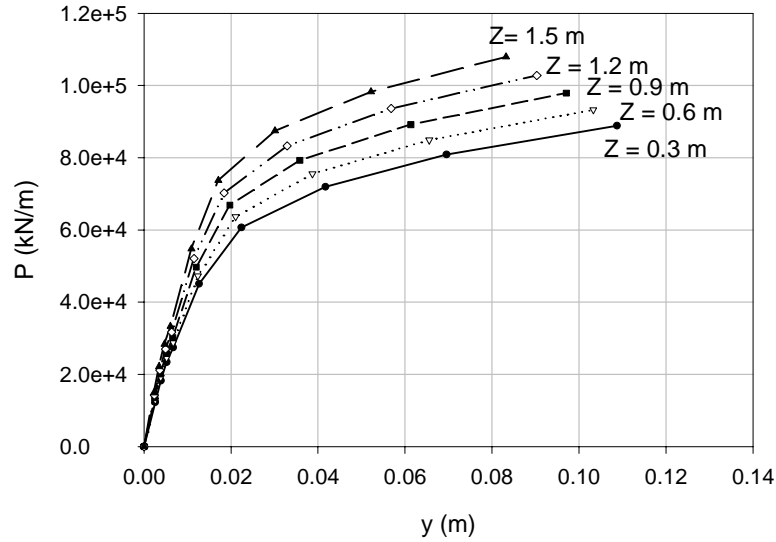
Figure 82. P-y Curves from F.E.M. Analysis with L/D = 7.5

As shown in Figure 82, the P-y curves from finite element analyses indicated an increase in initial secant slopes with depth. The coefficients of subgrade reaction were calculated from finite element-generated P-y curves. A major variable in the F.E.M. analyses was the depth of embedment. The depth of embedment affected the flexibility of the shaft. Such flexibility is manifested in the deformed shape, with a deflection profile that can be characterized as rigid body motion or restrained tip motion. Figure 83 shows the relationship between k_{h0}, based on secant modulus, and Z/D from the finite element analyses results.

The sudden increase in k_{h0} value with depth, as shown in Figure 83, may be explained by the difference in shear strain (γ) magnitude above and below the point of rotation. While soil above the point rotation was at or near the plastic yield, soil below the point of rotation was in elastic state. Accordingly, and in order to facilitate the analyses, it seems that coefficient of subgrade reaction (k_{h0}) can be modeled as a function of degree of fixity. A possible approach to facilitate the development of load deflection response comparable to that obtained in the field is to develop a function for estimation of the coefficient of subgrade reaction (k_{h0}) with depth, which is related to shaft relative degree of fixity.
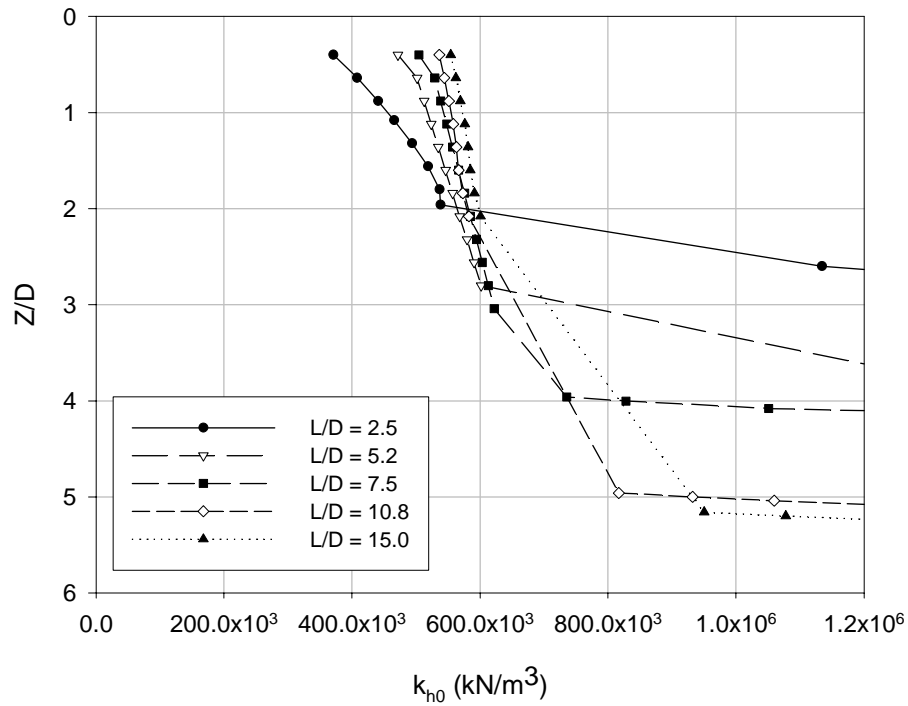
Figure 83. Calculated k_{h0} Results from F.E.M. Analyses

5.2.7 Proposed Model for k_{ho} in WR Profiles

Based on the analytical results presented in this study, it is recommended that the lateral subgrade response of a shaft subjected to lateral loading be modeled using two different characteristics, based on induced strain above and below the point rotation. As k_{h0} is a function of lateral modulus, and the modulus is consequently a function of shear strain, modeling with two different k_{h0} above and below the point of rotation will facilitate the analysis. As presented by Prakash and Kumar (1996), work by Mwindo (1992) indicated the dependency of modulus of subgrade reaction on the shear strain level in the soil. Mwindo presented a relationship based on analyzing 22 sets of load test data from piles embedded in different materials in which modulus of lateral subgrade reaction decreased exponentially with increasing shear strain. This was similar in logic to data by Seed and Idriss (1970) in which shear moduli values decreased exponentially with increasing shear strain level. As schematically illustrated in Figure 84, the lateral wedge providing resistance above the point of rotation involves a relatively small volume of soil with relatively higher shear strain as compared to that below the point of rotation with correspondingly low strain. Coupled with increase in confining stress with depth, the

114

increase in lateral modulus below the point of rotation can be modeled to be larger than the corresponding increase above the point of rotation in order to define degree of fixity and facilitate the analysis.
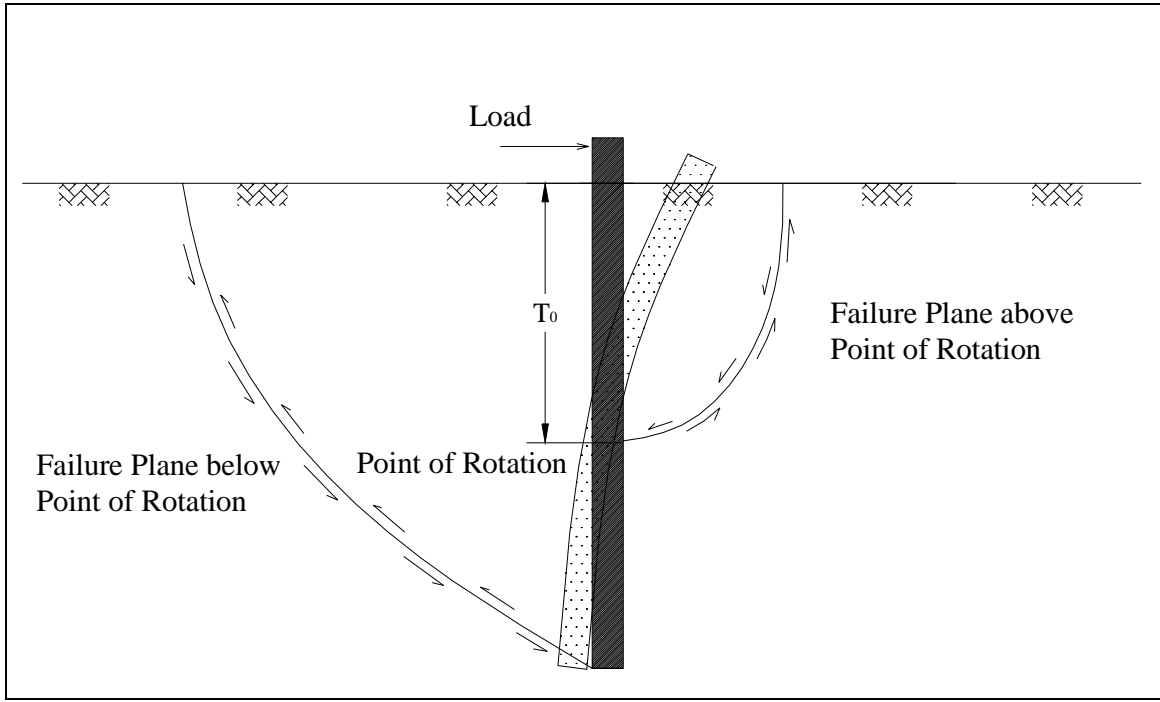
Figure 84. Possible Point of Rotation under Lateral Load

As the general deflection of a shaft can be expressed by the following function (Prakash, 1990), the following procedure is recommended for estimation of k_{h0}:

$$y = f(x, T, L, k_h, EI, Q, M) \tag{56}$$

Where, x = depth of embedment;

T = relative stiffness factor = $(\dfrac{EI}{n_h})^{1/5}$;

L = pile length;

k_h = modulus of subgrade reaction;

n_h = constant of subgrade reaction;

EI = pile stiffness;

Q = lateral load applied at the pile head; and,

M = moment applied at the pile head.

In the Chapter 2, Literature Review, the flexibility factor (K_R) was introduced as follows (Poulos and Davis, 1980).

$$K_R = \frac{E_p I_p}{E_s L^4} \qquad (57)$$

K_R is a dimensionless factor that describes the relative stiffness of the shaft with respect to soil. The elastic modulus, E_s, of weathered rock can be determined using data from the rock dilatometer as previously explained. However, in many situation, such data are not available. In these cases, the following equation (Hoek and Brown, 1997) can be used to estimate the rock modulus:.

$$E_s \ (GPa) = \sqrt{\frac{\sigma_{ci}}{100}} 10^{[(GSI-10)/40]} \qquad (58)$$

Where, σ_{ci} = compressive strength of rock (GPa); and

GSI = Geotechnical Strength Index.

Using results from the field and laboratory testing as well as from the finite element analyses, Table 22 summarizes the point of rotation normalized as a function of shaft-length (T_0/L) versus flexibility factors, K_R. These data are also plotted in Figure 85 which has semi-log scale for the flexibility factor. The data shown in Table 22 included a wide range of length from very short to long shafts.

Table 22. Summary of Points of Rotation versus Flexibility Factor

F.E.M. Analyses		Field Tests		Laboratory Test	
K_R	T_0/L	K_R	T_0/L	K_R	T_0/L
0.0001	0.2694	0.0401	0.7500	0.0132	0.6179
0.0009	0.4574	0.0193	0.7292		
0.0034	0.5786	0.0091	0.6140		
0.0061	0.6000	0.0098	0.6186		
0.0426	0.7286				
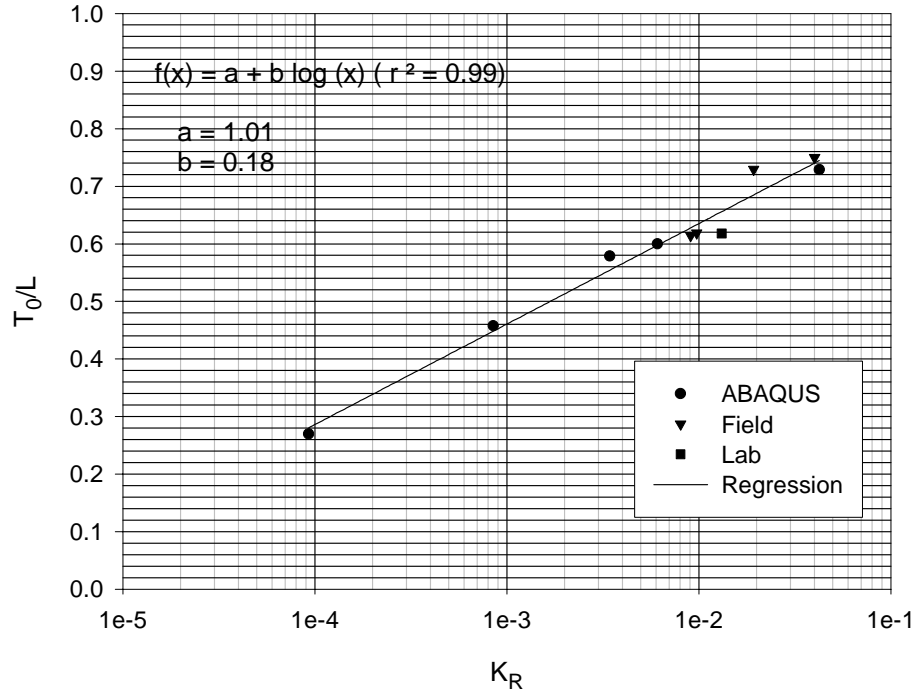
Figure 85. Points of Rotation vs. Flexibility Factor

Based on data in Figure 85, the following equation is proposed for preliminary estimation of point of rotation:

$$\frac{T_0}{L} = 1 + 0.18 \log K_R \quad (K_R \le 1) \tag{59}$$

The model value of the subgrade reaction, as empreically correlated to geologic properties, was assumed equal to the elastic modulus of weathered rock can be calculated as follows:

$$k_{ho} = 0.65 \frac{\sqrt{\sigma_{ci} \times 10^4}}{D(1 - v_r^2)} \quad 10^{[(GSI-10)/40]} \quad (\text{kN/m}^3) \tag{60}$$

Where, σ_{ci} = unconfined compression strength of intact rock (kPa).

The proposed model calls for an increase in the value of k_{h0} using a multiplier, I_T, which was estimated from the field and finite element data. The value of I_T, can be determined from Figure 86 or using equation 62 as follows:

$$I_T = -28 - 383 \log(\frac{T_0}{L}) \qquad \mathbf{I_T} \geq 1 \tag{62}$$
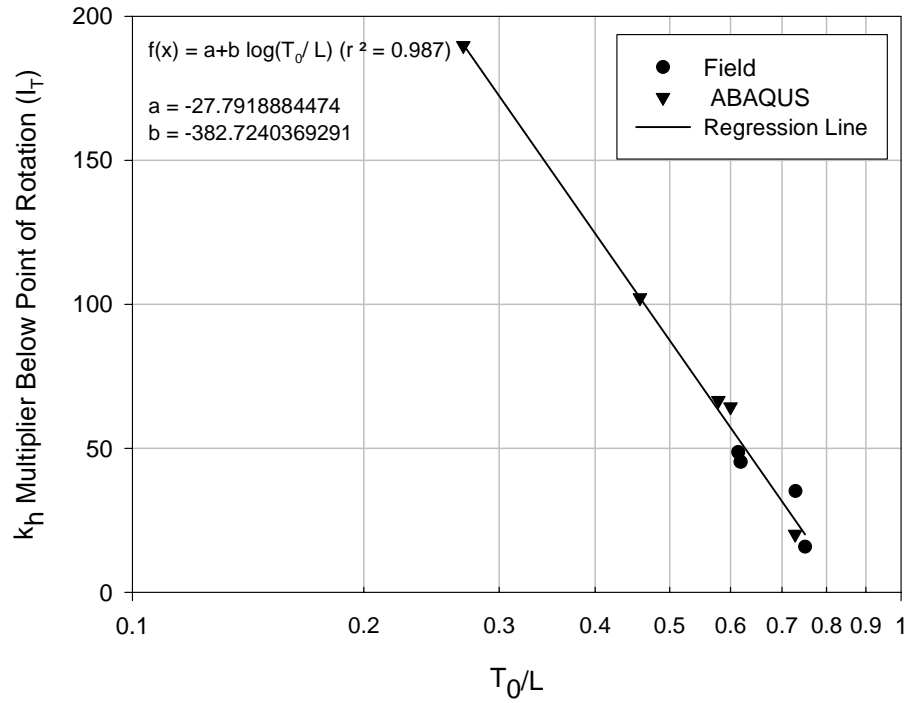
Figure 86. Increment of k_{h0} below Point of Rotation (I_T)

Accordingly, the modulus of subgrade modulus (k_h) for the proposed P-y curve model can then be obtained using following equations:

$$k_h = (k_{h0} + n_h z)B \qquad (0 \leq z \leq T_0) \tag{63}$$

$$k_h = \{(k_{h0} + n_h T_0) + n_h(z - T_0)I_T\}B \qquad (T_0 < z \leq L) \text{ and } \mathbf{I_T} \geq 1 \tag{64}$$

5.3 Ultimate Resistance (P_{ult}) for Weathered Rock

The ultimate resistance (P_{ult}) of weathered rock is one of two parameters needed for the proposed P-y model. The ultimate resistance can be measured from load tests if the applied load is large enough to fail the shaft. However, the field and laboratory tests do not normally yield the ultimate resistance at every location along the shafts The tests conducted for this study only produced local failure at shallower depths, near the surface.

The ultimate resistance can be obtained from curve fitting and extrapolation assuming the shape of P-y curve to be hyperbolic. P_{ult} was estimated from the field

backcalculated P-y curves by taking the inverse of the 'b' parameter as suggested by Konder et al (1963). However, a gross margin of error can be expected for estimating P_{ult} from curves with small deflections. Specifically, these were data obtained from locations around the point of rotation.

5.3.1 Laboratory Test Results

The ultimate resistance (P_{ult}) was estimated from the surcharge and no surcharge load tests. Few data points near the point of rotation were not used, as errors in the estimation procedure were amplified given the small deformation magnitude at these locations. Figure 87 depicts the distribution of P_{ult} with depth for the laboratory tests.
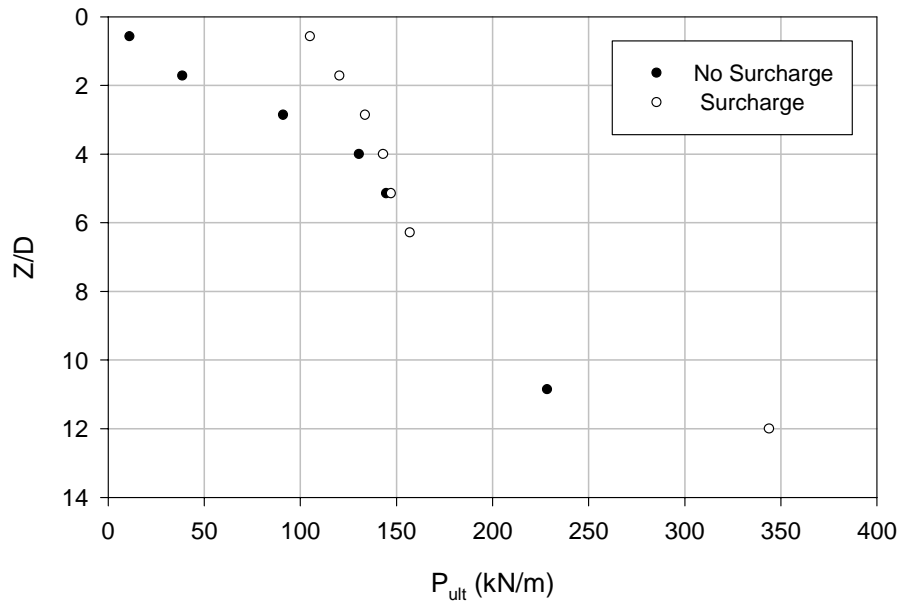
Figure 87. Depth vs. P_{ult} – ABC Tests (Surcharge and No Surcharge)

As shown in Figure 87, the test with no surcharge indicated a P_{ult} of approximately zero at the ground surface. With increased confining stresses, an increase in P_{ult} was obtained.   However, after a depth of approximately 0.36 meter (Z/D $\cong$ 6) the ability to predict P_{ult} becomes questionable due to small deformation levels and the limited number of data points.

Analytical estmation of P_{ult} can be conducted using the Hoek-Brown failure criterion for rock masses (1998).   The generalized failure criterion for jointed rock masses was explained in Chapter 2, Literature Review. This criterion was used by Zhang (1999) to determine the normal limit stress p_L and subsequently P_{ult}. Zhang and Einstein

(2000) also used work by Briaud and Smith (1983) and Carter and Kulhawy (1992) in which P_{ult} was expressed as follows:

$$P_{ult} = (p_L + \tau_{max})B \tag{65}$$

Where, p_L = the normal limit stress;

$$p_L = \sigma_1{}' = \gamma' z + \sigma_c \left(m_b \frac{\sigma_3{}'}{\sigma_c} + s \right)^a \tag{66}$$

γ' = effective unit weight of the rock mass;

z = depth from the rock mass surface; and,

$$\tau_{max} = 0.20(\sigma_c)^{0.5} \text{ (MPa) for a smooth rock socket (Zhang 1999)} \tag{67}$$

Utilizing these relationships, P_{ult} values based on laboratory test parameters were calculated and compared to values estimated, or extrapolated, from backfigured P-y curves. The geologic parameters in Table 23 were used in the calculations of P_{ult}. The results are compared and presented in Figure 88.

Table 23. Parameters for Estimation of P_{ult}

Property	Value
GSI	10
m_i	10
s	0
a	.55
σ_c	σ'*tan (52 degrees)

These results indicated a close match between laboratory-estimated P_{ult} and values computed using Zhang and Einstein (2000) recommendations. Accordingly, the failure criterion and estimation procedure for P_{ult}, by Zhang and Einstein (2000), were used further for comparison with field test results.
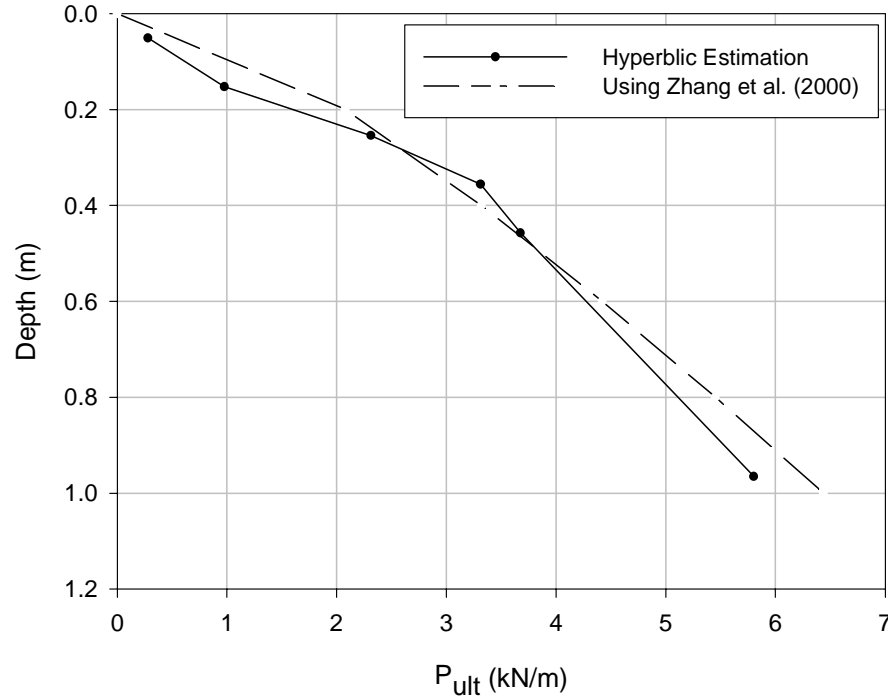
Figure 88. Comparison of P$_{ult}$ from Curve Fitting vs. Zhang's Approach

5.3.2 Applicability of P$_{ult}$ to Field Results

The P$_{ult}$ from field tests were obtained from curve fitting procedures as previously described for the laboratory testing analyses. As for the lab data from the area around the point of rotation posed an inherent problem due to the small deformation levels. Therefore, these data have been excluded from the analysis.

The geological conditions in the immediate vicinity of each shaft at the Caldwell county test site were considered to be identical. In contrast, and as presented in Chapter 4, Field Tests, the Wilson County short shaft exhibited larger lateral resistance, as compared to the long shaft, due to differences in geological conditions. The method proposed by Zhang and Einstein (2000) was used to estimate P$_{ult}$ for the field results. The geologic parameters used to estimate P$_{ult}$ in this case are summarized in Table 24. Field-evaluated versus model-computed P$_{ult}$ values are compared in Figure 89.

As shown in Figure 89, it was possible to predict the backfigured P$_{ult}$ using Zhang and Einstein (2000) method and reasonable estimate of geologic parameters. Accordingly, the method by Zhang and Einstein (2000) is recommended for estimation of P$_{ult}$ value with depth for the purpose of constructing P-y curves.

Table 24. Parameters for Estimation of P$_{ult}$

Property	Value		
	Caldwell County	**Wilson County (Long Shaft)**	**Wilson County (Short Shaft)**
GSI	30	25	40
m$_i$	33	9	9
m$_b$	1.59	0.62	1.06
S	0	0.00024	0.00127
a	0.50	0.50	0.55
σ_c	60 MPa	58 MPa	62 MPa
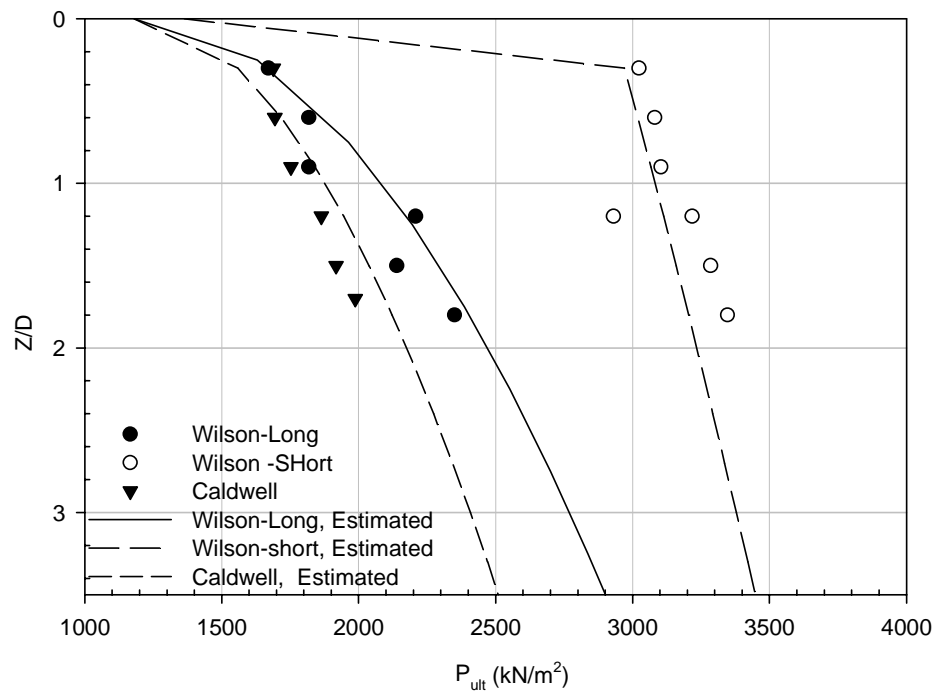
Figure 89. Comparisons of P$_{ult}$

5.4 Validation of Proposed P-y Model

The proposed method for the construction of P-y curves in weathered rock was validated using results from field tests performed in Caldwell and Wilson Counties. This work simply shows that the proposed method is valid in the sense of being able to estimate the data used in developing the model. Therefore, as we are predicting response for the shafts from which data the method was developed, it should be expected that computed and measured behavior match closely. As mentioned earlier, the properties required for the construction of P-y curves include lateral modulus and ultimate shaft resistance with depth. These two parameters can be evaluated using various approaches. One approach is to use index rock properties such as RQD, fissure size and recovery, and correlate them to a GSI value (Hoek and Brown, 1997). This GSI value, in conjunction with unconfined compressive strength of rock core samples, can be used for estimating the lateral WR modulus and P_{ult}. Alternatively, the rock dilatometer can be used to measure the in-situ rock modulus while P_{ult} will still need to be computed, as the deformation induced by the rock dilatometer is normally not large enough to induce failure. The use of an in situ estimated modulus should provide more accurate results as compared to values estimated using index rock properties from core samples.

5.4.1 Comparison with Field Data

Estimation of k_{h0} and P_{ult} using geological properties requires rock core samples in order to define the index properties of the rock along the length of the shaft. However, when the weathered rock is severely weathered and highly fractured, it is difficult to obtain core samples for testing, and one of the alternatives is to use the rock dilatometer.

Rock dilatometer tests were conducted at the locations of the long and short shafts in Caldwell County, and the short shaft in Wilson County. Using the proposed P-y method with rock dilatometer data, BMCOL76 analyses were performed and comparative results are presented in Figures 90 through 94. Data in these figures include shaft-top deflection versus applied load for the following cases: (1) field load-deflection data measured during load testing using dial gages, (2) estimated load-deflection data based on P-y curves back-calculated from measured strain and inclinometer data, (3) estimated

123

load-deflection relationship based on P-y curves developed using index geological properties, and (4) estimated load-deflection relationship based on P-y curves with the modulus obtained from the rock dilatometer.

Figure 90 shows comparative shaft top deflection data from the long shaft at Nash County test site. As shown in Figure 90, the estimated results from proposed P-y curve model shows reasonable agreement with the measured response.
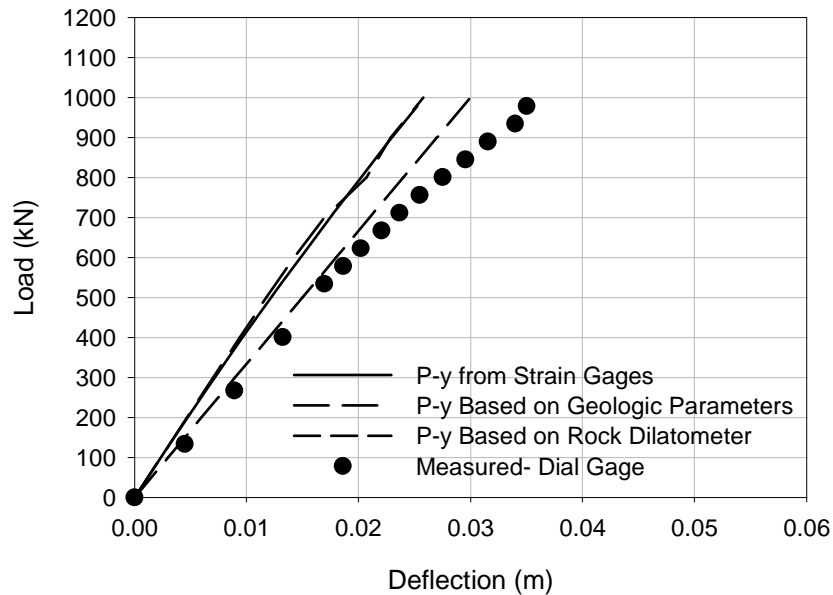
Figure 90. Verification of P-y Curve Model – Nash County Long Shaft

Figures 91 and 92 show the shaft-top deflections of the Caldwell County short and long shafts. The measured deflections from the dial gage are close to computed values from back-calculated P-y curves based on strain gage data as well as the calculated values using P-y curves based on geological properties. Data based on the rock dilatometer slightly overestimated the measured response, but consistently yield the closest computed response as compared to that estimated using geological properties.
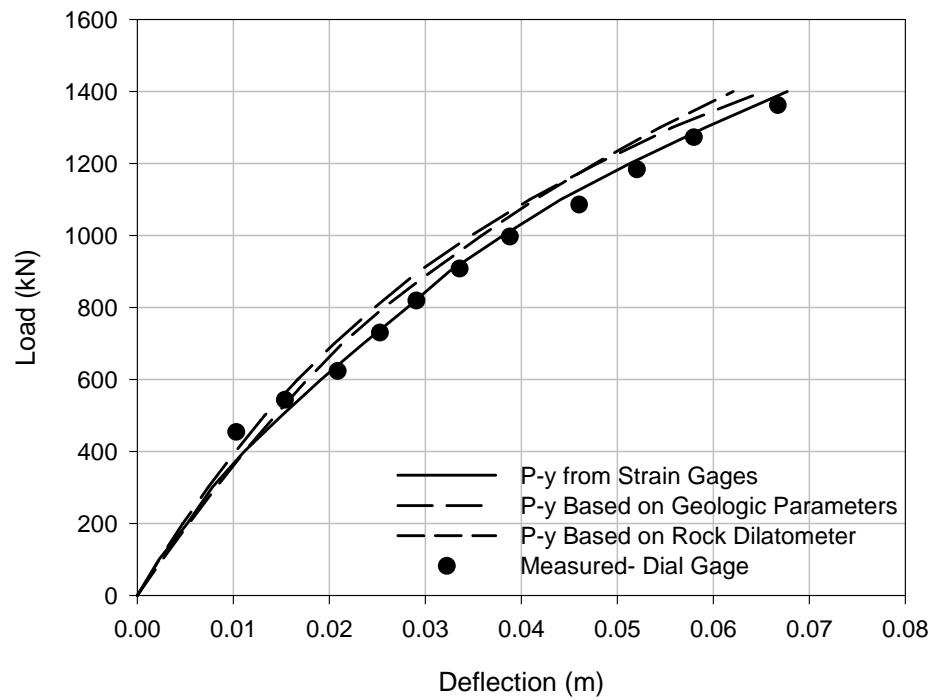
Figure 91. Verification of P-y Curve Model – Caldwell County Short Shaft
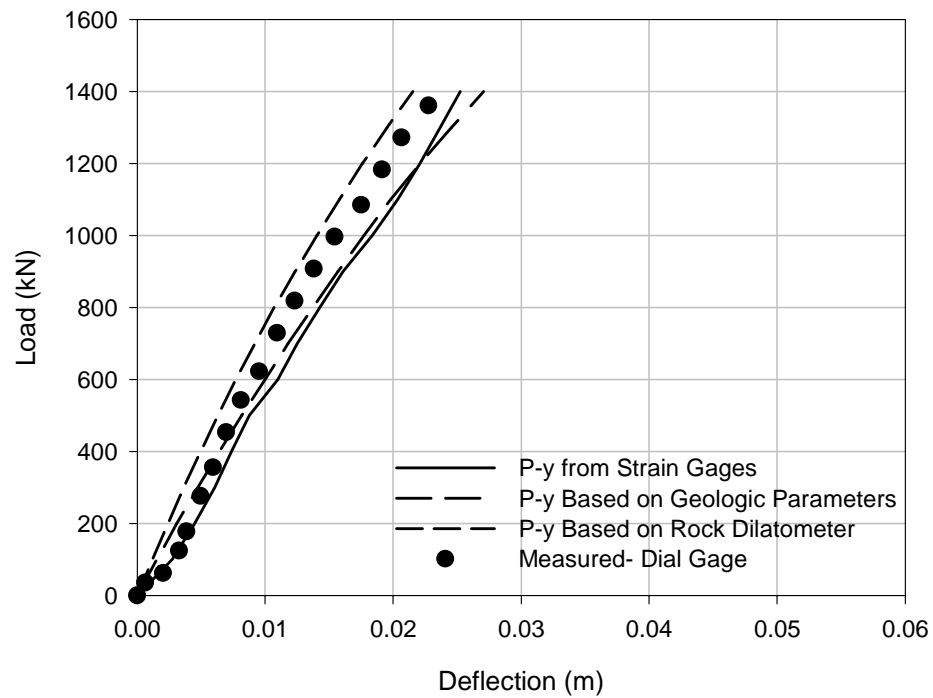
Figure 92. Verification of P-y Curve Model – Caldwell County Long Shaft

125

Figure 93 shows a similar comparison of the Wilson County short shaft. No predictions using rock dilatometer data for the long shaft are presented are presented as no test was performed due to the collapse of the bore hole at this location. Figure 94 shows the shaft-top deflection comparison for the Wilson County long shaft. As shown in the figure, the calculated top deflections from the P-y curves back-calculated from strain gages, and from P-y curves estimated from geological properties are close to those measured by dial gage measurement data.

A comparison of Figures 93 and 94 shows that a softer deformation response was obtained for the long shaft, as RQD value of 13% was estimated at its location versus 59% at the location of the short shaft. It is noteworthy to mention, however, computations based on geologic parameters yielded a response similar to field data, which suggest the ability of the model to account for variable geologic condition within the same site. Un general, the measured and calculated deflection values compared well to each other.
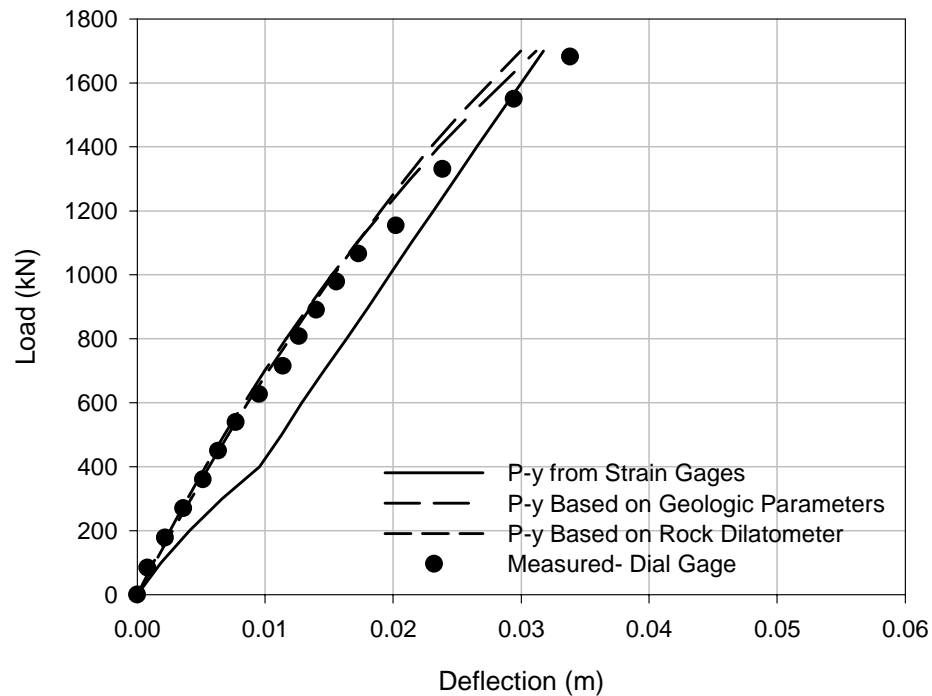
Figure 93. Verification of P-y Curve Model – Wilson County Short Shaft
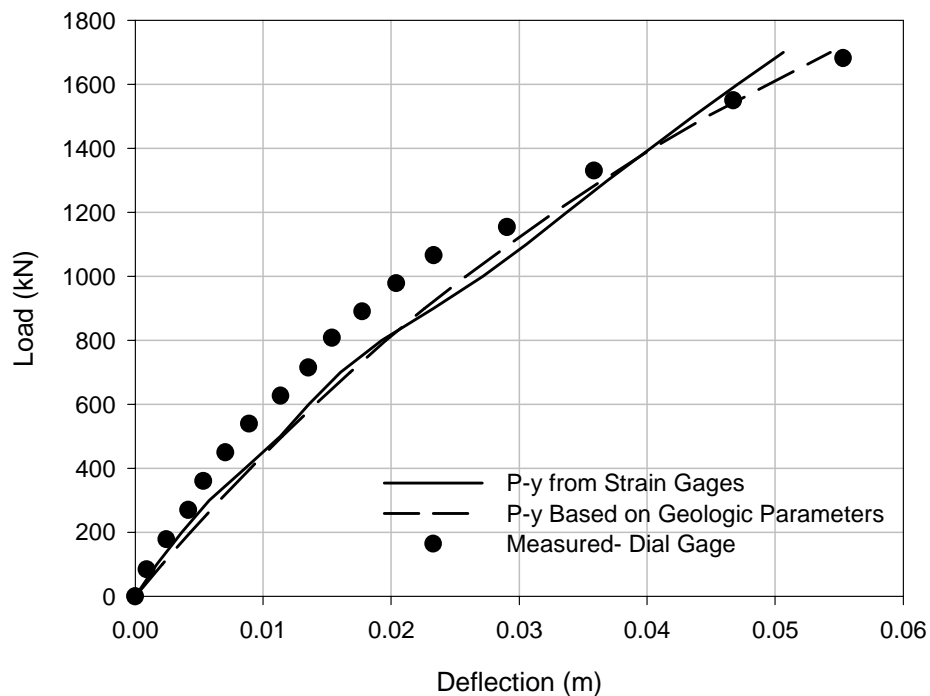
Figure 94. Verification of P-y Curve Model – Wilson County Long Shaft

In general, it seems that using rock dilatometer data to estimate lateral modulus for the development of P-y curves provided a more accurate estimation of load-deflection response as compared to method using index geological properties. Therefore, if a project requires a high accuracy of estimating lateral load-deflection response, or the geologic conditions of site are highly variable, the rock dilatometer should be used to measure in situ properties of the weathered rock at each shaft location. The developed model using geological properties will, however, yield increasingly more accurate results as better characterization of the weathered rock is provided and a data base of rock properties for the piedmont area is assembled as a resource for the design engineer.

In general, and as shown in Figures 90 through 94, the proposed P-y model for weathered rock provided reasonably well estimates of lateral deflection behavior in the different geological setting tested. However, the proposed model was based on the relatively small database of load test developed for this study. In order to further evaluate the reliability of the proposed P-y model, a comparison analysis with published field test results is presented.

5.4.2 Comparison with Published Load Test (Reese, 1997)

Results presented by Reese (1997) included lateral load test data with shafts embedded in weathered rock. The load test was performed by the California Department of Transportation (Speer, unpublished report, 1992). The test site was underlain by sandstone as found from geological investigation. Twenty (20) values of RQD were reported, ranging from zero to 80 %, with an average of 45 %. The sandstone was very fractured with bedding planes, joints, and fracture zones. Pressuremeter tests were conducted and the results, as reported by Reese (1997), are shown in Figure 95 in terms of variation of elastic modulus with depth.
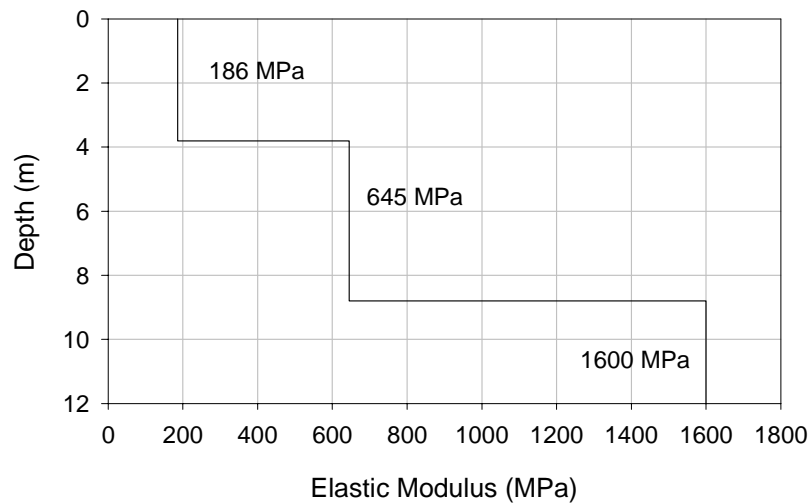
Figure 95. Initial Moduli of Rock from Pressuremeter (Reese, 1997)

At the test site, two concrete shafts were laterally loaded. The geometric and stiffness properties of the test shafts are summarized in Table 25.

Table 25. Properties of Test Piles

	Pile A	Pile B
Diameter (m)	2.25	2.25
Length (m)	12.5	13.8
EI (kN-m^2)	35.15×10^6	35.15×10^6

In order to use the proposed P-y curve model, GSI values must be determined. As explained before, GSI value can be determined using Figure 13 in Chapter 2, or based on Rock Mass Rating (RMR) method. The compression strength values of the weathered rock reported in the paper (0-3.9 m; qu=1.86MPa, 3.9-8.8 m; qu=6.45 MPa, and below 8.8 m; qu=16 MPa) were assumed based on elastic moduli measured from pressuremeter, with reducing the moduli values by factor of one hundred (100). However, this assumption of a reduction factor of 100 might be too conservative for use in the P-y model, proposed herein, based on geologic data. This is especially considered since the proposed P-y model accounts for rock weathering through GSI value, and is based on laboratory-evaluated qu values. In the analysis herein, the compressive strength for the weathered rock was assumed based on a database for sandstone with a possible range of rock properties.

Axial compression yielded a value of sandstone compressive strength in the range of 19.6 – 167 MPa (Farmer, 1968). Lama and Vutukuri (1978) published a database of rock properties for various rock types. The unconfined compressive strengths of sandstone were listed for 217 cases. The distribution of compressive strength values is shown in Figure 96. The distribution shows a typical shape of log-normal distribution.
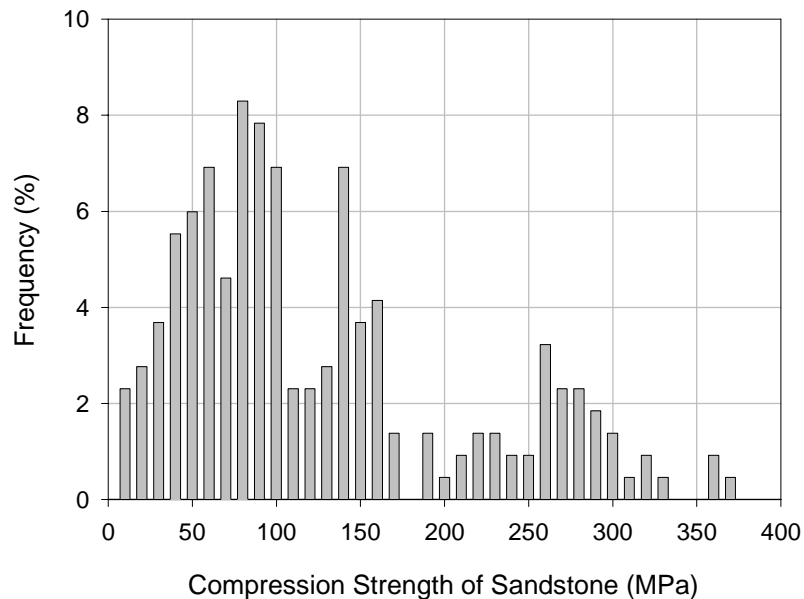
Figure 96. Distribution of Unconfined Compression Strength (σ_c) of Sandstone

The average and standard deviation, presented in Table 26 were calculated by assuming that the distribution of data is a log-normal. Using one standard deviation above (maximum) and below (minimum) the mean value, a range of possible strengths were obtained as shown in Table 26.

Table 26. Summary of Statistical Analysis of Sandstone Property

Item	Log-Normal Distribution	Value
Average	4.25	69.9 MPa
Standard Deviation	1.05	-
Possible Maximum Value	5.30	200.1 MPa
Possible Minimum Value	3.20	24.4 MPa

To estimate subgrade modulus values based on geological properties, the spacing of joints and conditions of joints were assumed as presented in Table 27. The point of rotation, the increment of subgrade modulus, and the subgrade modulus along length of pile were calculated using equations 56 through 64.

Table 27. RMR Estimation for the Weathered Rock

Item	Value	Rating
Strength (MPa)	24.4 – 200.1	4-12
RQD (%)	0-80	3-17
Spacing of joint	(50-300 mm) - (1-3 m) (assumed)	10-25
Condition of joint	-	6-25
Ground water	Set to 10 (Hoek's Recommendation, 1997)	10
Sum		33-89

Figure 97 shows the comparisons between dial gage measurement results and calculated results using the proposed P-y curve model. The comparisons show good agreement and validate the proposed model as a possible tool to estimate lateral load-deflection response of a shaft embedded in weathered rock.

Figure 97. Top Deflection Comparisons with Data from Reese (1997)

CHAPTER 6. VERIFICATION OF P-y MODEL

Four additional full-scale field load tests were performed for verification of the P-y model for weathered rock presented in Chapter 5. Load-deformation predictions of the four test shafts were performed using data from the rock dilatometer prio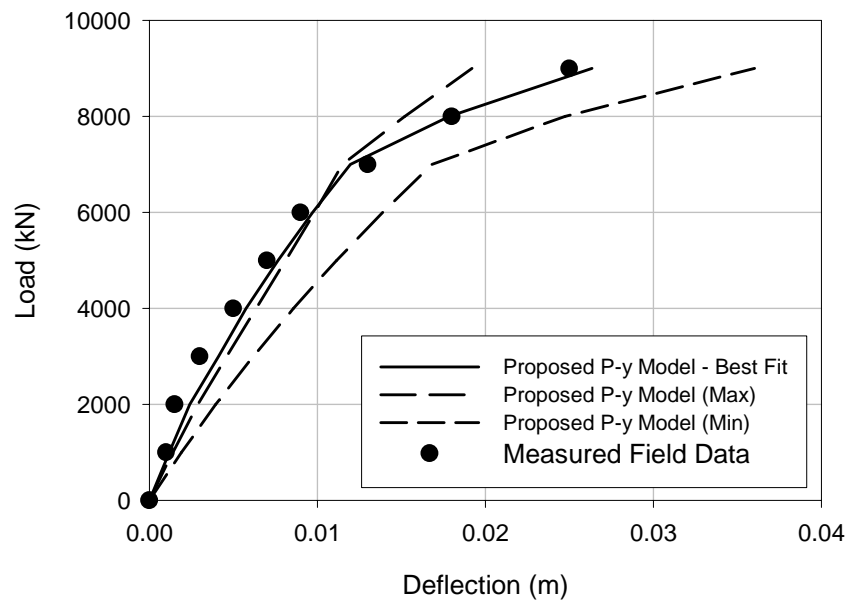r to field testing. In addition, performance predictions were developed using the proposed WR P-y model based on geologic parameters, Reese's method for P-y curves in weak rock (Reese, 1997), and the Stiff Clay Model (Reese, Cox, and Koop, 1975). During the progress of the load tests, measured pile head deflections were plotted against the a'priori predictions in the presence of Mr. Eric Williams, NCDOT.

6.1 Test Sites Description

The verification load tests were performed at two sites in Durham County, North Carolina. Two tests were performed at a site situated inside the cloverleaf interchange of Interstate 40 (I-40) West and North Carolina Highway 55, in southern Durham County. Two more tests were carried out inside the exit ramp area of the interchange between Interstate 85 (I-85) North and Gregson Street, in central Durham County.

The rock types encountered at each test site are listed in Table 28; the subsurface profiles consisted of residual soils, claystone, siltstone, and sandstone of the Durham Triassic Basin. At each test site, two 0.762 m diameter drilled shafts were constructed approximately 7.93 m apart. The shafts were drilled using a truck mounted rig and conventional rock augers; 12.7 mm-thick permanent steel casing was "screwed in" to shaft tip elevation of each test shaft. Figure 98 shows a picture of drilling a test shaft at the I-85 site. Permanent casing was utilized so that detectable deflections of the weathered rock could be realized without failure of the shaft. Testing setup was similar to that shown in Figure 31.

A loading frame supplied by the North Carolina Department of Transportation was used to transfer lateral load from a hydraulic jack to each test shaft. A 4,448 kN hydraulic jack and an electronic load cell were used to apply and monitor lateral loads during testing. Figure 99 shows a picture looking from the hydraulic jack to the long shaft at the I-40 test site. The test shafts were loaded in increments of approximately 89

kN up to 1512 kN. Unloading cycles, down to 89 kN, were performed as the test progressed.

Table 28. Verification Test Sites and Rock Types

Test Site	Rock Type
I-40	Triassic Claystone, Siltstone, and Sandstone
I-85	Triassic Claystone, Siltstone, and Sandstone

Figure 98. Drilling a Test Shaft – I-85 Site

6.1.1 Instrumentation Plan

Dial gages, strain gages, and slope inclinometers were used to measure deformations and strain with depth of the test shafts. Four surface dial gages were used to measure deflections and rotation. A fixed reference beam, in accordance with section 5.11 of ASTM D3966-90, was used to secure dial gages. Two dial gages were used to measure shaft rotation, so that deflection angles could be determined. One dial gage was used to measure deflection in the direction of loading, while another was used to measure movement perpendicular to the plane of loading.

Figure 99. Looking from the Hydraulic Jack, East to the Long Shaft
I-40 Load Test

Vibrating wire strain gages, mounted to 1 m- long sister bars, were attached to the tension side of the vertical reinforcement cages and cast into the test shafts. A CR-10x data logger, manufactured by Campbell Scientific, Inc., recorded strain and temperature measured from the vibrating wire gages.

A continuous chain of slope inclinometers was used to measure lateral deflection of the test shafts with depth. Electrolytic (EL) vertical in-place inclinometers were inserted into a plastic housing that was secured to the vertical reinforcement cage. A continuous chain of inclinometer probes consisted of sensors with wheels that are attached to each other at pivot points 0.5 m apart. Signal cables from each inclinometer extended up through the plastic housing to a data acquisition system, for monitoring and collection by a computer. Figure 100 is a picture of an instrumented reinforcement cage before insertion into the permanent casing; note that strain gages are on top as shown in the figure and inclinometer casing is opposite the gages.

Figure 100. Instrumented Reinforcement Cage

6.2 Interstate 40 Load Tests

The I-40 test site was situated at the northwest corner of the intersection of I-40 West and North Carolina Highway 55 in Durham County, North Carolina. The site was positioned within the confines of the cloverleaf exit ramp. Figure 101 is a local map of the area where the site is located. The test area footprint was 21 m by 12 m at the ground surface, and then sloped 3.1 m down to the test pad, El. 80.525 m. Figure 102 is a picture of the exposed rock at the elevation of the test pad.

Figure 101. Local Area Map of the I-40 Test Site

Figure 102. Exposed Rock at the Elevation of the Test Pad

6.2.1 Geology

There are two major Triassic Basins in North Carolina, The Dan River basin and the Deep River basin. The Deep River basin is divided into three separate basins, the Durham, Sanford, and Wadesboro sub-basins (Parish, 2001). The I-40 test site is located within the Durham Triassic Basin (DTB). The DTB is primarily comprised of sedimentary rocks including red conglomerate, arkosic sandstone, siltstone, claystone and mudstone (Parish, 2001). The residual soils at the test site were predominately dark brown to dark red-brown silty clays with mica. The transition to weathered rock was encountered approximately 3 m below the ground surface, EL. 83.698 m. RQD values of the material ranged from 72% to 100% at SB-1 and 89% to 100% at SB-2. The subsurface profile of the test site is shown in Figure 103.

6.2.2 Geotechnical Properties of the Test Site

Subsurface borings were performed at the location of each test shaft. Samples from standard penetration testing (SPT), in the residual soils, were dark brown to dark red-brown silty clay with mica. Blow counts (N-values) ranged from 9 (blows/300mm) to 16 (blows/300mm) at the surface and increased to 30 (blows/300mm) to 59 (blows/300mm) just above the weathered rock line, approximately 3.0 m below the ground surface. The weathered rock was cored using size H casing and NXWL core bits. The upper 3 m of
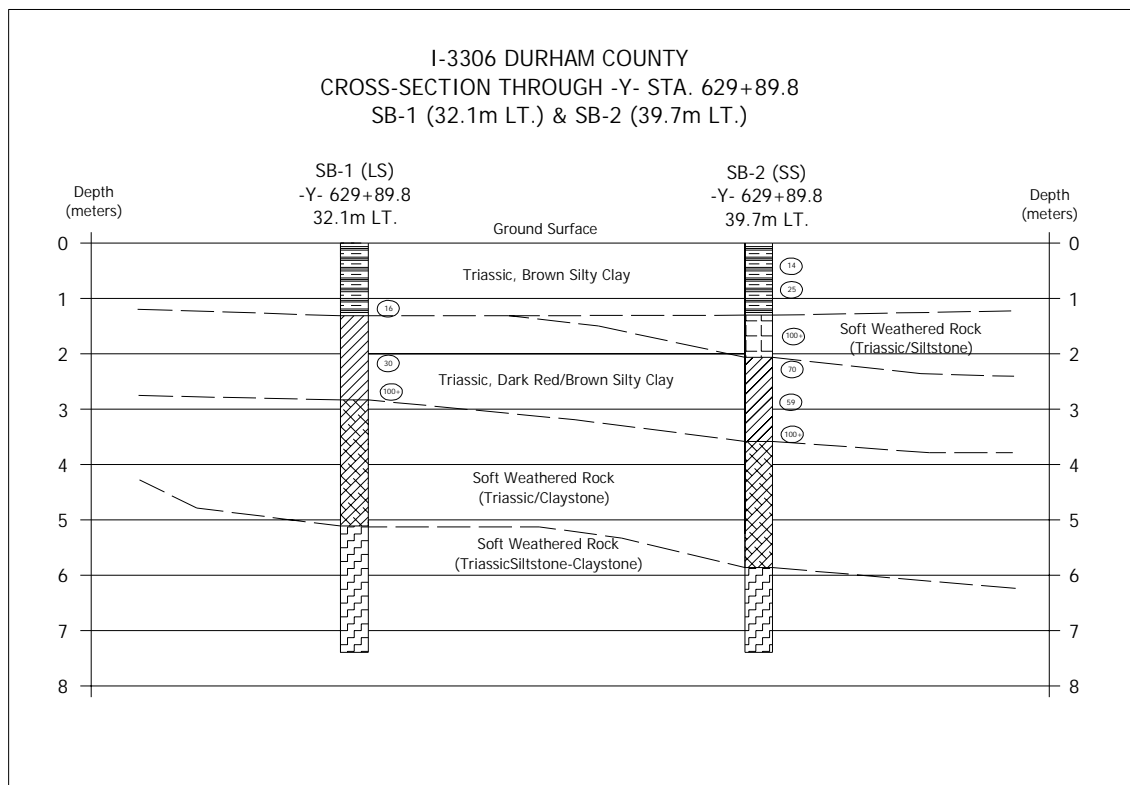
Figure 103. I-40 Test Site Subsurface Profile

weathered rock was claystone, after which there was a transition to siltstone then to sandstone. Core logs for each boring are given in Table 29. The NCDOT Materials and Test Unit tested core samples in unconfined compression. The unconfined compression (σ_{ci}) results are presented in Table 30 along with RQD values at corresponding depths. Upon completion of the rock coring, a rock dilatometer (model Probex 1 rock dilatometer manufactured by ROCTEST, Plattsburgh, NY) was used to

138

Table 29. I-40 Test Site Core Log

SB-1 – Long Shaft					
Depth (m)	Rate (min/0.5m)	Run (m)	Rec (m)	RQD (m)	Field Classification and Remarks
1.55 3.07	0:40 1:40 3:30	1.52	1.52 100%	1.52 100%	Dk. Red Brown, med. hard siltstone, only horizontal fractures 1.70, 2.05, 2.40, 2.60, 2.70, 2.90 meters
3.07 4.59	1:30 2:00 2:00	1.52	1.52 100%	1.10 72%	Dk. Red Brown, friable to indurated, soft to mod. hard siltstone, 1 joint from 3.80 to 4.05 meters
4.59 6.11	2:40 1:40 2:00	1.52	1.52 100%	1.52 100%	Dk. Red Brown, friable to indurated, med. hard to mod. hard siltstone and sandstone, 1 joint at 4.89 meters at 70 degrees
6.11 7.63	2:00 1:30 1:15	1.52	1.52 100%	1.19 78%	Dk. Red Brown, friable to indurated, soft to mod. hard siltstone and sandstone, 6.89 to 7.25 Red Brown hard clay, 7.25 meter Lt. Red, friable to indurated, mod. hard sandstone
SB-2 – Short Shaft					
1.54 3.06	1:39 1:24 2:35	1.52	1.30 86%		Dk. Red Brown, silty clay with rock fragments
3.06 4.58	2:21 1:43 1:56	1.52	1.52 100%	1.52 100%	Dk. Red Brown, silty clay to 3.41 meters, Dk. Red Brown, friable to indurated, med. hard to mod. hard, siltstone-claystone, no fractures
4.58 6.10	1:21 1:58 1:50	1.52	1.52 100%	1.35 89%	Dk. Red Brown, friable to mod. indurated, soft to mod. hard claystone-siltstone, no fractures
6.10 7.62	1:35 1:22 1:44	1.52	1.52 100%	1.36 89%	Dk. Red Brown, friable to mod. indurated, soft to mod. hard sandstone, 1 joint at 7.45 meters at 70 degrees

Table 30. I-40 Laboratory Test Results

Depth (m)	Unconfined Compressive Strength (MPa)	RQD (%)
6.20 – 6.39	25.9	78
3.50 – 3.63	12.2	72
5.24 – 5.41	12.2	89
6.10 – 6.25	34.9	100

measure pressure-volume data for the evaluation of the in situ rock-mass modulus of the weathered rock. Figures 104 and 105 show the pressure vs. volume curves obtained from the rock dilatometer testing for SB-1 and SB-2, respectively. The coefficient of subgrade reaction (k_{ho}) was determined, with depth, using measured rock dilatometer data and Equations 49 and 51; these data are presented in Table 31. The profile at the location of SB-1 has relatively higher modulus as presented in Table 31. At depths of 3.02 m and 4.02 m (in the case of SB-1) and 3.26 m (in the case of SB-2) there was lack of contact between the rock dilatometer probe and the sides of the core hole.

Table 31. I-40 Rock Dilatometer Results – k_{ho} Values

Boring Location	Depth (m)	k_{ho} (MN/m^3)
SB-1	5.02	394.5
	6.02	373.8
	7.02	349.1
SB-2	4.26	161.0
	5.26	195.6
	6.26	436.9
	7.26	396.4

MPa/m to pci: multiply by 3.684

6.2.3 Description of Drilled Shafts

Two drilled shafts, 0.762 m in diameter, were constructed 7.93 m apart at the test site. The long shaft was constructed at the location of subsurface boring SB-1 and the short shaft at SB-2. Due to the depth of the weathered rock at the test site, a 0.914 m temporary casing was first installed to the rock line at the location of each test shaft; the test shafts were drilled and constructed inside the temporary casing (this can be viewed in Figure 98). Each shaft was constructed using 27.6 MPa concrete with a vertical reinforcement cage made of 12 – #32 mm diameter rebar on a 245 mm radius. Shear spirals consisted of #16 mm diameter rebar at a 127 mm pitch. Each test shaft had a 12.7mm-thick permanent casing that extended to the tip elevations. The short shaft was embedded 3.356 m and the long shaft was embedded 4.057 m, each completely in weathered rock. Approximately 1 m of each shaft was left exposed to allow for the attachment of the load frame and surface instrumentation.
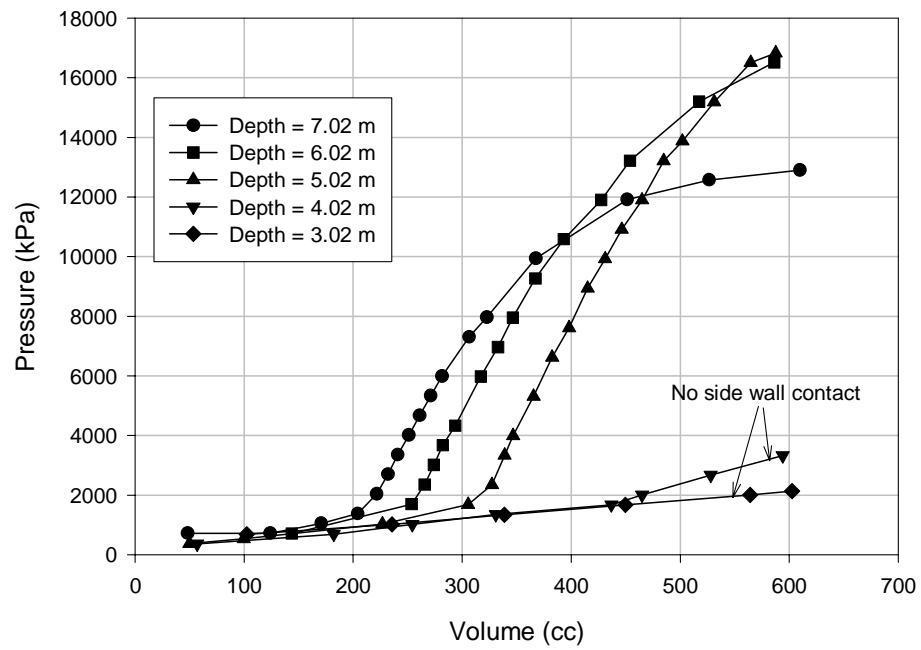
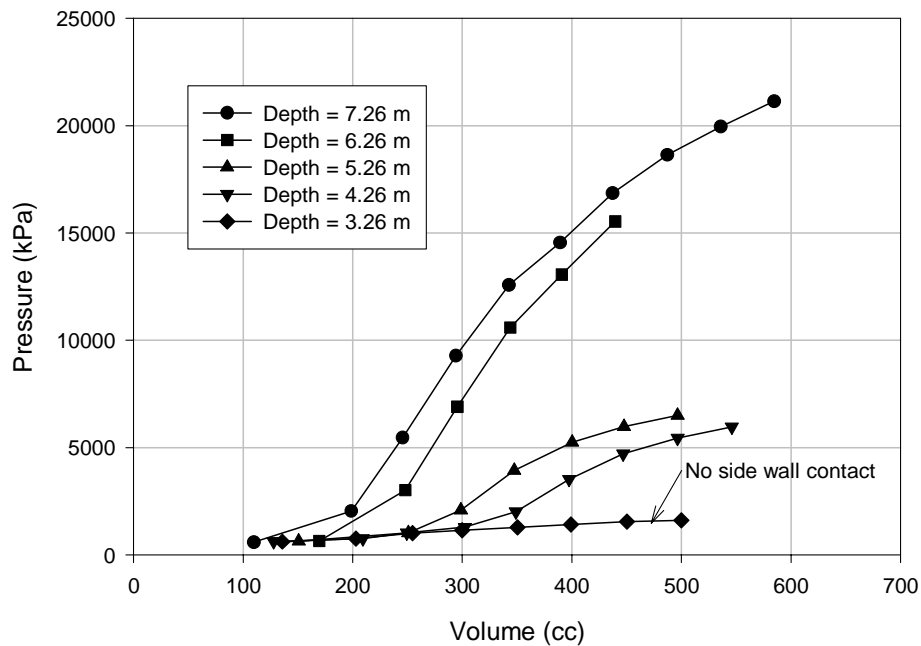**Figure 104. Rock Dilatometer Test Results – I-40 Test Site SB-1**

Figure 105. Rock Dilatometer Test Results – I-40 Test Site SB-2

141

The short shaft was instrumented with 7 vibrating wire strain gages attached to 1- m long sister bars. The long shaft had 9 strain gages similarly attached to the reinforcement cage using sister bars. Both shafts were instrumented with continuous slope inclinometer probes inserted into a plastic housing installed prior to concrete casting.

6.2.4 I-40 Load Test Performance Predictions

Four performance predictions were made for each shaft as follows:

1. "Predicted-Dilatometer" – P-y curves were computed based on k_{ho} from rock dilatometer test data and the proposed weathered rock criterion.
2. "Predicted-Geologic Based" – P-y curves were computed using the WR model with k_{ho} determined from empirical equations based on geologic index properties.
3. Reese's Method for P-y curves in weak rock and engineering properties as recommended by Reese (1997).
4. P-y Curves using stiff clay model (Reese, Cox, and Koop, 1975) and standard engineering properties used by the NCDOT.

6.2.4.1 I-40 Load Test – Predicted-Dilatometer

Using unconfined compressive strength test results and rock dilatometer data, the subsurface profiles at each shaft were analyzed in a number of layers. P-y curves as a function of depth were developed for each layer based on corresponding strength and modulus data. The parameters used for calculating the P-y curves for this set of predictions are listed in Table 32. The values of m_i and GSI were taken from Tables 3 and 4, respectively, as presented in the Literature Review. Because there were a limited number of samples tested in unconfined compression, a reference modulus ratio (k_h/σ_{ci}) based on data from the measured samples was used to establish the compressive strength for layers where data were not available.

The GSI value was determined by summing the ratings for each parameter listed in Table 4. The methodology for determining ratings for spacing of joints and condition of joints was to use those ratings that corresponded to measured RQD. Based on a recommendation put forth by Hoek and Brown (1997), a value of 10 was used for the ground water rating. Equation 64 was used to determine k_{ho} from rock dilatometer test results based on E from the rock dilatometer data. The average value of the elastic

modulus was determined by calculating a weighted average with depth. Depth to the point of rotation, T_o, was determined using Equation 59.

Table 32. Parameters for I-40 Predictions – Dilatometer

	Short Shaft			Long Shaft			
Layer Number	1	2	3	1	2	3	4
Layer Thickness (m)	1.8	1.0	0.5	1.2	1.4	1.0	0.6
γ' (kN/m^3)	25	25	25	25	25	15	15
σ_{ci} (MPa)	11.3	12.2	34.9	12.2	27.6	25.9	24.4
RQD (%)	100	89	89	72	100	78	78
GSI	87	74	76	57	66	76	74
m_i	9	9	19	9	14	14	14
E_s (GPa)	0.161	0.1456	0.4369	0.174	0.3945	0.3738	0.3491
k_{ho} (MN/m^3)	161.0	145.6	436.9	174.0	394.5	373.8	349.1
Avg. E_s (GPa)	0.1981			0.32			
K_R	3.895 x 10^{-2}			9.189 x 10^{-3}			
Calculated T_o (m)	2.46			2.66			
K_h Number, I_T	5.38			7.15			
# P-y Curves Used	13			19			

According to the proposed analyses procedure, equation 63 was then used to calculate k_{ho} above the initially estimated point of rotation, and Equation 64 was used below the point of rotation. P_{ult} was determined using Equations 26 and 65.

A spreadsheet was utilized to calculate values of k_h and P_{ult} for a number of P-y curves in each layer. These P-y curves were then entered into the computer program COM624P (Version 2.0, Reese and Wang, 1993) to evaluate the behavior of each shaft under incremental lateral loads. Figure 106 is presented to describe how the density of P-y curves was increased near layer interfaces; this allowed for a reduction in error imposed when the analysis software interpolated between curves. In an iterative process, the point of rotation determined from the COM624P analysis was reentered into the spreadsheet and a new set of P-y curves were generated. The new P-y curves were used for a second
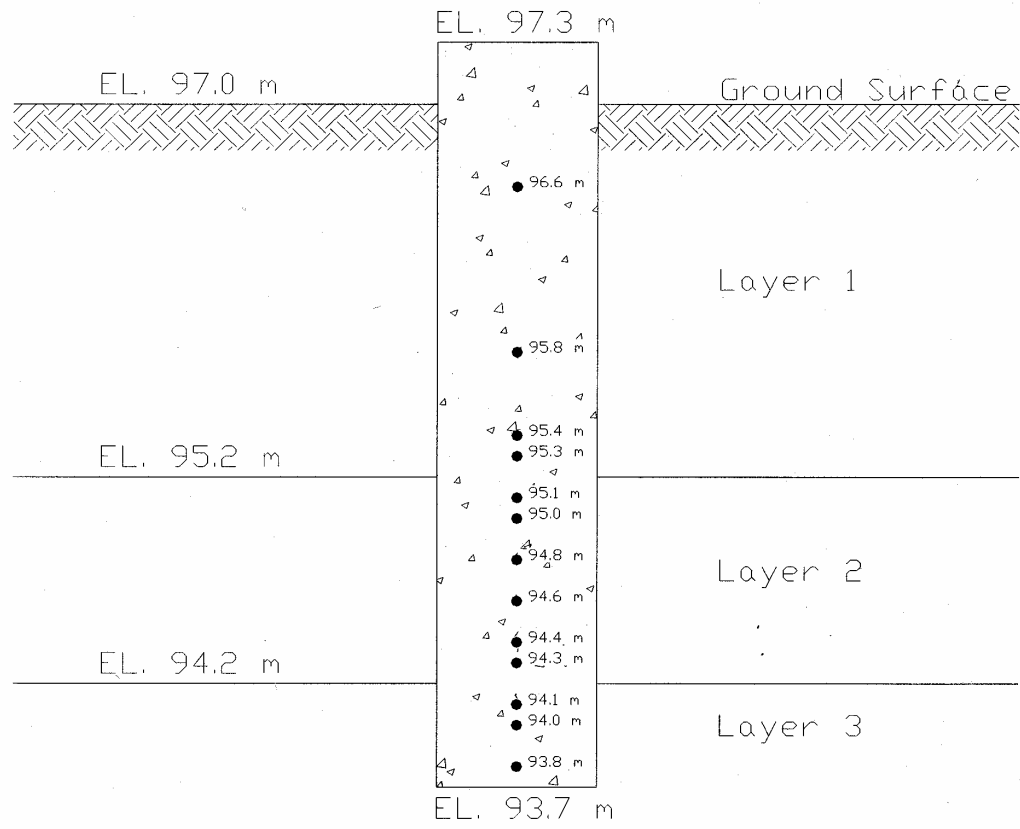
EL. 97.3 m

EL. 97.0 m

Ground Surface

● 96.6 m

Layer 1

● 95.8 m

EL. 95.2 m

● 95.4 m
● 95.3 m
● 95.1 m
● 95.0 m
● 94.8 m

Layer 2

● 94.6 m

● 94.4 m
● 94.3 m

EL. 94.2 m

● 94.1 m
● 94.0 m

Layer 3

● 93.8 m

EL. 93.7 m

Figure 106. Example of P-y Curve Distribution Used – I-40 Short Shaft Shown

iteration with this process repeated until the point of rotation converged to within 10% of the previous location. The point of rotation for the short shaft converged at 3.1 m below the point of load application, 0.64 m lower than the value initially calculated using the model in the first iteration. The point of rotation for the long shaft converged at a depth of 3.7 m below the point of load application, 1.04 m below the value initially calculated using the model. Table 33 lists the values of k_h and P_{ult} used to construct the P-y curves for both the short and long shaft predictions using dilatometer data. These values reflect the variability of rock strength and stiffness as obtained from laboratory and field testing.

Table 33. k_h and P_{ult} Values for I-40 Predictions – Dilatometer

Short Shaft					Long Shaft				
Layer #	Curve #	Depth[1] (m)	k_h (MPa)	P_{ult} (kN/m)	Layer #	Curve #	Depth[1] (m)	k_h (MPa)	P_{ult} (kN/m)
1	1	0.7	122.7	4746.0	1	1	0.7	132.6	1469.7
	2	1.5	122.7	4848.2		2	1.0	132.6	1529.2
	3	1.9	122.7	4898.6		3	1.3	132.6	1585.6
	4	2.0	122.7	4911.2		4	1.4	132.6	1604.3
2	5	2.2	110.9	3019.0	2	5	1.6	300.6	4330.0
	6	2.3	110.9	3033.7		6	1.7	300.6	4355.6
	7	2.5	110.9	3063.0		7	2.2	300.6	4481.2
	8	2.7	110.9	3092.0		8	2.6	300.6	4579.1
	9	2.9	110.9	3120.7		9	2.7	300.6	4603.3
	10	3.0	110.9	3135.0		10	2.8	300.6	4627.3
3	11	3.2	1790.6	8765.0	3	11	3.0	284.8	6579.8
	12	3.3	1790.6	8793.0		12	3.1	284.8	6601.1
	13	3.5	1790.6	8848.8		13	3.3	284.8	6643.5
CONVERSIONS MPa to psi: multiply by 145.04 kN/m to kips/inch: divide by 175.13						14	3.5	284.8	6685.6
						15	3.7	284.8	6727.5
						16	3.8	2036.0	6748.4
					4	17	4.0	1901.5	5969.4
						18	4.1	1901.5	5990.3
						19	4.3	1901.5	6032.0

6.2.4.2 I-40 Load Test – Predicted-Geologic Based

Predictions based on geologic parameters that are correlated with rock strength were developed using equations 58 and 60 for calculating E and k_{ho} (these equations utilize unconfined compressive strength data and GSI). The subsurface profile at each shaft was analyzed with the same number of layers and P-y curves used for dilatometer predictions. As the initial analysis of short shaft performance began, it was noticed that the calculated values of k_{ho} were large as compared to those determined from rock dilatometer testing. It was also noticed that the measured values of RQD for the I-40 rock cores were much larger than those from the Nash, Caldwell and Wilson field testing sites. The higher values of k_{ho} calculated from the empirical equations were a direct result of applying the previously described procedure for selecting GSI values. For

dilatometer predictions, GSI was used only for the calculation of ultimate strength, and modulus values were taken directly from rock dilatometer test results. With geologic-based predictions, GSI is used to establish both strength and modulus parameters; therefore, high RQD values lead to high GSI values, which results in high estimated modulus parameters (Note: GSI is the exponent of the equation for k_{ho}, therefore the effect of GSI on results of the equation is significant). A rational of "reduced GSI" was adopted to soften k_{ho} values from empirical equations so that predicted shaft head deflections would compare reasonably with dilatometer predictions.

GSI values were reduced by a multiplication factor determined by trial and error. The value of the reduction factor was varied until computed shaft head deflections were reasonable when compared with dilatometer predictions. Without reducing GSI, the predicted shaft head deflection for an applied lateral load of 1334 kN was 0.00499 m. When a reduction factor of 0.78 was applied to GSI values, shaft head deflection increased to 0.0135 m, compared to 0.0193 m predicted using dilatometer data. Table 35 lists the k_h values used to construct each P-y curve. Class B performance predictions for the long shaft utilizing the method presented in this section are given at the end of this chapter.

Table 34. k_h Values for I-40 Short Shaft Predictions – Geologic Based-Reduced GSI

Layer #	Curve #	Depth[1] (m)	k_h (MPa)
1	1	0.7	183.2
	2	1.5	186.9
	3	1.9	188.8
	4	2.0	189.3
2	5	2.2	167.4
	6	2.3	167.8
	7	2.5	168.8
	8	2.7	169.7
	9	2.9	170.6
	10	3.0	1452.3
3	11	3.2	2668.2
	12	3.3	2672.1
	13	3.5	2680.0

Note: Depth is referenced from the Point of Load, El. 81.0 meters.

MPa to psi: multiply by 145.04

6.2.4.3 I-40 Load Test– Reese's Method and Stiff Clay Model

P-y curves based on Reese's method were developed using the concepts presented in the Literature Review. The same number of layers and P-y curves were used for Reese's Method as used for predictions with the proposed WR P-y Model. Unconfined compressive strength from laboratory testing and elastic modulus from dilatometer testing were used to construct P-y curves by Reese's Method, along with an average of the range of k_{rm} values (0.000275) as reported by Reese (1997). These P-y curves were input to COM624P and pile head deflections, for incremental lateral loads, were determined.

COM624P contains a subroutine for the analysis of laterally loaded piles using the Stiff Clay Model. This selection was used with the following material properties: k_{ho} = 543,000 kN/m^3, cohesion = 200 kPa, and ε_{50} = 0.004. These material properties are standard for the North Carolina Department of Transportation when analyzing laterally loaded drilled shafts in weathered rock. Performance predictions for I-40 Short Shaft and Long Shaft are presented in Figures 107 and 108, respectively.
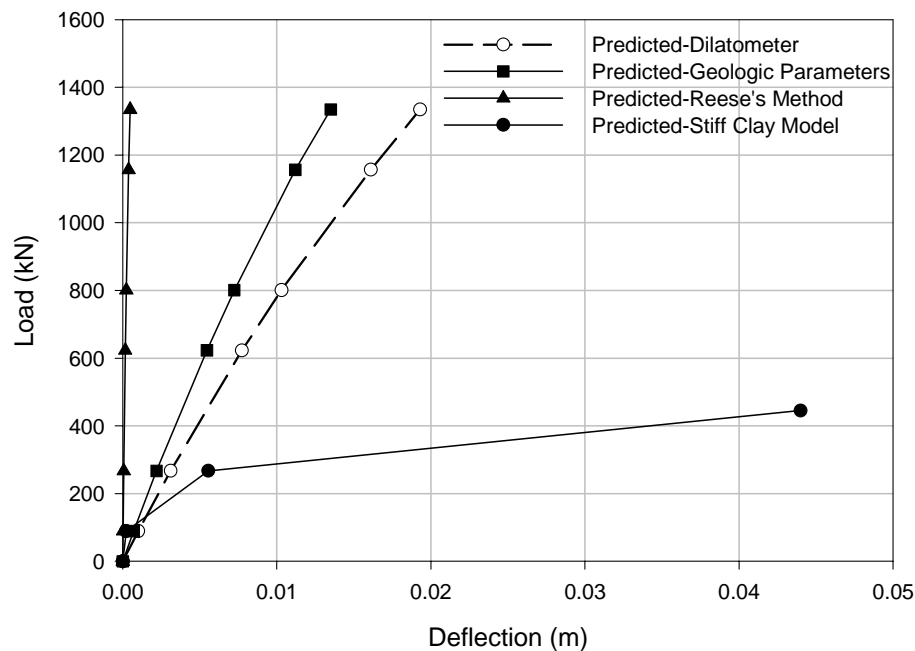
Figure 107. I-40 Short Shaft Performance Predictions
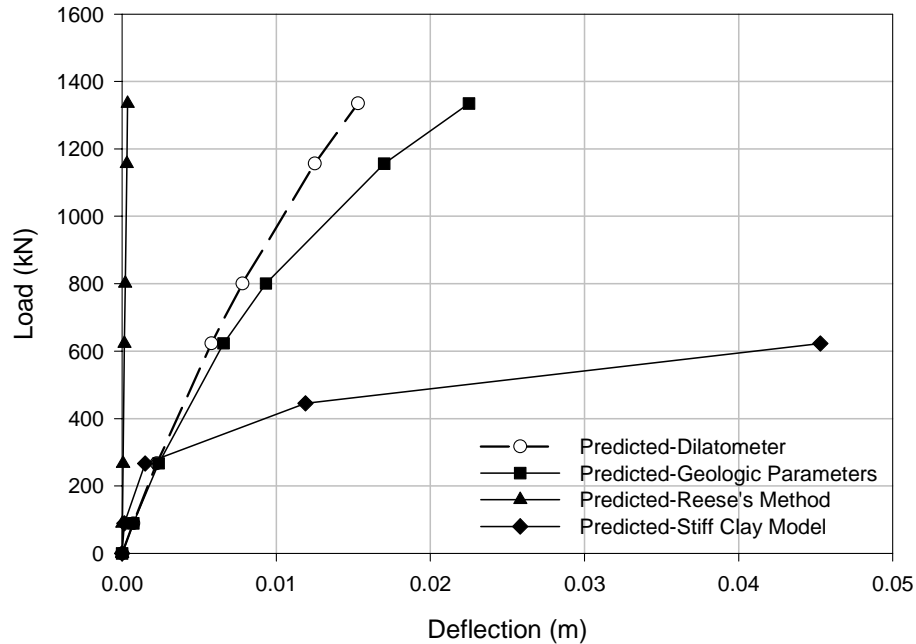
Figure 108. I-40 Long Shaft Performance Predictions

6.2.5 I-40 Load Test Results

Using a hydraulic ram with the loading frame in the field, lateral load was applied to both shafts in increments of 89 kN up to a maximum load of 1512 kN. For the maximum applied lateral load of 1512 kN, the short shaft experienced 0.0113 m of deflection at the point of load application, while the long shaft deflected 0.0161 m

6.2.5.1 Top Deflections and Inclinometer Readings

Dial gages were used to monitor shaft deflections above the ground surface for each increment of lateral load applied to the test shafts. Measured deflections for both shafts are presented in Figure 109. Both shafts exhibited nearly linear load-deflection behavior up to the maximum applied load. The larger deflections measured at the long shaft can be attributed to poorer quality of joints as well as close spacing of joints and effect of standing water. The long shaft was located on the lower end of the testing area, where perched water and rainwater accumulated. Triassic Weathered Rock is known to slake (degrade in strength) in the presence of water (Parish, 2001). It is postulated that slaking of the rock near the surface at the long shaft was the cause of the larger measured deflections. An axial statnamic test conducted for NCDOT showed a reduction in side
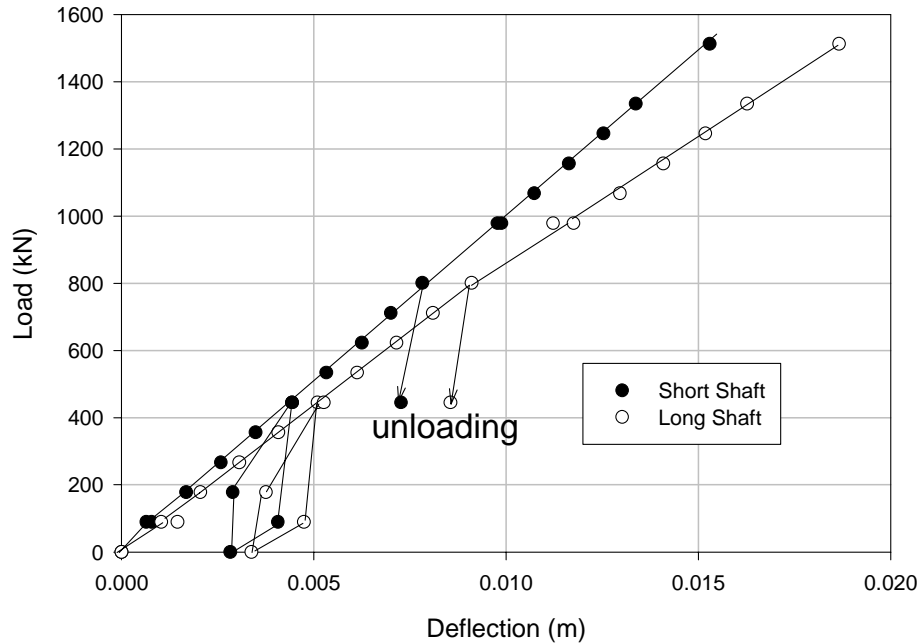
Figure 109. Top Deflections of I-40 Short and Long Shafts: Measured from Dial Gages

shear capacity of Triassic Weathered Rock, of up to 54%, due to soaking an augured shaft hole for a period of 24 hours (AFT, 2002).

As mentioned earlier, a system of continuous slope inclinometers was used to measure the deflection profile with depth for both the short and long shafts. Inclinometer data were recorded as the cumulative sum of successive gage deflections beginning with the bottom-most gage. Since neither string of inclinometers extended below the shaft tip, the data need to be adjusted to a known value of deflection. Shaft head deflections measured from dial gages were used to adjust these data. The deflection profiles before dial gage adjustment for both the short and long shafts are presented in Appendix I. The adjusted deflection profiles for the short and long shafts are given in Figures 110 and 111, respectively.
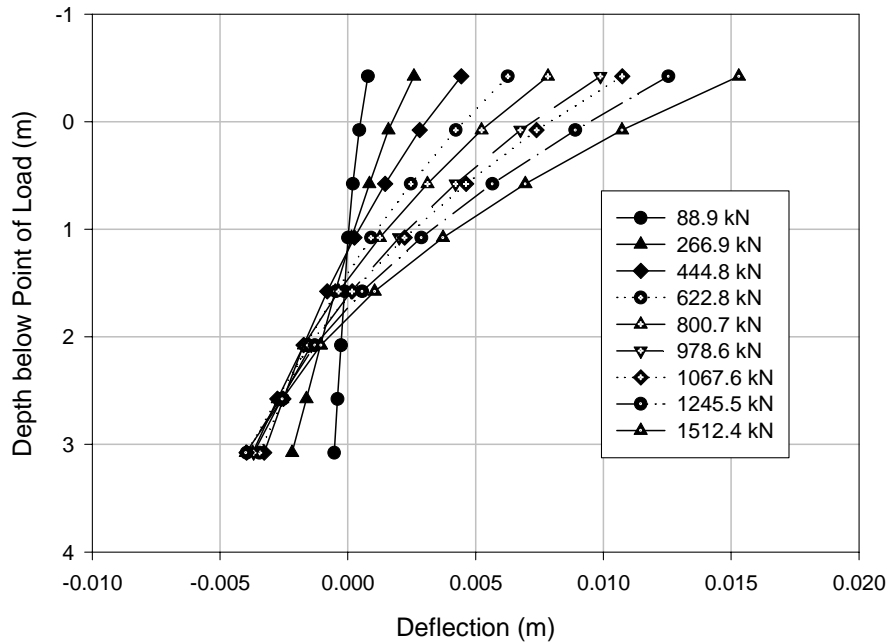
Figure 110. Deflection Profiles after Dial Gage Adjustment – I-40 Short Shaft
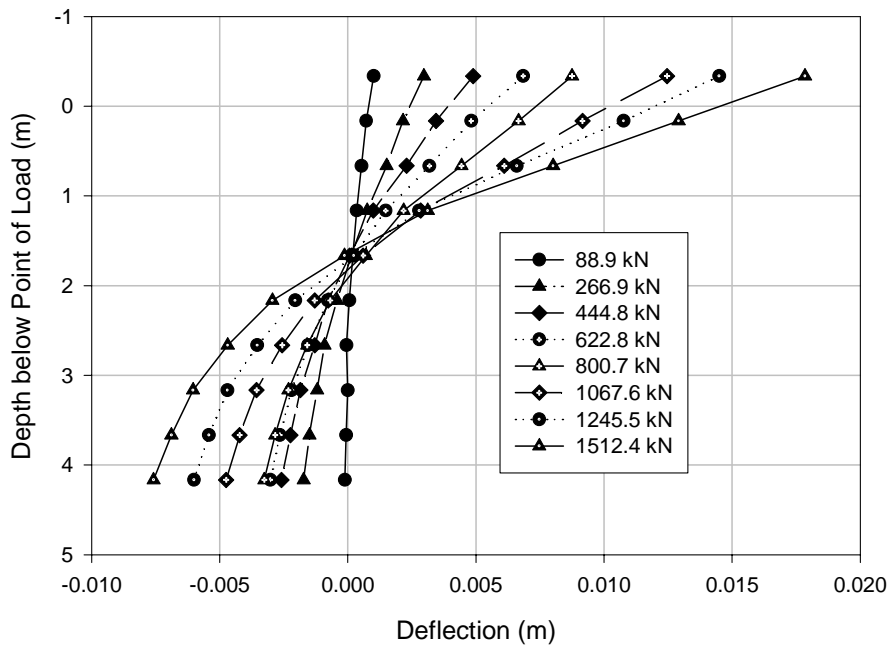
Figure 111. Deflection Profiles after Dial Gage Adjustment – I-40 Long Shaft

The tips of both shafts deflected considerably into the passive region. The weathered rock below the point of rotation at the location of the long shaft had a lower

strength than that of the short shaft, due to the suspected softening of the material due to slaking. In order to sustain larger loads, the weathered rock had to continue to deform; therefore it is hypothesized that the slaking of the rock caused the larger shaft-head deflections, even though the "long" shaft had a greater embedded length.

6.2.5.2 Predicted and Measured Shaft Performance

Comparison between predicted and measured shaft behavior, shown in Figures 113 and 114, suggest the applicability of the proposed WR P-y Model. The geologic-based predictions compared favorably with the measured short shaft deflections, and the dilatometer prediction can be considered a good conservative estimate in this case. As for the long shaft, the dilatometer predictions seem to model the behavior of the shaft relatively well. The predictions based upon geologic parameters performed well up to 600 kN, after which the effect of softening P_{ult} became evident.

Predictions using the stiff clay model with input parameters traditionally used by NCDOT consistently showed softer response as compared to measured data. Perhaps, such a finding emphasized the need for this research and the fact that NCDOT was well aware of the high degree of conservatism embedded in assuming weathered rock to behave as stiff clay. On the other end of the spectrum, the Reese (1997) rock model consistently yielded much stiffer responses than those measured. This finding is explained by the fact that Reese introduced a modulus multiplier, to obtain k_h, that increased from 100 at the rock surface to 500 at a depth/diameter ratio of 3. Such distribution of k_h variation with depth results in a stiff layer at relatively shallow depth, which considerably impacts the estimated lateral response of the shafts, as shown in Figures 113 and 114.

6.2.5.3 Back Calculated P-y Curves

Using the strain measurements with depth, moment curves were back calculated for each load increment using the concepts presented in the Literature Review. A fourth order regression equation was used to fit moment data; the soil reaction (P, kN/m) with depth was calculated from the second derivative of moment curves. Deflection (y, meters) was evaluated directly from inclinometer data. The back calculated P-y curves from strain gage and inclinometer data are shown in Figures 114 and 115.
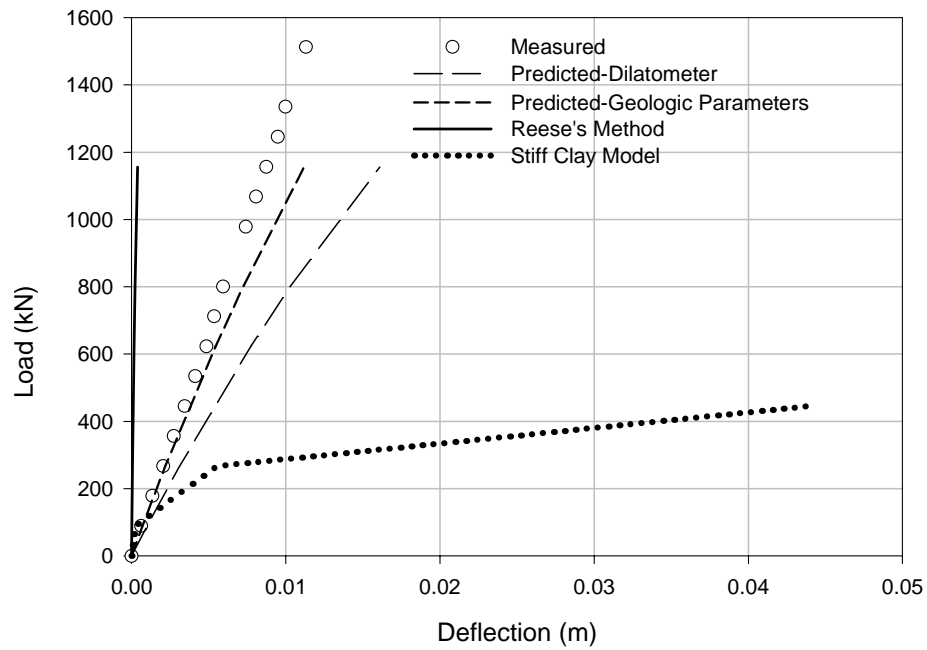
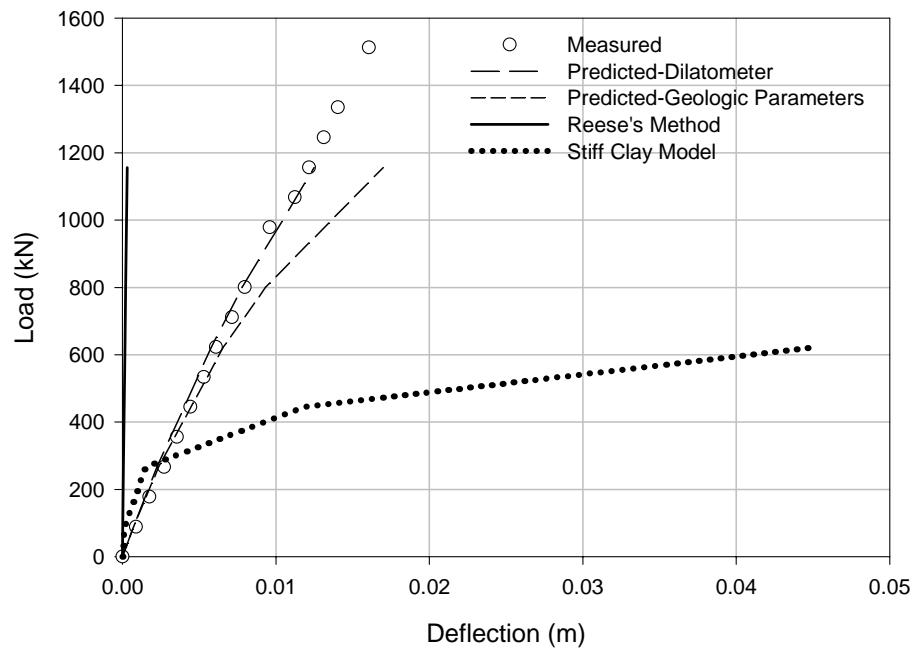**Figure 112. I-40 Short Shaft Pile Head Deflection Performance**

Figure 113. I-40 Long Shaft Pile Head Deflection Performance

152

The back calculated P-y curves show that k_h increased with depth; however a decrease in k_h from 2.3 m to 3.8 m for the long shaft was measured. This could be attributed to changes in rock properties that were not detected in the subsurface
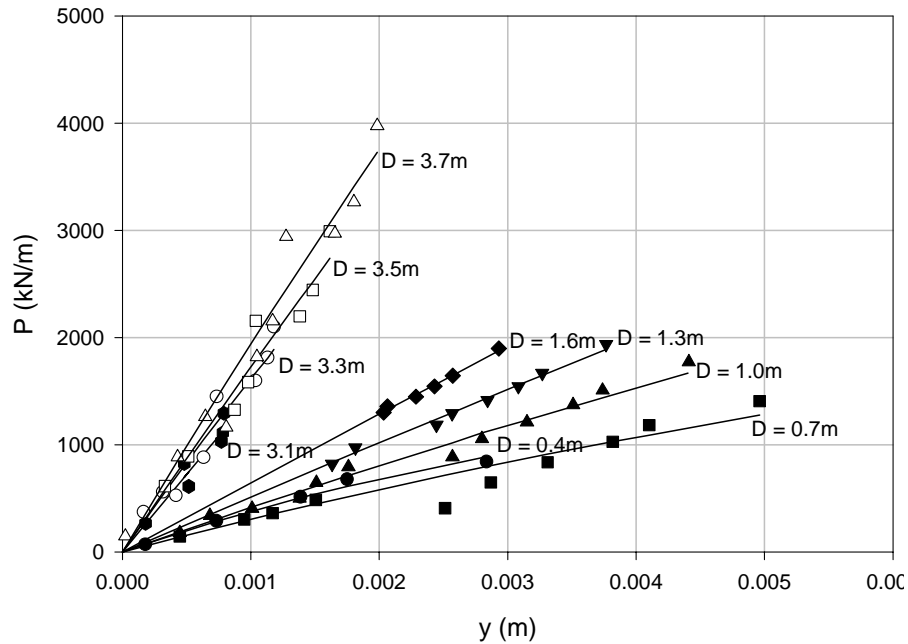

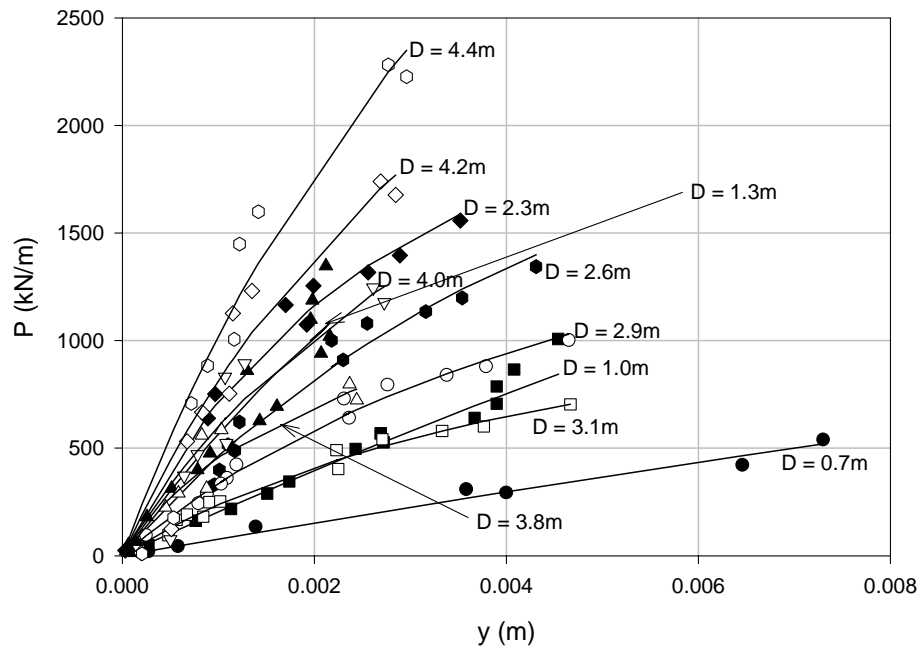**Figure 114. Back Calculated P-y Curves for the Weathered Rock – I-40 Short Shaft**

Figure 115. Back Calculated P-y Curves for the Weathered Rock – I-40 Long Shaft

153

investigation, or to error introduced in the back calculation process, partly due to small deflections around the point of rotation. Transformed axes plots were used to curve fit the back calculated P-y data. These plots were used to establish the values of k_h and P_{ult} for the back calculated P-y curves. Two examples are shown in Figures 116 and 117, and the remainder of the data are presented in Appendix E.
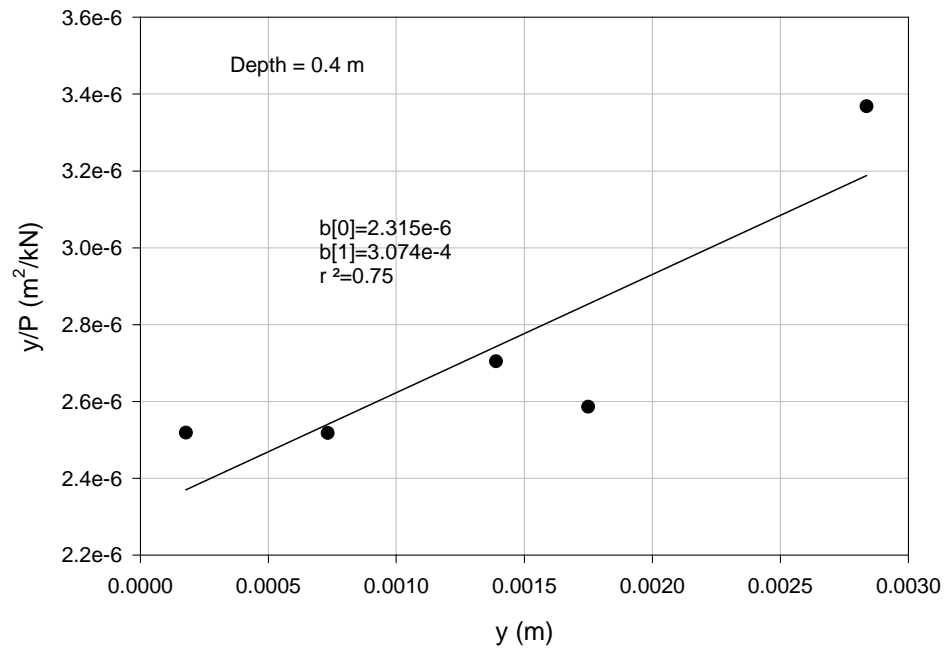
Figure 116. Curve Fitting Results – I-40 Short Shaft
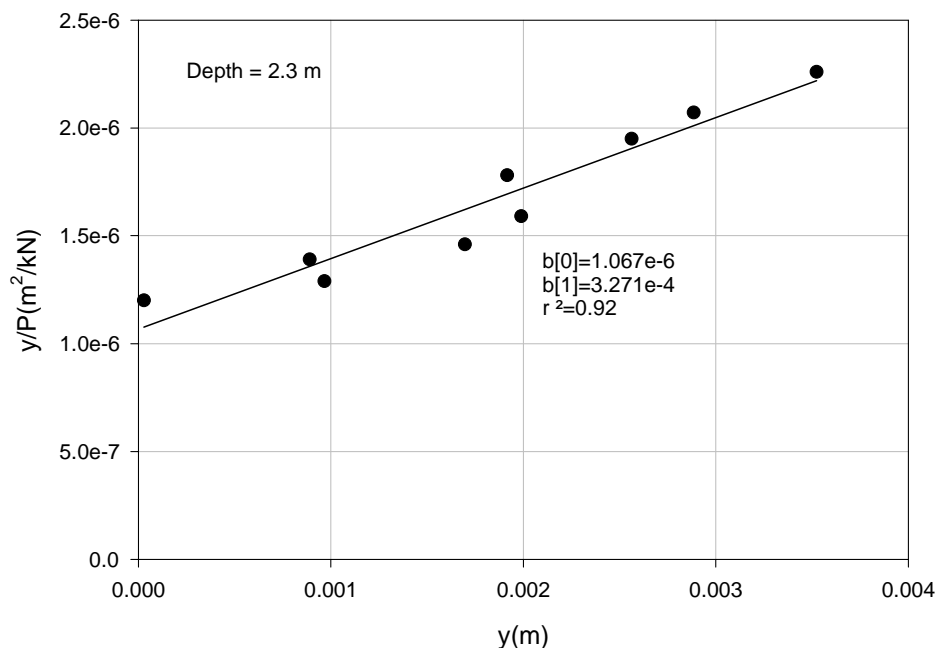
Figure 117. Curve Fitting Results – I-40 Long Shaft

6.2.5.4 Predicted and Back Calculated P-y Curves

Figures 118 through 123 are presented to compare P-y curves generated using the Weathered Rock Model to those back calculated from measured strain and deflection data. Because there was little variation in k_h and P_{ult} in the divided subsurface profiles, one estimated P-y curve is shown for each layer. For the sake of such estimation, an average depth was used (for example, in Figure 118, an average depth of 0.8 m was used in computations). For individual comparison purposes these graphs are plotted on differing scales.

In general, the WR P-y Model seems to underpredict the available resistances near the ground surface and somewhat over predict resistance at deeper depths (see Figure 123). However, the overall balance is such that there appears to be a compensating effect, in that shaft-head deflections at any given lateral load are reasonably well represented.
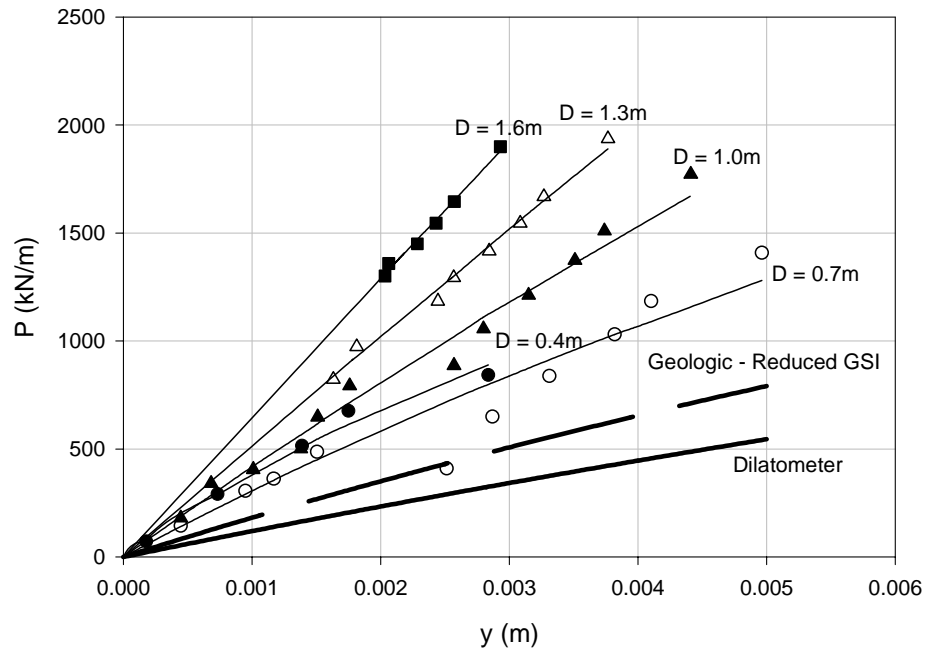
Figure 118. Predicted and Back Calculated P-y Curves – I-40 Short Shaft Layer 1
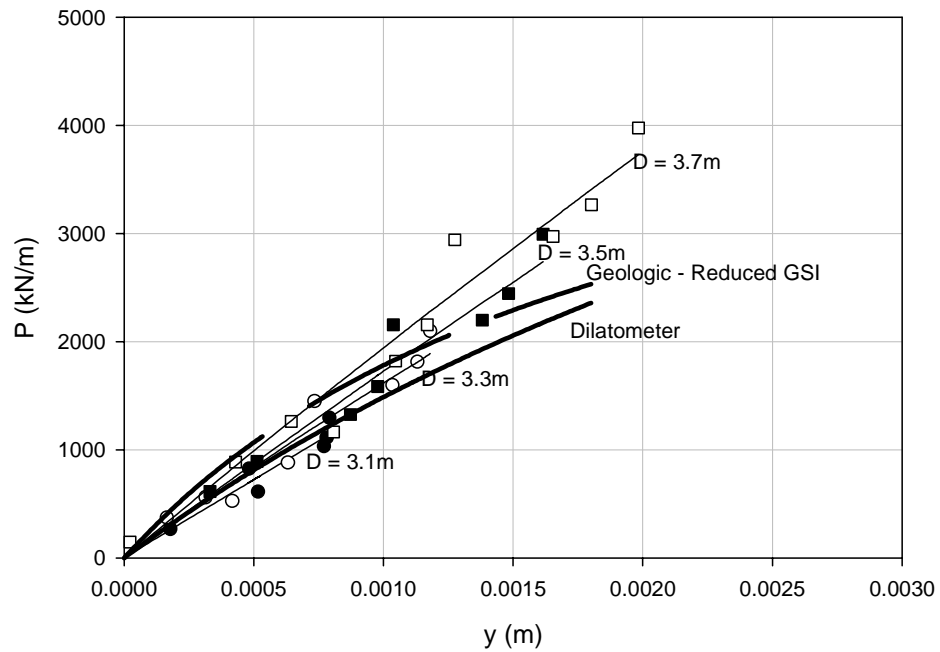
Figure 119. Predicted and Back Calculated P-y Curves – I-40 Short Shaft Layer 3
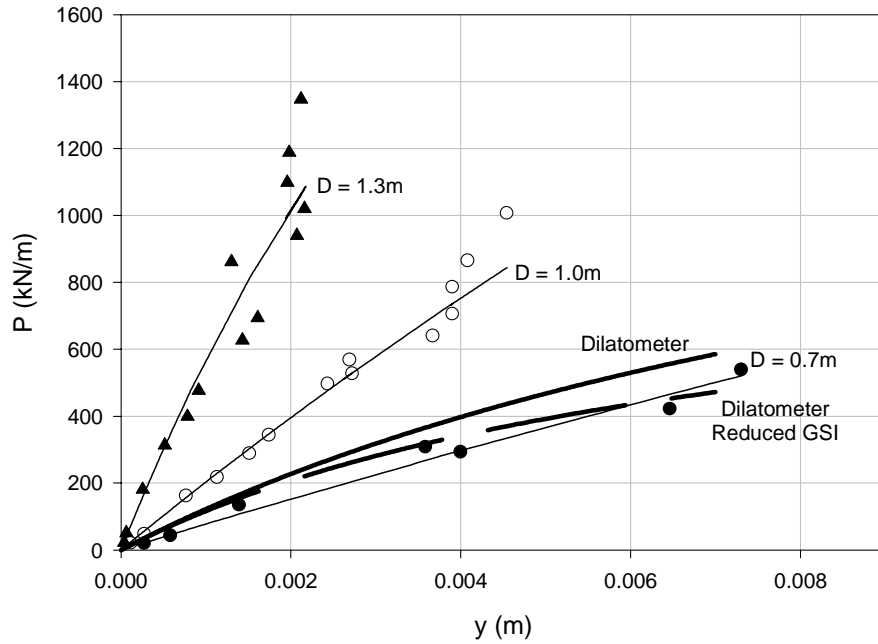
Figure 120. Predicted and Back Calculated P-y Curves – I-40 Long Shaft Layer 1
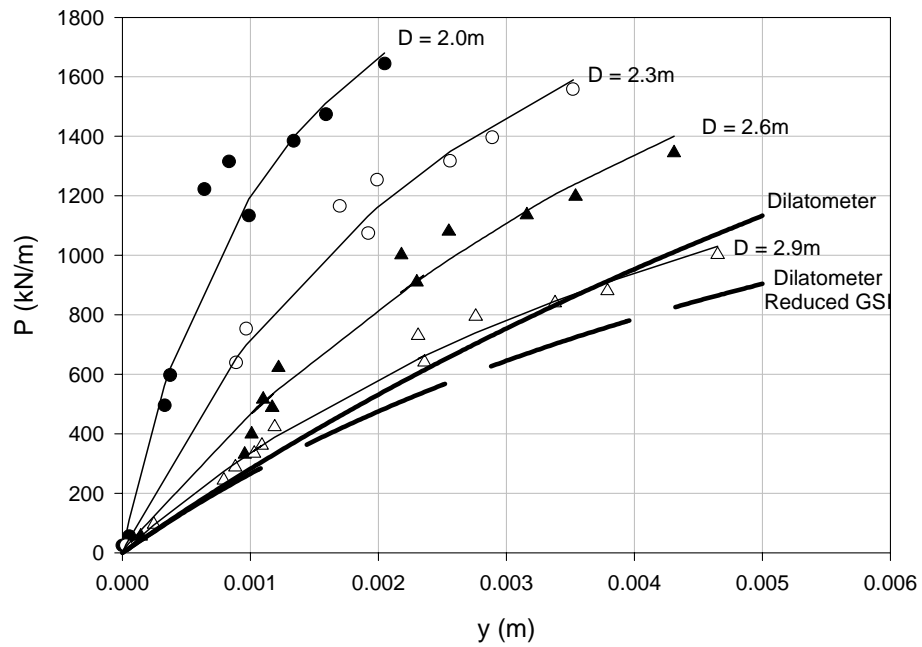
Figure 121. Predicted and Back Calculated P-y Curves – I-40 Long Shaft Layer 2
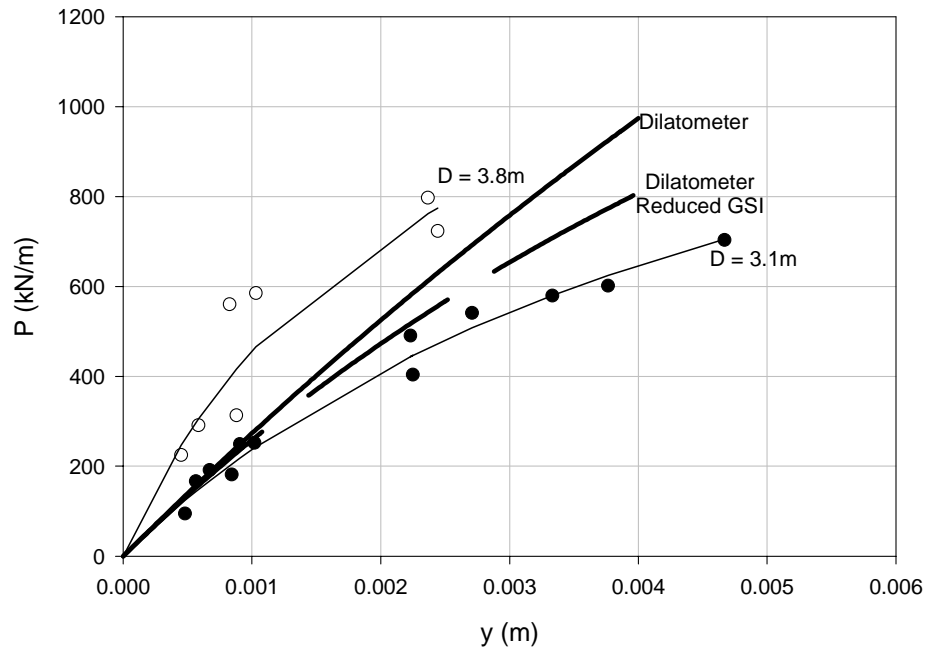
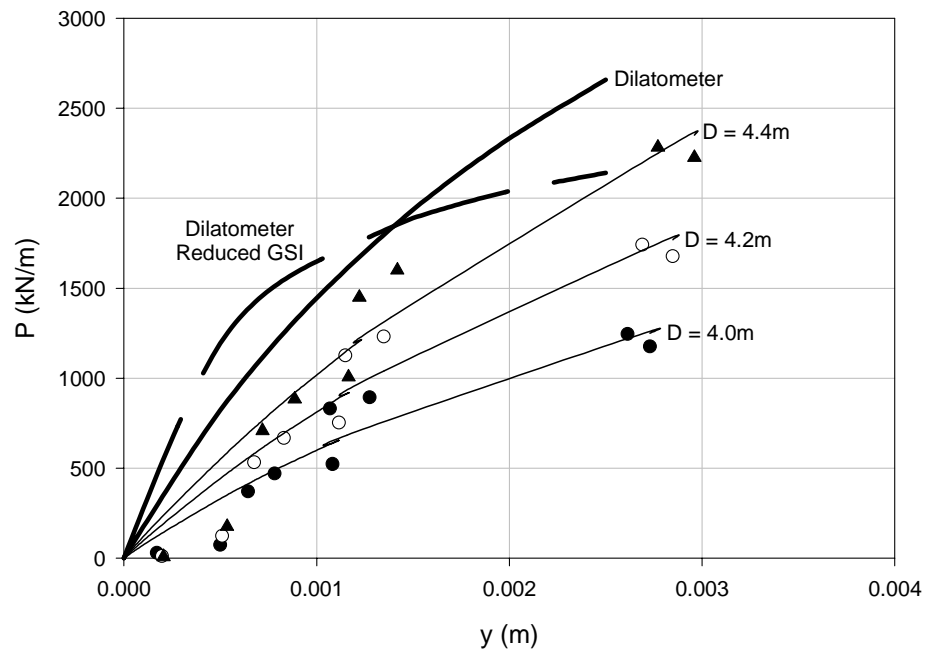**Figure 122. Predicted and Back Calculated P-y Curves – I-40 Long Shaft Layer 3**

Figure 123. Predicted and Back Calculated P-y Curves – I-40 Long Shaft Layer 4

6.3 Interstate 85 Load Tests

The I-85 test site was located within the exit ramp area of the Interstate 85 North and Gregson Street interchange, in central Durham County. Figure 124 is a local area map showing the site location. The test area was approximately 12 m by 8 m, and was excavated 1.5 m down to the test pad elevation, El. 97.6 m. Figure 125 is a picture of the exposed rock at the elevation of the test pad.

6.3.1 Geology

The I-85 test site was located on the northwestern portion of the Durham Triassic Basin (DTB). Approximately 1.2 m of residual soil was overlying the weathered rock at the test site. Coring was terminated approximately 5.1 m below the rock line in Triassic weathered rock. RQD values ranged from 49% to 96% at B1-Dur and 44% to 72% at B2-Dur (Parish, 2001). A subsurface profile of the test site is shown in Figure 126.

Figure 124. Local Area Map of the I-85 Test Site

159

Figure 125. Exposed Rock Profile at the Elevation of the Test Pad
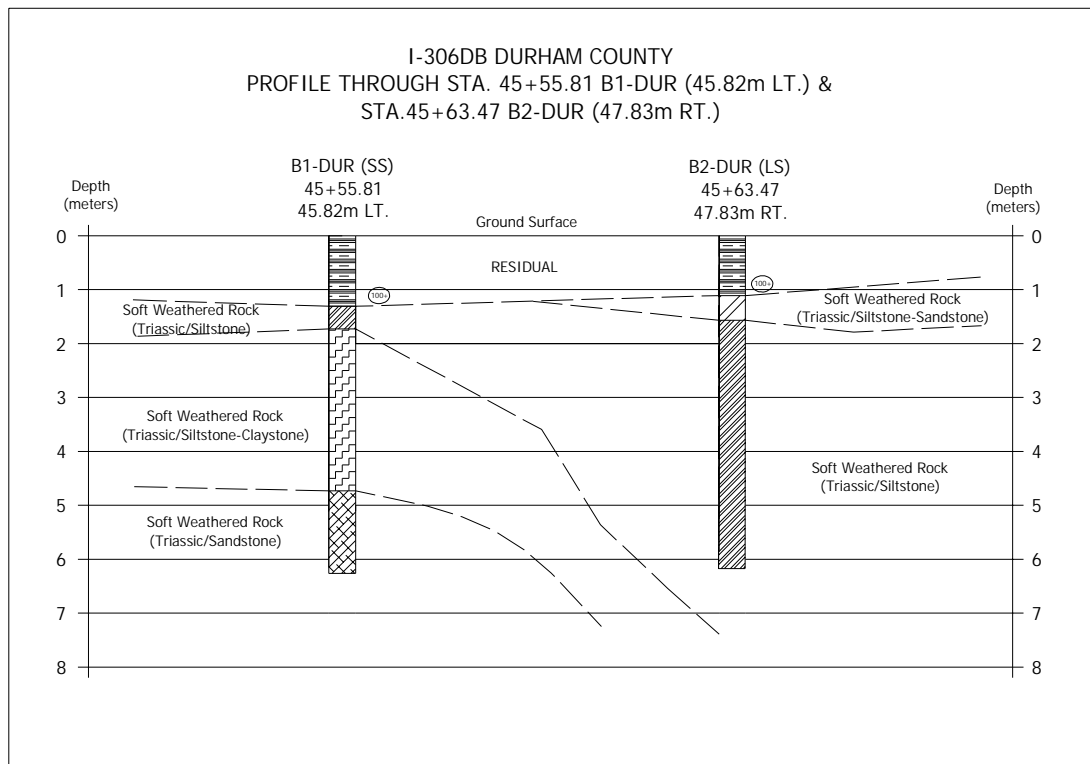
Figure 126. I-85 Test Site Subsurface Profile

6.3.2 Geotechnical Properties of the Test Site

Two subsurface borings were performed, one each at the location of each shaft. Information pertaining to the type of residual soil at the test site was not documented; the transition to weathered rock occurred approximately 1.2 m below the ground surface. The weathered rock was cored using size H casing and NXWL core bits. The upper 4.5 m of weathered rock was Triassic siltstone and claystone, after which there was a transition to Triassic sandstone. Table 35 presents a description of the core runs taken at each boring. Core samples were selected for unconfined testing by North Carolina State University researchers; results are presented in Table 36. This site was also a part of a comprehensive research program into the Slake Durability and Engineering Properties of Durham Triassic Basin Rock, (Parish, 2001). After the rock coring was completed, a rock dilatometer (model Probex 1 rock dilatometer manufactured by ROCTEST, Plattsburgh, NY) was used to measure pressure-volume data for the evaluation of the in-situ rock-mass modulus. Figures 127 and 128 show pressure vs. volume curves for B1-Dur and B2-Dur, respectively. The coefficient of subgrade reaction (k_{ho}) was determined

Table 35. I-85 Test Site Core Log

Depth (m)	Rate (min/0.5m)	Run (m)	Rec (m)	RQD (m)	Field Classification and Remarks
B1-Dur – Short Shaft					
1.46 1.67	Time not taken	0.21	0.21 100%	0.12 57%	Red Brown to Gray, Severely Weathered, Moderate to Extremely Fractured Weathered Rock (Triassic Siltstone)
1.76 3.19	1:14 0:59 1:10	1.43	1.43 100%	0.7 49%	Red Brown to Gray, Moderately to Severely Weathered, Slightly to Extremely Fractured Weathered Rock (Triassic Siltstone-Claystone) Sandstone Layer: 1.77 – 1.86 meters
3.19 4.71	1:05 1:26 1:16	1.52	1.52 100%	0.98 64%	Red Brown to Gray, Moderately to Severely Weathered, Slightly to Extremely Fractured Weathered Rock (Triassic Siltstone-Claystone) Sandstone Layer: 4.08 – 4.17 meters
4.71 6.23	1:26 1:14 1:31	1.52	1.52 100%	1.46 96%	Red Brown to Gray, Moderately Weathered, Moderately to Slightly Fractured, (Triassic Siltstone-Sandstone) Siltstone: 4.72 – 5.09m & 5.94 – 6.16m Sandstone: 5.09 – 5.94m & 6.16 – 6.25m
B2-Dur – Long Shaft					
1.19 1.65	Time not taken	0.46	0.46 100%	0.27 59%	Moderately Fractured, Severely Weathered, Gray Weathered Rock (Triassic Siltstone-Sandstone)
1.65 3.17	1:10 1:05 0:47	1.52	1.52 100%	0.67 44%	Moderately to Extremely Fractured, Severely Weathered, Red Brown to Gray Weathered Rock (Triassic-Siltstone)
3.17 4.69	0:52 1:18 1:02	1.52	1.52 100%	0.67 44%	Slightly to Extremely Fractured, Moderately to Severely Weathered, Red Brown Weathered Rock (Triassic Siltstone)
4.69 6.21	1:26 1:22 0:59	1.52	1.46 96%	1.10 72%	Slightly to Extremely Fractured, Moderately to Severely Weathered, Red Brown Weathered Rock(Triassic Siltstone)

Table 36. I-85 Laboratory Test Results (Parish, 2001)

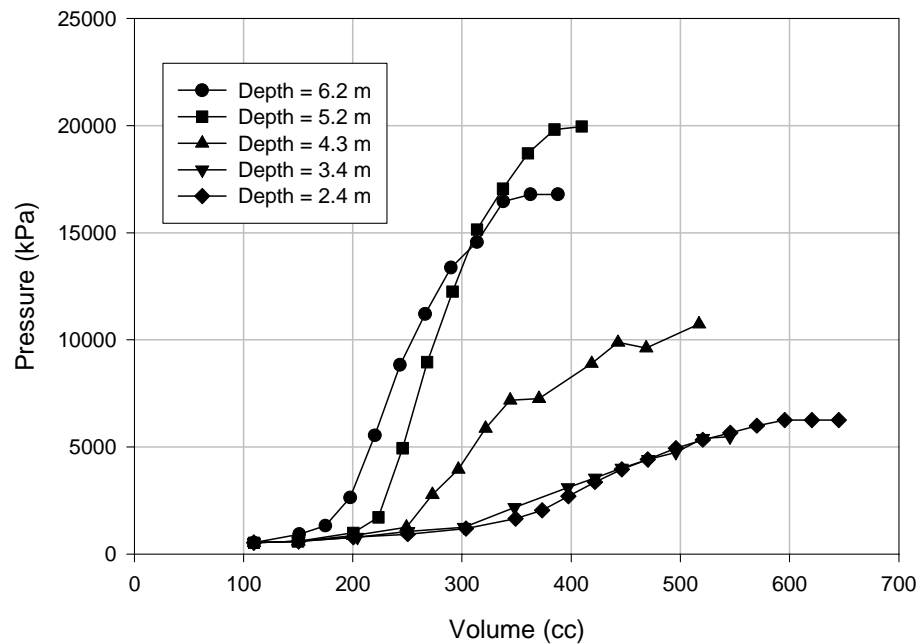| Depth (m)	Unconfined Compressive Strength (MPa)	RQD (%)
3.0 – 3.9	28.7	44%
3.6 – 4.7	45.5	64%
4.3 – 5.4	33.0	100%
4.7 – 5.5	28.5	44%
5.4 – 6.2	35.8	72%
5.5 – 6.1	30.8	96%

MPa to psi: multiply by 145.04

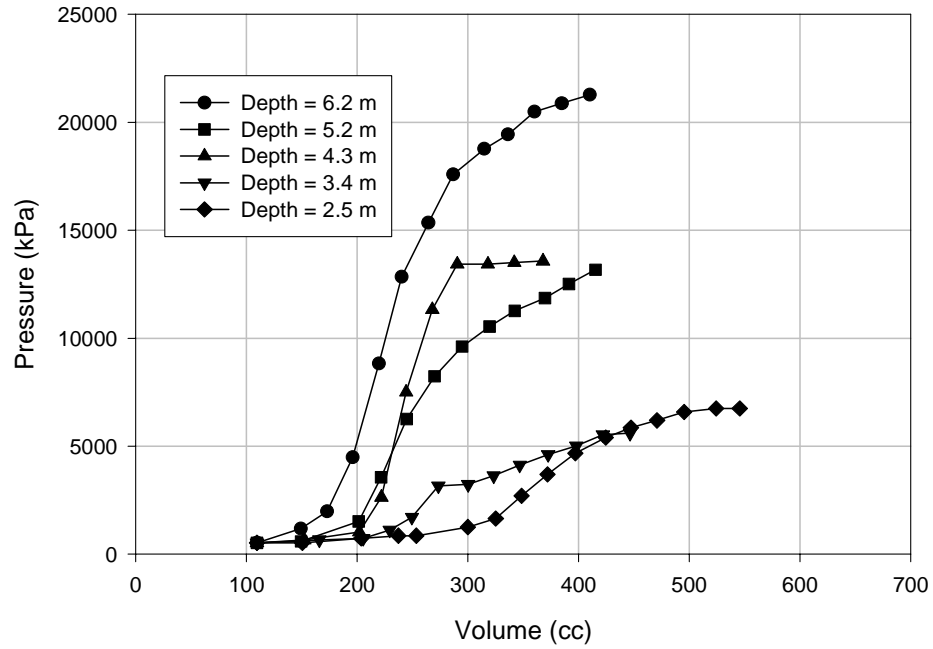**Figure 127. Rock Dilatometer Test Results – I-85 Test Site B1-Dur**

Figure 128. Rock Dilatometer Test Results – I-85 Test Site B2-Dur

with depth using the measured rock dilatometer data and Equations 49 and 51; these results are presented in Table 37.

Table 37. I-85 Rock Dilatometer Results – k_{ho} Values

Boring Location	Depth (m)	k_{ho} (MPa/m)
B1-Dur	2.4	107.9
	3.4	92.1
	4.3	336.2
	5.2	876.9
	6.1	707.4
B2-Dur	2.5	224.2
	3.4	106.3
	4.3	1151.9
	5.2	604.6
	6.2	1132.0

MPa/m to pci: multiply by 3.684

6.3.3 Description of Drilled Shafts

Two drilled shafts, 0.762 m in diameter, were constructed 7.93 m apart at the test site. The short shaft was constructed at location B1-Dur and the long shaft at B2-Dur. To aid in shaft construction, a 0.914 m temporary casing was installed through the overburden down to the rock line at each test shaft. Construction of the test shafts took place inside the temporary casings. The test shafts were constructed using 27.6 MPa concrete with a vertical reinforcement cage made from 10 - #32 mm diameter rebar on a 245 mm radius. Shear spirals consisted of #16 mm diameter rebar at a 127 mm pitch. Each test shaft had a 12.7 mm thick permanent steel casing down to the design tip elevations. The short shaft had an embedment depth of 2.789 m; the long shaft was embedded 4.21 m. Both shafts were completely embedded in weathered rock. Approximately 1 m of each shaft was left exposed to allow for the attachment of the load frame and surface instrumentation.

The short shaft was instrumented with 6 vibrating wire strain gages attached to 1m sister bars; the long shaft with 9 strain gages similarly attached to the reinforcement cage using sister bars. Both shafts had continuous slope inclinometer probes inserted into a plastic housing. The instrumentation scheme allowed for the measurement of both stain and deflection with depth.

6.3.4 I-85 Load Test Performance Predictions

Similar to I-40 case study, four performance predictions were developed for each shaft as described below:

1. "Predicted-Dilatometer" – P-y curves were computed based on k_{ho} from rock dilatometer test data and the proposed weathered rock criterion.

2. "Predicted-Geologic Based" – P-y curves were computed using the WR model with k_{ho} determined from empirical equations based on geologic index properties.

3. Reese's Method for P-y curves in weak rock and engineering properties as recommended by Reese (1997).

4. P-y Curves using stiff clay model (Reese, Cox, and Koop, 1975) and standard engineering properties used by the NCDOT.

6.3.4.1 I-85 Load Test Performance Predictions

Performance predictions for the 1-85 load tests were calculated as described in Section 6.2.4.1 through 6.2.4.3 with the following exception; the reduced GSI concept was not utilized. Table 38 lists the parameters used in making the "Predicted-Dilatometer" and "Predicted-Geologic Based" computations for both the short and long shaft. Table 39 lists the k_h and P_{ult} values used to construct P-y curves for calculating the lateral response of the short and long shaft. Table 40 gives k_h values calculated using the WR P-y Model based on geologic parameters. These values were used to make the "Predicted-Geologic Based" predictions.

Table 38. Parameters for I-85 Performance Predictions – Dilatometer and Geologic Based

	Short Shaft			Long Shaft			
Layer Number	1	2	3	1	2	3	4
Layer Thickness (m)	1.2	0.7	0.76	1.5	1.0	0.7	0.98
γ' **(kN/m^3)**	15	15	15	15	15	15	15
σ_{ci} **(MPa)**	29.1	24.8	45.5	25.0	28.7	33.0	33.0
RQD (%)	53	64	64	44	44	44	72
GSI	59	59	59	38	38	38	59
m_i	9	9	9	9	9	9	9
E_s **(GPa)**	0.1079	0.092	0.3362	0.2242	0.1064	1.1519	0.6046
k_{ho} **(MN/m^3)**	107.9	92.0	336.2	224.2	106.4	1151.9	604.6
Avg. E_s (GPa)	0.1689			0.4405			
K_R	1.082×10^{-1}			6.805×10^{-3}			
Calculated T_o (m)	2.5			2.55			
K_h **Number, I_t**	3.76			6.35			
# P-y Curves Used	15			18			

Note: k_{ho} values presented are based on rock dilatometer testing, k_h from empirical equations given in Table 18.

Table 39. k_h and P_{ult} Values for I-85 Load Test Predictions – Dilatometer

Short Shaft					Long Shaft				
Layer #	Curve #	Depth (m)	k_h (MPa)	P_{ult} (kN/m)	Layer #	Curve #	Depth (m)	k_h (MPa)	P_{ult} (kN/m)
1	1	0.47	82.2	3131.1	1	1	0.55	170.8	1444.3
	2	0.85	82.2	3209.7		2	1.05	170.8	1574.7
	3	1.2	82.2	3280.2		3	1.55	170.8	1689.0
	4	1.35	82.2	3309.9		4	1.7	170.8	1721.0
2	5	1.52	70.1	2942.5	2	5	1.9	81.0	1915.9
	6	1.65	70.1	2967.5		6	2.05	81.0	1947.1
	7	1.8	70.1	2995.8		7	2.4	81.0	2017.3
	8	1.9	70.1	3014.6		8	2.55	81.0	2046.3
	9	2.05	70.1	3042.6		9	2.65	81.0	2065.3
3	10	2.22	256.2	4972.4	3	10	2.95	877.7	2301.6
	11	2.35	256.2	4997.7		11	3.05	877.7	2320.5
	12	2.5	963.9	5026.7		12	3.2	877.7	2348.5
	13	2.6	963.9	5045.9		13	3.35	877.7	2376.0
	14	2.8	963.9	5084.2	4	14	3.55	460.7	4081.4
	15	2.9	963.9	5103.2		15	3.65	460.7	4099.1
CONVERSIONS MPa to psi: multiply by 145.04 kN/m to kips/inch: divide by 175.13						16	3.88	2927.4	4139.6
						17	4.13	2927.4	4183.1
						18	4.38	2927.4	4226.2

Note: Depth is referenced from the Point of Load, El. 97.83 m

Table 40. k_h Values for I-85 Load Test Predictions – Geologic Based

Short Shaft				Long Shaft			
Layer #	Curve #	Depth[1] (m)	k_h (MPa)	Layer #	Curve #	Depth[1] (m)	k_h (MPa)
1	1	0.47	219.8	1	1	0.55	61.2
	2	0.85	223.3		2	1.05	62.9
	3	1.2	226.6		3	1.55	64.6
	4	1.35	227.9		4	1.7	65.1
2	5	1.52	212.7	2	5	1.9	70.1
	6	1.65	213.9		6	2.05	70.6
	7	1.8	215.3		7	2.4	71.8
	8	1.9	216.3		8	2.55	72.3
	9	2.05	217.6		9	2.65	72.6
3	10	2.22	290.6	3	10	2.95	78.3
	11	2.35	291.8		11	3.05	78.6
	12	2.5	1495.7		12	3.2	79.2
	13	2.6	1500.4		13	3.35	79.7
	14	2.8	1509.9	4	14	3.55	243.3
	15	2.9	1514.6		15	3.65	243.7
MPa to psi: multiply by 145.04					16	3.88	2155.7
					17	4.13	2163.2
					18	4.38	2170.6

Note: Depth is referenced from the Point of Load, El. 97.83 m

Performance predictions for the short and long shafts are presented in Figures 129 and 130, respectively. The trend of the results is similar to that obtained for the I-40 load tests. Predictions from the stiff clay model yielded the softest load-deformation response while those using Reese's (1997) weak rock model yielded the stiffest response. Predictions using the rock dilatometer data and index geologic are reflection of the properties used for each shaft. At the location of the short shaft, higher RQD values were recorded, but a lower dilatometer modulus was estimated, as compared to the values at the location of the long shaft (where a lower RQD values were measured with a higher dilatometer modulus.) As will be presented in the next section, the rock dilatometer modulus better reflected the soil stiffness, as was evidenced from the load test data.
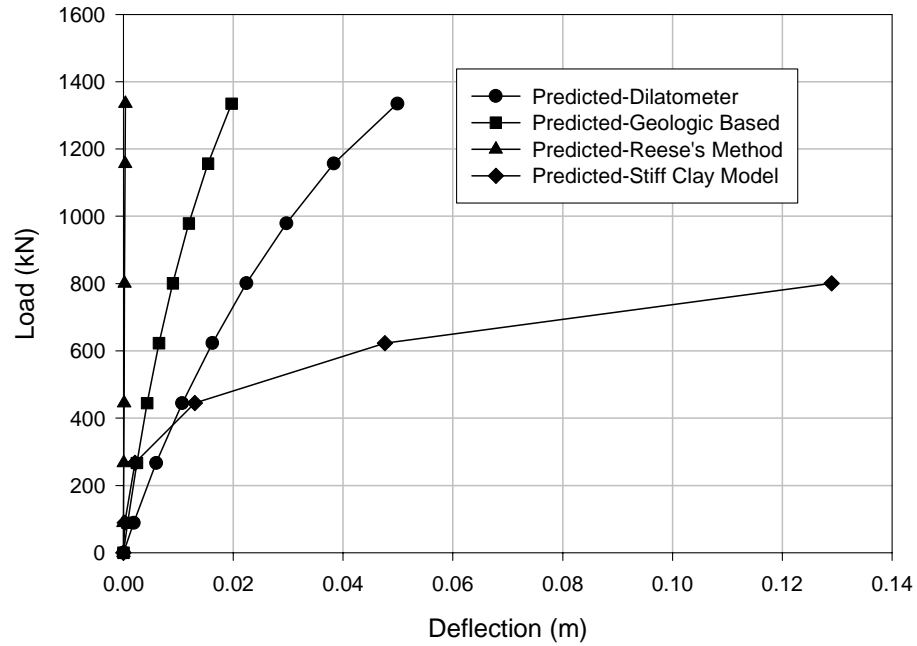
Figure 129. I-85 Short Shaft Performance Predictions
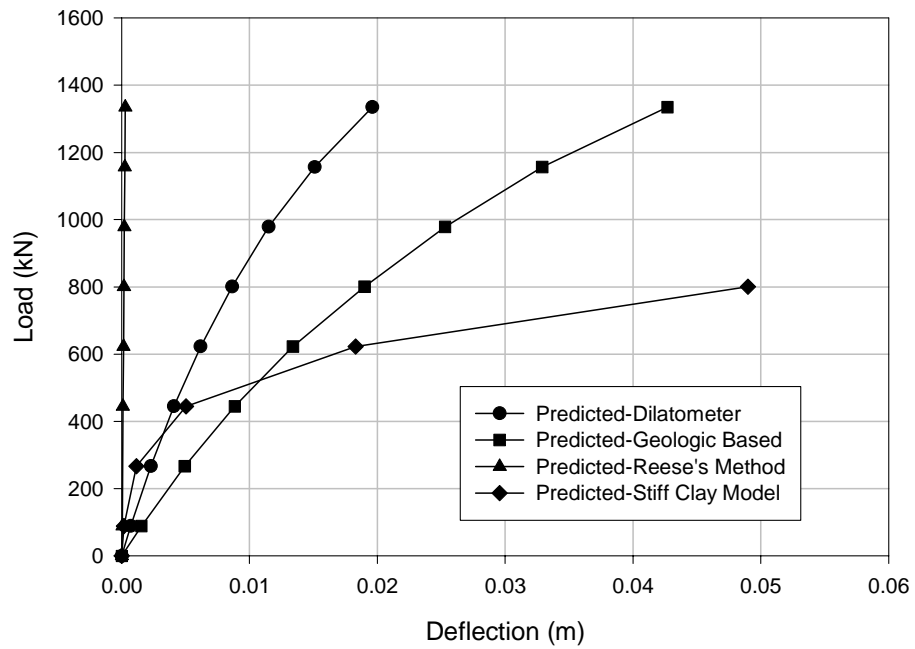
Figure 130. I-85 Long Shaft Performance Predictions

169

6.3.5 I-85 Load Test Results

Using a hydraulic jack, lateral load was applied to both shafts in increments of 89 kN up to a maximum load of 1334 kN. At the maximum applied lateral load of 1334 kN, the short shaft deflected 0.0478 m and the long shaft experienced 0.0172 m of deflection.

6.3.5.1 Top Deflections and Inclinometer Readings

Deformation above the ground surface for both shafts was monitored with dial gages. Shaft-head deflections for both the short and long shaft are presented in Figure 132. Unloading data were not obtained for the long shaft due to a dial gage malfunction. The short shaft yielded a non-linear deflection response as the maximum load was approached; however the long shaft produced nearly linear increments of deflection up to the maximum applied load.
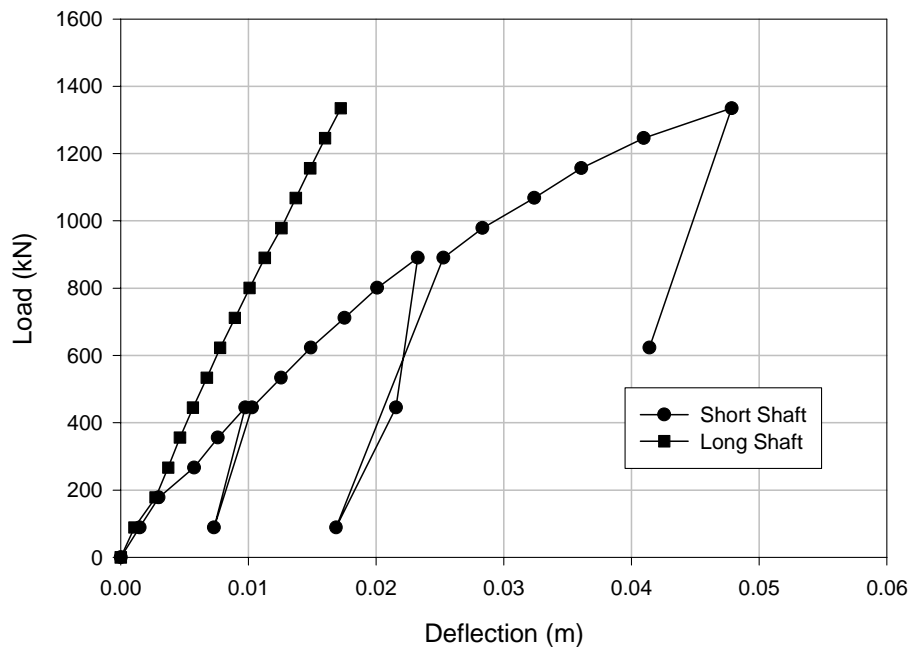
Figure 131. Top Displacements of the Short and Long Shaft Measured from Dial Gages

A system of continuous slope inclinometers was used to measure deflection profiles with depth for both the short and long shafts. Inclinometer data are recorded as the cumulative sum of successive gage deflections, beginning with the bottom-most gage.

Since neither string of inclinometers extended below the shaft tip, the data must be adjusted to a known value of deflection. Shaft head deflections, measured from dial gages, were used to adjust the inclinometer data. Deflection profiles, before dial gage adjustment, for both the short and long shaft are presented in the Appendix I. Adjusted deflection profiles are given in Figures 132 and 133.
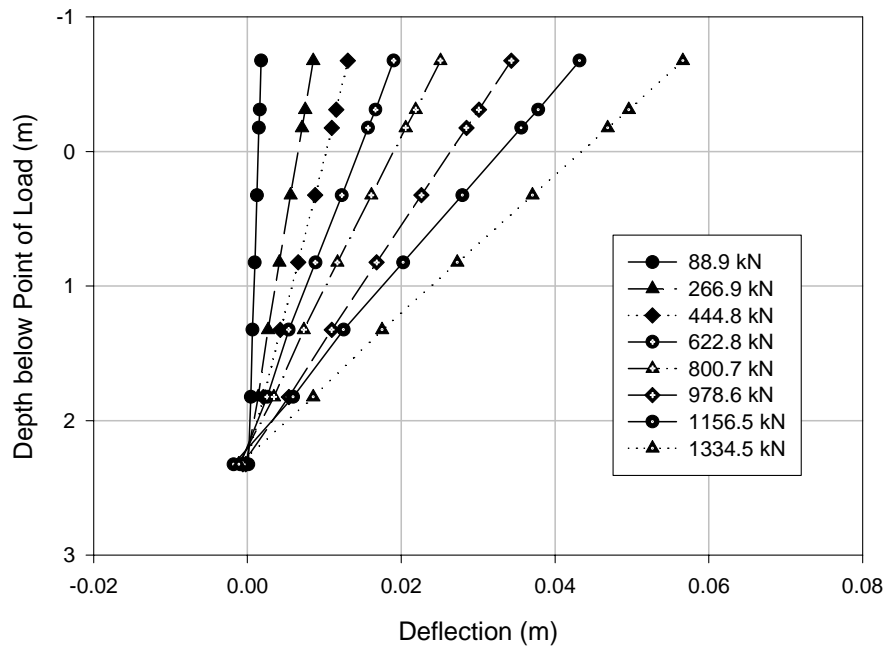
Figure 132. Deflection Profiles after Dial Gage Adjustment – I-85 Short Shaft
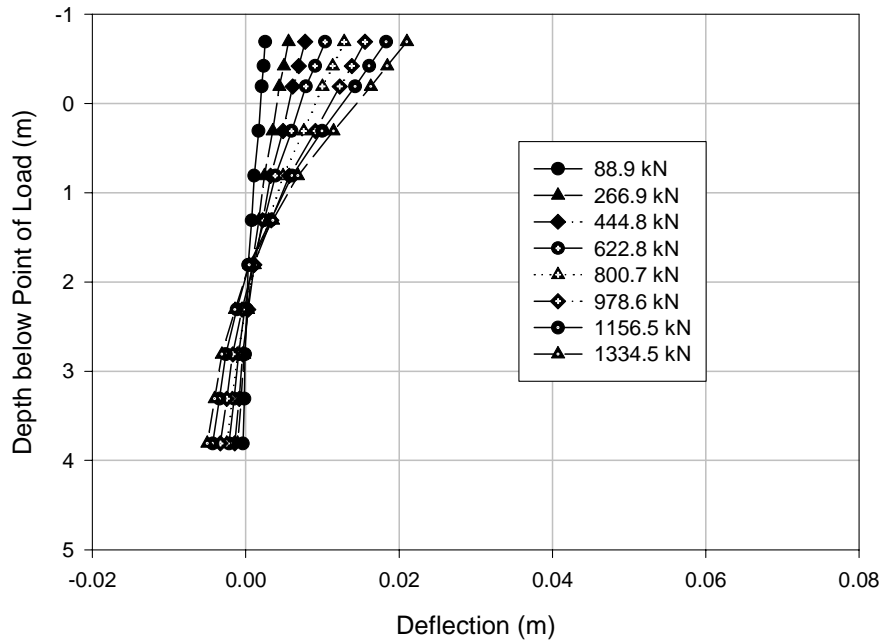
Figure 133. Deflection Profiles after Dial Gage Adjustment – I-85 Long Shaft

6.3.5.2 Predicted and Measured Test Shaft Performance

Based on predicted and measured shaft behavior, Figures 134 and 135 demonstrate the applicability of the WR P-y Model. The dilatometer predictions seemed to model the behavior of both the short and long shaft fairly well. Discrepancies between deflections predicted using geologic data and measured deflections could be attributed to the inherent problems associated with Triassic basin rock. The claystone tends to have a relatively large RQD value due to the dispersive nature of the clay mineral but relatively low strength. The GSI is based on an empirical equation and RQD values do not reflect the proper in-situ properties.
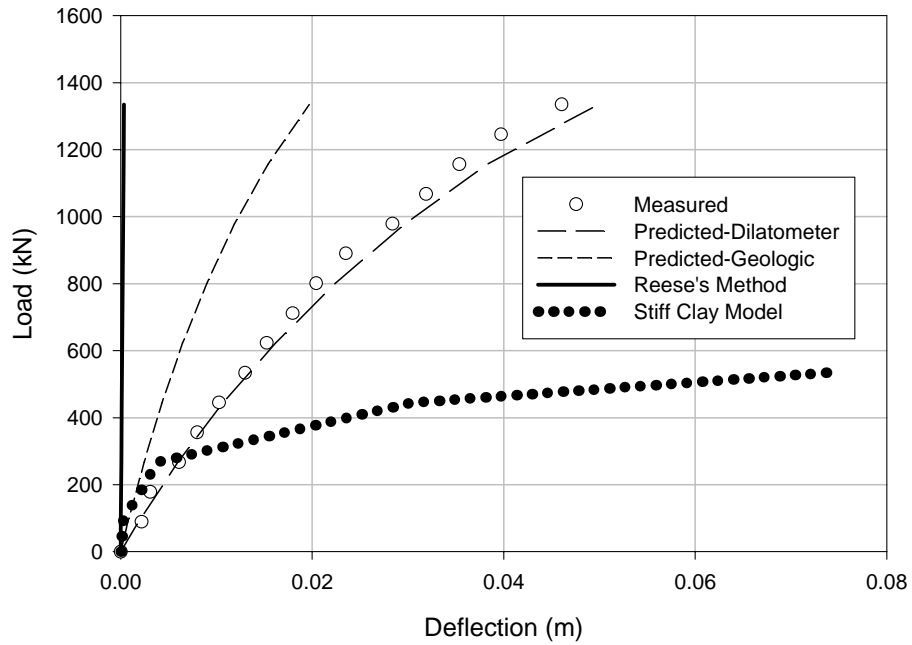
Figure 134. I-85 Short Shaft Pile Head Deflection Performance
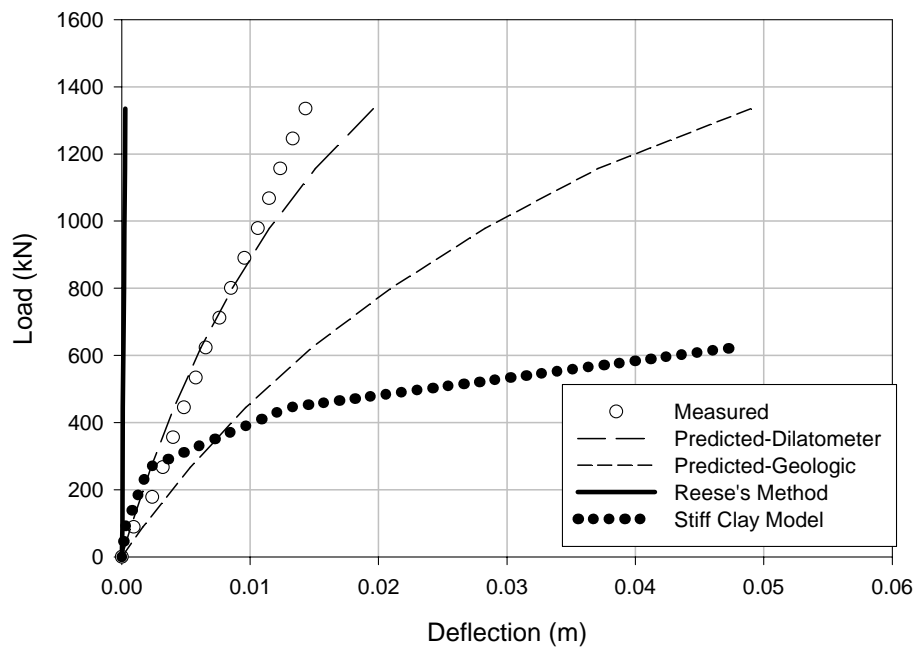
Figure 135. I-85 Long Shaft Pile Head Deflection Performance

173

6.3.5.3 Back Calculated P-y Curves

Using the strain measurements with depth, moment curves were developed for each load increment as described in the Literature Review. A fourth order equation was used to regress the moment data; the soil reaction (P, kN/m) with depth was calculated from the second derivative of the moment curves. Deflection (y, meters) was taken directly from the inclinometer readings. Back calculated P-y curves from strain gage and inclinometer data are shown in Figures 136 and 137.

The back calculated P-y curves show the k_h to increase with depth; however the decrease in k_h from 2.6 m to 3.0 m for the long shaft should be noted. This could be attributed to changes in rock properties that were not discovered in the subsurface investigation, or a precision error introduced in the back calculation process, partly due to small deflections around the point of rotation.

Transformed axes plots were used to curve fit the back calculated P-y data, as presented in Literature Review. These plots were used to establish the values of k_h and P_{ult} from the back calculated P-y curves. Two examples are shown in Figures 138 and 139; the remainder are presented in the Appendix E.
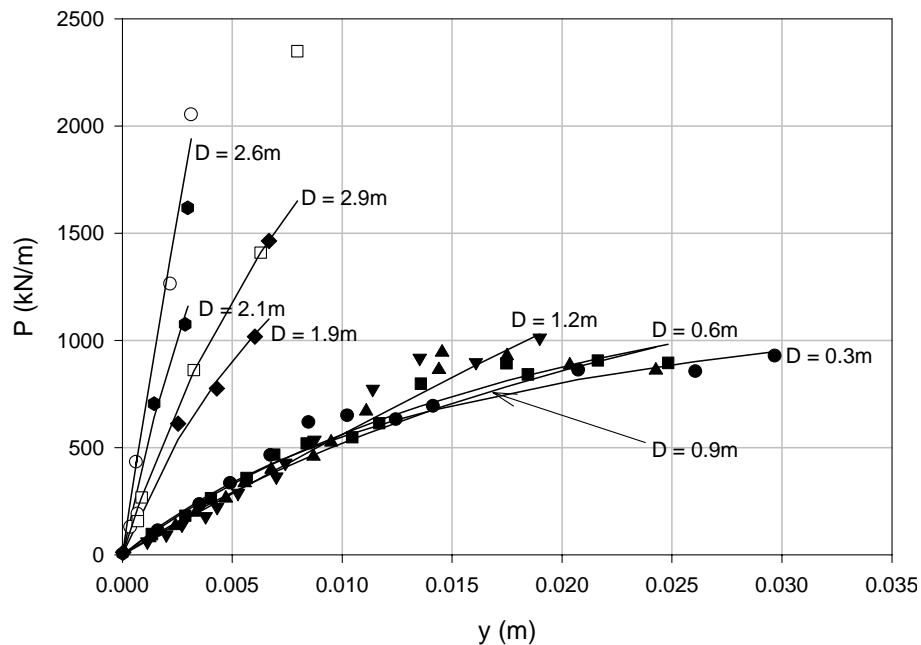
Figure 136. Back Calculated P-y Curves for the Weathered Rock – I-85 Short Shaft
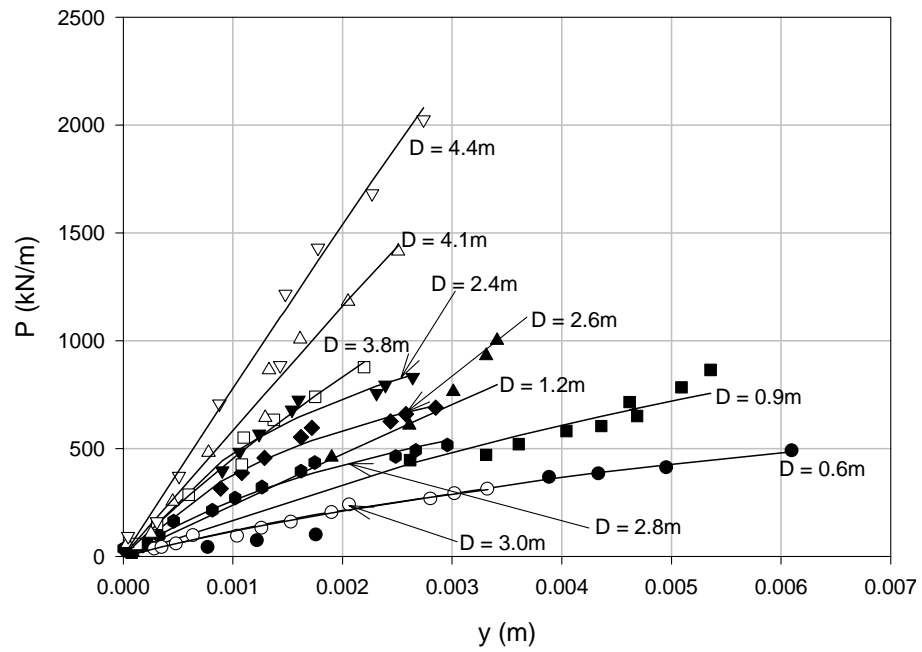
Figure 137. Back Calculated P-y Curves for the Weathered Rock – I-85 Long Shaft
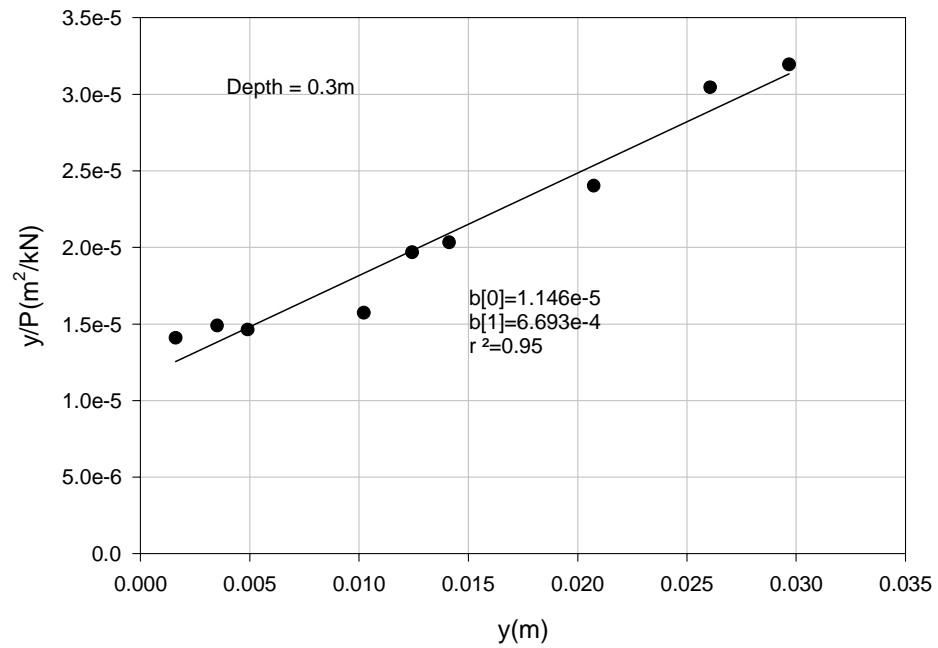
Figure 138. Curve Fitting Results – I-85 Short Shaft
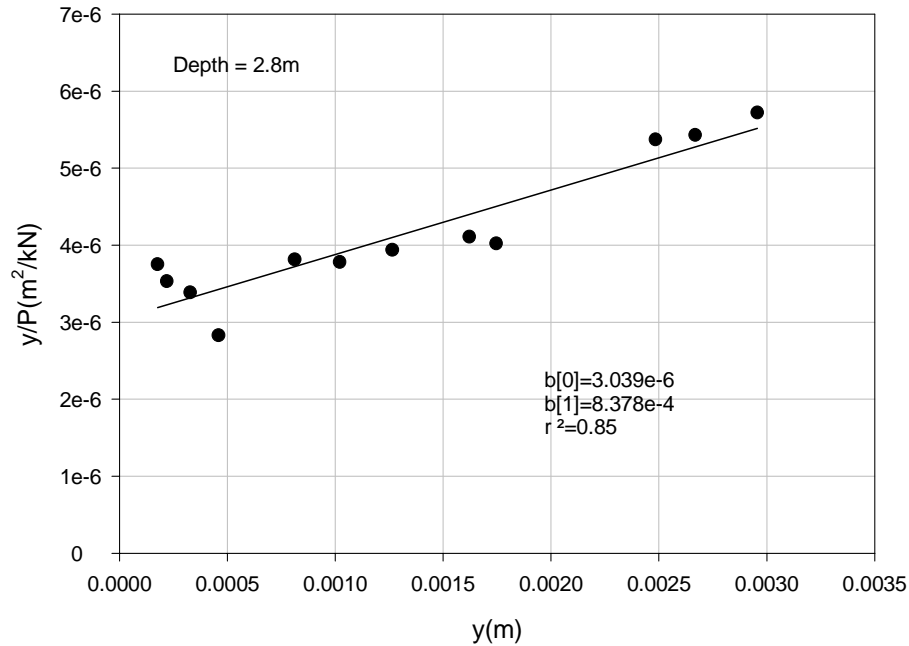
Figure 139. Curve Fitting Results – I-85 Long Shaft

6.3.5.4 Predicted and Back Calculated P-y Curves

Figures 140 through 146 show a comparison of P-y curves generated using the proposed P-y model and those back calculated from measured strain and deflection data. Due to the lack of rock properties with depth, one predicted P-y curve is shown for a given layer. For clarity, the graphs are plotted on differing scales.

As was the case for the I-40 load test results, the WR P-y model seems to under predict available resistance near the ground surface and over predict it at deeper depths. However, there seems to be an overall balance based on the reasonably good comparison between predicted and measured shaft deflections at the ground surface.
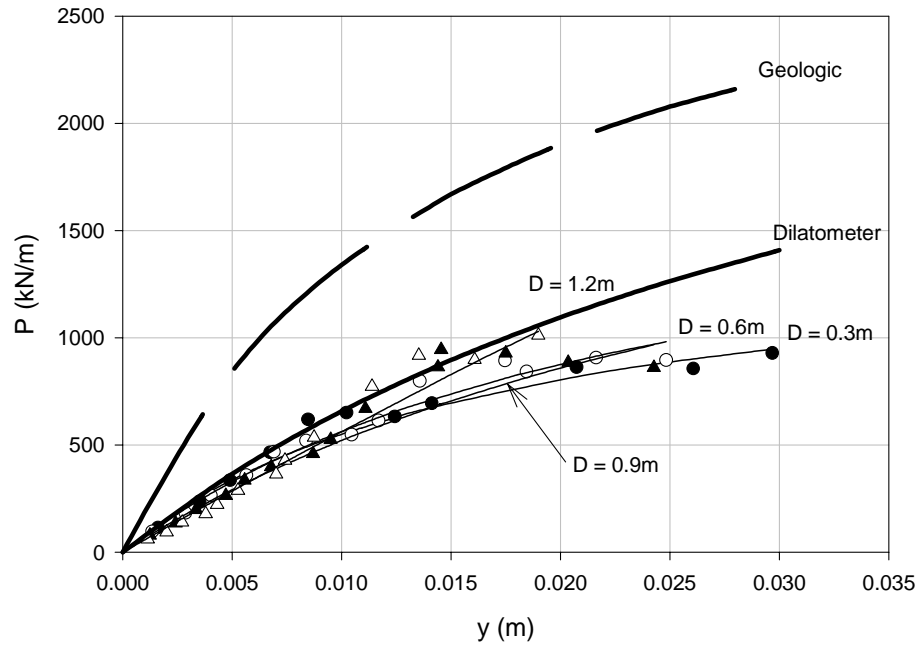
Figure 140. Predicted and Back Calculated P-y Curves – I-85 Short Shaft Layer 1
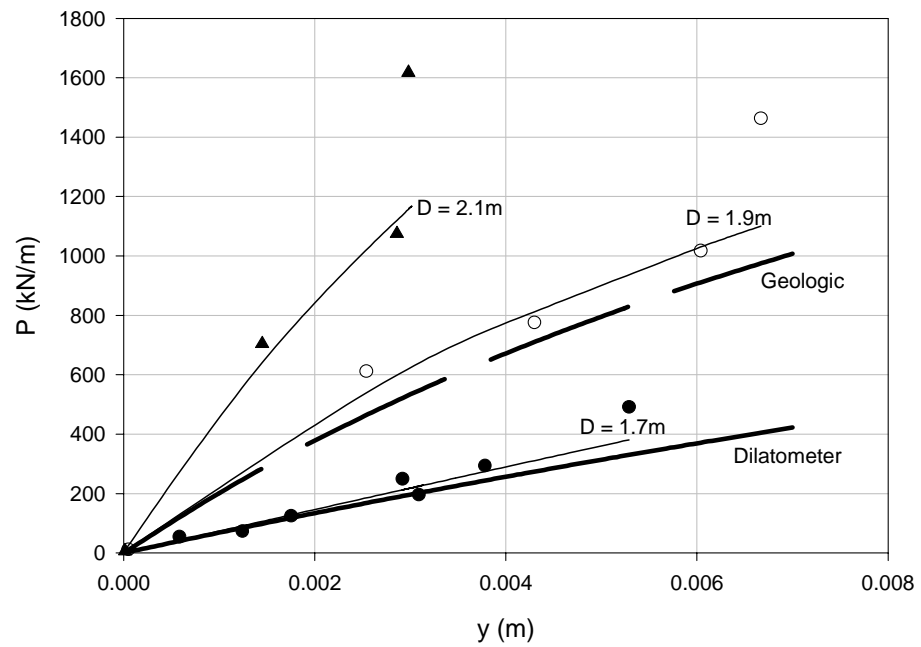
Figure 141. Predicted and Back Calculated P-y Curves – I-85 Short Shaft Layer 2
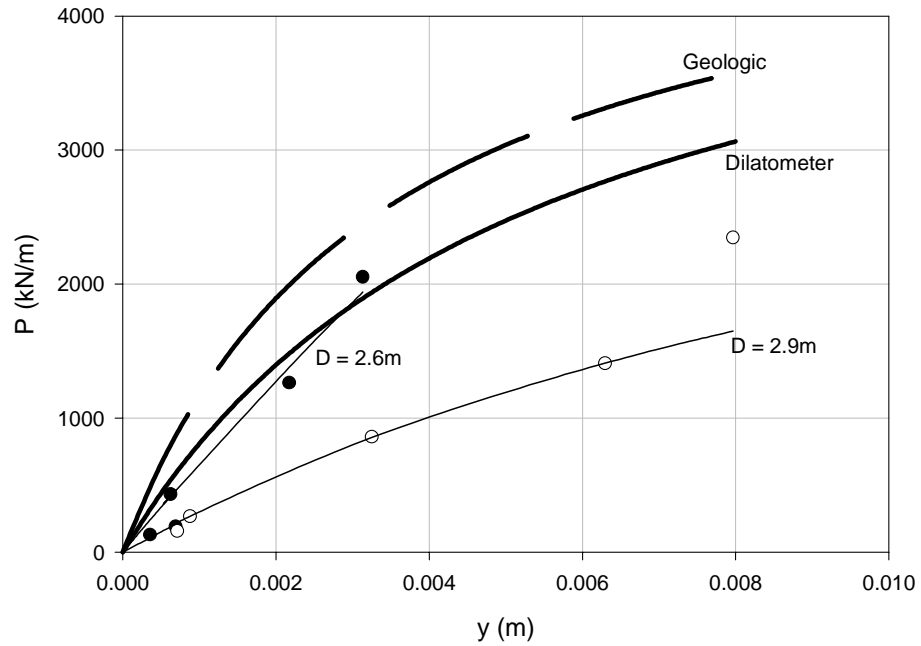
Figure 142. Predicted and Back Calculated P-y Curves – I-85 Short Shaft Layer 3
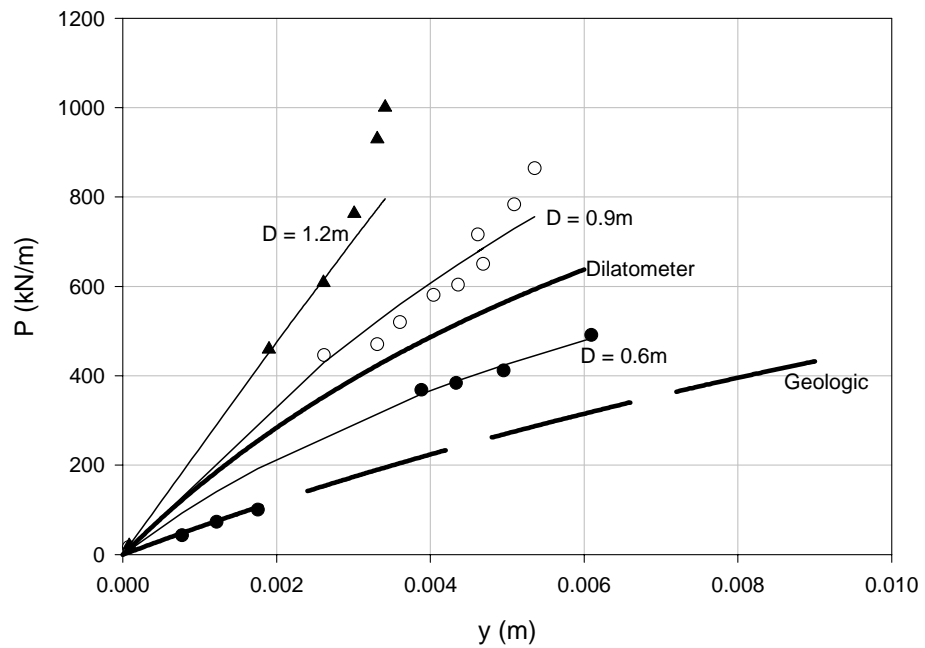
Figure 143. Predicted and Back Calculated P-y Curves – I-85 Long Shaft Layer 1
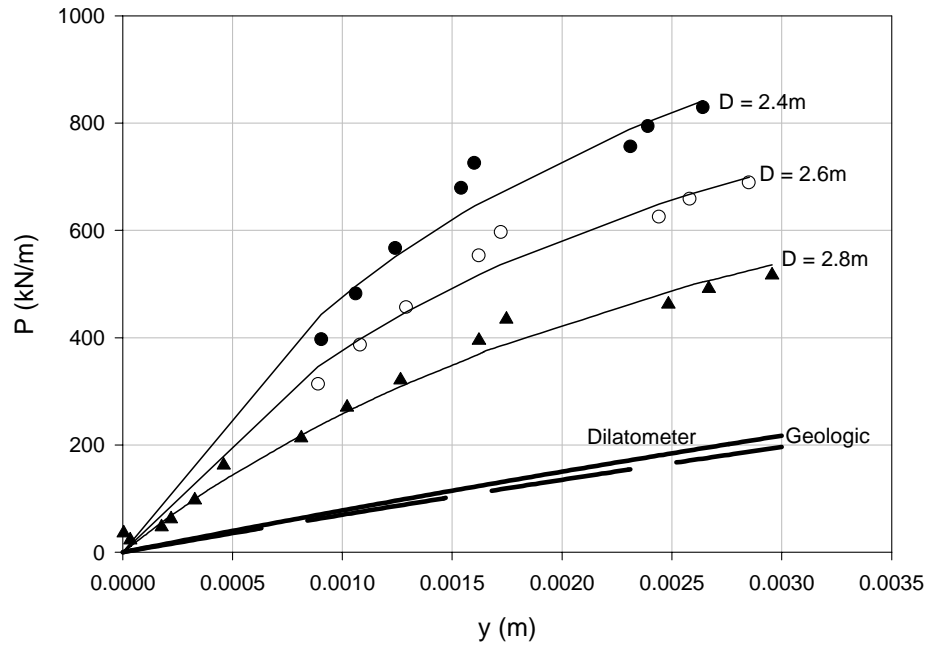
Figure 144. Predicted and Back Calculated P-y Curves – I-85 Long Shaft Layer 2
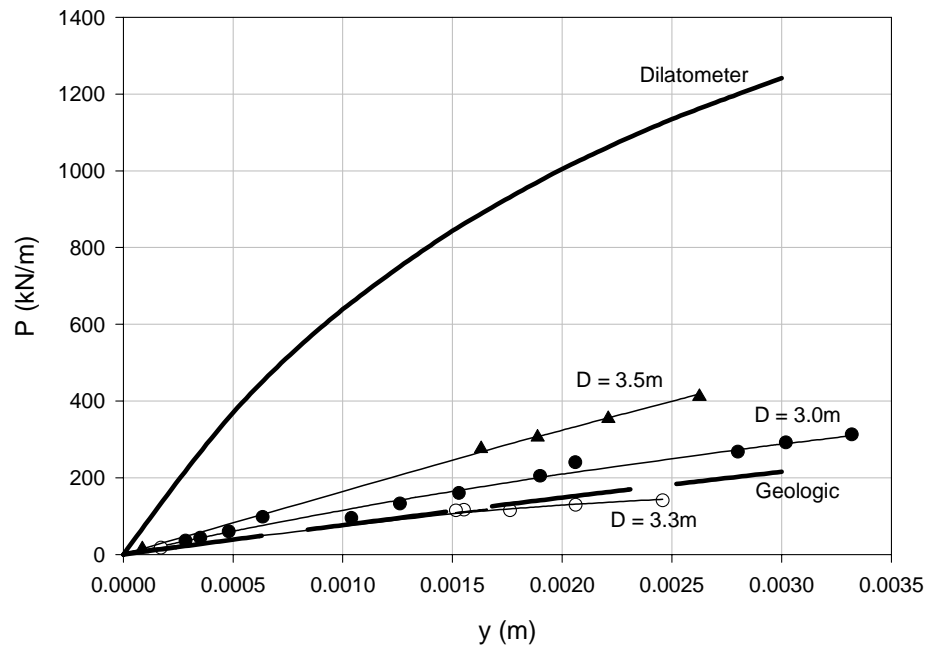
Figure 145. Predicted and Back Calculated P-y Curves – I-85 Long Shaft Layer 3
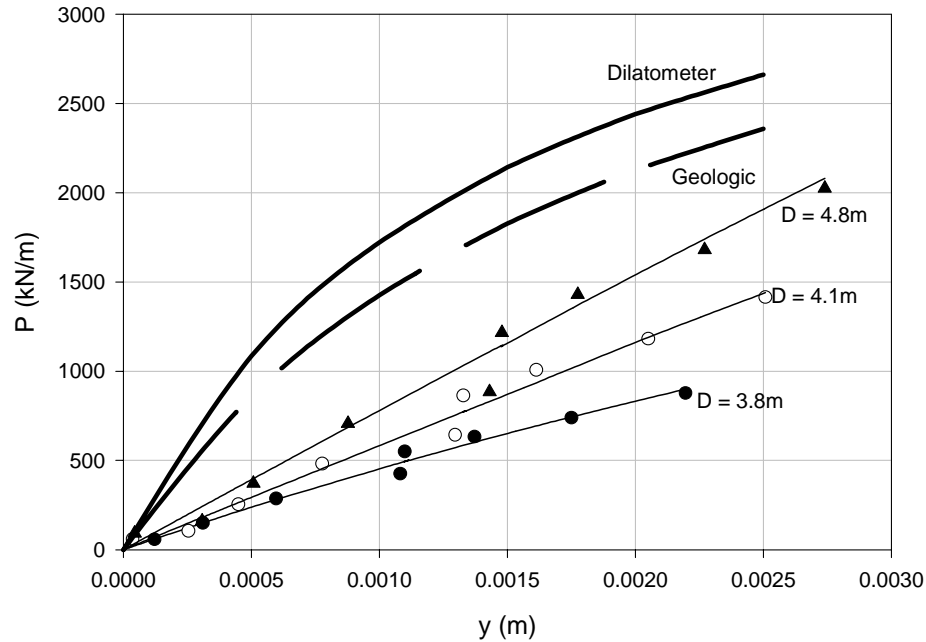
Figure 146. Predicted and Back Calculated P-y Curves – I-85 Long Shaft Layer 4

6.4 Distribution of the Subgrade Reaction (k_h)

The subgrade reaction (k_h) was determined by evaluating the initial slope of a P-y curve; the coefficient of subgrade reaction (k_{ho}) was then calculated by dividing k_h by the diameter of the test shaft. Figure 147 presents the distribution of k_{ho} evaluated from the I-40 and I-85 load tests. On the average, the value of k_{ho} increased from approximately 200 MN/m^3 at the surface to 2000 MN/m^3 at a depth/diameter ratio of 6. In the case of I-40 short shaft, the k_{ho} increased from approximately 400 MN/m^3 at the surface to 4000 MN/m^3 (value extrapolated) at a depth/diameter ratio of 6. The weathered rock at the location of the I-40 short shaft was significantly stiffer than that at the long shaft. This was also observed from the measured load-deformation response. Under applied load of 1000 kN, the lateral deformation of I-40 short shaft was 10 mm; the smallest value of the four validation test shafts. This finding emphasized the variability of rock properties, even on a local scale.
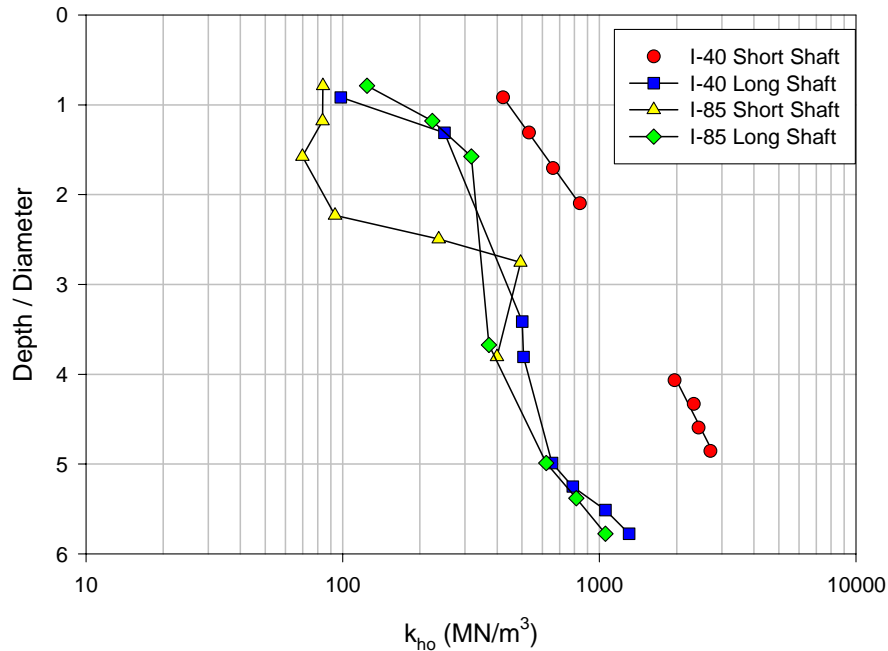
Figure 147. Measured k_{ho} from Verification Tests

6.5 Proposed Design Procedures

Based on the proposed WR P-y curve model and the verification testing presented in this chapter, the following procedures for the analysis of drilled shafts embedded in weathered rock are proposed.

6.5.1 Design of Laterally Loaded Drilled Shafts using Dilatometer Data

The following recommendations and procedures are based on the research work and the results of verification testing presented herein. The proposed design procedures are advanced based on P-y curves computed from either index geologic parameters or from rock dilatometer test data.

Step 1: Calculation of GSI value

GSI is the summation of the ratings for the five parameters outlined in Table 4. Each parameter (strength of intact rock material, RQD, spacing of joints, condition of joints, and groundwater level) is given a rating based on available in-situ data. If

181

sufficient data are unavailable, especially for spacing and condition of joints, ratings on the basis of measured RQD values can be used (for example, if RQD = 80%, RQD rating = 17, Spacing of Joints rating = 25, Condition of Joints rating = 20). A groundwater rating of 10 was always used for the verification testing predictions. GSI values used for the predictions for both I-40 and I-85 load tests are listed in Tables 33 and 40.

Step 2: Calculation of Weathered Rock Modulus of Elasticity

The modulus of elasticity is expressed as follows:

$$E_s(GPa) = \sqrt{\frac{\sigma_{ci}}{100}} 10^{\{(GSI-10)/40\}} \tag{67}$$

where, σ_{ci} = compressive strength of rock (GPa). The coefficient of subgrade reaction can then be calculated as follows:

$$k_{ho} = 0.65 \frac{\sqrt{\sigma_{ci} \times 10^4}}{D(1-\nu_r^2)} \quad 10^{[(GSI-10)/40]} \quad (kN/m^3) \tag{68}$$

When multiple layers of weathered rock are encountered, the modulus of elasticity for each layer should be calculated, and then a representative value for the entire profile can be determined from a weighted average.

Step 3: Calculation of Flexibility Factor

A flexibility factor is computed as follows (Poulos and Davis, 1972):

$$K_R = \frac{E_p I_p}{E_s L^4} \tag{68}$$

where, E_p = modulus of elasticity of shaft,

I_p = moment of inertia of shaft,

L = length of shaft embedded in weathered rock.

Step 4: Calculation of the Point of Rotation

The following equation is used to define the turning point as a function of the embedded shaft length:

$$\tag{69}$$

182

$$\frac{T_0}{L} = 1 + 0.18 \log K_R \quad (K_R \leq 1) \tag{70}$$

where, T_o = turning point,

L = embedded length of shaft.

Step 5: Calculation of the I_T Number

Once T_o is estimated from step 4, the I_T number for depths below the point of rotation can be determined as follows:

$$\mathbf{I_T = -28 - 383 \log(\frac{T_0}{L}) \quad I_T \geq 1} \tag{71}$$

Step 6: Calculation of Coefficient of Subgrade Reaction

For rock dilatometer test data, the coefficient of subgrade reaction can be calculated as follows (another procedure is presented later if only geologic parameters are available):

$$\mathbf{k_{ho} = \frac{0.65 E_s}{D(1 - v_r^2)} [\frac{E_s D^4}{E_p I_p}]^{1/12}} \ (kN/m^3) \tag{72}$$

where,

$$\mathbf{E_s = 2(1 + \upsilon_r) \times (v_0 + v_m) \times \frac{1}{(\frac{\Delta v}{\Delta p - \Delta p_i}) - c}}$$

v_o = normal initial or at rest volume of the deflated probe (1,950 cc; for the ROCTEST Model Probex 1)

v_m = mean additional volume

μ_r = Poisson's ratio of membrane (0.3)

Δp_i = change of the pressure of the dilatable membrane (kPa)

Δp = applied pressure increment (kPa)

c = volume correction factor

EpIp = shaft stiffness

By performing multiple dilatometer tests within the weathered rock profile a distribution of k_{ho} with depth can be generated.

Step 7: Calculation of the Subgrade Reaction

$$k_h = (k_{ho})B \quad (0 \le z \le T_o) \tag{73}$$

$$k_h = (k_{ho})I_T B \quad (T_o < z \le L) \tag{74}$$

Step 8: Calculation of the Normal Limit Stress

$$p_L = \gamma' z + \sigma_{ci} \left(m_b \frac{\gamma' z}{\sigma_{ci}} + s \right)^a \tag{75}$$

where, γ' = effective unit weight of the rock mass, kN/m^3,

z = depth from the rock mass surface, m,

σ_{ci} = compressive strength of the rock (kPa),

m_b, S, and a = coefficients based on GSI from Table 3.

Step 9: Calculation of the Shearing Resistance along the sides of a Drilled Shaft

The side shear resistance is calculated based on the compressive strength of rock as follows:

$$\tau_{max} = 0.20\sqrt{\sigma_{ci}} \text{ (MPa)} \tag{76}$$

Step 10: Calculation of the Ultimate Resistance

Based on p_L and τ_{max}, the P_{ult} is computed as:

$$P_{ult} = (p_L + \tau_{max})B \tag{77}$$

Step 11: Construction of the P-y Curve

Once, k_h and P_{ult} are evaluated, the P-y curves are constructed using the following hyperbolic equation:

$$P = \frac{y}{\left(\dfrac{1}{k_h}\right) + \left(\dfrac{y}{P_{ult}}\right)} \tag{78}$$

Any number of P-y curves can be developed throughout the profile depending on the density of curves desired for an analysis.

6.5.2 Design of Laterally Loaded Drilled Shafts using Geologic Data

Geologic data are used together with a set of empirical equations to calculate the coefficient of subgrade reaction of weathered rock. The geologic method can be used in place of dilatometer data; however, results of the verification testing suggested that the empirical equations do not model the insitu properties as accurately as the rock dilatometer. For the design of laterally loaded drilled shafts using geologic data, Steps 1 through 5 are carried out as described above, followed by Steps 6 through 8 presented below.

Step 6: Calculation of the Coefficient of Subgrade Reaction

In this case, k_{ho} is computed as a function of σ_{ci} and GSI as follows:

$$k_{ho}(kN/m^3) = \sqrt{(\sigma_{ci}x10^3)}10^{\frac{GSI-10}{40}} \tag{79}$$

Note: GSI reduction factor, α_{GSI}, should be used for Triassic Weathered Rock; rational is presented below.

Step 7: Calculation of the Distribution of the Coefficient of the Subgrade Reaction

Based on the distribution of n_h with depth, the following empirical equation is advanced for the evaluation of n_h values based on the relative stiffness of the shaft to soil and the shaft geometric properties:

$$n_h = \frac{2E_p I_p}{k_{ho}L^4} \times 10^5 \tag{80}$$

where, k_{ho} = coefficient of subgrade reaction for weathered rock at surface (kN/m^3)

L = embedded shaft length, m

Step 8: Calculation of the Modulus of Subgrade Reaction

The magnitude of the modulus of subgrade reaction is estimated based on the location of the turning point as follows:

$$k_h = (k_{ho} + n_h z)B \qquad (0 \leq z \leq T_o) \tag{81}$$

$$k_h = \{(k_{h0} + n_h T_0) + n_h(z - T_0)I_T\}B \qquad (T_0 < z \leq L) \text{ and } I_T \geq 1 \tag{82}$$

185

Equations 75, 76, and 77 are proposed to calculate the ultimate resistance of the weathered rock. Equation 78 is proposed to construct P-y curves for any values of k_h and P_{ult}.

For the Triassic Weathered Rock tested in the verification tests, the geologic model, as described above, generally under predicted head deflections with the exception of the I-85 Long Shaft. Based on these results it is proposed to adjust GSI values by a reduction factor such that the geologic model matches or, consistently, conservatively predicts head deflections. Table 41 presents GSI values for each verification test shaft as determined using the method described in Section 6.5.1 (Step 1); to the left of these values, in parenthesis, are the GSI values that were needed in order to estimate shaft deflections that closely represented those measured.

Table 41. GSI Values for the Verification Load Tests

Layer No.	Parameter	I-40 Load Tests		I-85 Load Tests	
		Short Shaft	Long Shaft	Short Shaft	Long Shaft
1	Strength	2	2	4	4
	RQD	20	13	13	8
	Spacing	30	20	20	10
	Condition	25	12	12	6
	Groundwater	10	10	10	10
	Total GSI	(77) **87** (0.89)	(41) **57** (0.72)	(43) **59** (0.73)	(38) **38** (1.0)
2	Strength	2	4	4	4
	RQD	17	20	13	8
	Spacing	25	30	20	10
	Condition	20	25	12	6
	Groundwater	10	10	10	10
	Total GSI	(61) **74** (0.82)	(79) **89** (0.89)	(43) **59** (0.73)	(38) **38** (1.0)
3	Strength	4	4	4	4
	RQD	17	17	13	8
	Spacing	25	25	20	10
	Condition	20	20	12	6
	Groundwater	10	10	10	10
	Total GSI	(63) **76** (0.83)	(63) **76** (0.83)	(43) **59** (0.73)	(38) **38** (1.0)
4	Strength		2		4
	RQD		17		13
	Spacing		25		20
	Condition		20		12
	Groundwater		10		10
	Total GSI		(61) **74** (0.82)		(59) **59** (1.0)

GSI reduction factors (α_{GSI}) are determined from the ratio between the two values and are presented in Figure 150.
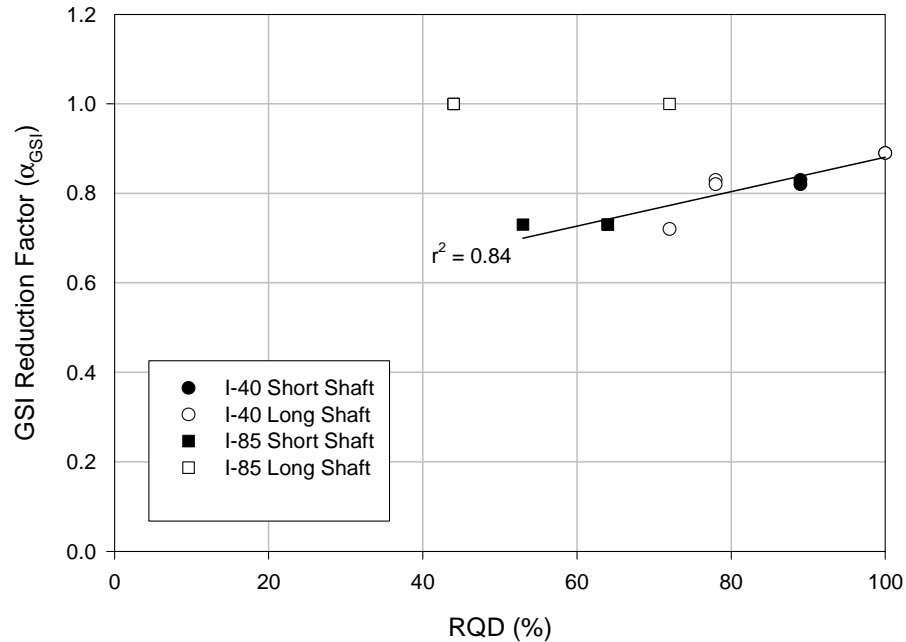
Figure 148. GSI Reduction Factor, α_{GSI}, for Triassic Weathered Rock

Figures 151 through 154 are presented to compare the measured test results with the recommended design procedures. The "Recommended-Dilatometer" curves are the same as those presented as "Predicted-Dilatometer" in previous sections. "Recommended-Geologic Based (Class B)" were developed using the GSI reduction factor, α_{GSI} .

The results of the verification testing discussed in the preceding sections have proven that the rock dilatometer provides the most accurate means, in this study, of predicting in situ modulus when estimating lateral drilled shaft behavior with the proposed WR P-y model. While the proposed geologic parameters produced conservative results, the design engineer should use good judgment based on all of the material presented in this report when analyzing laterally loaded drilled shafts with geologic data.
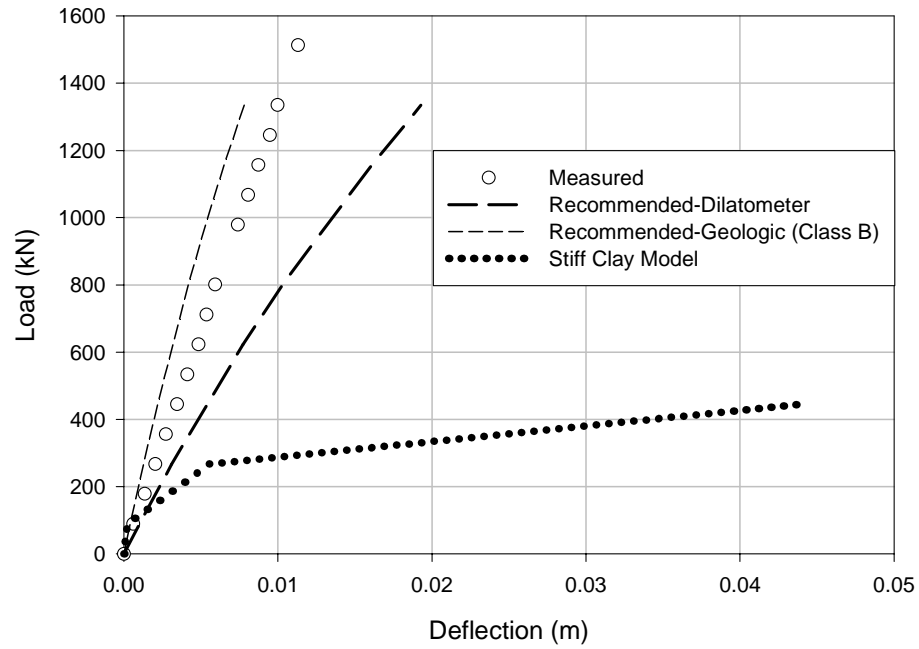
Figure 149. I-40 Short Shaft Pile Head Deflections with Recommendations
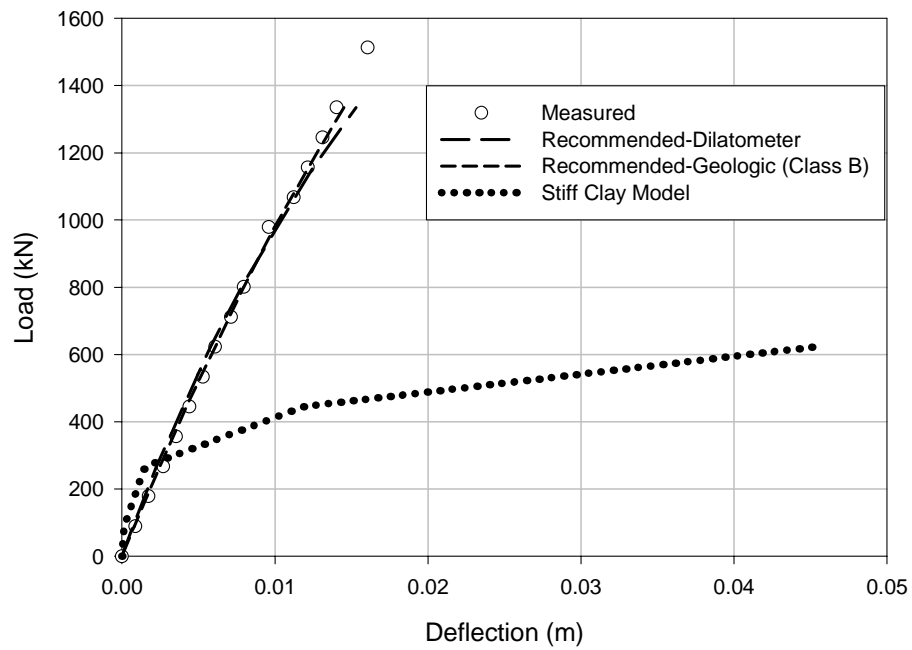
Figure 150. I-40 Long Shaft Pile Head Deflections with Recommendations
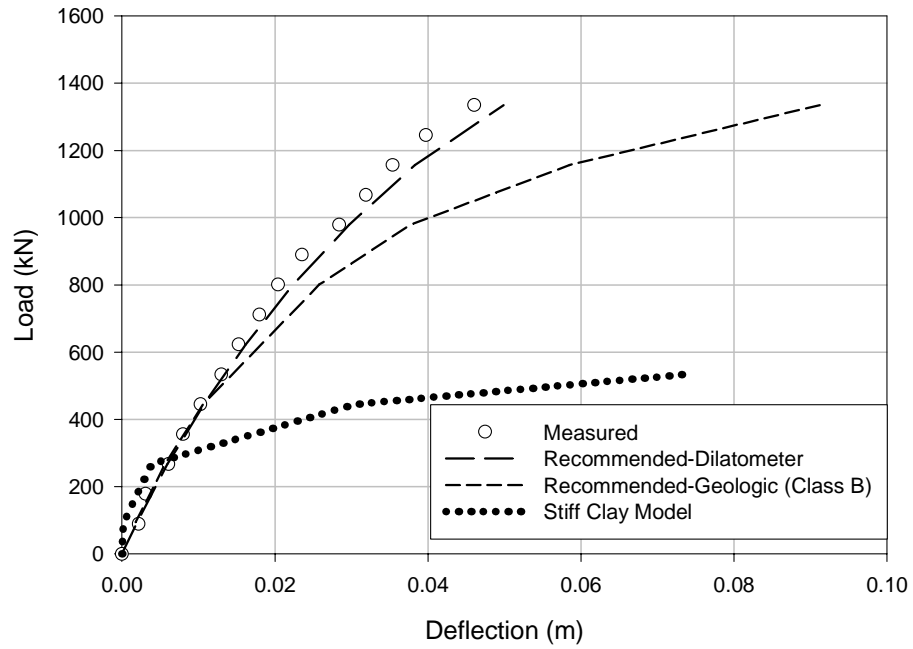
Figure 151. I-85 Short Shaft Pile Head Deflections with Recommendations
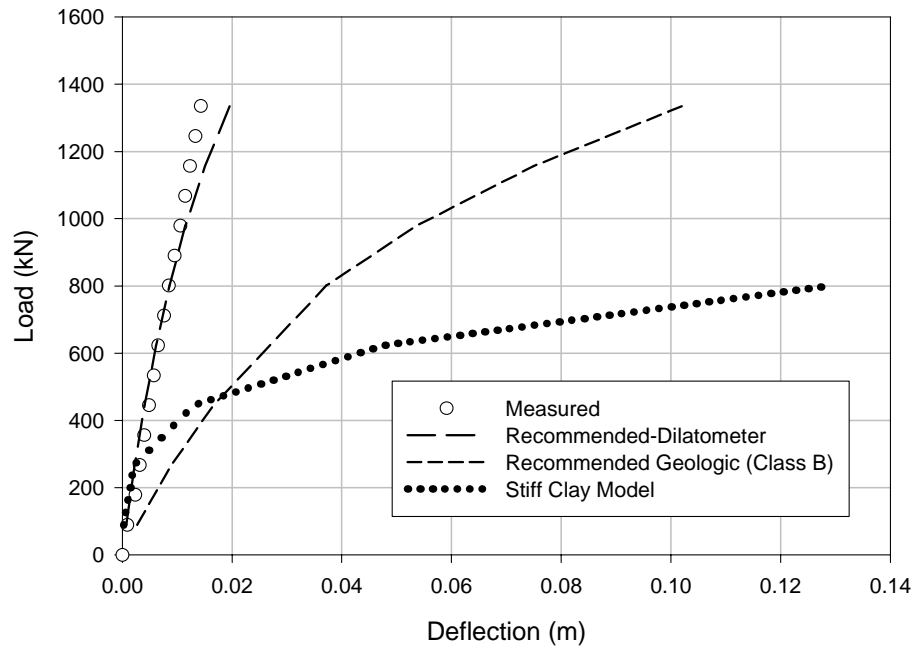
Figure 152. I-85 Long Shaft Pile Head Deflections with Recommendations

6.6 Inclusion of the Weathered Rock Model in the Computer Program LTBASE (Borden and Gabr, 1987)

The computer program LTBASE was developed for the analysis of laterally loaded drilled shafts with slope and base effects at North Carolina State University by Borden and Gabr (1987). With the development of the proposed WR P-y model, a subroutine was added to the computer code to allow engineers to use this method when designing for weathered rock profiles. The program allows for layered profiles of soil and weathered rock. In addition to the Weathered Rock Model, the program code contains many of the other popular design models for soils. Table 42 presents the form of input file used in LTBASE; steps for analysis when using the Weathered Rock Model follow along with a description of the input variables presented in Appendix J.

Table 42. LTBASE Input File Format

Input File Format	Input Variables
ANALYSIS OF SHAFT	TITLE
NCDOT Example	PROJECT NUMBER
NCDOT	PROJECT LOCATION
Initials	OPERATOR NAME
10/11/02	DATE
0	NOPTION
20. 0.0 1 1.5	PT ,BC2,KODE,FSCR
30. 0.2 .001 4.0 100 5 -1 1 1 1	D,H,TOL,DEFCR,N,NU,NTYPE*,NCHOICE,IPRINT,IOUT
15.4 .319E+12	TP, EIP
0. 0.	THETA,THETAU
1	NX
30.0 30. 159.1 35.0 9. 3626. .000 -4	TH(1),DIA(1),GAM(1),FPHI(1),SK(1),CSHO(1),EP50(1),NPC(1)
1	I
.319E+12 20.0	RR(J), XX(J)

A description of the input variables is presented in the Appendix J.

6.6.1 Steps for LTBASE Analysis

Once the input file has been created, the following steps should be used when analyzing laterally loaded drilled shafts with the proposed WR P-y model:

1. Determine the initial depth to the point of rotation using the concepts of the Weathered Rock Model or simply assume it.

2. Perform an initial run of the LTBASE program using the input file with the initial depth to the point of rotation.

3. Evaluate the depth to the point of rotation from output file (for the load increment of interest).

4. Update the input file with the new depth to the point of rotation.

5. Repeat process until depth to the point of rotation from the output matches that in the input file.

6.7 Summary of Verification Testing

The WR P-y model presented in Chapter 5 was used to develop performance predictions of four drilled shafts embedded in weathered rock of the Durham Triassic Basin. This type of rock profile is substantially different from rock profiles in which tests used as a part of model development were conducted. Performance predictions were also created using two other models for the design of laterally loaded drilled shafts, Reese's Method for P-y Curves for Weak Rock (Reese, 1997) and the Stiff Clay Model (Reese, Cox, and Koop, 1975) which was mainly used by NCDOT for design of these types of foundation. Results of the verification testing show that the proposed WR P-y model can reasonably predict the behavior of laterally loaded drilled shafts. However, further data are needed to establish the model's validity. Two recommended design procedures are advanced. The first is based on measurement of in situ properties using rock dilatometer data and the second is based on using empirical equations and index geologic parameters.

CHAPTER 7. SUMMARY AND CONCLUSIONS

Review of existing literature indicated that currently proposed P-y curve approaches to the design of drilled shafts embedded in weathered rock profiles of the piedmont region yielded unreasonable estimates of load-deflection responses of laterally loaded shafts. The P-y model proposed by Reese (1997) overestimated shaft resistance. This was partly due to the distribution of k_h with depth in which the soil modulus was multiplied by a factor of 100 at the ground surface (Reese, 1997). Such an increase in E created a stiff layer near the shaft top which led to very stiff load-deformation response. On the other hand, the stiff clay model currently being used by NCDOT to design shafts embedded in weathered rock was shown to significantly underestimate available lateral resistance.

The research reported herein was performed for the development of a more appropriate P-y model in weathered rock. The work proceeded along four complementary tasks. The first task involved 3-D Finite Element modeling using the ABAQUS computer program, the second task included laboratory work to study the characteristics of P-y curves in simulated material, the third task included field testing using full scale shafts to develop and validate P-y curves in natural weathered rock materials, and the final task involved the application of the developed P-y curve model to field load tests. Six field load tests were part of the model development. These tests were performed in Sandstone, Mica Schist, and crystalline rock. The results from these tests were used to validate the proposed model. In addition, the model was verified by comparing model results with published test results as well as with results from four field tests performed in the Durham Triassic Basin; a geological rock type that was different from those used as a part of model development. Recommended design procedures are proposed based on the results of experimental and analytical studies.

The proposed weathered rock (WR) P-y model was developed as a hyperbolic function as this shape was found to best fit the laboratory and field data. An analysis method is advanced by which different lateral subgrade responses are assigned in the model based on the location of the point of rotation. Above the point of rotation, a coefficient of lateral subgrade reaction is assigned on the basis of evaluated modulus as

computed from rock dilatometer data or from index geologic properties. A stiffer lateral subgrade reaction is assigned below the point of rotation in order to model the relatively small shear strains in this region.

The proposed WR P-y model showed good agreements with field test results. The load-deflection characteristics of drilled shafts were shown to be a function of relative stiffness of the shaft and the in situ material. A model to evaluate stiffness properties of weathered rock by utilizing the in-situ rock dilatometer was demonstrated, and a database for weathered rock subgrade reaction, as backfigured from the field load tests was presented. The use of coefficient of subgrade reaction as evaluated based on data from the rock dilatometer data provided a more precise estimation of measured load response as compared to estimations based on index geological properties. Therefore, if a project requires a high degree of accuracy in the estimation of lateral response, or the geological condition of a site is highly variable, it is recommended that the in-situ rock dilatometer test be performed to measure the modulus of weathered rock. The proposed P-y model, based on geological properties, can be used to accurately estimate lateral response if information regarding joint conditions and RQD are obtained during subsurface investigation, and the strength properties of cored sample are evaluated from laboratory testing. The proposed WR P-y model developed herein somewhat underpredicted field results, for load tests performed in various rock profiles

Verification testing was performed as a means of validating the WR P-y model independent of the field data used for development. The verification testing also added Triassic weathered rock properties to the database established from the previous testing program. The results of the verification testing further reinforced the conclusion that the current accepted standards of practice along with standard material properties presented previously for designing laterally loaded drilled shafts in weathered rock do not model the field behavior accurately. The Weathered Rock model, accompanied with quality dilatometer data, consistently predicted the behavior of laterally loaded drilled shafts embedded in weathered rock well.

The results of this research provide a cost effective method for designing drilled shaft foundations. Because the design depth of embedment of drilled shafts under lateral loading is often governed by the P-y response, a significant cost savings in terms of the

quantity of rock drilling and construction materials, can be realized if the shaft length is reduced. These savings in material and labor are due to a more accurate determination of the P-y response as well as a better estimation of the weathered rock properties. For example, the cost to drill a 42-inch diameter shaft is approximately $1000/ft with material costs on the order of $200/ft. Therefore, a $6000 cost saving could be realized by shortening a shaft 5 ft. Analysis performed using the "stiff clay model" for the Caldwell County short shaft test demonstrate potential length reduction by using the proposed model. In order to have a shaft that produced the measured shaft-top deflection under maximum applied load, the stiff clay model analysis yielded a shaft over 80 feet in length (assuming the same diameter as the tested shaft.) The Caldwell County short shaft, as tested, was only 14 feet long. The outcome of this research should be utilized to increase design efficiency and decrease the cost of drilled shafts constructed in weathered rock profiles, while maintaining adequate levels of safety.

REFERENCES

Ashford, S. A., and Juirnarongrit, T., 2003, Evaluation of Pile Diameter Effect on Initial Modulus of Subgrade Reaction, Journal of Geotechnical and Geoenvironmental Engineering, ASCE, v 129 (3) Nov., ASCE, pp. 234-242.

Briaud, J-L, 1992, The Pressuremeter, A. A. Balkema, Rotterdam, Netherlands.

Gabr, M. A. and R. H. Borden, "LTBASE: Lateral Analysis of Piers Including Base and Slope Effects: Program Documentation," Transportation Research Record No. 1169, Transportation Research Board, Washington, D.C., April 1988, pp. 83-93.

Gabr, M., and Borden, R. H., 1992, Lateral Analysis of Piers on Sloping Profiles, Closure, Journal of Geotechnical Engineering, V. 118(6), pp. 969-972.

Gabr, M., 1993, Analysis of Laterally Loaded Shafts in Rock, Discussion of Paper by Carter and Kulhawy, Journal of Geotechnical Engineering, ASCE, 119 (12), pp. 2015-2018.

Hassan K. M, O'Neill, M. W., Sheikh, S. A., and Ealy, C. D., 2002 " Design Method for Drilled Shafts in Soft Argillaceous Rock,"Journal of Geotechnical and Geoenvironmental Engineering -- March 1997 -- Volume 123, Issue 3, pp. 272-280

Hoek, E., and Brown, E. T., 1988, The Hoek-Brown Criterion – A 1988 Update, Proc. 15th Canadian Rock Mechnical Symp. University of Toronto, Toronto, Canada, pp. 31-38.

Hoek, E, and Brown, E. T., 1997, Practical Estimation of Rock Mass Strength, Int. Rock Mechanics Sci., Pergamon, Oxford, U.K., 34(8), pp. 1165-1186.

Hoek, E., and Bray J., 1981, Rock Slope Engineering 3rd Edition, The Institution of Mining and Metallurgy, London, U.K., pp. 100.

Kagawa T., and Kraft L. M. (1980) "Lateral Load-Deflection Relationships of Piles Subjected to Dynamic Loading," Soils and Foundation, Tokyo, Japan, 20(4), 19-34.

Lama, R.D., Vutukuri, V.S., 1978, Handbook on Mechanical Properties of Rocks – Testing Techniques and Results Vol. 2, Trans Tech Publications, Clausthal, Germany.

Matlock, H., and Reese, L. C., 1960. "Generalized solutions for laterally loaded piles."J. Soil Mech. and Found. Div., ASCE, **86**(5), 63–91.

Matlock, H., Bogard, D., and Lam, I. P., 1981, A Computer Program for the Analysis of Beam-Columns under Static Axial and Lateral Loading, University of Texas, Austin, Texas.

Mwindo, J. M., 1992 "Strain Dependent Soil Modulus of Horizontal Subgrade Reaction," MS Thesis, University of Missouri, Rolla

North Carolina Department of Transportation, 1998, Geotechnical Report-Bridge Foundation Investigation for Structure on –L- (NC 43) over Fishing Creek, State Project 8.1321301 (B-2594), Federal Project BRSTP-43(1), Nash and Halifax County, NCDOT Geotechnical Unit, Raleigh, North Carolina.

Parish, D. W., 2001, Slake Durability and Engineering Properties of Durham Triassic Basin Rock, Ph.D. Dissertation, North Carolina State University, Raleigh, North Carolina, pp. 62-83.

Poulos, H. G., 1971, Behavior of Laterally Loaded Piles: I – Single Piles, Journal of Soil Mechanics and Foundations, ASCE, 97(5), pp. 711-731.

Prakash S., 1962 "Behavior of Pile Group Subjected to Lateral Loads," Ph.D. Thesis, University of Illinois, Urbana, Ill.

Prakash S., and Sharma H. F., 1990 " Analysis and Design of Pile Foundation Under Lateral Loads," Pile Foundation in Engineering Practice, John Wiley and Sons, New York, N.Y.

Seed H. B, and Idriss, 1970 "Soil Moduli and Damping Factors for Dynamic Response Analysis," Report No. EERC70-10. Earthquake Engineering Research Center, University of California, Berkeley.

Reese, L. C., and Welch, R. C., 1975, Lateral Loadings of Deep Foundation in Stiff Clay, Journal of Geotechnical Engineering, ASCE, 101(7), pp. 633-649.

Reese, L. C., 1997, Analysis of Laterally Loaded Piles in Weak Rock, Journal of Geotechnical and Geoenvironmental Engineering, ASCE, v 123 (11) Nov., ASCE, pp. 1010-1017.

Rocktest Limited, 1999, Dilatometer Model Probex-1 Instruction Manual, Rocktest Inc., Plattsburgh, New York.

Zhang, L., and Einstein, H. H., 2000, Nonlinear Analysis of Laterally Loaded Rock-Socketed Shafts, Journal of Geoenvironmental Engineering, ASCE, Vol. 126, pp. 955-968.

BIBLIOGRAPHY

Bogard, D., and Matlock, H., 1980, Simplified Calculation of P-y Curves for Laterally Loaded Piles in Sand, Rep., Earth Technology Corp., Inc., Houston, Texas.

Briaud, J-L, and Smith, T. D., 1983, Using the Pressuremeter Curve to Design Laterally Load piles, Proc., 15th Offshore Technology Conference, pp. 495-502.

Broms, B. B., 1964a, Lateral Resistance of Piles in Cohesive Soils, Journal of Soil Mechanics and Foundations, ASCE 90(2), 27-63.

Broms, B. B., 1964b, Lateral Resistance of Piles in Cohesionless Soils, Journal of Soil Mechanics and Foundations, ASCE 90(3), 123-156.

Carter, J. P., Kulhawy, F. H., 1992, Analysis of Laterally Loaded Piles in Rock, Journal of Geotechnical Engineering, ASCE, Vol. 118 (6), ASCE, pp. 839-855.

Coates, D. F., 1970, Rock Mechanics Principles, Department of Energy Mines and Resources, Mine Branch Monograph, pp. 874.

Coon, R. F. and A. H. Merrit, 1970, Predicting In situ Modulus of Deformation Using Rock Quality Indexes, Determination of the In situ Modulus of Deformation of Rock, ASTM STP 477, pp. 154-173.

Deere, D. U., and Patton, F. D., 1971, Slope Stability in Residual Soils, Proceeding of the 4th Pan-American Conference on Soil Mechanics and Foundation Engineering Vol. I, pp. 87-170.

Digioia, A. M. Jr., Rojas-Gonzalez, L. F., 1994, Laterally Loaded Rock-Socketed Foundation, IEEE Transactions on Power Delivery, v 9 (3) Jul 1994 USA pp. 1570-1576.

Fleming, W. G. K., Weltman, A. J., Randolph, M. F., and Elson, W. K., 1992, Piling Engineering, Blackie, Glasgow, and London, U.K.

Goodman, R. E., Van, T. K., and Heuze, F. E., 1968, The Measurement of Rock Deformability in Boreholes, Proc. 10th Symp. On Rock Mechanics, AIME, Austin, TX, pp. 523-555.

Hansen, B. J., 1961, The Ultimate Resistance of Rigid Piles against Transversal Forces, Bull. No. 12, Geotknist Institute, Copenhagen, Netherlands.

Hartman, J. P., 1974, Finite Element Parametric Study of Vertical Strain Influence factors and the Pressuremeter Test to Estimate the Settlement of Footing in Sand, Ph. D. dissertation, University of Florida, Gainesville, Floroda.

Heartz, W. T., 1977, An Overview of Pressuremeter Research and a Suggested Miniature Prototype Design, North Carolina State University CE 598.

Hoek, E., and Brown, E. T., 1980, Empirical Strength Criterion for Rock Masses, Journal of Geotechnical Engineering, ASCE, 106(9), pp. 1013-1035.

Hoek, E. and Bray, J., 1981, Rock Slope Engineering, 3rd edition, The Institution of Mining and Metallurgy, London, U.K., pp. 100.

Jamiolkowski, M., and Garassino, A., 1997, Soil Modulus for Laterally Loaded Piles, Proc., 9th Int. Conf. S. M. F. E., Balkema, Rotterdam, Netherlands, pp. 87-92.

Kulhawy F. H., Trautmann C. H., and O'Rourke T. D., 1991, Soil Rock Boundary: What Is It and Where Is It?, Geotechnical Special Publication No. 28, ASCE, pp. 1-15.

Matlock, H, 1970, Correlations for Design of Laterally Loaded Piles in Soft Clay, Proc. 2nd Offshore Technology Conf., Vol. 1, pp. 577-594.

Mattlock, H., 1970 "Correlations for Design of Laterally Loaded Piles in Soft Clay", Paper no. OTC 1204, Offshore Technology conference, Dallas, Texas.

Peck, R. B., 1976, Rock Foundations for Structures, Proceeding of the Specialty Conference on Rock Engineering, ASCE, Vol. II, Boulder, Colorado, pp. 1-21.

Poulos, H. G., and Davis, E. H., 1980, Pile Foundation Analysis and Design, Wiley, New York.

Prakash, S, and Sharma, H. D., 1990, Pile Foundations in Engineering Practice, John Wiley and Sons, Inc, New York, New York

Prakash, S, 1962, "Behavior of Pile Groups Subjected to Lateral Loads," Ph.D. Thesis, University of Illinois, Urbana.

Randolph, M. F., and Houlsby, G. T., 1984, The Limiting Pressure in a Circular Pile Loaded Laterally in Cohesive Soil, Geotechnique, London, U, K., 34(4), pp. 613-623.

Reese, L. C., Cox, W. R., Koop, F. D., 1974, "Analysis of Laterally Loaded Piles in Sand", Paper No. 2080, Offshore Technology Conference, Dallas, Texas. 1974.

Reese, L. C., Cox, W. R., Koop, F. D., 1975, Field Testing and Analysis of Laterally Loaded Piles in Stiff Clay, Paper No. 2312, Offshore Technology Conference, Dallas, Texas.

Reese, L. C., 1997, Analysis of Laterally Loaded Piles in Weak Rock, Journal of Geotechnical and Geoenvironmental Engineering, ASCE, v 123 (11) Nov., ASCE, pp. 1010-1017.

Smith, R. E., Gabr, M. A., and Kula, J. R., 1991, Soil-Rock Transition Zone: Uncertainties for Design and Construction, Geotechnical Special Publication No. 28, ASCE, pp. 91-106.

Sowers,G.F., and Richardson, T. L., 1983, Residual Soils of Piedmont and Blue Ridge, Transportation Research Record 919, Transportation Research Board, Washington D. C.

Stevens, J. B., and Audibert, J. M. E., 1979, Re-examination of P-y Curve Formulations, Proc. 11th Offshore Technology Conf., Vol. 2, pp. 379-403.

Sun, K., 1994, Laterally Loaded Piles in Elastic Media, Journal of Geotechnical Engineering, ASCE, 120(8), pp. 1324-1344.

Zhang, L, 1999, Analysis and Design of Drilled Shafts in Rock, Ph.D. Thesis, Massachusetts Institute of Technology, Cambridge, Massachusetts.

Zhang, L., and Einstein, H. H., 1998, End Bearing Capacity of Drilled Shafts in Rock, Journal of Geoenvironmental Engineering, ASCE, 124(7), pp. 574-584.

APPENDIX A

Calculation of Deflection of the Rock during Dilation

Equation A-1 may be derived in several ways, one of which Hartman (1974) attributes to Boresi as follows. As shown in Figure A-1 and Figure A-2, it can be considered that the membrane is expanded as uniform cylindrical expansion of a hole. The equilibrium equation for this axisymmetric condition with no body force is

$$\frac{\partial \sigma_r}{\partial r} + \frac{\sigma_r - \sigma_\theta}{r} = 0 \qquad\qquad (A-1)$$

where, σ_r = radial stress

σ_θ = tangential stress

r = radial distance
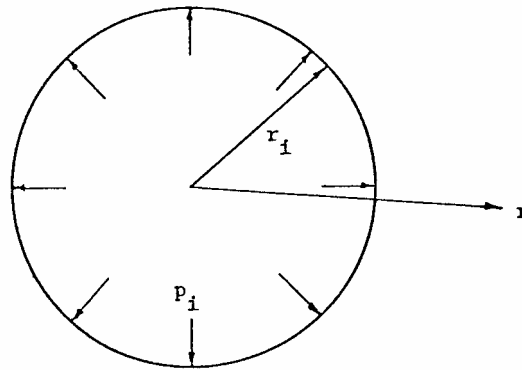
Figure A-1. Geometry for Uniform Cylindrical Expansion in an Infinite Elastic Medium (after, Heartz, 1977)
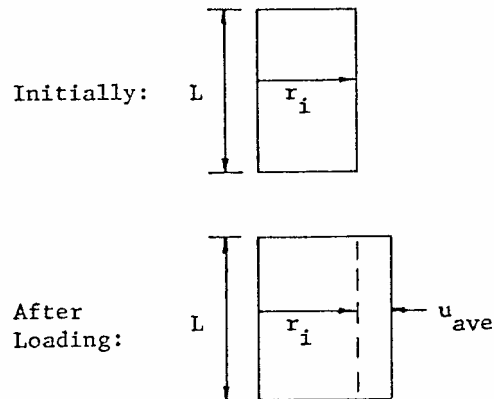
Figure A-2. Geometry for Average Radial Displacement and Volume Relationship for Measuring Cell (after, Heartz, 1977)

The stress-displacement relations for an isotropic elastic material for the cylindrical case can be written:

$$\sigma_r = \frac{E}{(1+v)(1-2v)}\left[v\frac{u}{r} + (1-v)\frac{\partial u}{\partial r}\right] \tag{A-2}$$

$$\sigma_\theta = \frac{E}{(1+v)(1-2v)}\left[v\frac{\partial u}{\partial r} + (1-v)\frac{u}{r}\right] \tag{A-3}$$

where, E = elastic modulus

   v = Poisson's ratio

   r = radial distance

By differentiating equation A-2 and then substituting the result as well as equation A-2 and A-3 into equation A-1, the following differential equation is obtained:

$$\frac{\partial^2 u}{\partial r^2} + \frac{1}{r}\frac{\partial u}{\partial r} - \frac{u}{r^2} = 0 \tag{A-4}$$

This is recognized as a linear, homogeneous, second order differential equation. The general solution of equation A-4 is

$$u = \frac{A}{r} + Br \tag{A-5}$$

where, A and B = constants to be determined from the specific boundary

   conditions

For the case of cylindrical expansion is an infinite medium, the first boundary requirement is that as radius increases to infinity, the displacement, u, must equal to zero. Thus,

$$Limit_{r \to 0} \quad (\frac{A}{r} + Br) = 0 \tag{A-6}$$

This can only be possible if the constant B equals to zero. Thus general solution reduces to;

$$u = \frac{A}{r} \tag{A-7}$$

For the second boundary condition, it is noted that the radial stress at the inner radius, r_i, is the loading pressure P_i. Thus,

$$\sigma_r = -P_i \quad at \; r = r_i \tag{A-8}$$

where, the negative sign is because of the compressive loading. By differentiating equation A-7, substituting in equation A-2, and applying the boundary conditions of equation A-8, the constant A is obtained:

$$A = \frac{P_i(1+v)r_i^2}{E} \tag{A-9}$$

The general displacement as a function of radial distance is thus

$$u(r) = \frac{P_i(1+v)r_i^2}{rE} \tag{A-10}$$

For the case of the displacement at the inner radius, r_i, equation A-10 becomes

$$u_{r=r_i} = \frac{P_i(1+v)r_i}{E} \tag{A-11}$$

To apply equation A-11 to a cylindrical loading case where the volume of displacement is measured, and not the radial displacement, the average radial displacement is calculated using the geometry shown in Figure A-3. Initially the volume of the cylinder is

$$V_0 = \pi r_i^2 L \tag{A-12}$$

where, V_0 = initial volume of the measuring cell

L = length of cylindrical measuring cell

After a pressure, P_i, is applied, the wall displaces. If the average wall displacement is considered, the new volume can be calculated as

$$V = \pi (r_i + u_{ave})^2 L \tag{A-13}$$

where, V = volume after pressure P_i is applied

u_{ave} = average radial displacement of wall surface

The change is volume can then be calculated by expanding equation A-13 and then subtracting equation A-12, which results in:

$$\Delta V = \pi L 2 r_i u_{ave} + \pi L u_{ave}^2 \tag{A-14}$$

where, ΔV = change in measuring cell volume

If the u_{ave}^2 term is neglected, the following very simple relationship results for the displacement as a function of the volume:

$$u_{ave} = \frac{\Delta V}{V_0} \frac{r_i}{2} \tag{A-15}$$

Using equation A-15, the displacements from measured volume from rock dilatometer testing can be calculated.

APPENDIX B
Rock Dilatometer Test Data
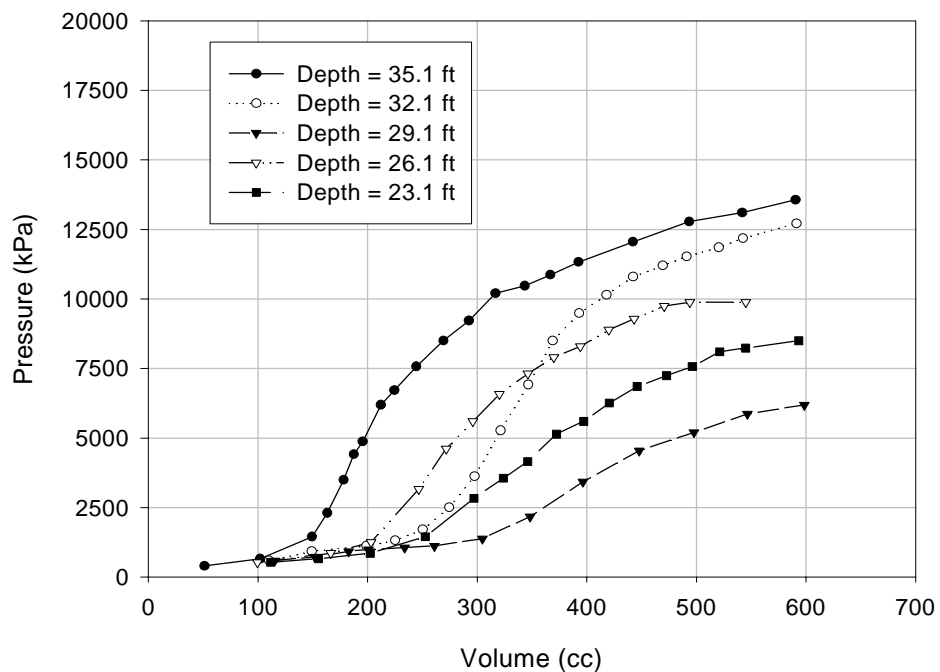
Figure B-1. Rock Dilatometer Test Result (Pressure vs. Volume) – Caldwell Site A
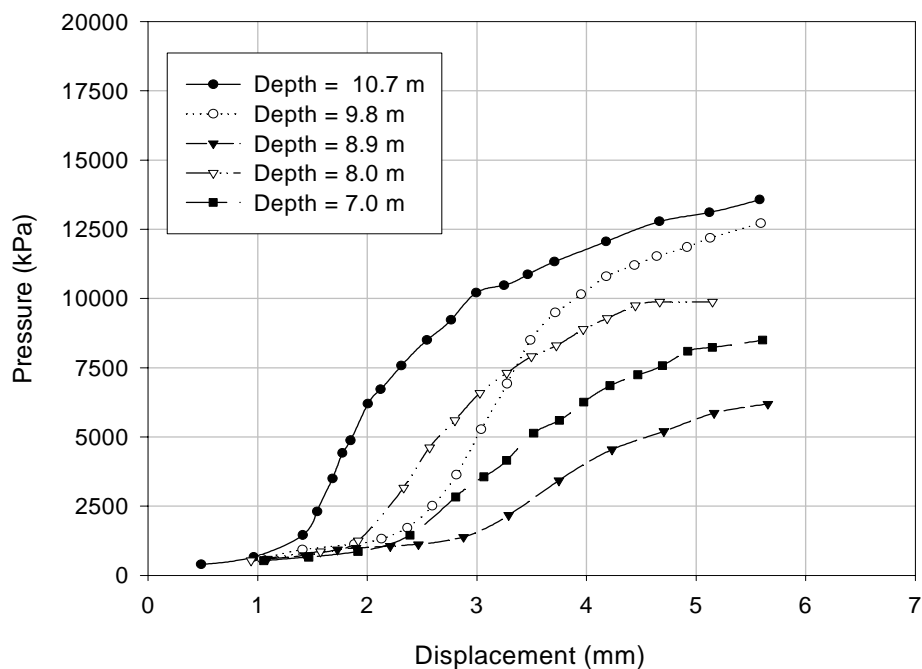
Figure B-2. Rock Dilatometer Test Result (Pressure vs. Displacement) – Caldwell

Site A
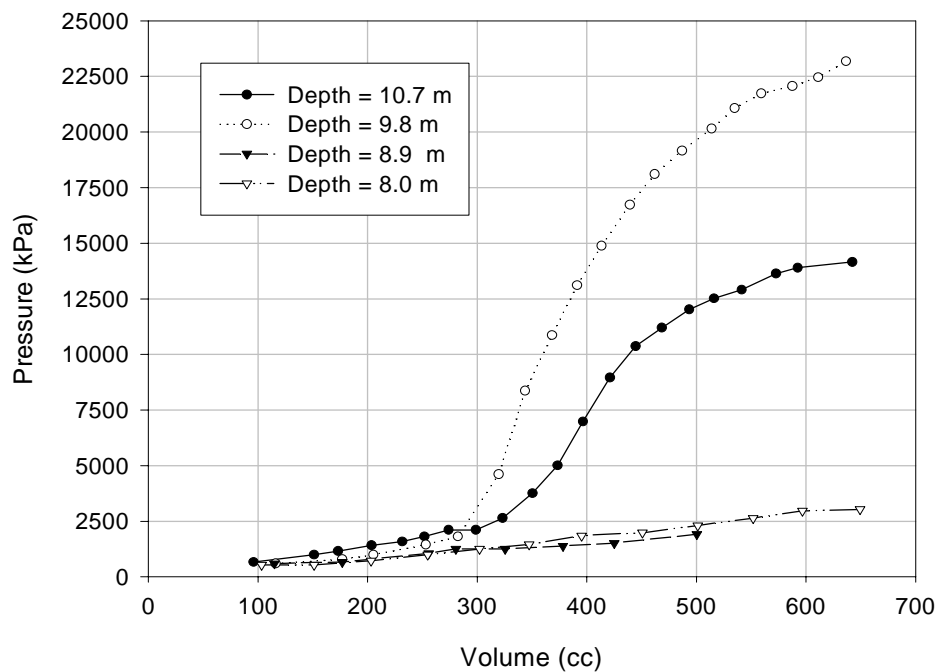
Figure B-3. Rock Dilatometer Test Result (Pressure vs. Volume) – Caldwell Site B
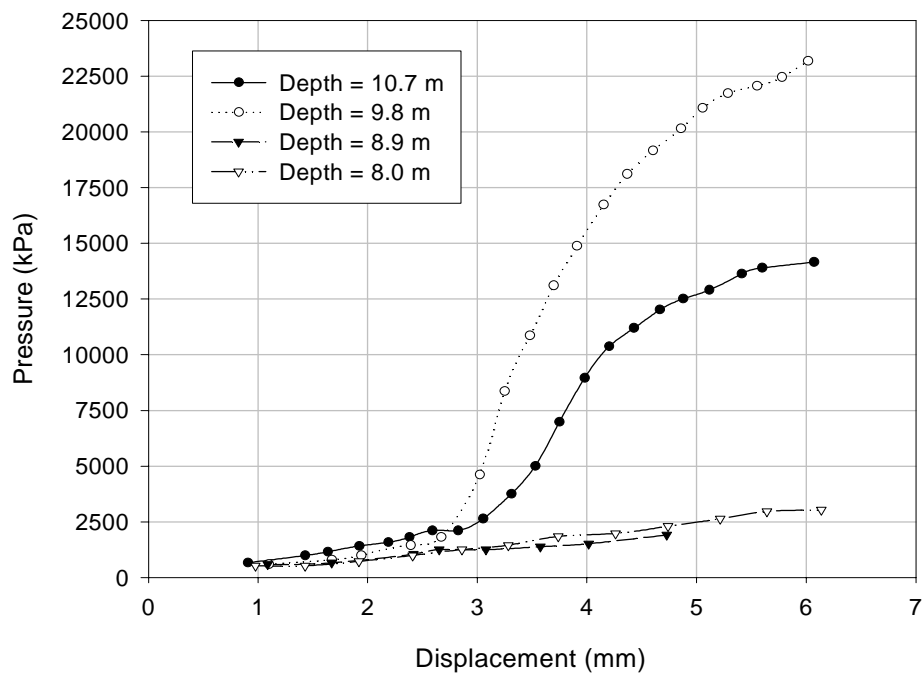
Figure B-4. Rock Dilatometer Test Result (Pressure vs. Displacement) – Caldwell

Site B
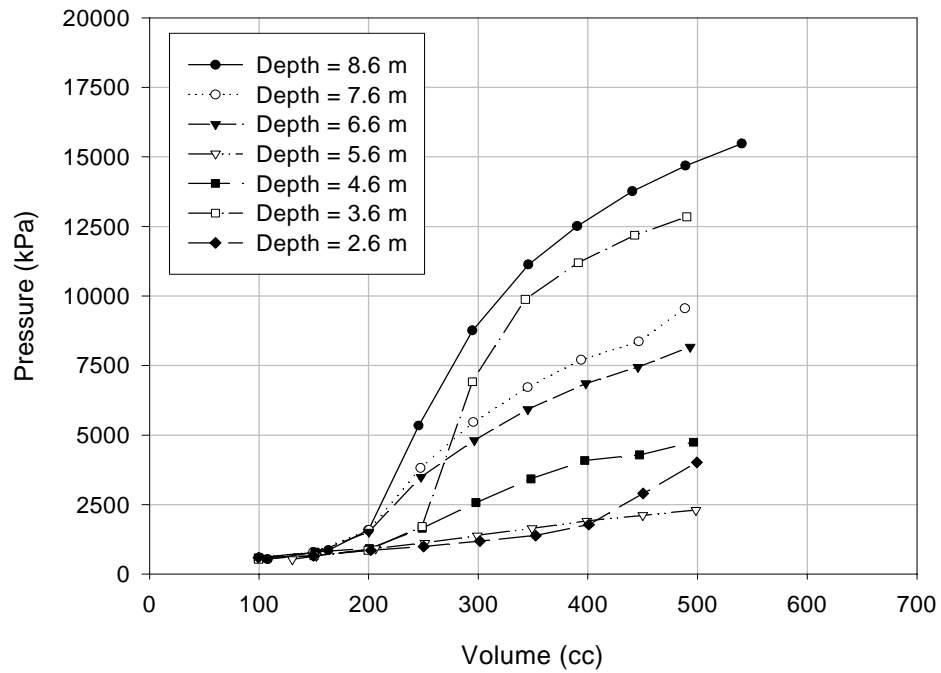
Figure B-5. Rock Dilatometer Test Result (Pressure vs. Volume) – Wilson
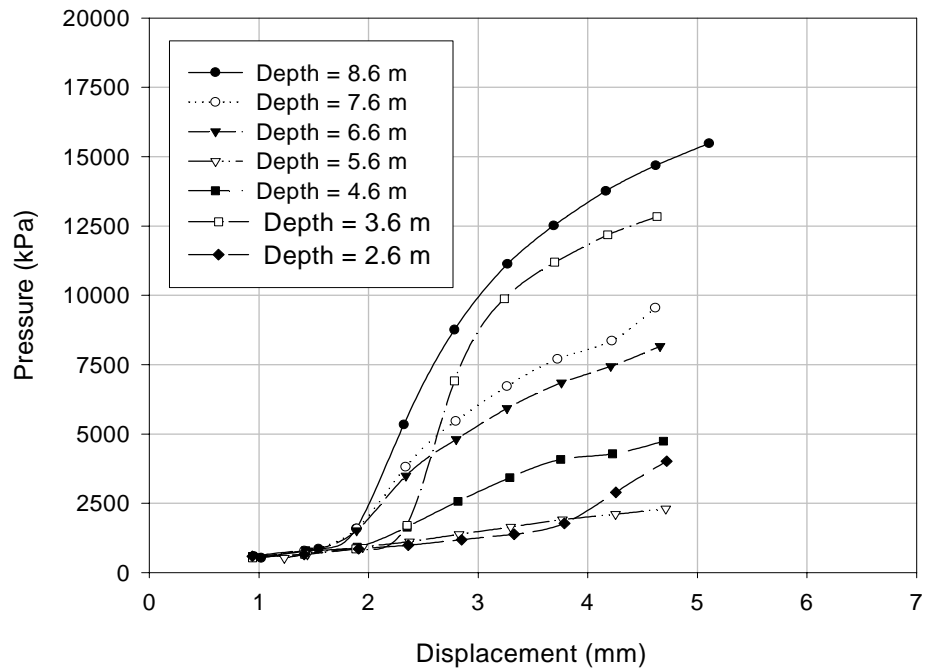
Figure B-6. Rock Dilatometer Test Result (Pressure vs. Displacement) – Wilson

208
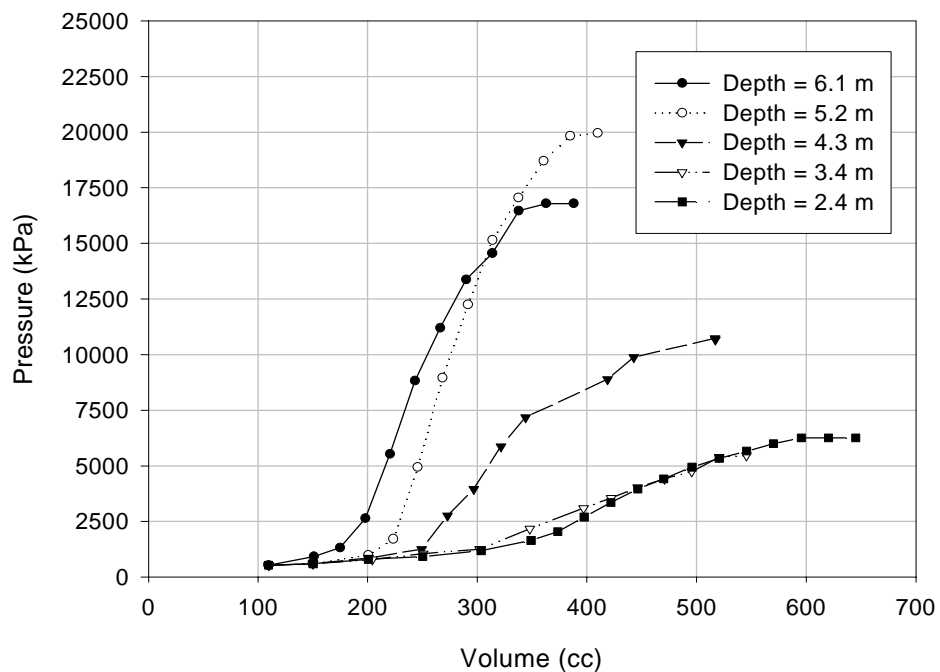
Figure B-7. Rock Dilatometer Test Result (Pressure vs. Volume) – Durham Site A
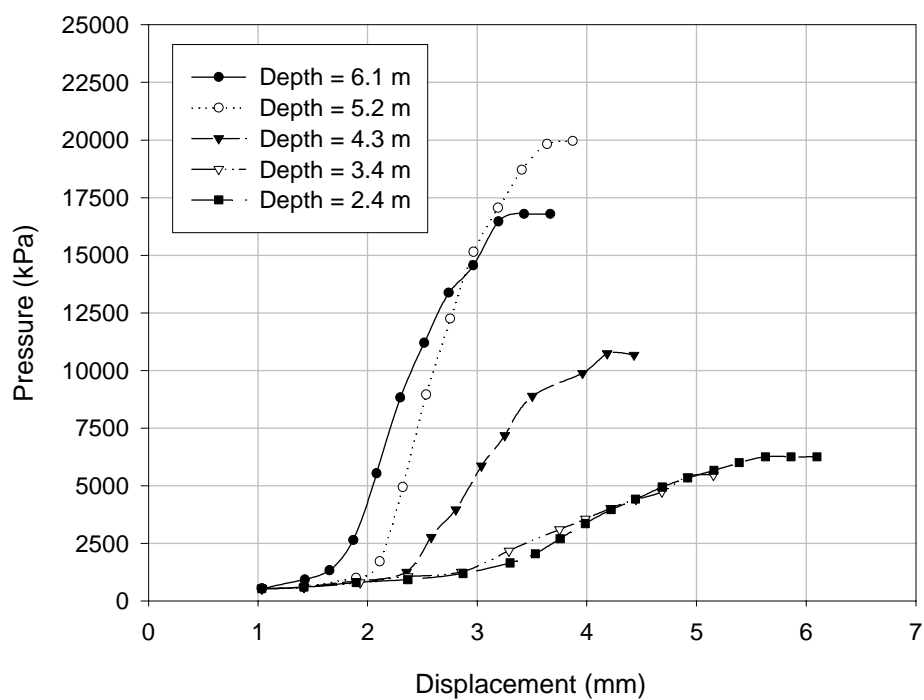
Figure B-8. Rock Dilatometer Test Result (Pressure vs. Displacement) – Durham

Site A
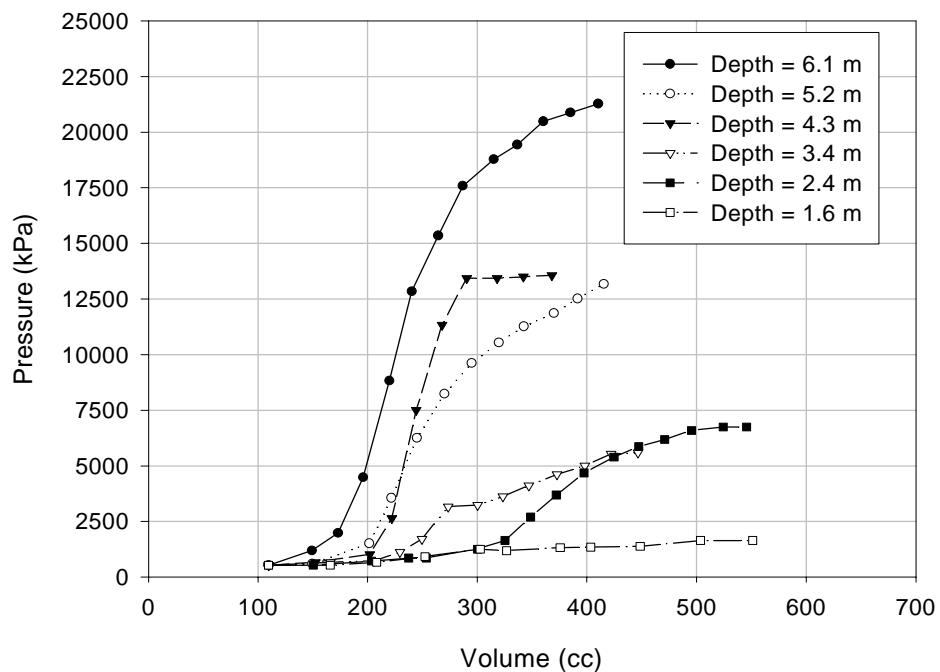
Figure B-9. Rock Dilatometer Test Result (Pressure vs. Volume) – Durham Site B
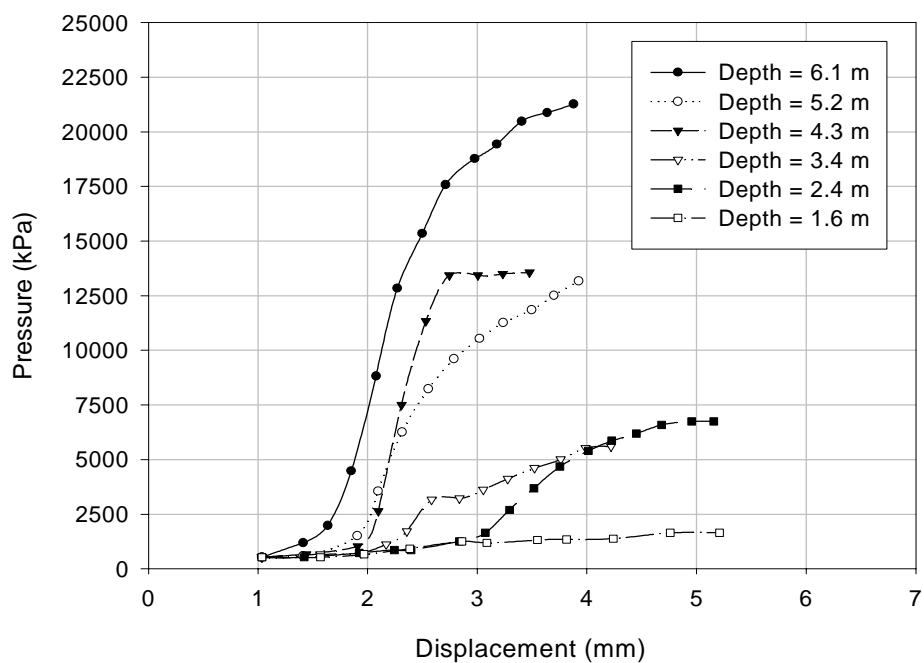
Figure B-10. Rock Dilatometer Test Result (Pressure vs. Displacement) – Durham Site B
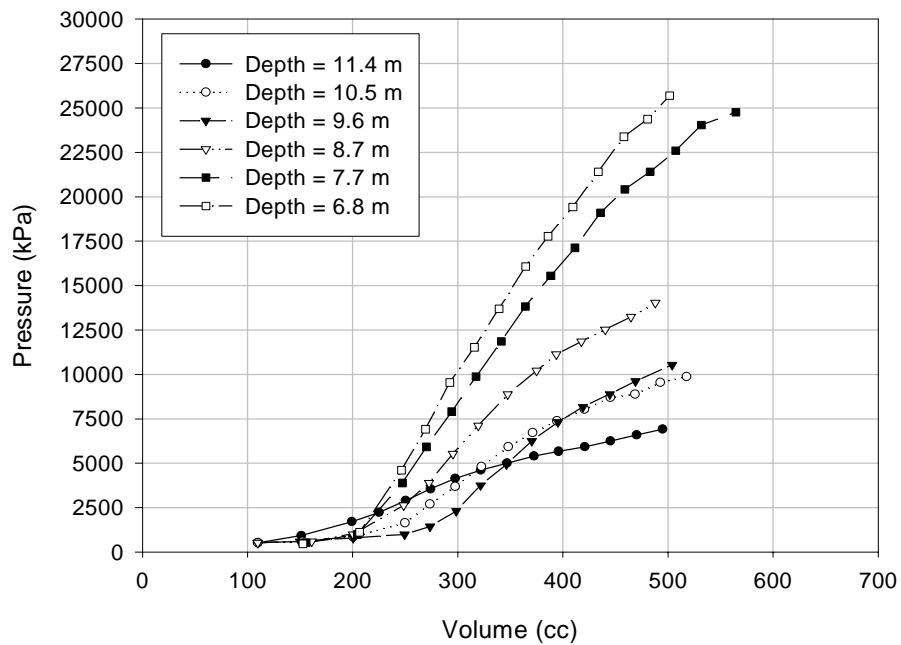
Figure B-11. Rock Dilatometer Test Result (Pressure vs. Volume) – Wake
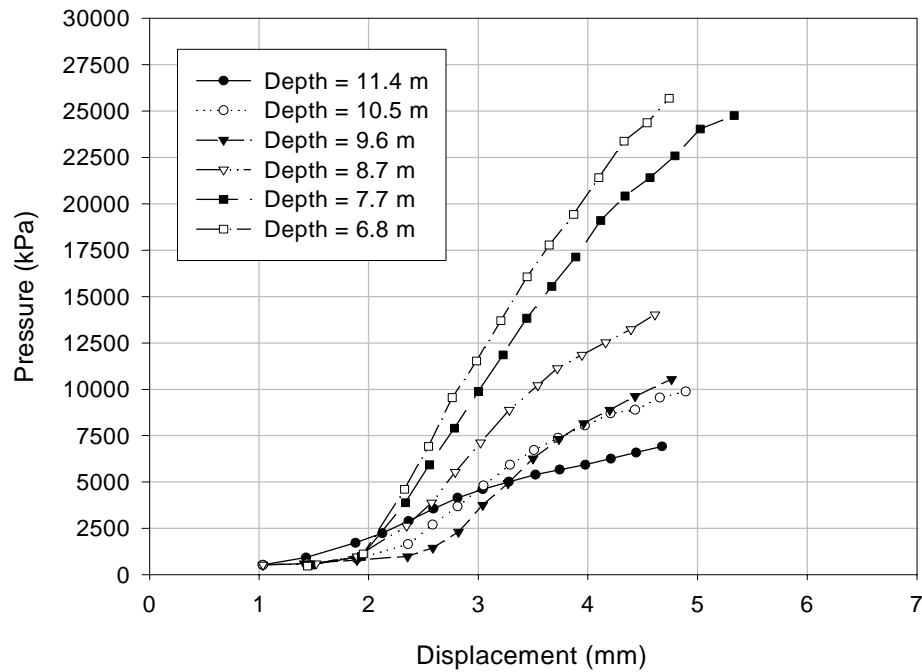
Figure B-12. Rock Dilatometer Test Result (Pressure vs. Displacement) – Wake

APPENDIX C
Locations of Test Site (Local Map)

Figure C-1. Nash County Test Site Location
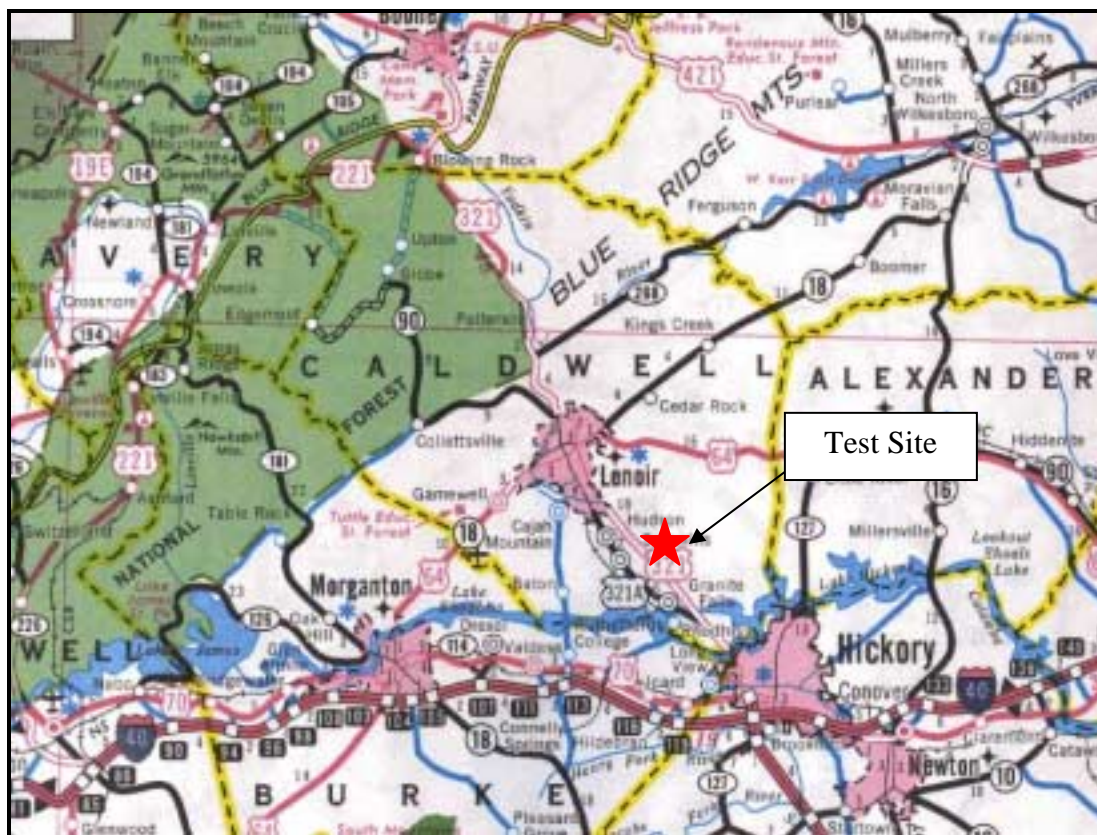
Figure C-2. Caldwell County Test Site Location

Figure C-3. Wilson County Test Site Location

APPENDIX D

Boring Logs and Rock Core Report at Test Sites

PROJECT NO. 8.2732201	ID. B-2937	COUNTY CALDWELL	GEOLOGIST C.A. YOUNGBLOOD	
SITE DESCRIPTION DILATOMETER TESTING				GROUND WATER
BORING NO. B2-CA	BORING LOCATION 16+55	OFFSET 30' LT	ALIGNMENT L1	0 HR. N/A
COLLAR ELEVATION 1097.8'	NORTHING 0.00	EASTING 0.00		24 HR. N/A
TOTAL DEPTH 35.4'	DRILL MACHINE CME-550	DRILL METHOD WASH BORING	HAMMER TYPE AUTOMATIC	
START DATE 8/8/00	COMPLETION DATE 8/9/00	SURFACE WATER DEPTH N/A	DEPTH TO ROCK N/A	

ELEV.	DEPTH (FT.)	BLOW COUNT 0.5'|0.5'|0.5'	PEN. (FT.)	BLOWS PER FOOT 0 25 50 75 100	SAMPLE NUMBER	MOI.	LOG	SOIL AND ROCK DESCRIPTION
1097.8								
1095.0								**RESIDUAL:** TAN TO BROWN, MEDIUM DENSE, SILTY TO FINE COARSE SAND MICACEOUS & SAPROLITIC (DESCRIPTION FROM B1-CA LOG)
1090.0								
1085.0								
1080.0	16.6	44 36 64	1.4	100 X				SOFT TO HARD WEATHERED ROCK (GNIESS)
1075.0	20.4	31 56 44	1.3	100 X				
1070.0	25.4	67 33	1.3	100 X				
1065.0	30.4	100	0.7	100 X				
1060.0				CORING TERMINATED AT ELEVATION 1062.4 IN SOFT WEATHERED ROCK (GNIESS)				
1055.0								
1050.0								
1045.0								
1040.0								
1035.0								
1030.0								
1025.0								
1020.0								

Figure D-1. Caldwell County Test Area Boring Log

CORE BORING REPORT

PROJECT: 8.2732201   ID: B-2937   COUNTY: CALDWELL   BORING NO: B2-CALD

DESCRIPTION: DILATOMETER TESTING

LOCATION OF BORING: 16+55, 30' LT.   COMPLETION DATE: 8/9/00

COLLAR or GROUND ELEVATION: 1097.8 ft   CORE SIZE: 2"   GEOLOGIST: C.A. YOUNGBLOOD

CORE EQUIPMENT: CME-550, N-CASING   DRILLER: H.R. CONLEY

ELEV (ft)	DEPTH (ft)	DRILL RATE (min/ft)	RUN (ft)	REC (ft) (%)	RQD (ft) (%)	SAMPLE NUMBER	FIELD CLASSIFICATION and REMARKS
1079.8	18.0	Time not		1.2	0.0		SPT TAKEN BEFORE RUN 1 WITH OF TOTAL PENETRATION OF 1.4'
		taken due	2.4				EXTREMELY FRACTURED, MODERATELY SEVERE WEATHER GNIESS WITH QUARTZITE.
		to the					SALT AND PEPPER TEXTURE.
		length of		(50%)	(0%)		
1077.4	20.4	the run					SPT TAKEN BETWEEN RUN 1 AND 2 WITH A TOTAL PENETRATION OF 1.3'.
1077.4	21.7	1:15		2.3	0.0		MODERATELY TO EXTREMELY FRACTURE, MODERATE WEATHER GNIESS WITH QUARTZITE
		1:00	3.7				AND BIOTITE. SALT AND PEPPER TEXTURE.
		0:45					
		1:39		(62%)	(0%)		
1073.7	25.4	1:05					SPT TAKEN BETWEEN RUN 2 AND 3 WITH A TOTAL PENETRATION OF 0.7'.
1073.7	26.1	1:12		3.8	1.3		MODERATELY TO EXTREMELY FRACTURED, SEVERE WEATHER GNIESS WITH QUARTZITE
		1:12					AND BIOTITE. SALT AND PEPPER TEXTURE.
		1:01	4.3				A CLAY LAYER WAS OBSERVED BETWEEN 30.0'-30.2'.
		0:55		(88%)	(30%)		
1069.4	30.4	1:30					SPT TAKEN BETWEEN RUN 3 AND 4 WITH A TOTAL PENETRATION OF 0.5'.
1069.4	30.9	1:31		3.4	1.2		MODERATELY TO EXTREMELY FRACTURE, MODERATE WEATHER GNIESS WITH QUARTZITE,
		0:57					BIOTITE AND GARNETS.
		0:50	4.5				
		0:47		(76%)	(27%)		
1064.9	35.4	0:40					
		TOTALS:	14.9	10.7 (72%)	2.5 (17%)		BOREHOLE TERMINATED AT ELEVATION OF 1062.4 FEET, IN SWR.

Figure D-2. Caldwell County Test Site Rock Core Report

NORTH CAROLINA DEPARTMENT OF TRANSPORTATION
GEOTECHNICAL UNIT BORING LOG

PROJECT NO. 8.1340801	ID. U-3472	COUNTY WILSON		GEOLOGIST G. CAMPBELL	

SITE DESCRIPTION					GROUND WATER
BORING NO. DT-3	BORING LOCATION 86+64.00	OFFSET 11.00 RT	ALIGNMENT -L-		0 HR.
COLLAR ELEV. 0.00	NORTHING 0.00	EASTING 0.00			24 HR.
TOTAL DEPTH 7.76	DRILL MACHINE CME 550	DRILL METHOD WASH BORING		HAMMER TYPE AUTOMATIC	
START DATE 4/9/1	COMPLETION DATE 4/9/1	SURFACE WATER DEPTH		DEPTH TO ROCK	

Boring log chart columns: ELEV., DEPTH, BLOW COUNT (15cm 15cm 15cm), PEN. (m), BLOWS PER 30cm (0 25 50 75 100), SAMPLE NUMBER/MOI., LOG, SOIL AND ROCK DESCRIPTION.

ARTIFICAL FILL: TAN, SANDY GRAVEL

CRYSTALLINE ROCK

BORING TERMINATED AT DEPTH OF 7.76 M

Figure D-3. Wilson County Test Area Boring Log – Long Shaft

219

NORTH CAROLINA DEPARTMENT OF TRANSPORTATION
GEOTECHNICAL UNIT BORING LOG

SHEET I OF I

PROJECT NO. 8.1340801	ID. U-3472	COUNTY WILSON		GEOLOGIST G. CAMPBELL	
SITE DESCRIPTION					GROUND WATER
BORING NO. DT-4	BORING LOCATION 86+56.00	OFFSET II.00 RT	ALIGNMENT -L-		0 HR.
COLLAR ELEV. 0.00	NORTHING 0.00	EASTING 0.00			24 HR.
TOTAL DEPTH 9.12	DRILL MACHINE CME 550	DRILL METHOD WASH BORING	HAMMER TYPE AUTOMATIC		
START DATE 4/10/1	COMPLETION DATE 4/10/1	SURFACE WATER DEPTH		DEPTH TO ROCK 2.3	

ELEV.	DEPTH	BLOW COUNT 15cm 15cm 15cm	PEN. (m)	BLOWS PER 30cm 0 25 50 75 100	SAMPLE NUMBER	▼ / MOI.	LOG	SOIL AND ROCK DESCRIPTION
0.00								ARTIFICAL FILL: TAN, SANDY GRAVEL
-2.00								
-4.00								CRYSTALLINE ROCK
-6.00								
-8.00								
-10.00				BORING TERMINATED AT A DEPTH OF 9.12M				
-12.00								
-14.00								
-16.00								
-18.00								
-20.00								

Figure D-4. Wilson County Test Area Boring Log – Short Shaft

CORE BORING REPORT

PROJECT: **8.1340801**   ID: **U-3472**   COUNTY: **Wilson**   BORING NO: **DT-3**

DESCRIPTION: Dilotometer Testing

LOCATION OF BORING: L, 86+64   COMPLETION DATE: 04/09/01

COLLAR or GROUND ELEVATION: n/a m   CORE SIZE: NX   GEOLOGIST: Gene Campbell

CORE EQUIPMENT: NX WL, CME 550   DRILLER: HRC

ELEV (m)	DEPTH (m)	DRILL RATE (min/0.5m)	RUN (m)	REC (m) (%)	RQD (m) (%)	SAMPLE NUMBER	FIELD CLASSIFICATION and REMARKS
####	2.18		1.02	0.65 (64%)	0.00 (0%)		Green-Grey, very severely weathered, hard to soft, very closely fractured, metavolcanic
####	3.20						
####	3.20		1.52	1.00 (66%)	0.20 (13%)		Green-Grey, very severely weathered, hard to very soft, close to very closely fractured, metavolcanic
####	4.72						
####	4.72		1.52	0.80 (53%)	0.00 (0%)		Green-Grey, very severely to moderately severly weathered, soft to hard, close to very closely fractured, metavolcanic
####	6.24						
####	6.24		1.52	1.20 (79%)	0.35 (23%)		Green-Grey, very severly to moderately severly weathered, soft to hard, close to very closely fractured, meatvolcanic
####	7.76						
		TOTALS:	5.58	3.65 (65%)	0.55 (10%)		##

Figure D-5. Wilson County Rock Core Report – Long Shaft

221

CORE BORING REPORT

PROJECT: __8.1340801__   ID: __U-3472__   COUNTY: __Wilson__   BORING NO: __DT-4__

DESCRIPTION: __Dilotometer Testing__

LOCATION OF BORING: __I, 86+56, 11m RT__   COMPLETION DATE: __04/10/01__

COLLAR or GROUND ELEVATION: __n/a__ m   CORE SIZE: __NX__   GEOLOGIST: __BAP__

CORE EQUIPMENT: __NXWL, CME 550__   DRILLER: __HRC__

ELEV (m)	DEPTH (m)	DRILL RATE (min/0.5m)	RUN (m)	REC (m) (%)	RQD (m) (%)	SAMPLE NUMBER	FIELD CLASSIFICATION and REMARKS
####	2.30		0.74	0.74 (100%)	0.40 (54%)		Green-Grey, moderate to moderately severly weathered, soft to hard, very close to closely fractured metavolcanic, fractures at 30 degrees at 2.90 and 2.94 meters
####	3.04						
####	3.04		1.52	1.52 (100%)	0.90 (59%)		Green-Grey, moderate to slightly weathered, medium hard to hard, close to moderately closely fractured, metavolcanic, fractures from 20 to 45 degrees at 3.91 and 3.96 meters, a fracture zone from 3.04 to 3.56 meters
####	4.56						
####	4.56		1.52	1.32 (87%)	0.42 (28%)		Green-Grey, very severly to moderately severely weathered, soft to hard, very closely to closely fractured, metavolcanic, fracture zone from 4.56 to 5.33 meters.
####	6.08						
####	6.08		1.52	1.40 (92%)	0.00 (0%)		Dark Green-Grey, severely to moderately severely weathered, soft to medium hard, very closely to closely fractured, meatvolcanic. Entire run is severly fractured.
####	7.60						
####	7.60		1.52	1.42 (93%)	0.58 (38%)		Dark Green-Grey, moderately severely to slightly weathered, moderate hard to medium hard, close to moderately close fractured, metavolcanic. Fracture zone at 8.57 to 9.12 meters. Fractures at 30 to 40 degrees at 7.83, 8.23, and 8.33 meters.
####	9.12						
	TOTALS:		6.82	6.40 (94%)	2.30 (34%)	##	

Figure D-6. Wilson County Rock Core Report – Short Shaft

APPENDIX E
Hyperbolic Curve Fittings
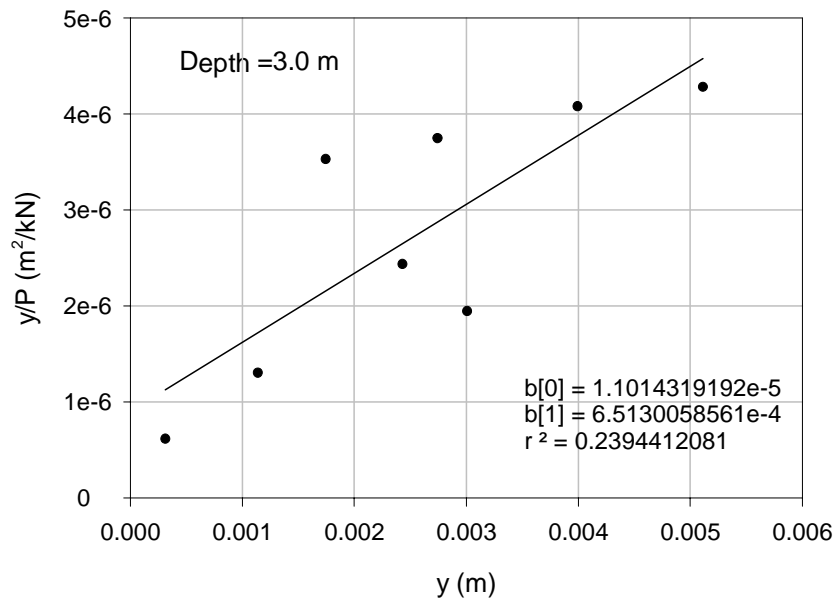
Figure E-1. Curve Fitting Result for Field Tests – Nash Long Shaft
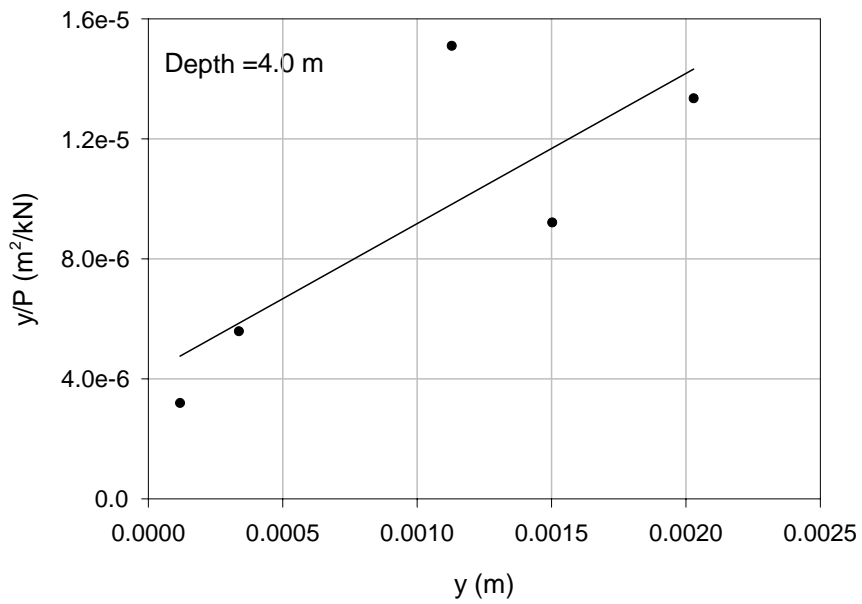
Figure E-2. Curve Fitting Result for Field Tests – Nash Long Shaft
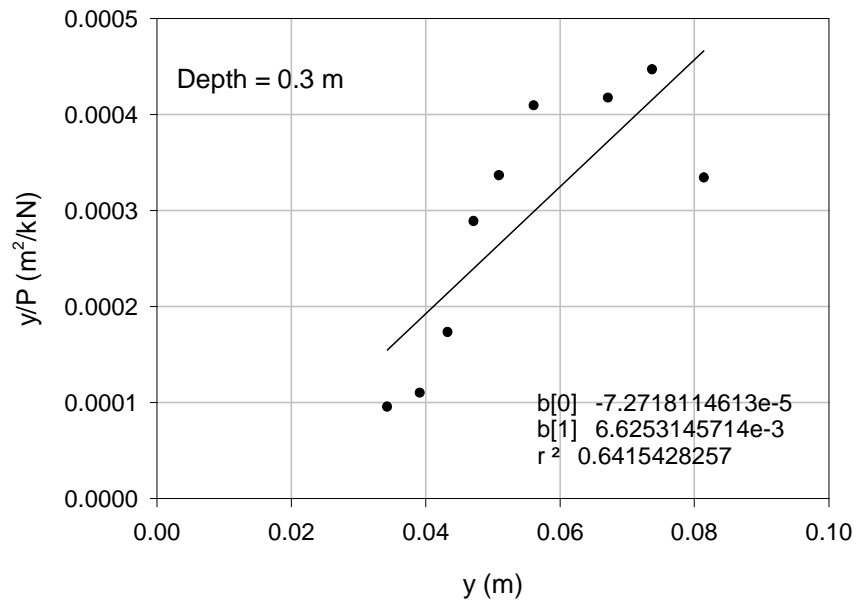
Figure E-3. Curve Fitting Result for Field Tests – Caldwell Short Shaft
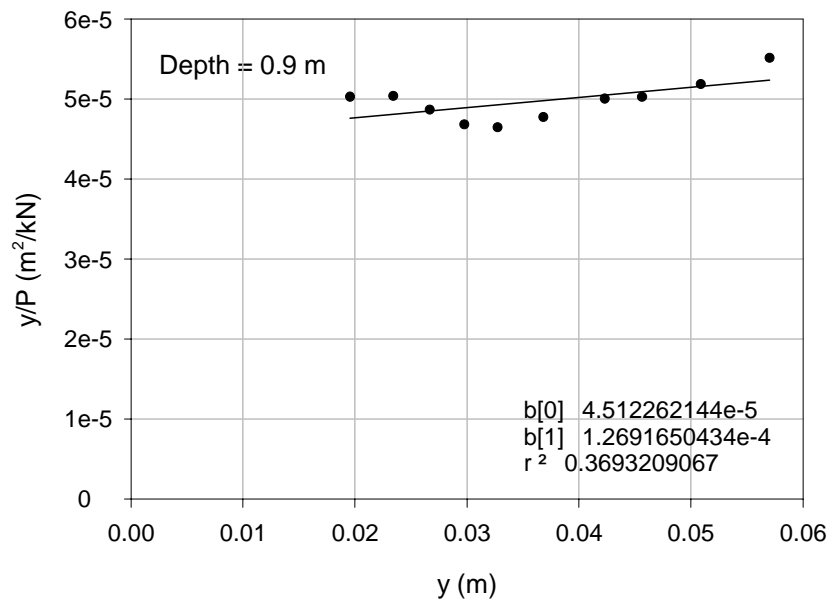
Figure E-4. Curve Fitting Result for Field Tests – Caldwell Short Shaft
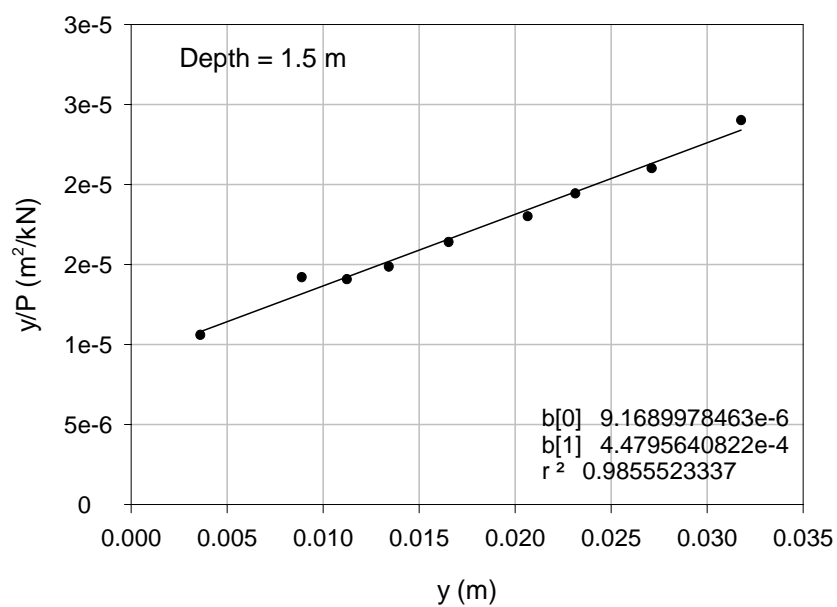
Figure E-5. Curve Fitting Result for Field Tests – Caldwell Short Shaft
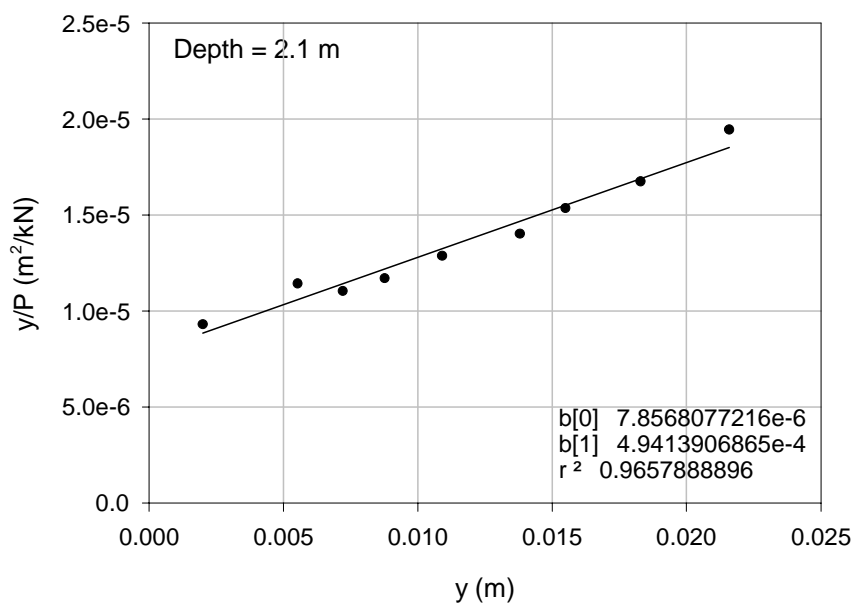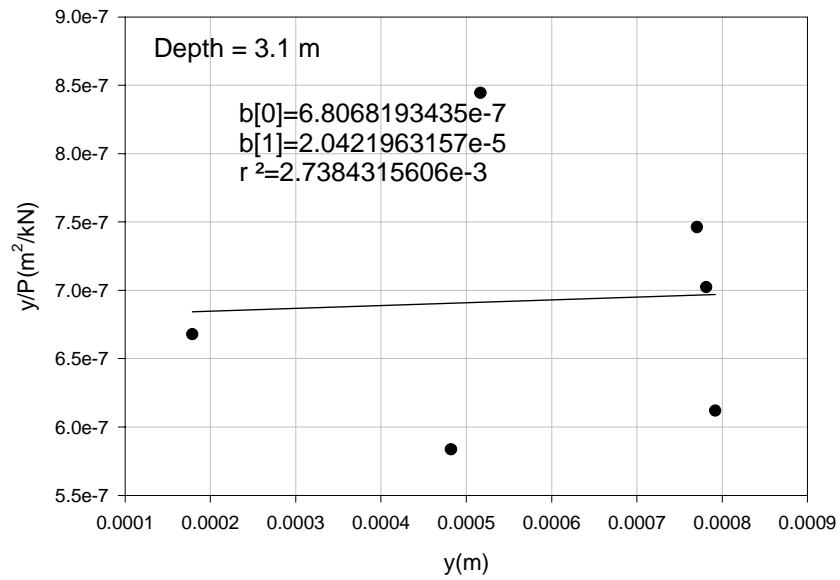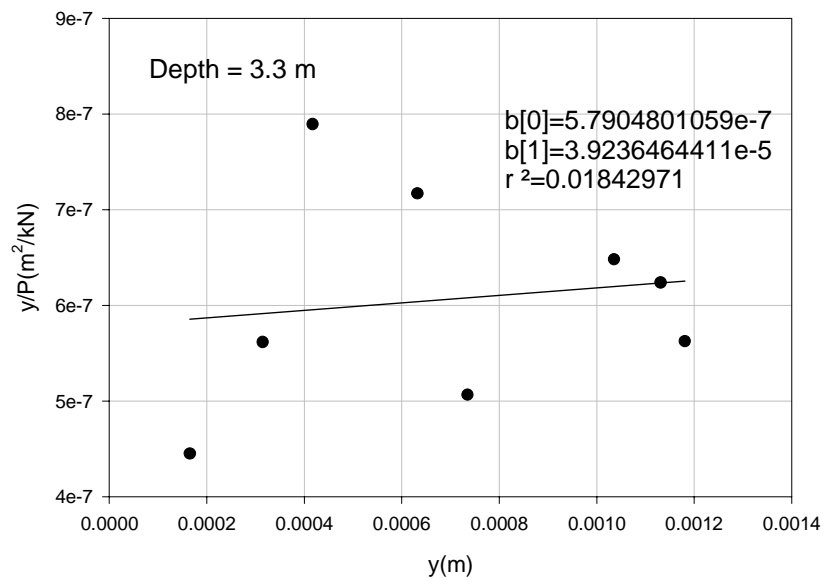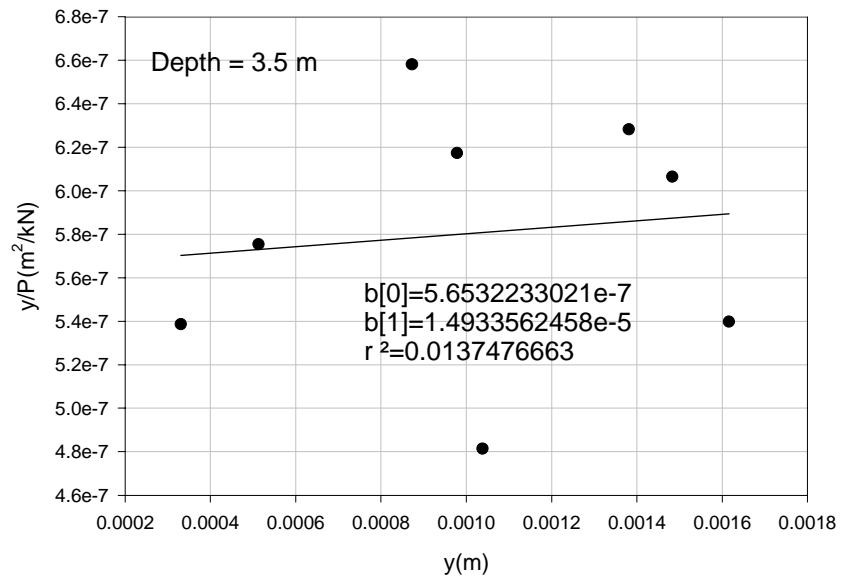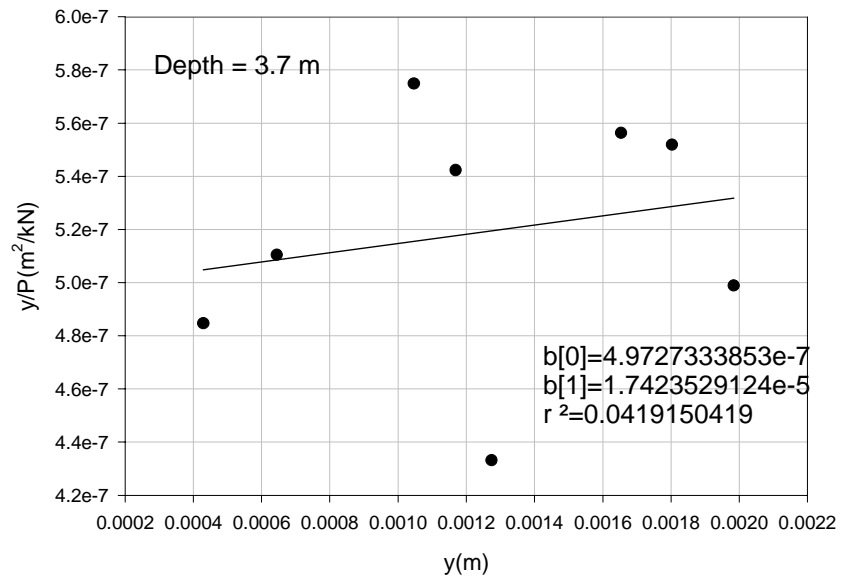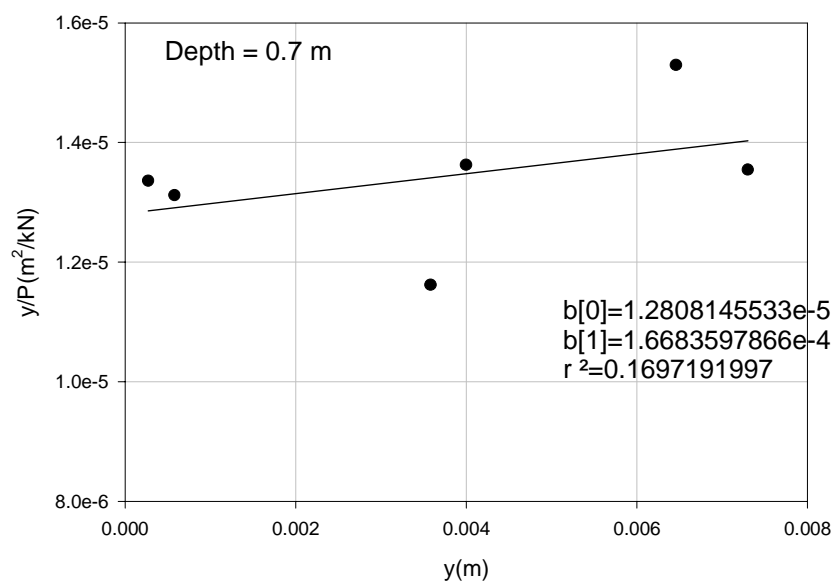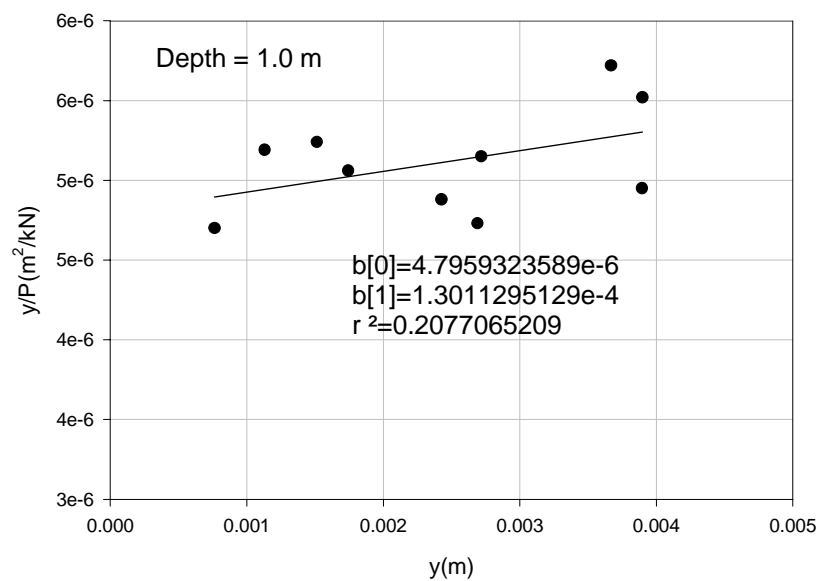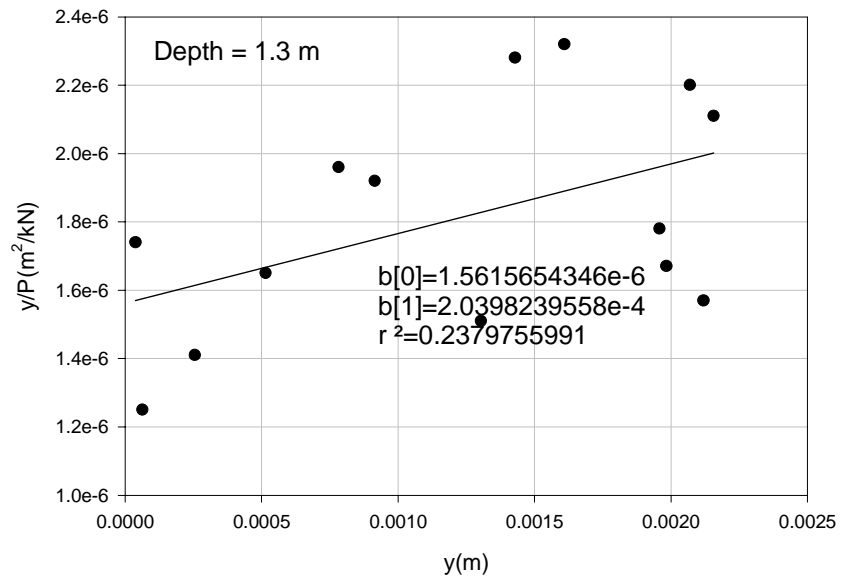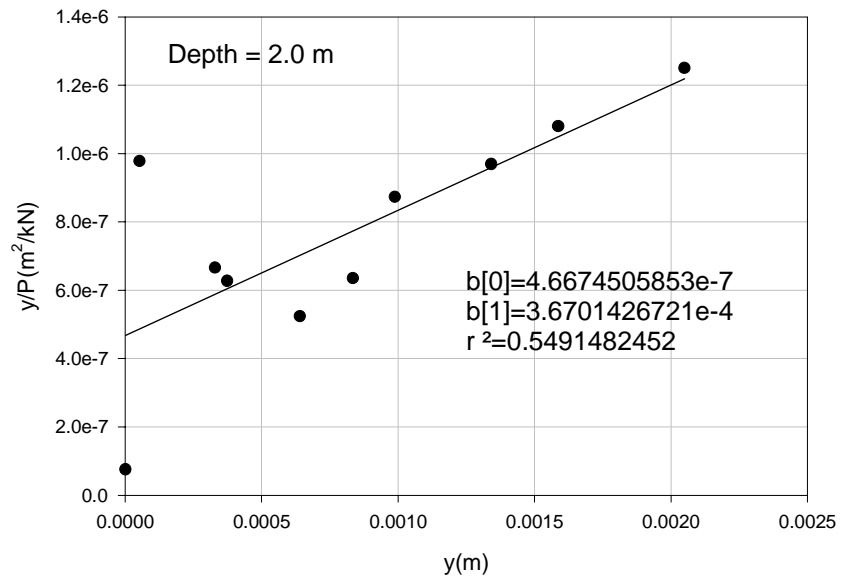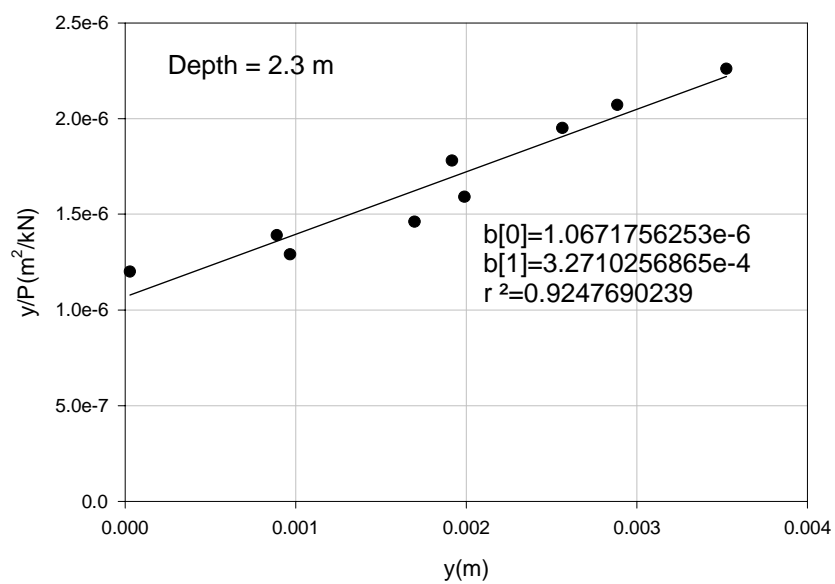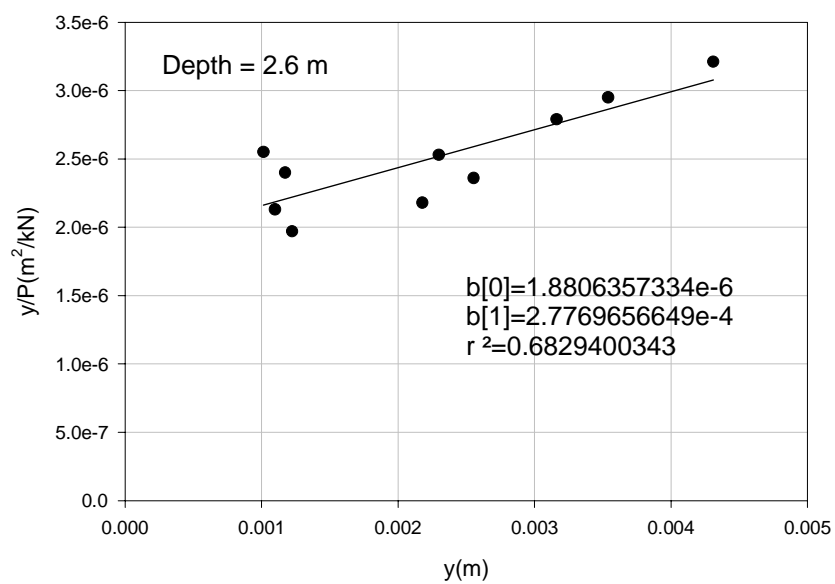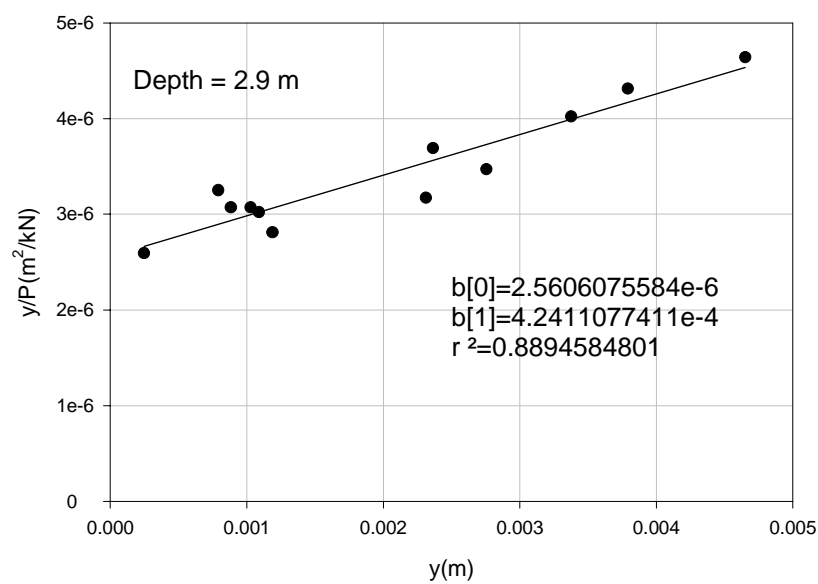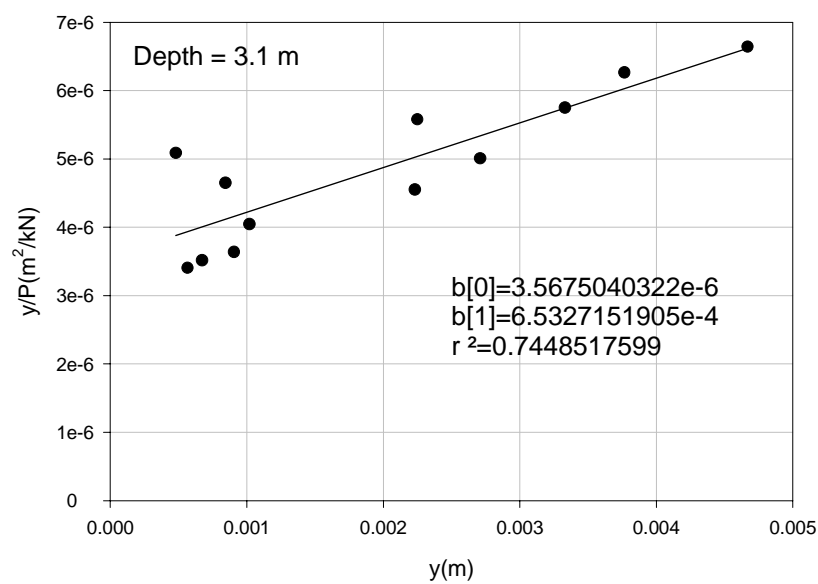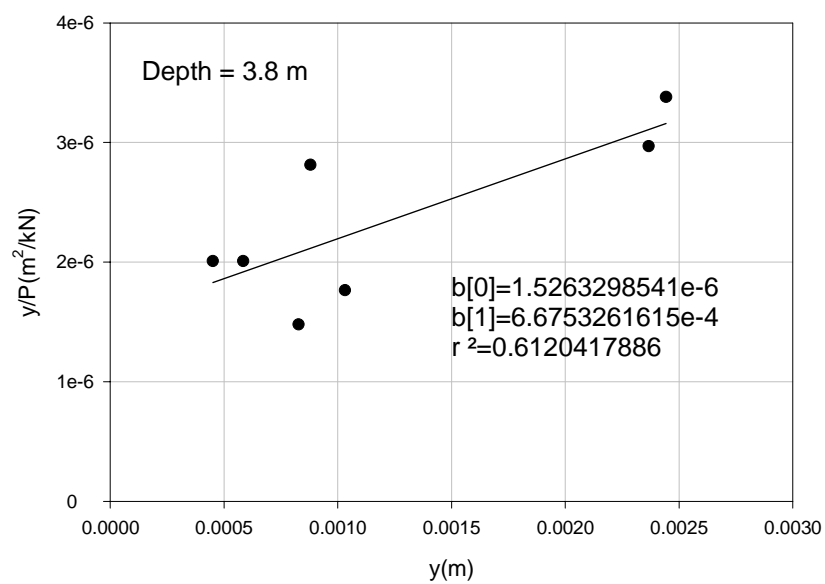

Figure E-6. Curve Fitting Result for Field Tests – Caldwell Short Shaft
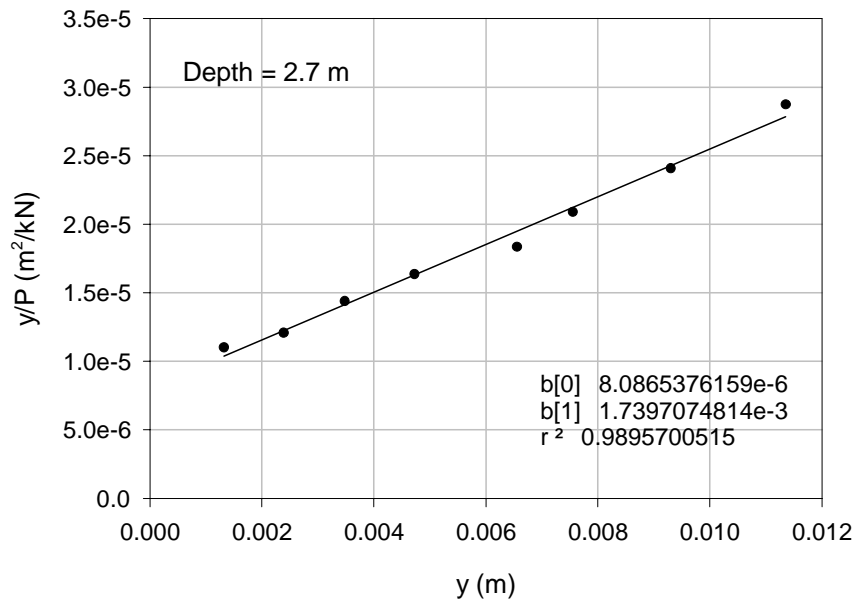
Figure E-7. Curve Fitting Result for Field Tests – Caldwell Short Shaft
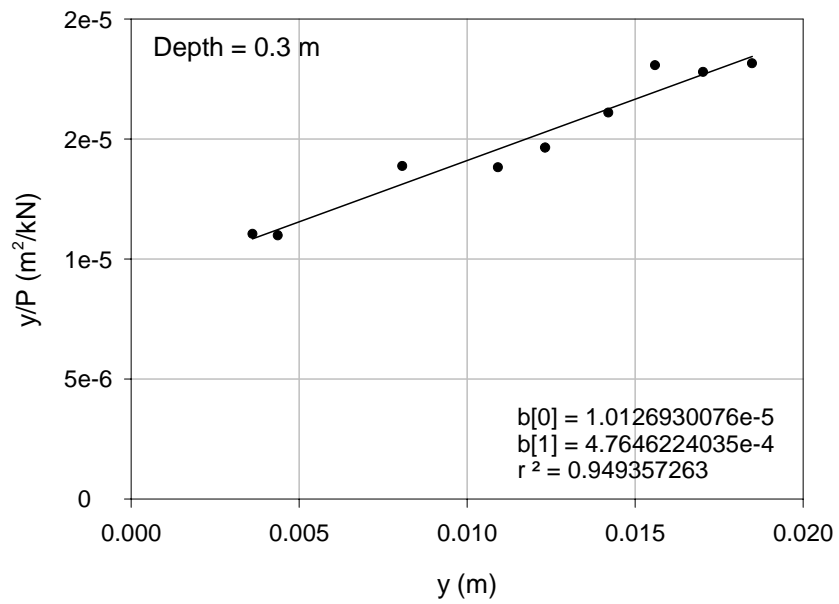
Figure E-8. Curve Fitting Result for Field Tests – Caldwell Long Shaft
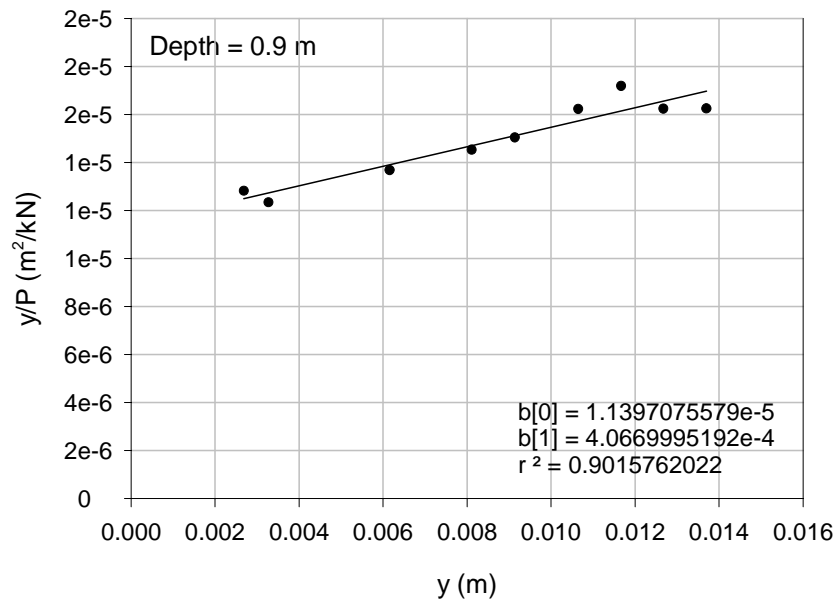
Figure E-9. Curve Fitting Result for Field Tests – Caldwell Long
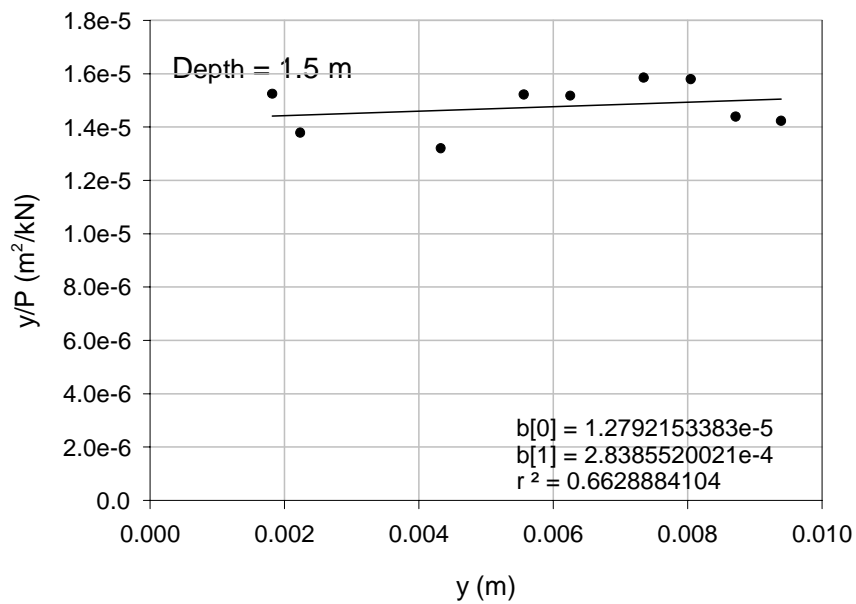
Figure E-10. Curve Fitting Result for Field Tests – Caldwell Long Shaft
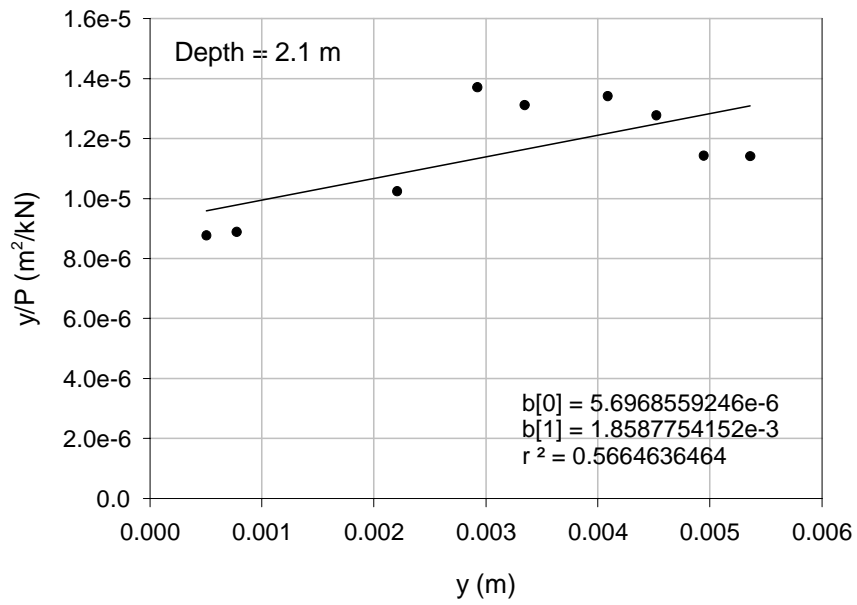
Figure E-11. Curve Fitting Result for Field Tests – Caldwell Long Shaft
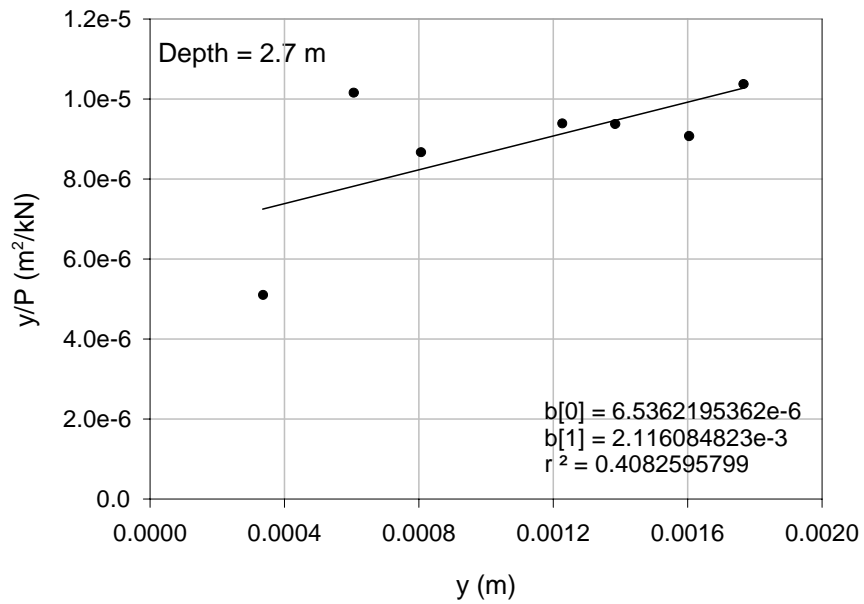
Figure E-12. Curve Fitting Result for Field Tests – Caldwell Long Shaft
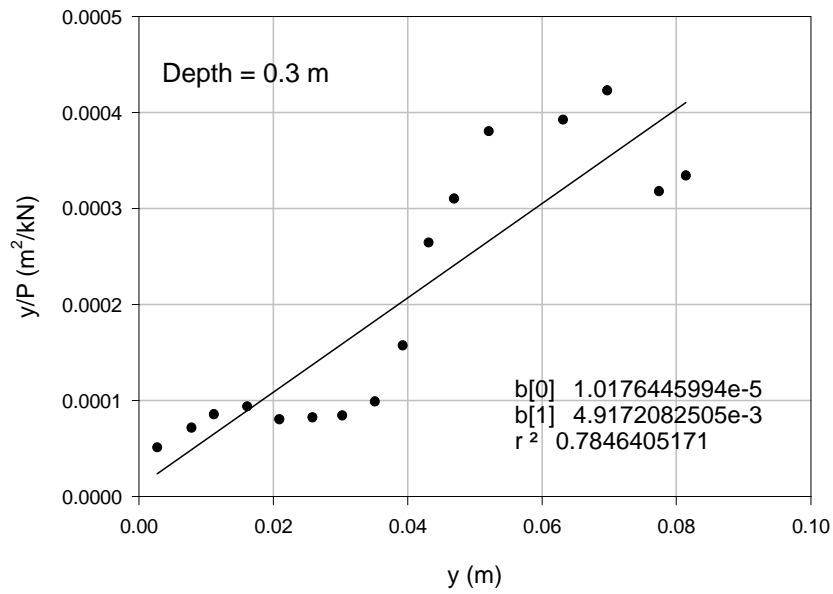
Figure E-13. Curve Fitting Result for Field Tests – Wilson Short Shaft
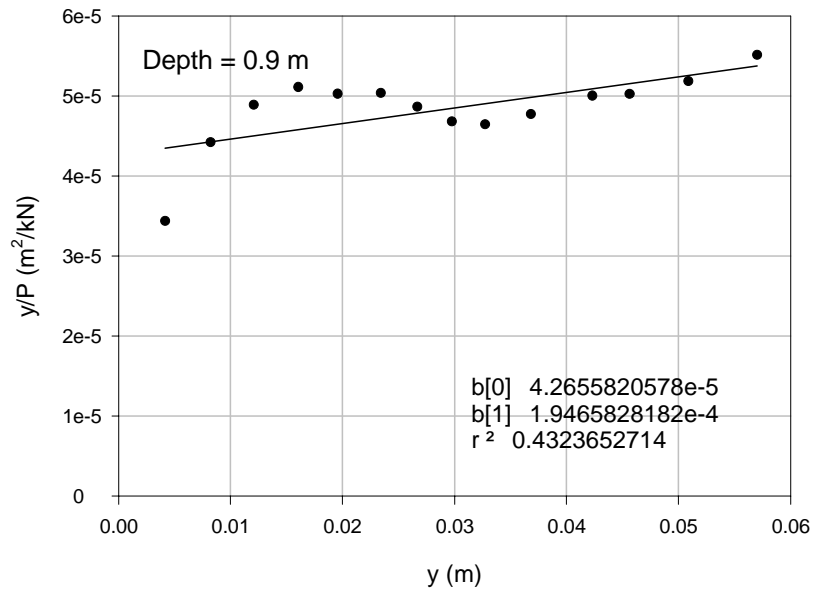
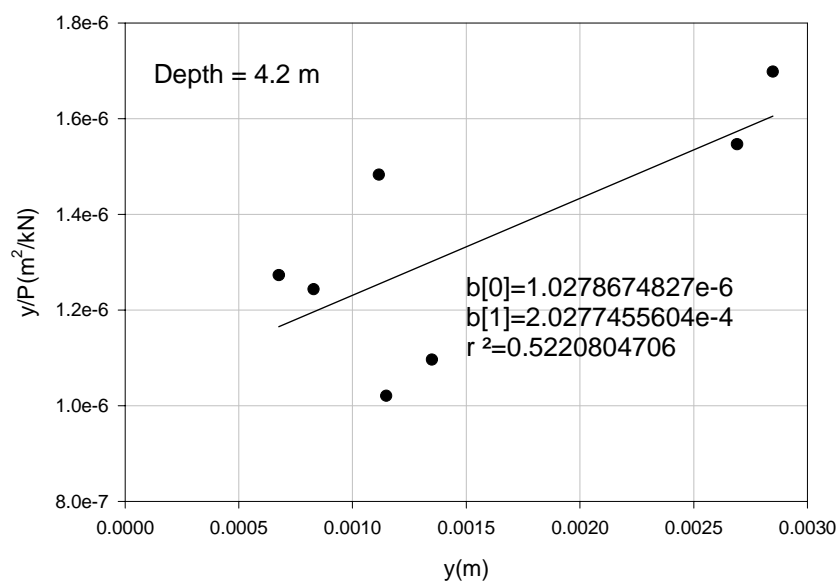**Figure E-14. Curve Fitting Result for Field Tests – Wilson Short Shaft**

230
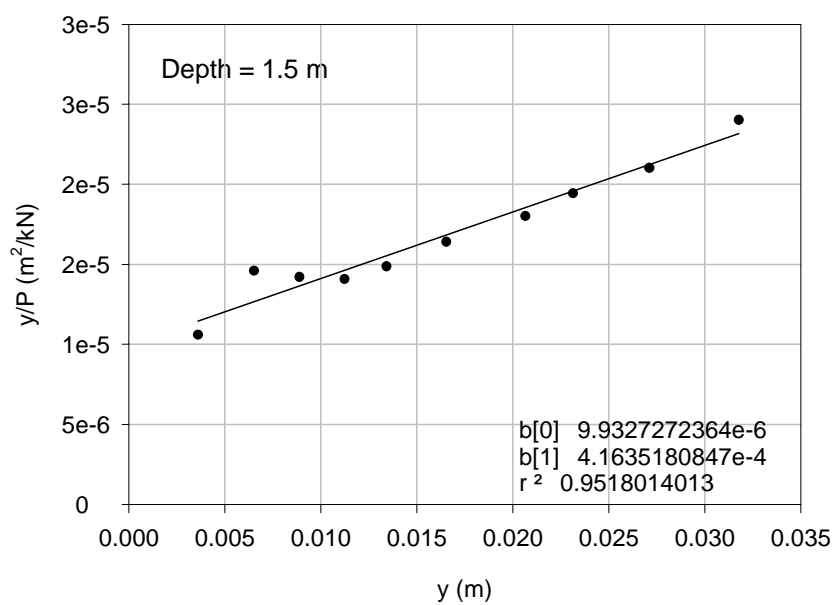
Figure E-15. Curve Fitting Result for Field Tests – Wilson Short Shaft
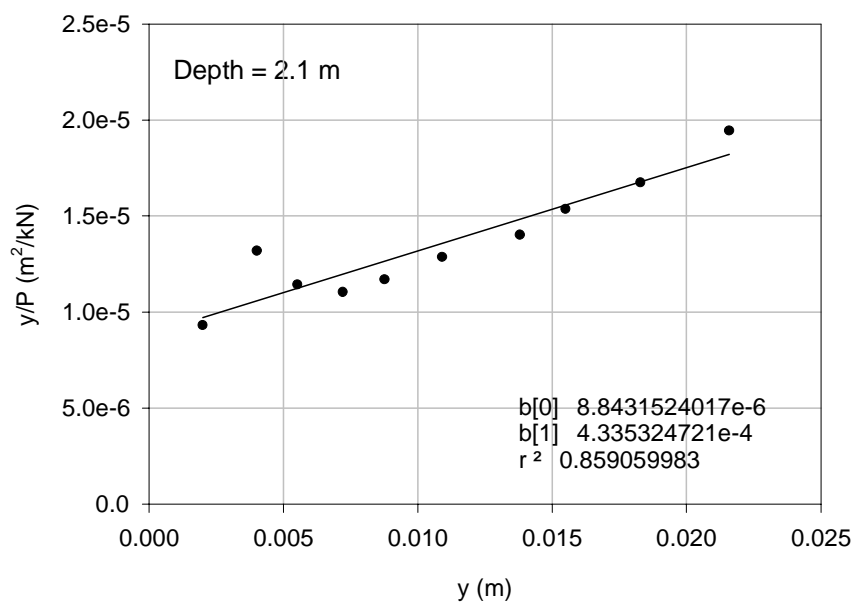
Figure E-16. Curve Fitting Result for Field Tests – Wilson Short Shaft
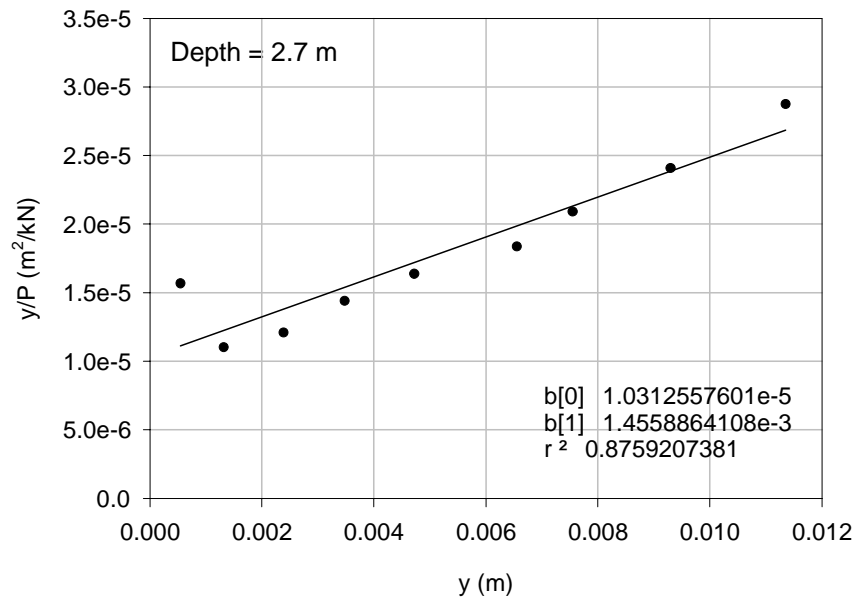
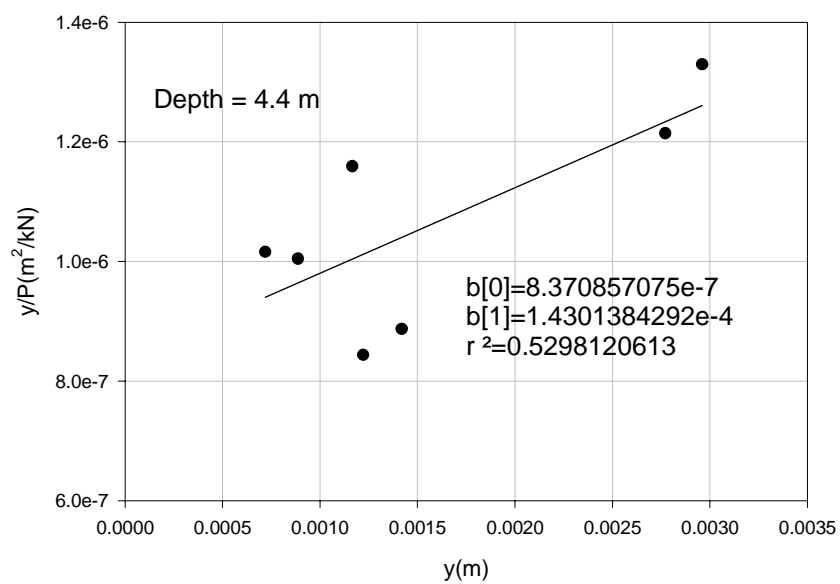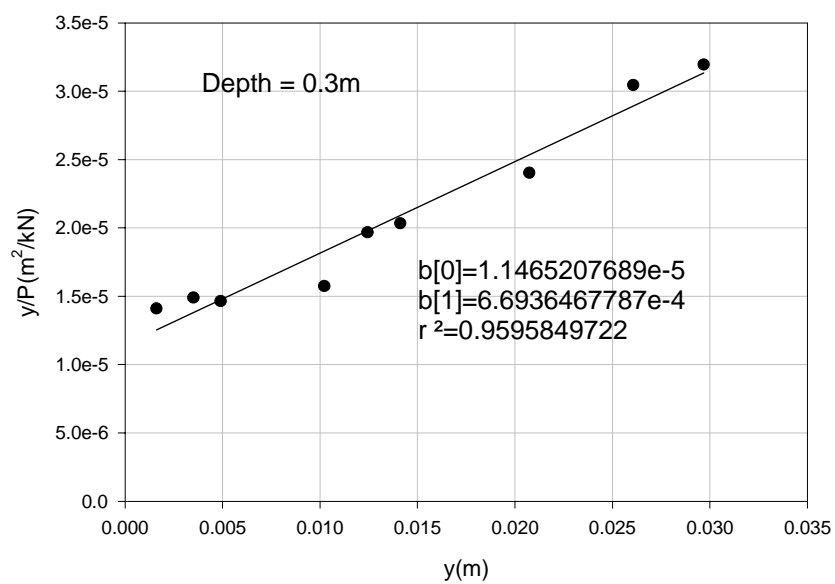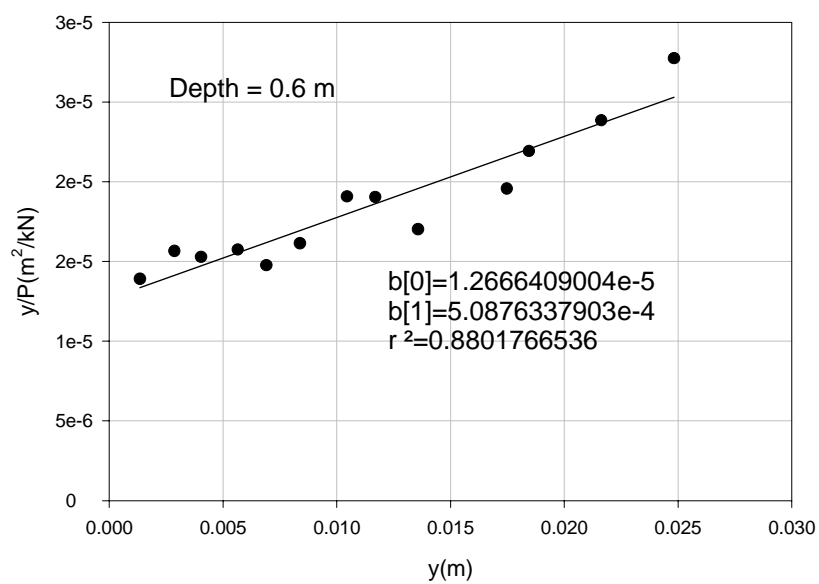**Figure E-17. Curve Fitting Result for Field Tests – Wilson Short Shaft**
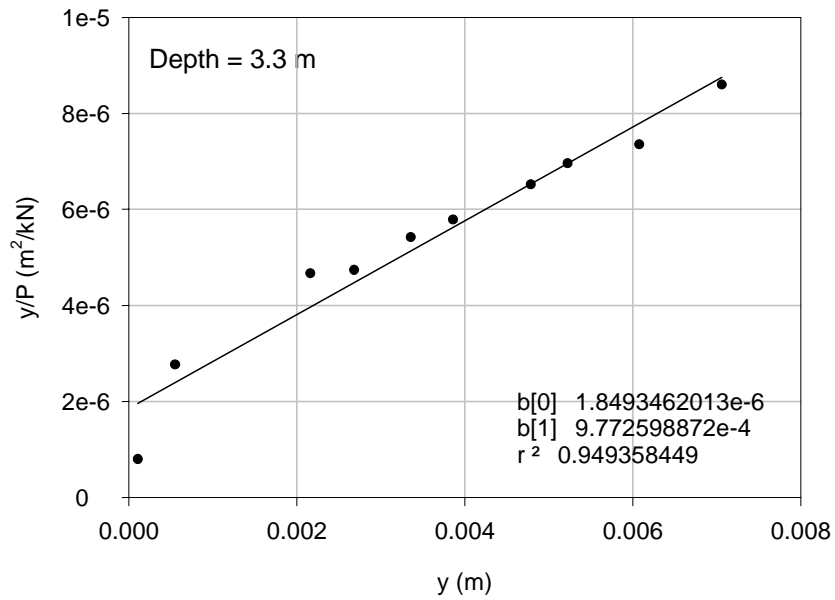
Figure E-18. Curve Fitting Result for Field Tests – Wilson Short Shaft
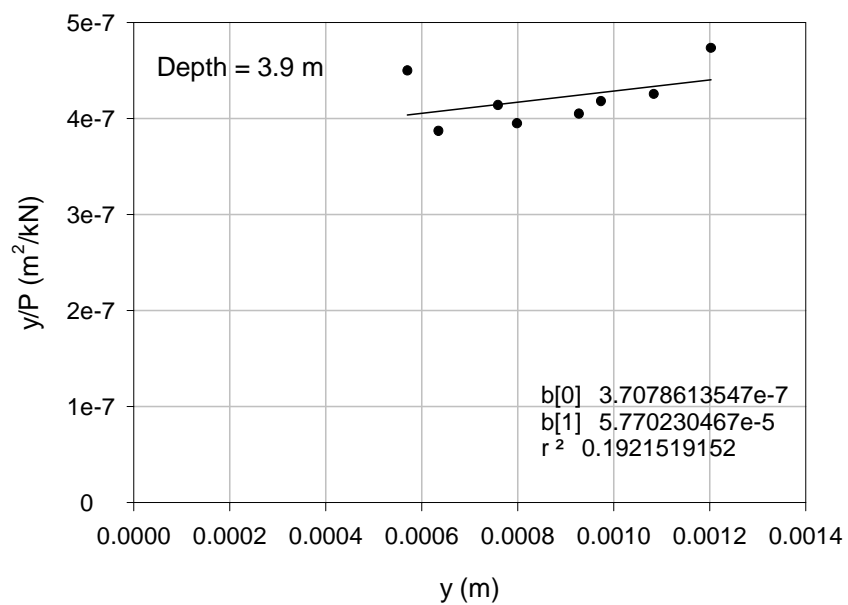
Figure E-19. Curve Fitting Result for Field Tests – Wilson Short Shaft
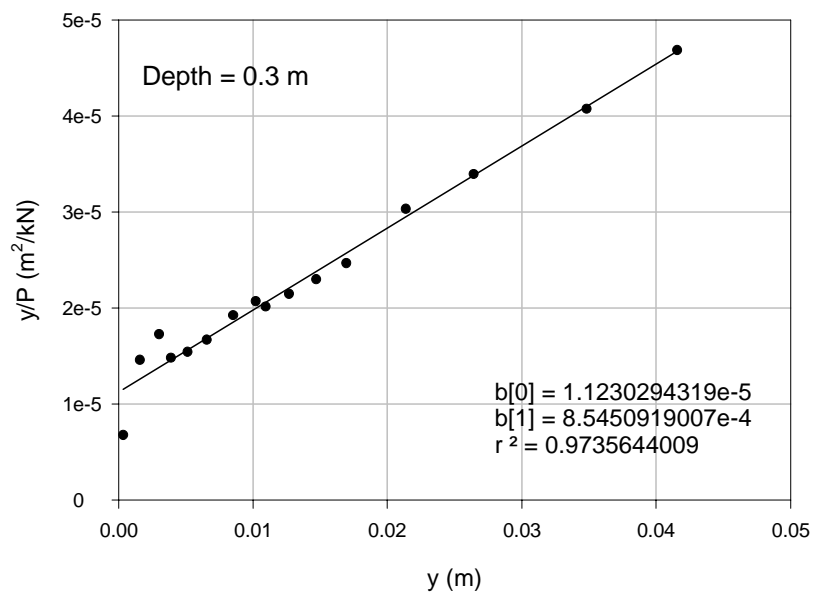
Figure E-20. Curve Fitting Result for Field Tests – Wilson Long Shaft
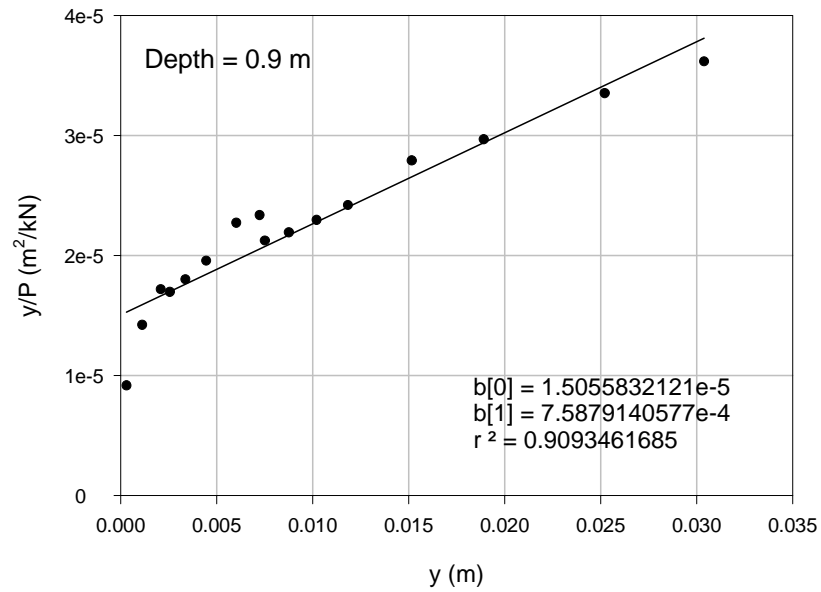
Figure E-21. Curve Fitting Result for Field Tests – Wilson Long Shaft
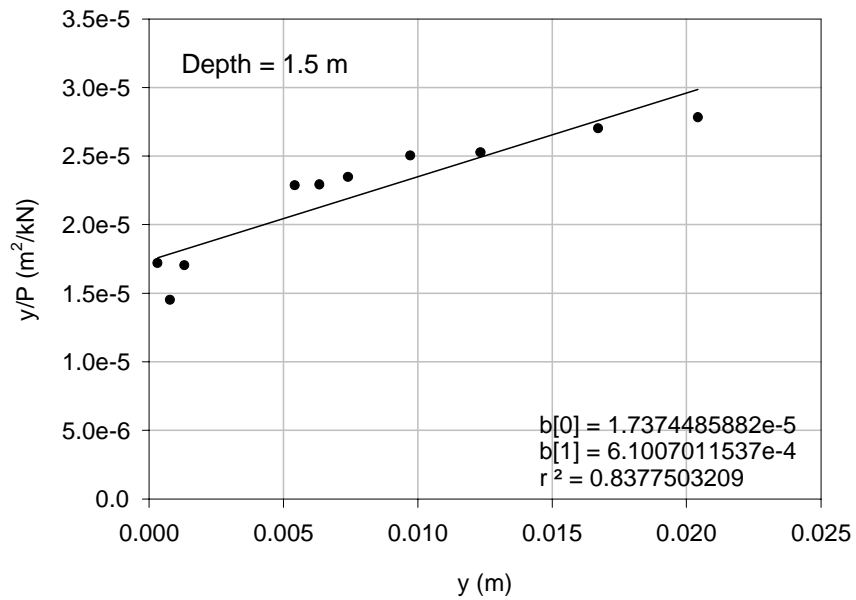
Figure E-22. Curve Fitting Result for Field Tests – Wilson Long Shaft
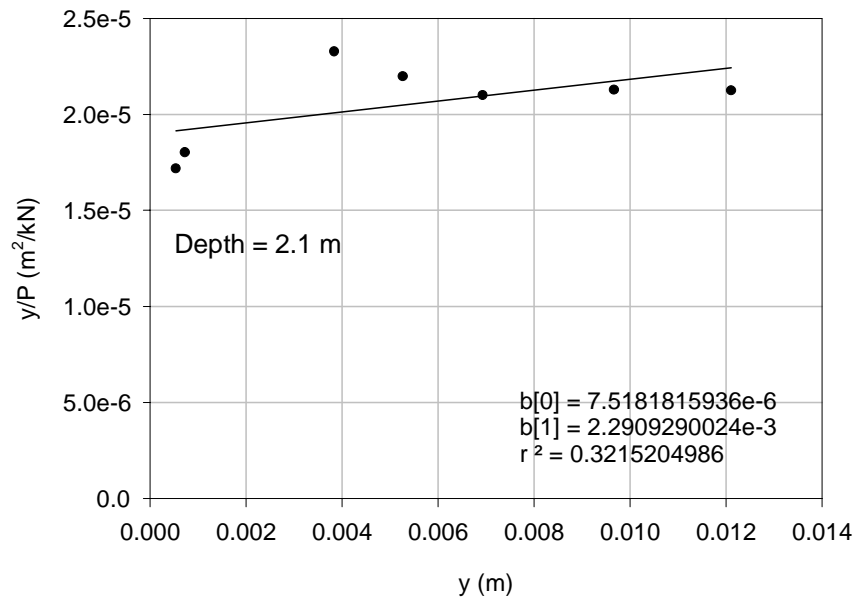
Figure E-23. Curve Fitting Result for Field Tests – Wilson Long Shaft
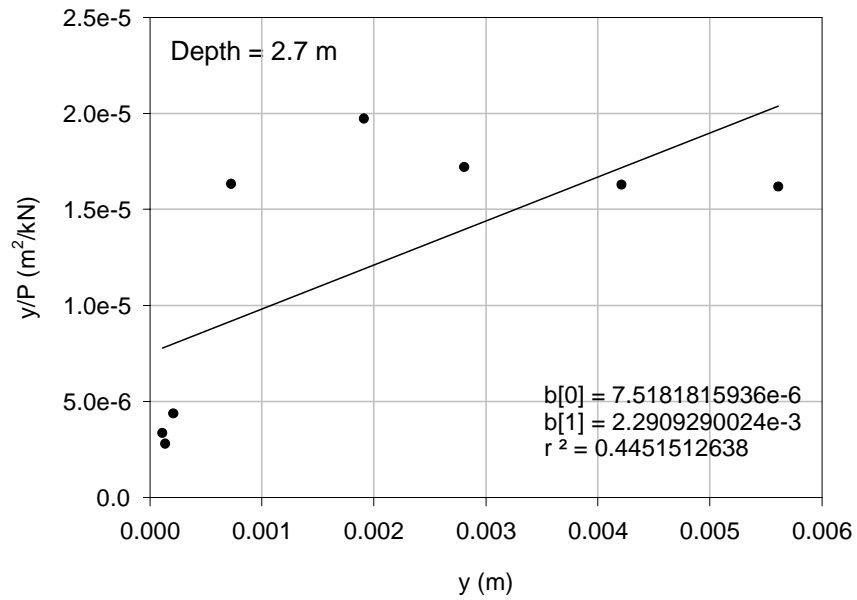
Figure E-24. Curve Fitting Result for Field Tests – Wilson Long Shaft
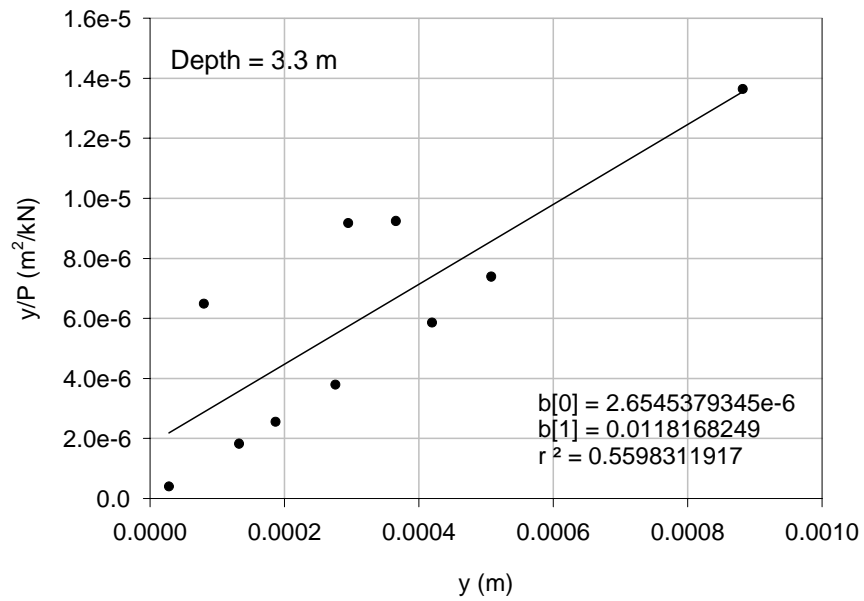
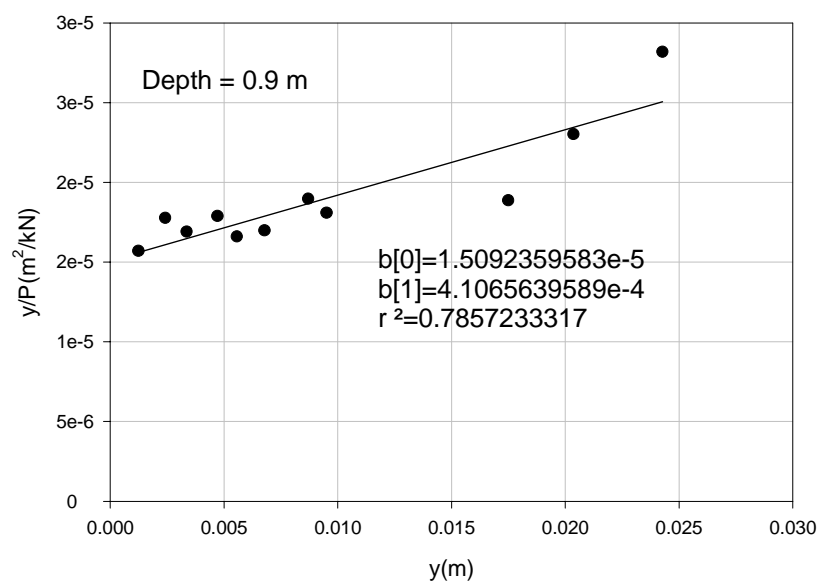**Figure E-25. Curve Fitting Result for Field Tests – Wilson Long Shaft**
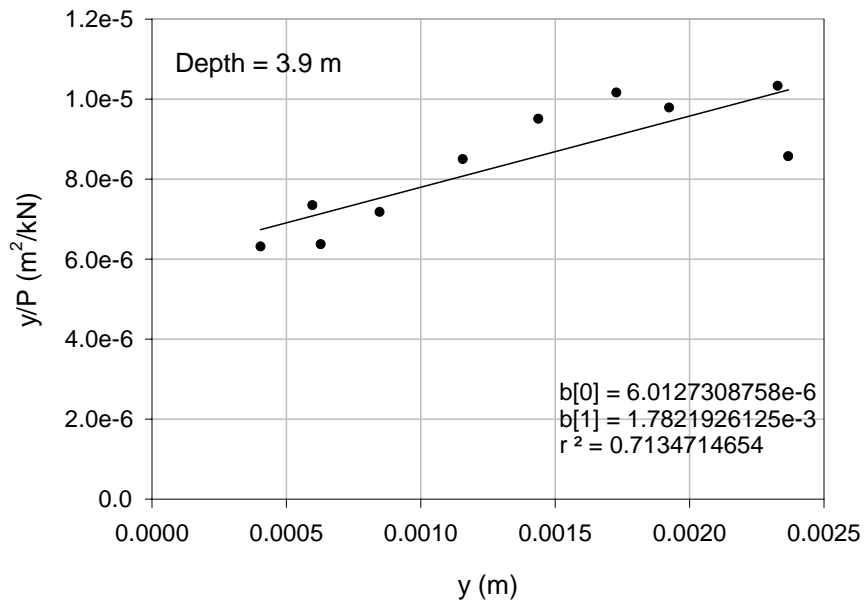
Figure E-26. Curve Fitting Result for Field Tests – Wilson Long Shaft
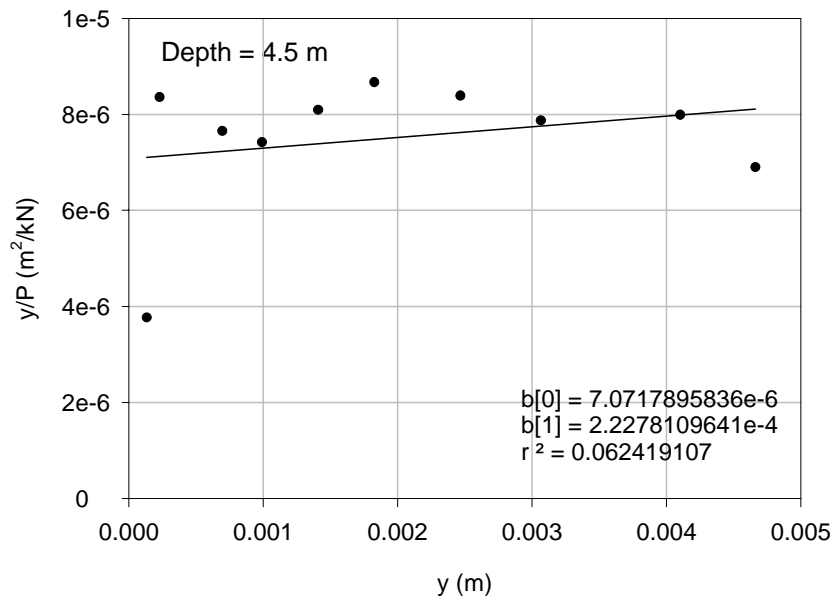
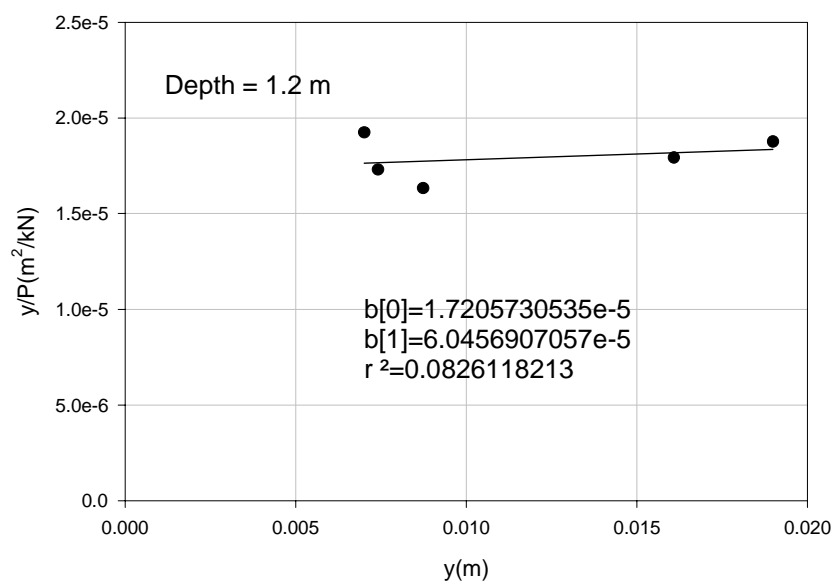**Figure E-27. Curve Fitting Result for Field Tests – Wilson Long Shaft**
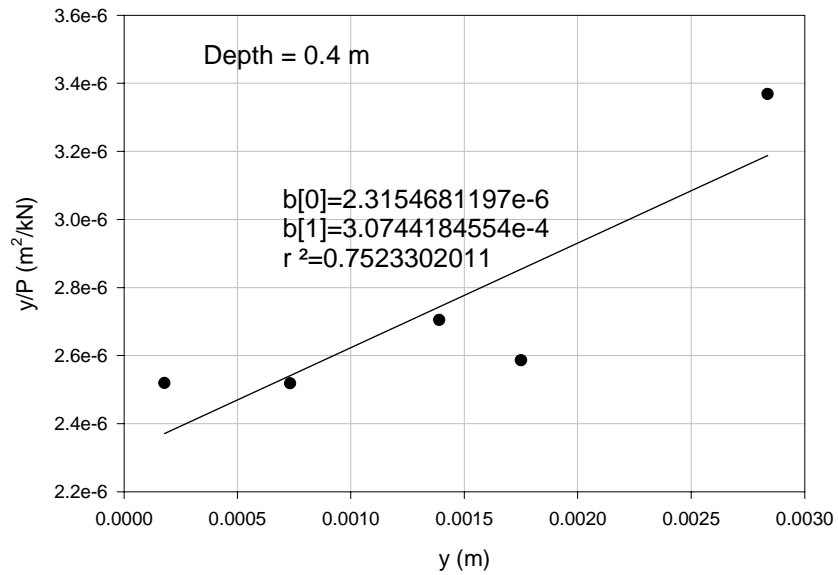
Figure E-28. Curve Fitting Result for Field Tests – I-40 Short Shaft

237
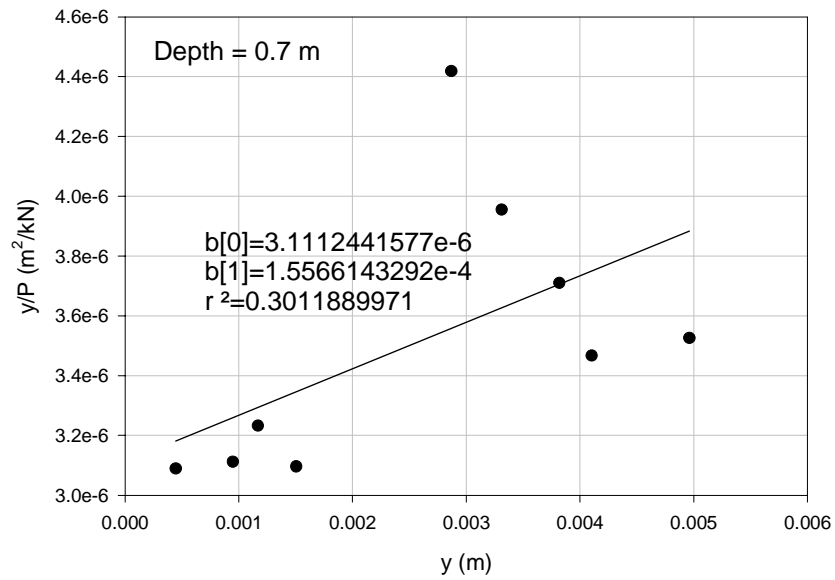
Figure E-29. Curve Fitting Result for Field Tests – I-40 Short Shaft
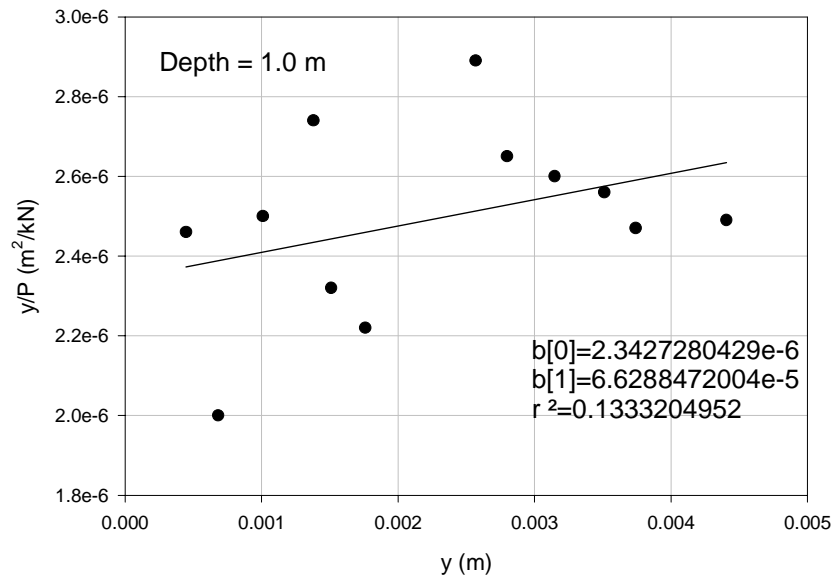
Figure E-30. Curve Fitting Result for Field Tests – I-40 Short Shaft
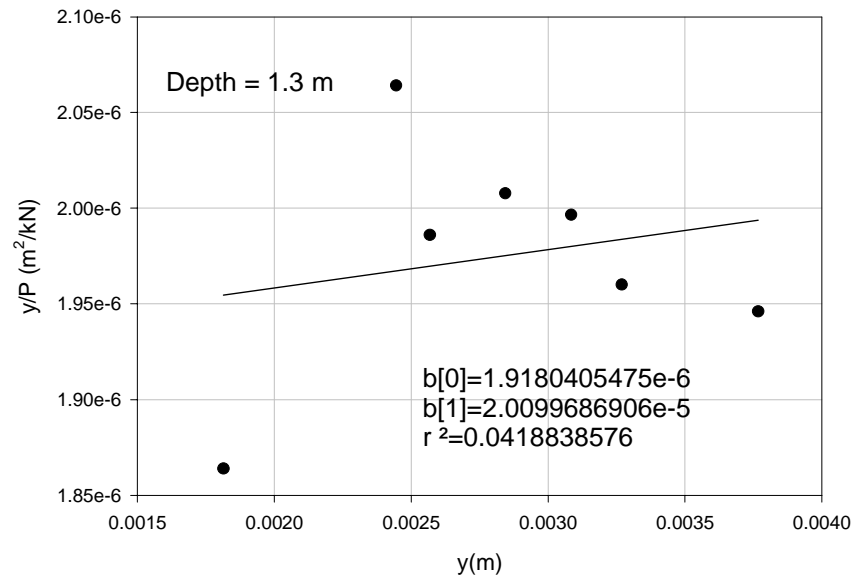
Figure E-31. Curve Fitting Result for Field Tests – I-40 Short Shaft
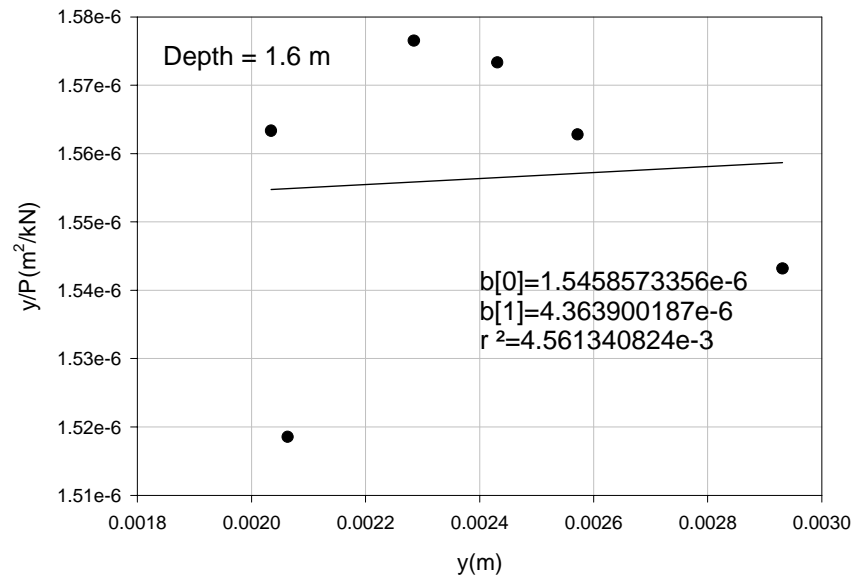
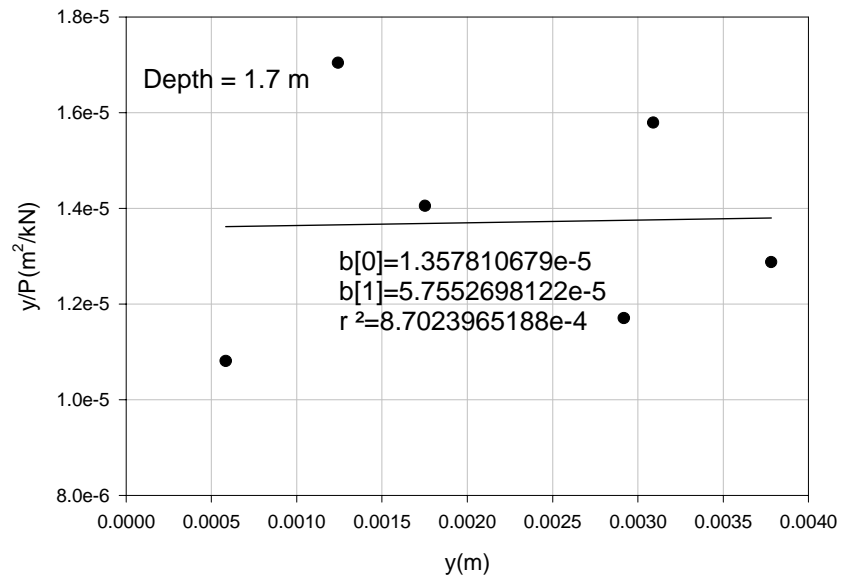**Figure E-32. Curve Fitting Result for Field Tests – I-40 Short Shaft**

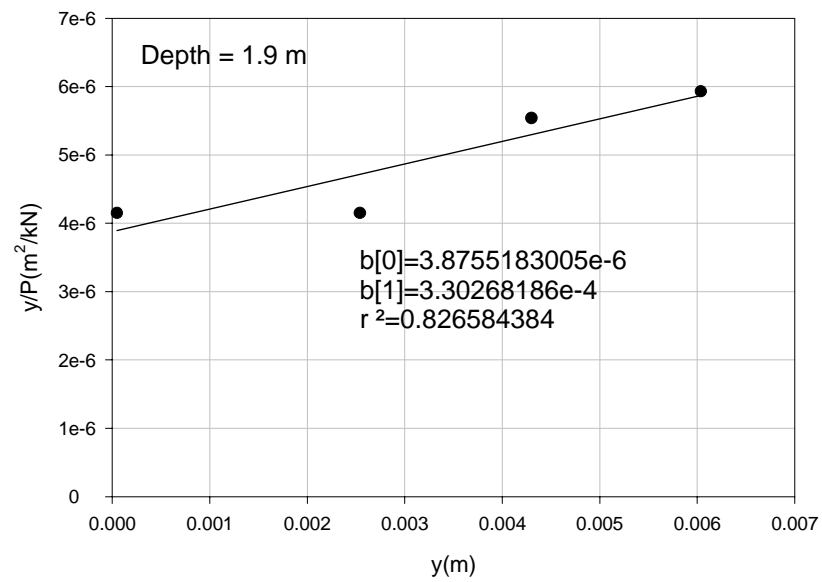**Figure E-33. Curve Fitting Result for Field Tests – I-40 Short Shaft**

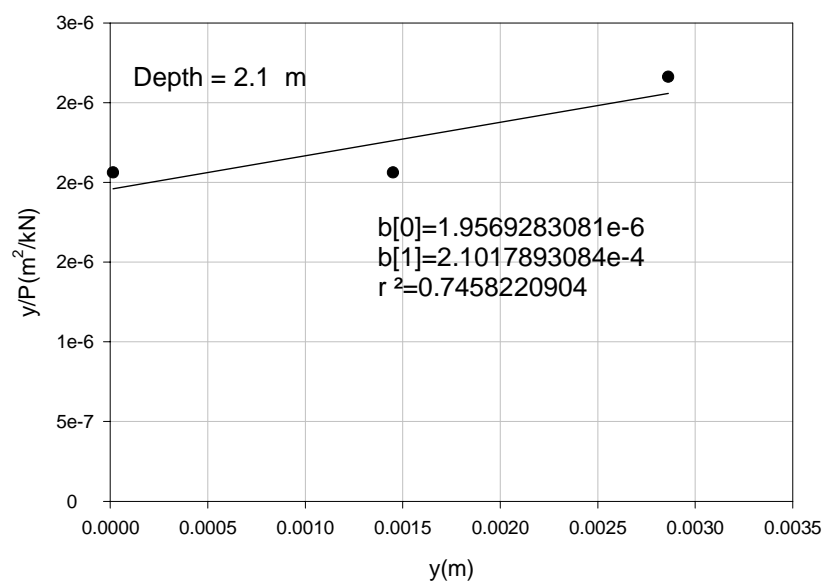**Figure E-34. Curve Fitting Result for Field Tests – I-40 Short Shaft**

240

Depth = 3.5 m

b[0]=5.6532233021e-7
b[1]=1.4933562458e-5
r ²=0.0137476663

Figure E-35. Curve Fitting Result for Field Tests – I-40 Short Shaft

Depth = 3.7 m

b[0]=4.9727333853e-7
b[1]=1.7423529124e-5
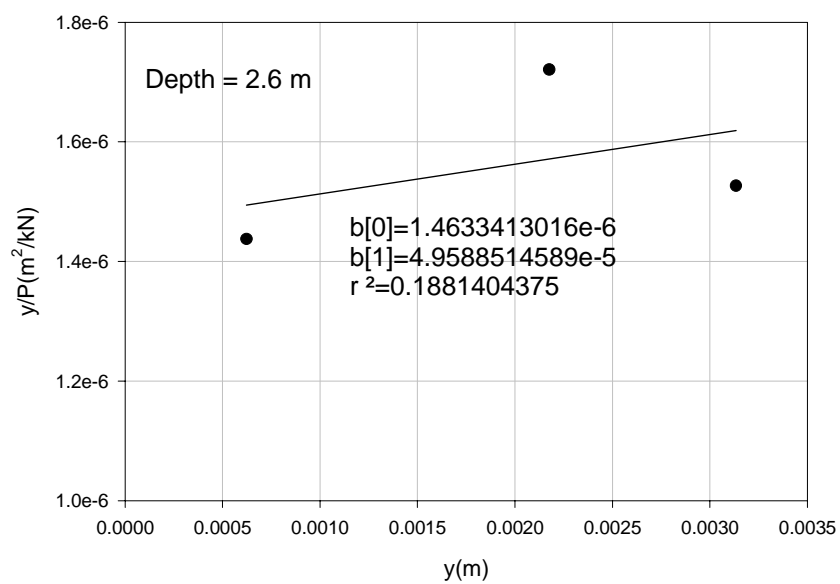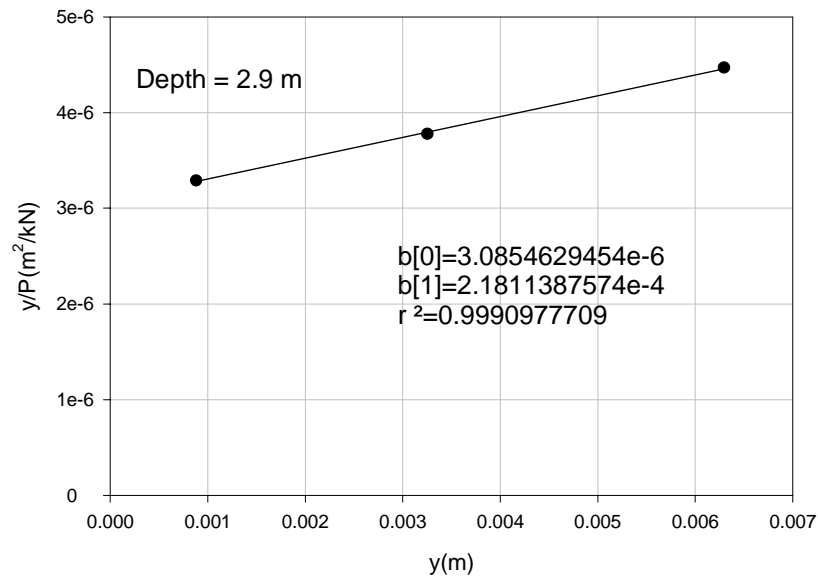r ²=0.0419150419

Figure E-36. Curve Fitting Result for Field Tests – I-40 Short Shaft

Figure E-37. Curve Fitting Result for Field Tests – I-40 Long Shaft
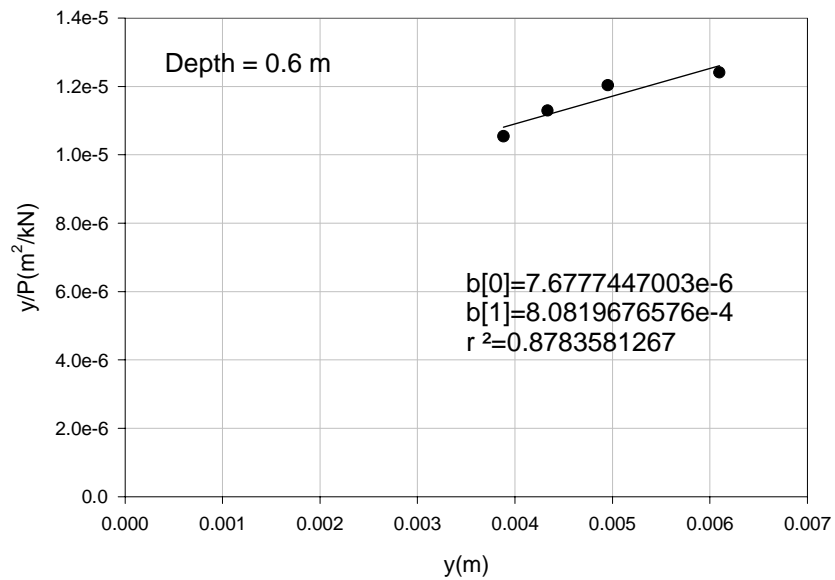

Figure E-38. Curve Fitting Result for Field Tests – I-40 Long Shaft

Figure E-39. Curve Fitting Result for Field Tests – I-40 Long Shaft

Figure E-40. Curve Fitting Result for Field Tests – I-40 Long Shaft

Figure E-41. Curve Fitting Result for Field Tests – I-40 Long Shaft
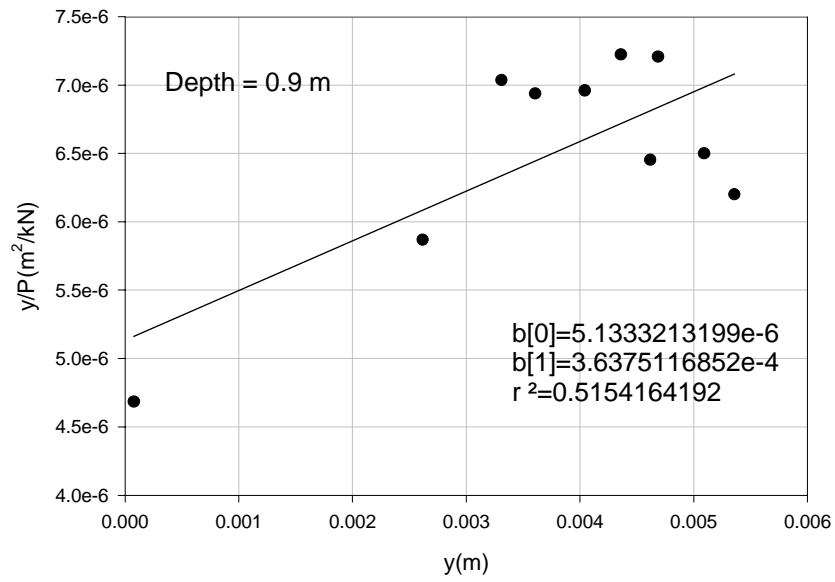

Figure E-42. Curve Fitting Result for Field Tests – I-40 Long Shaft

Figure E-43. Curve Fitting Result for Field Tests – I-40 Long Shaft

Figure E-44. Curve Fitting Result for Field Tests – I-40 Long Shaft
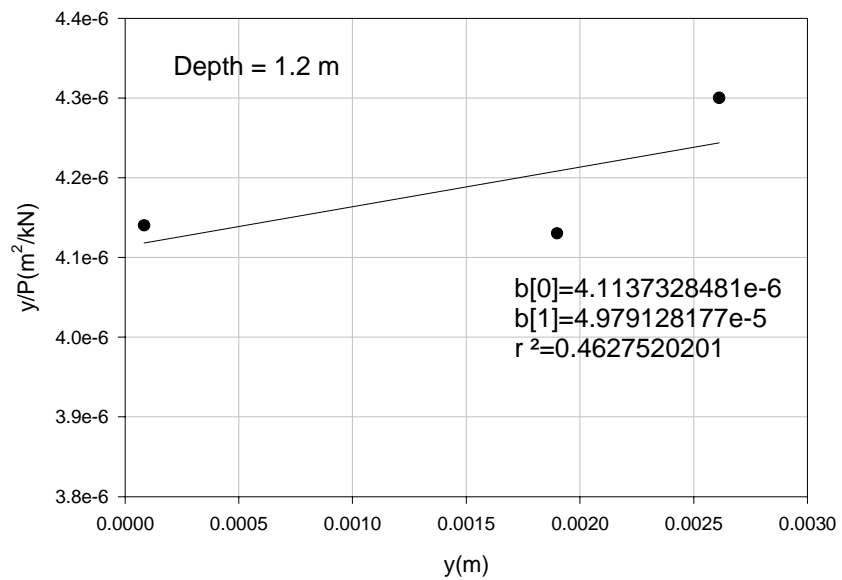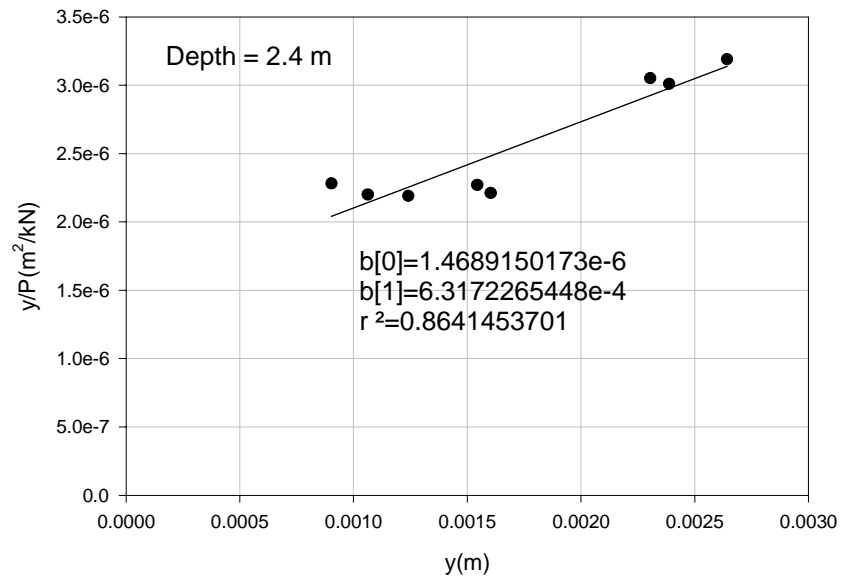
Figure E-45. Curve Fitting Result for Field Tests – I-40 Long Shaft
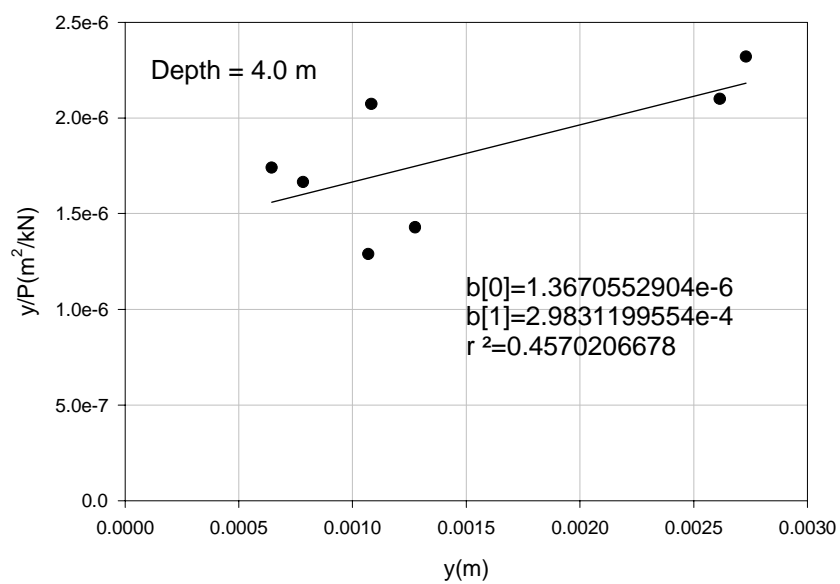
Figure E-46. Curve Fitting Result for Field Tests – I-40 Long Shaft

Figure E-47. Curve Fitting Result for Field Tests – I-40 Long Shaft

Figure E-48. Curve Fitting Result for Field Tests – I-40 Long Shaft

247

Figure E-49. Curve Fitting Result for Field Tests – I-85 Short Shaft

Figure E-50. Curve Fitting Result for Field Tests – I-85 Short Shaft

Figure E-51. Curve Fitting Result for Field Tests – I-85 Short Shaft
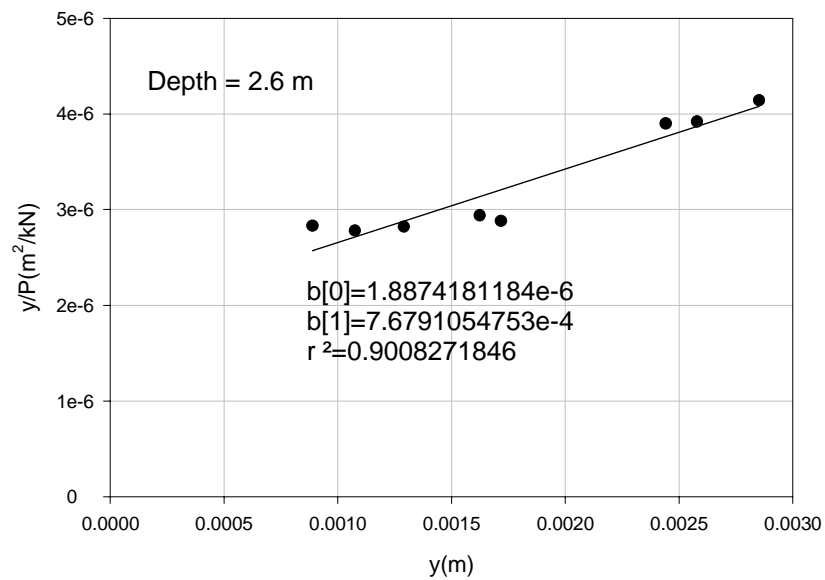

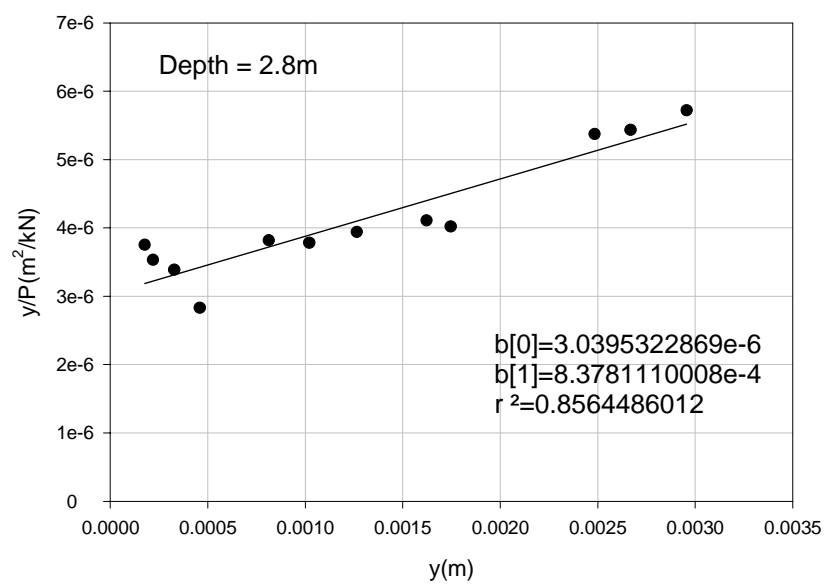**Figure E-52. Curve Fitting Result for Field Tests – I-85 Short Shaft**

Figure E-53. Curve Fitting Result for Field Tests – I-85 Short Shaft

Figure E-54. Curve Fitting Result for Field Tests – I-85 Short Shaft

Figure E-55. Curve Fitting Result for Field Tests – I-85 Short Shaft

Figure E-56. Curve Fitting Result for Field Tests – I-85 Short Shaft

Figure E-57. Curve Fitting Result for Field Tests – I-85 Short Shaft

Figure E-58. Curve Fitting Result for Field Tests – I-85 Long Shaft

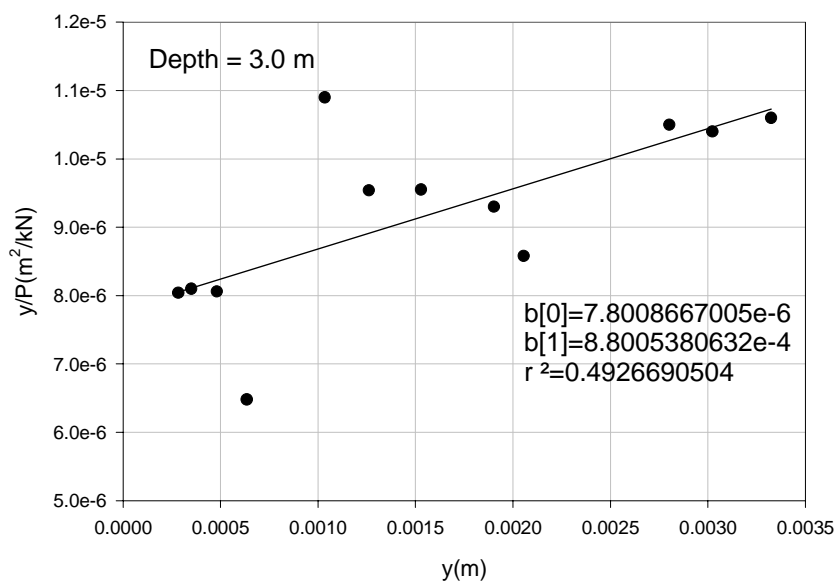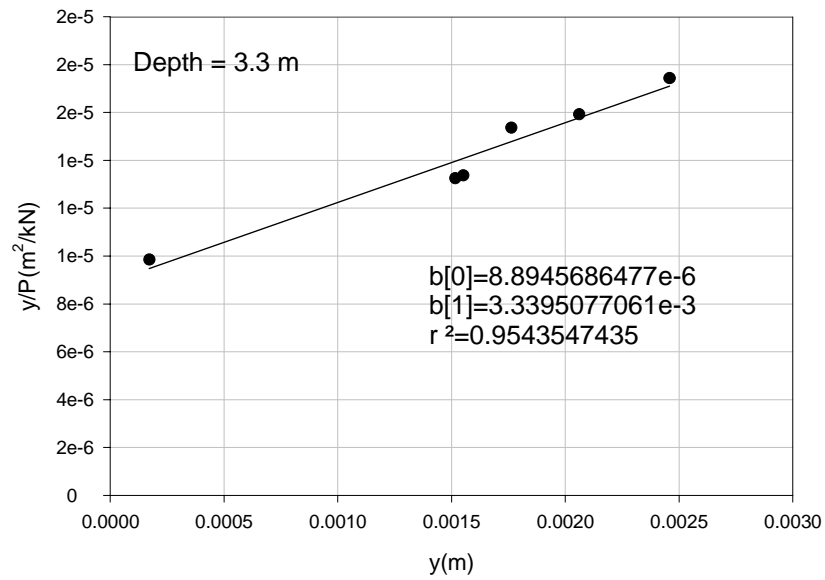**Figure E-59. Curve Fitting Result for Field Tests – I-85 Long Shaft**
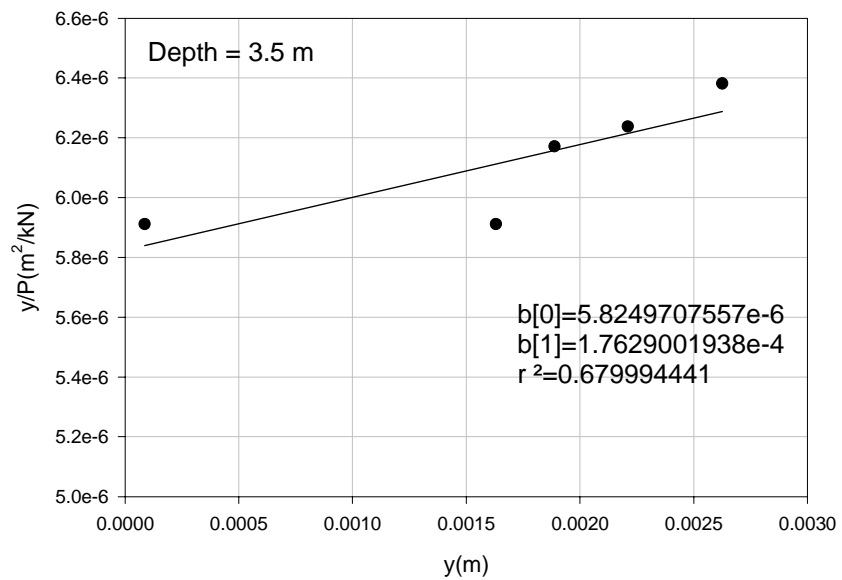

Figure E-60. Curve Fitting Result for Field Tests – I-85 Long Shaft

Figure E-61. Curve Fitting Result for Field Tests – I-85 Long Shaft

Figure E-62. Curve Fitting Result for Field Tests – I-85 Long Shaft

Figure E-63. Curve Fitting Result for Field Tests – I-85 Long Shaft

Figure E-64. Curve Fitting Result for Field Tests – I-85 Long Shaft

Figure E-65. Curve Fitting Result for Field Tests – I-85 Long Shaft

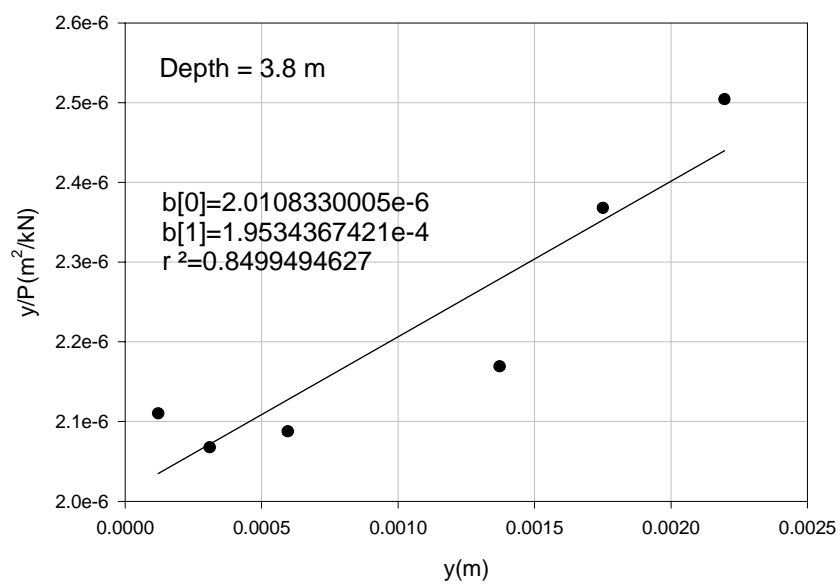**Figure E-66. Curve Fitting Result for Field Tests – I-85 Long Shaft**

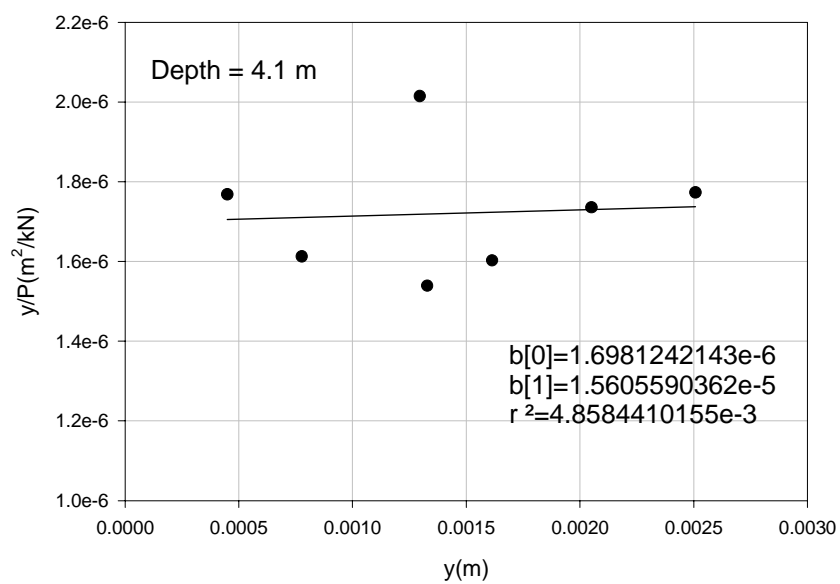**Figure E-67. Curve Fitting Result for Field Tests – I-85 Long Shaft**

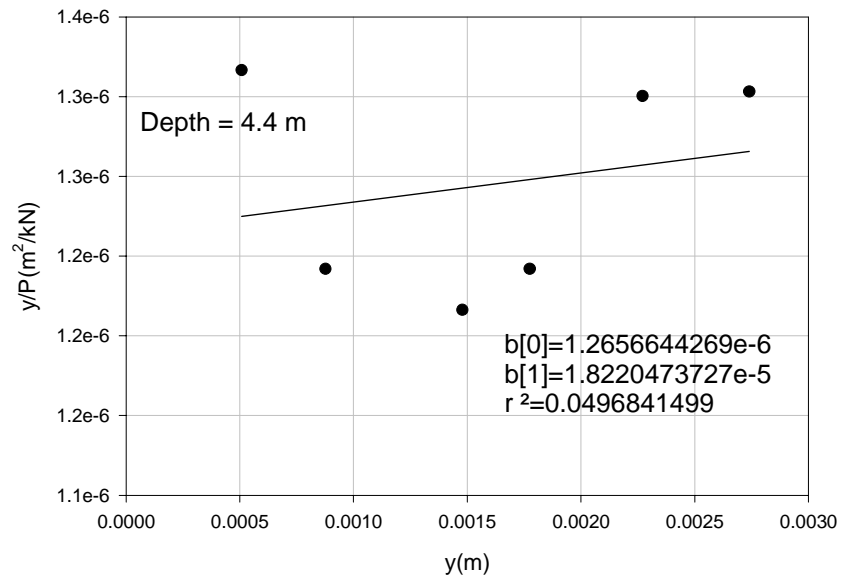**Figure E-68. Curve Fitting Result for Field Tests – I-85 Long Shaft**

257

Figure E-69. Curve Fitting Result for Field Tests – I-85 Long Shaft

APPENDIX F
Cases of F.E.M. Analysis

Table F-1. List of F.E.M. Analyses

No. of Running	L/D	Load (kips)
1		100
2		200
3		300
4		400
5	2.5	500
6		700
7		900
8		1300
9		1700
10		2000
11		100
12		200
13		300
14		400
15	5.2	500
16		800
17		1100
18		1500
19		2000
20		2500
21		100
22		200
23		300
24		400
25	7.5	500
26		1000
27		1500
28		2000
29		2500
30		3000

Table F-1. List of F.E.M. Analyses (continued)

No. of Running	L/D	Load (kips)
21	10.8	100
22		200
23		300
24		400
25		500
26		1000
27		1500
28		2000
29		2500
30		3000
31	15.0	100
32		200
33		300
34		400
35		500
36		1000
37		1500
38		2000
39		2500
40		3000

APPENDIX G

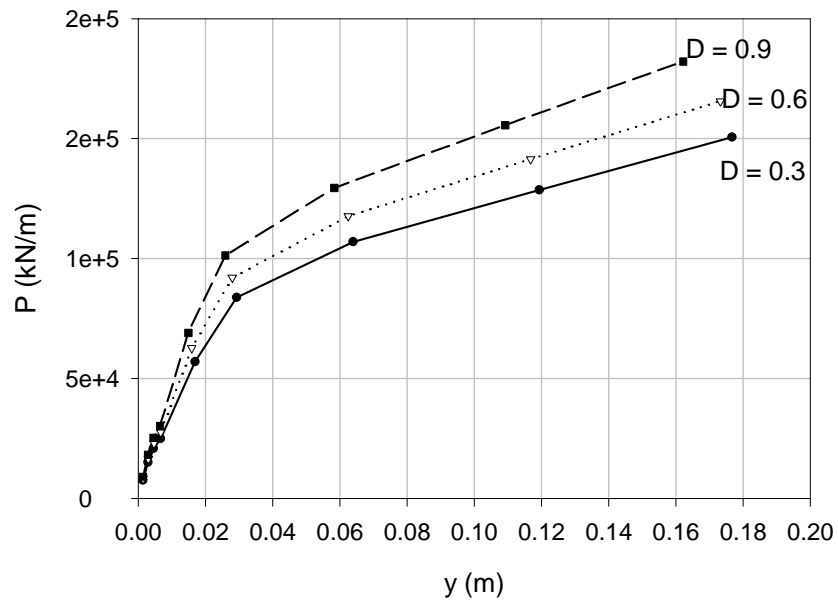## P-y Curve from F.E.M. Analysis

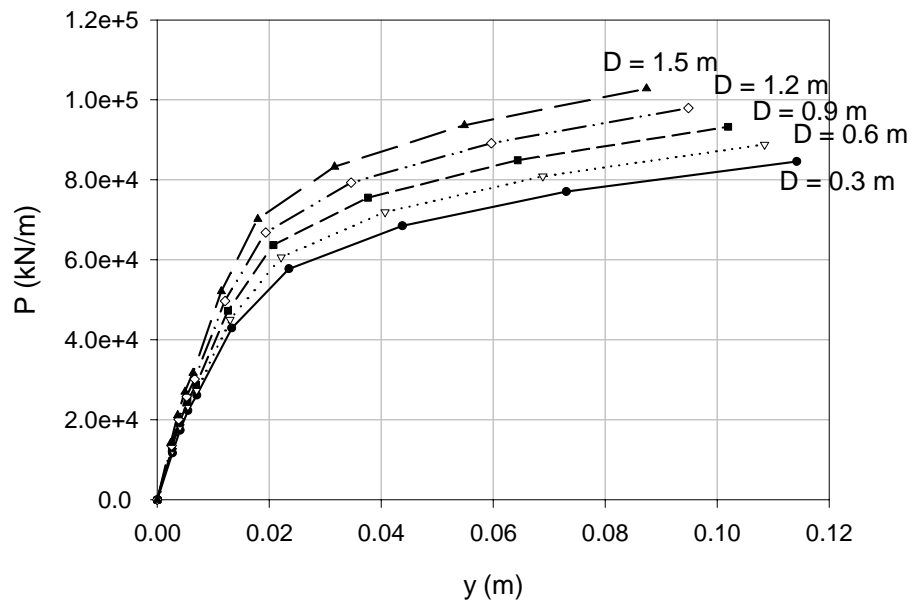**Figure G-1. P-y Curves from F.E.M. Analysis (L/D = 2.5)**

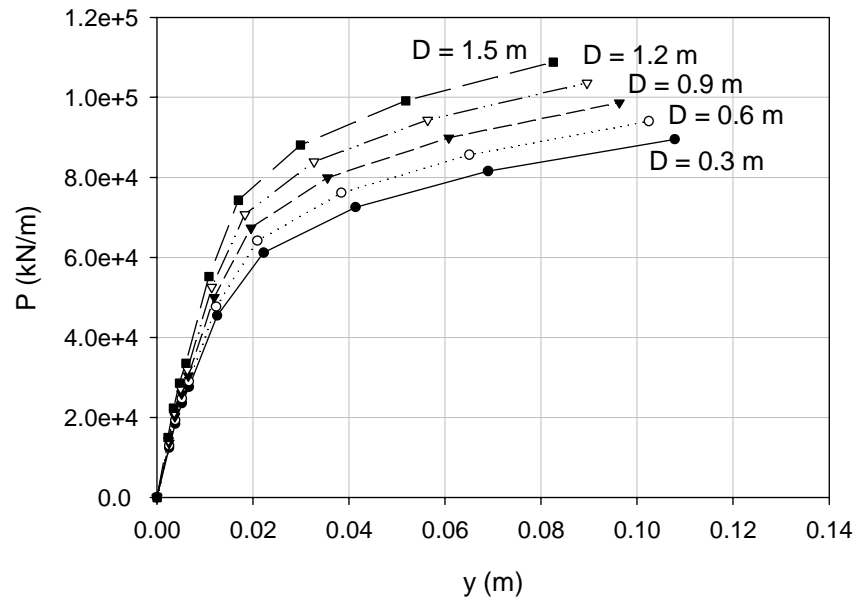

Figure G-2. P-y Curves from F.E.M. Analysis (L/D = 5.2)

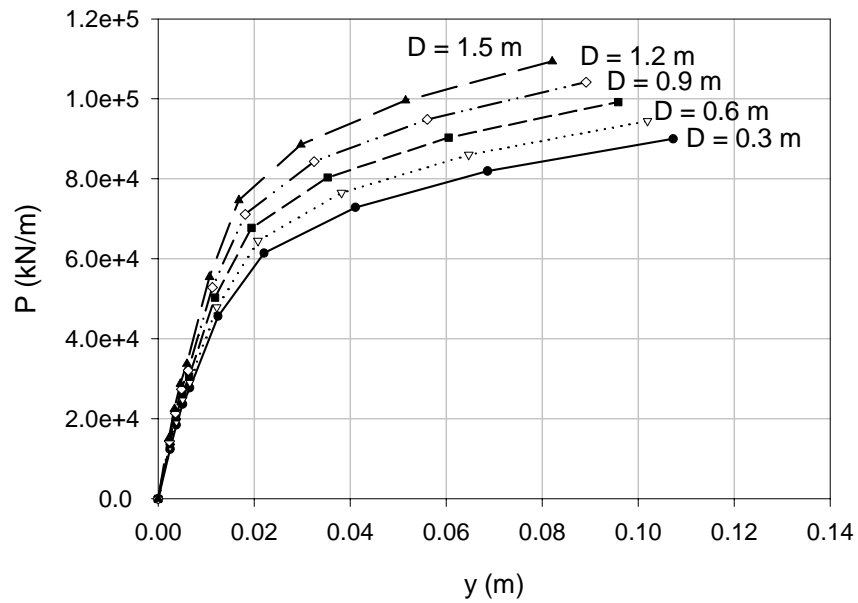**Figure G-3. P-y Curves from F.E.M. Analysis (L/D = 10.8)**

Figure G-4. P-y Curves from F.E.M. Analysis (L/D = 10.8)
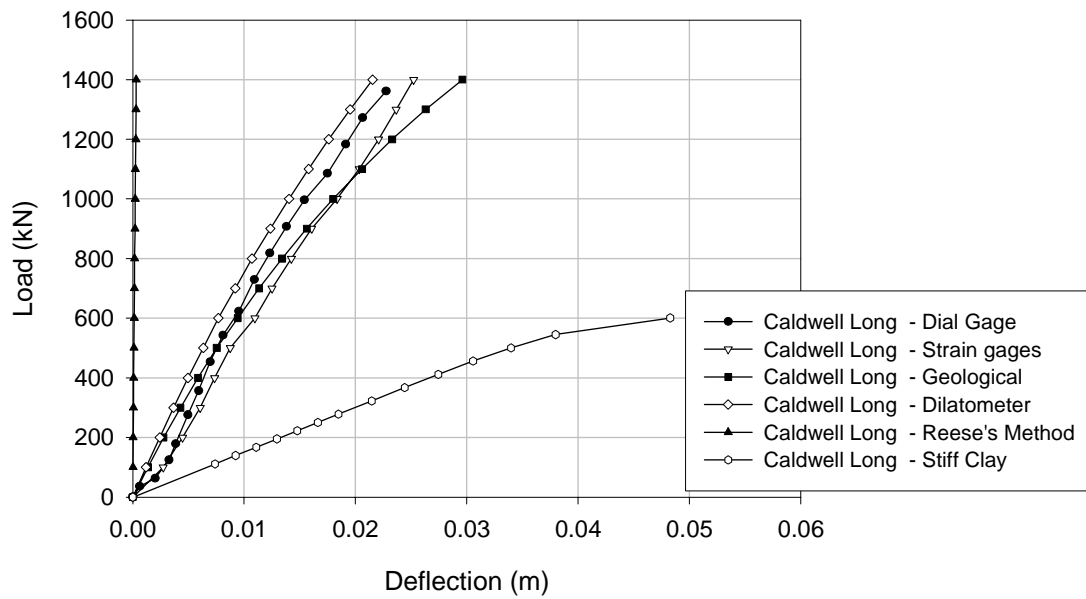
APPENDIX H

Proposed P-y Model- Estimate Comparisons

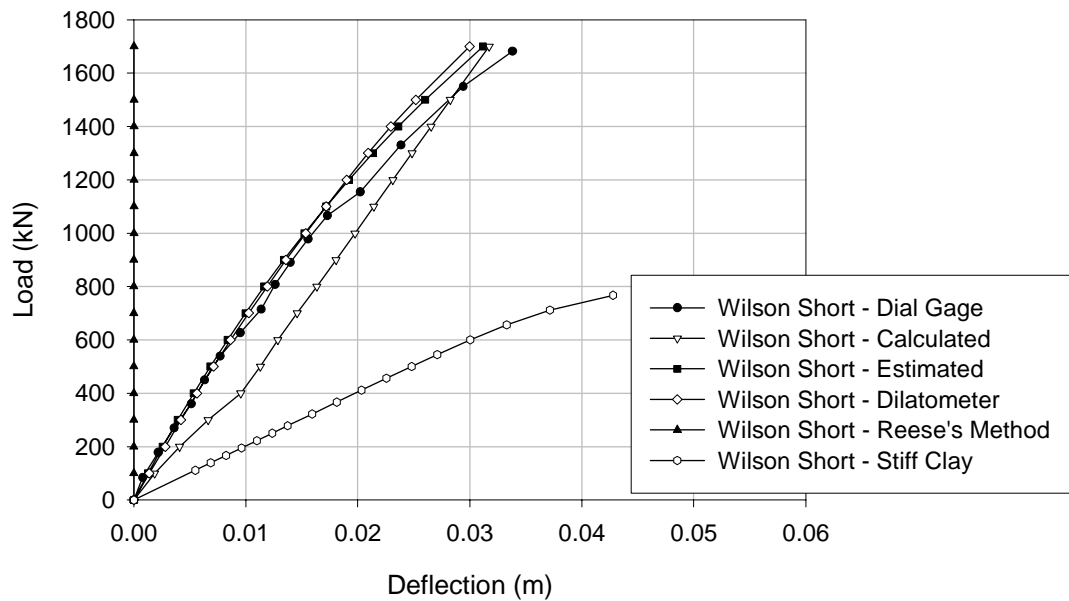**Figure H-1. Model Comparisons for Caldwell Long Shaft**

Figure H-2. Model Comparisons for Wilson Short Shaft

266

APPENDIX I

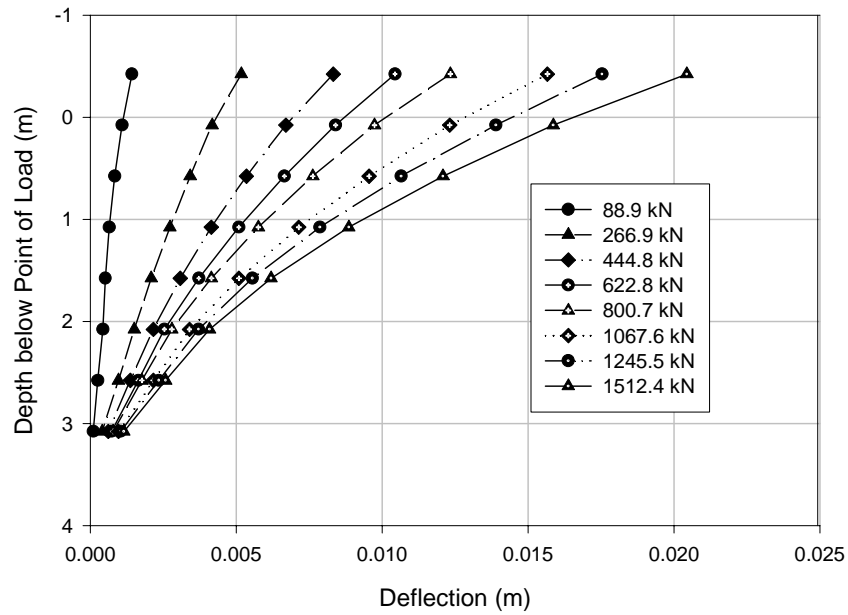Inclinometer Deflection Profiles

Figure I-1. Deflection Profiles before Dial Gage Adjustment – I-40 Short Shaft

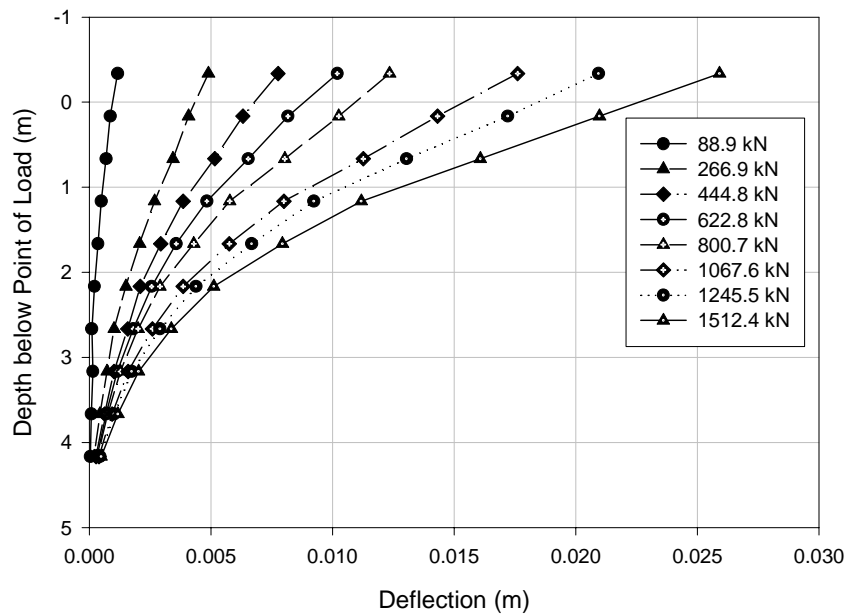**Figure I-2. Deflection Profiles before Dial Gage Adjustment – I-40 Long Shaft**
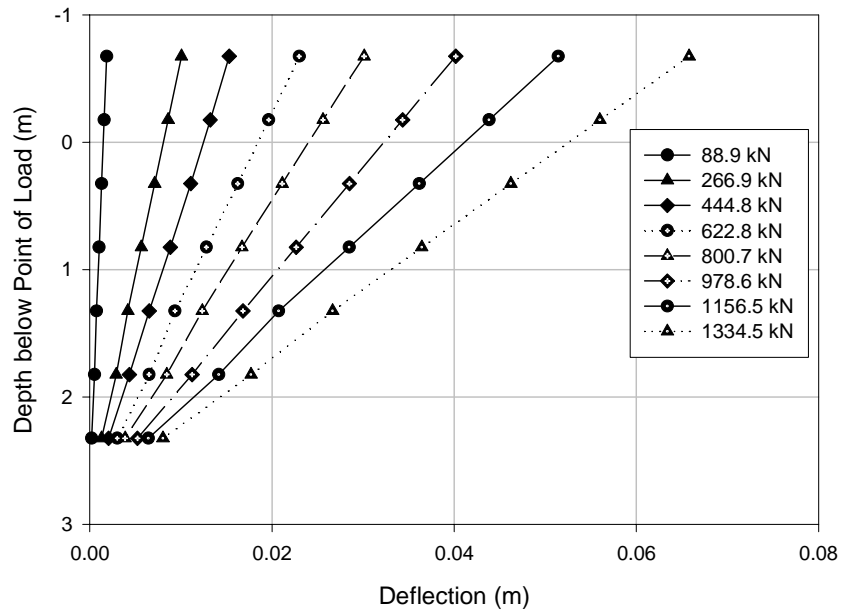
268

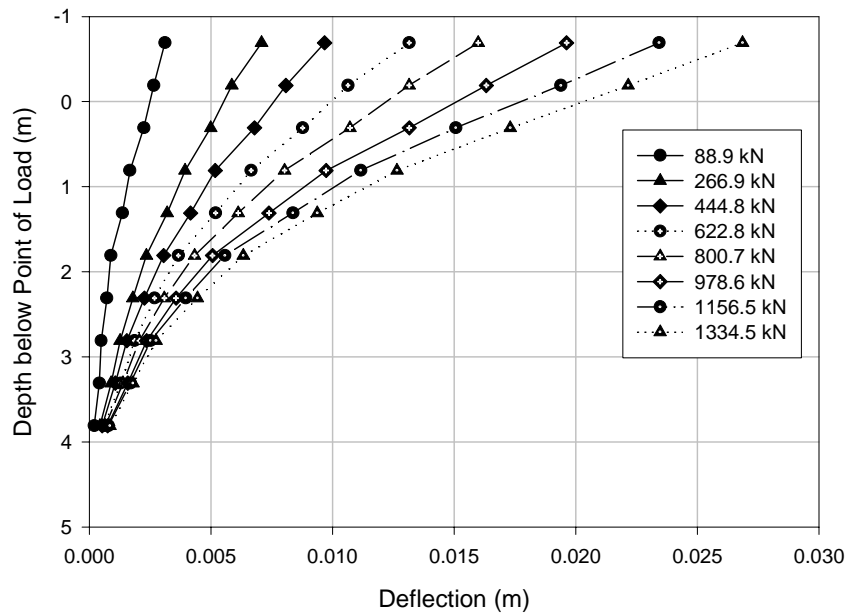**Figure I-3. Deflection Profiles before Dial Gage Adjustment – I-85 Short Shaft**

Figure I-4. Deflection Profiles before Dial Gage Adjustment – I-85 Long Shaft

APPENDIX J

Description of Input Variables for LTBASE Computer Program

(Gabr and Borden, 1987) with inclusion of the Weathered Rock

Model

LTBASE input file	Description:
ANALYSIS OF SHAFT	TITLE
NCDOT Example	PROJECT NUMBER
NCDOT	PROJECT LOCATION
Initials	OPERATOR NAME
10/11/02	DATE
0	NOPTION
20. 0.0 1 1.5	PT ,BC2,KODE,FSCR
30. 0.2 .001 4.0 100 5 -1 1 1 1	D,H,TOL,DEFCR,N,NU,NTYPE*,NCHOICE,IPRINT,IOUT
15.4 .319E+12	TP, EIP
0. 0.	THETA,THETAU
1	NX
30.0 30. 159.1 35.0 9. 3626. .000 -4	TH(1),DIA(1),GAM(1),FPHI(1),SK(1),CSHO(1),EP50(1),NPC(1)
1	I
.319E+12 20.0	RR(J), XX(J)

Lines 1-5: General Information

ANALYSIS OF SHAFT	TITLE
NCDOT Example	PROJECT NUMBER
NCDOT	PROJECT LOCATION
Initials	OPERATOR NAME
10/11/02	DATE

Line 6: Analysis Option

0	NOPTION, =1 Length is internally incremented
	=0 Single run analysis

Line 7: Loading Conditions

20. 0.0 1 1.5	PT ,BC2,KODE,FSCR
	PT = Initial lateral load to be applied at top of shaft, (kips)
	BC2 = Moment from shear force, (kip-ft) if KODE = 1
	= Slope, (in/in) if KODE = 2
	= Moment/slope, (kip-ft) if KODE = 3
	KODE = Code to control boundary condition at top of shaft
	FSCR = Limiting factor of safety criterion.

Line 8: Shaft dimensions and analysis control

30. 0.2 .001 4.0 100 5 -1 1 1 1	D,H,TOL,DEFCR,N,NU,NTYPE,NCHOICE,IPRINT,IOUT
	D = Shaft diameter at the ground surface. (inches)
	H = Total length of the pier / No. of increments (N), (feet) (100 maximum)
	TOL = Tolerance of solution convergence, recommended value 0.001
	DEFCR = Allowable deflection value at the top of the shaft, (inches)
	N = No. of increments into which the shaft is divided.
	NU = No. of pier increments above the ground surface
	NTYPE = Analysis option, 0 for SOIL case and -1for Weathered Rock Model

	NCHOICE = P-y curve generation option:
	      = 1, the program generates P-y curves initially.
	      = 0, user inputs P-y curves.

	IPRINT = 1, P-y curves are printed internally by the program = 0, printing of P-y curves is suppressed.
	IOUT = 1, Output file "*.OUT" is printed. = 0, Printing of "*.OUT" is suppressed

Line 9: Input depth to point of rotation and EI

15.4 .319E+12	TP, EIP
	TP = Input depth to point of rotation from ground surface (feet)
	EIP = Shaft stiffness, (psi)

Line 10: Slope analysis option

0. 0.	THETA,THETAU
	THETA = Slope angle of the ground surface in the front of shaft, (degrees).
	THETAU = Slope angle of the ground surface in the back of shaft, (degrees).

Line 11: Input and generation of P-y curves

1	NX = Number of the layers in the subsurface profile to be analyzed, if NCHOICE = 1

Line 12: Soil/rock properties

30.0 30. 159.1 35.0 9. 3626. .000 -4	TH(1),DIA(1),GAM(1),FPHI(1),SK(1),CSHO(1),EP50(1),NPC(1)
	TH(2),DIA(2),GAM(2),FPHI(2),SK(2),CSHO(2),EP50(2),NPC(2)
	TH(3),DIA(3),GAM(3),FPHI(3),SK(3),CSHO(3),EP50(3),NPC(3)
	For soil:
	TH(K)= Distance from ground surface to the end of the layer (feet)
	DIA(K)= Diameter of shaft at the mid-height of the layer (inches)
	GAM(K) = Effective or total unit weight of soil at the mid-height of the layer (pcf)
	FPHI(K)= Angle of internal friction soil at the mid-height of the layer, (degrees).
	SK(K) = Coefficient of lateral subgrade reaction at the mid-height of the layer, (pci).
	CSHO(K) = Undrained shear strength of the soil at the mid-height of the layer, (psi)
	EP50 (K) = Strain corresponding to 50% stress level at the mid-height of the layer
	NPC(K) = Code to control the type of P-y curves to be generated:
	= -1, P-y curves are generated using the Unified method.
	= 0, P-y curves are generated using the procedure developed by Reese et al. for sand.
	= 1, P-y curves are generated using the procedure developed by Parker et al. and O'Neill et al. for soil layer possessing both friction angle and cohesion.
	For rock:
	TH(K)= Distance from ground surface to the end of layer (feet).
	DIA(K)= Diameter of shaft at the mid-height of the layer (inches).
	GAM(K) = Effective or total unit weight of rock at the mid-height of the layer (pcf).
	FPHI(K)= GSI value of rock at the mid-height of the layer.
	SK(K) =m_i value of rock at the mid-height of the layer.
	CSHO(K) = Unconfined compressive strength of rock at the mid-height of the layer, (psi).
	EP50 (K) = 0.00 for the rock sub-layer
	NPC(K)= Code to control the type of P-y curves to be generated:
	= -4 P-y curves generated using the Weathered Rock Model

Line 13: Pier stiffness

1	I = Number of different shaft cross-sections

Line 14: Pier stiffness (2)

.319E+12 20.0	RR(J), XX(J)
	RR (J) = EI value (psi)
	XX (J) = Depth from top of shaft to point where cross-section changes (feet)

IMPORTANT NOTE: In the output file depth is referenced from the top of the shaft. However, in the input file depth to the point of rotation is referenced for the ground surface.

Save input file with .dat extension

Load vs. deflection results are given in the *.prn file.